Chemistry of the sea ice/ snowpack/ atmosphere system in coastal Antarctica

A thesis submitted to the

School of Environmental Sciences

of the

University of East Anglia

in candidature for the degree of

Doctor of Philosophy

By

Zak Buys

May 2014

Research was conducted at the

British Antarctic Survey

© This copy of the thesis has been supplied on condition that anyone who consults it is understood to recognise that its copyright rests with the author and that use of any information derived there from must be in accordance with current UK Copyright Law. In addition, any quotation or extract must include full attribution.

Abstract

Tropospheric Ozone Depletion Events (ODEs) have been known to occur during springtime in polar regions for over 20 years. During such events, ozone concentrations can fall from background amounts to below instrumental detection limits within a few minutes and remain suppressed for on the order of hours to days. The chemical destruction of ozone is driven by halogens (especially bromine radicals) that have a source associated with the sea ice zone. There is much debate over the source of bromine radicals in the atmosphere that drive polar boundary layer ODEs and few observations of speciated inorganic bromine against which to test current theory.

In 2007, year round measurements were made at the British Antarctic Survey station Halley, in coastal Antarctica, using a Chemical Ionisation Mass Spectrometer (CIMS). During specific periods in the spring the CIMS was configured to measure concentrations of BrO, Br_2 and BrCl. In addition, concurrent measurements of surface ozone and local meteorology were made.

Presented here is an analysis of these datasets in terms of both chemistry, and the broader meteorological situation at play during the onset and termination of ODEs, in a move towards developing a generalised picture for ODEs at Halley. In order to explore halogen release, the MISTRA model is used to consider emissions from specific source regions, identified using HYSPLIT air parcel back trajectories.

A new snow-photochemistry module has been developed for MISTRA which includes chemistry which takes place in the liquid like layer on frozen surfaces (MISTRA-SNOW; Thomas et al., 2011). Understanding these surface processes is of great importance to our understanding of the chemistry which initiates a bromine explosion. MISTRA-SNOW is initialised using measurements made at Halley station to explore both the chemical and meteorological conditions required to produce tropospheric ODEs in polar regions.

Contents

List of Tables

List of Illustrations

List of illustrations cont'd

List of illustrations cont'd

Acknowledgements

I would like to start by thanking my supervisors, Dr Anna Jones and Dr Roland von Glasow for their continual encouragement and advice, as well as the many helpful (and informative) discussions we had along the way. Thanks also go to Neil Brough, from the British Antarctic Survey, for the hours he spent working with me on the initial data work-up, and advice on analysis techniques with IGOR. I would like to thank Tony Phillips of the British Antarctic Survey for giving me access to an experimental service providing web access to IDL based PP plotting routines of ECMWF operational analysis data. Thanks are also made to Phil Anderson (formerly of BAS), for his advice on meteorological matters at Halley.

Finally I would like to thank my family for their constant support (both moral and financial), and for believing in me when I wasn't sure I believed in myself.

This study is part of the British Antarctic Survey Polar Science for Planet Earth programme. My studentship was funded by the Natural Environment Research Council through a BAS Algorithm grant.

1. Introduction

1.1. Halley dataset and project description

In 2007, year round measurements were made at the British Antarctic Survey station Halley (75° 35'S, 26° 19'W), in coastal Antarctica, using a Chemical Ionisation Mass Spectrometer (CIMS). Measurements were made by Neil Brough (British Antarctic Survey) during part of a 14 month field campaign at Halley station. During the austral spring, the CIMS instrument was configured to perform high resolution measurements of BrO, Br_2 and BrCl. In addition, concurrent measurements of surface ozone and local meteorology were made (Normal BAS routine). Although such observations have been made in the Arctic (Neuman et al., 2010; Liao et al., 2011a; Liao et al., 2011b; Liao et al., 2012b), this is the first such suite of measurements made in Antarctica. The CIMS instrument (along with the ozone instrument) was located in the Clean Air Sector Laboratory (CASLab), which is run and maintained by the Chemistry and Past Climate group at the British Antarctic Survey.

Locating this measurement campaign at Halley makes a lot of sense, as it is partly influenced by air masses that have passed over the sea ice zone prior to their arrival at Halley. This is important as the sea ice zone is thought to be a source of reactive bromine species, a key driver of ozone depletion events (ODEs). The polar boundary layer is a unique atmospheric chemistry system that has received huge interest over recent years, and exploration of snow-atmosphere interaction in this region is a current topic of debate for many atmospheric chemists. The halogen activation process on the snow/ ice surface is not well understood, but processes linked to new sea ice formation do drive emissions of halogens, especially bromine.

Air masses arrive at Halley after passing over the sea ice zone of Precious Bay to the south west of Halley, meaning the chemical influence of the sea ice can be observed. Air arriving at Halley also often comes from over the continent rather than the sea ice zone, which gives the opportunity to measure background halogen compounds and ozone mixing ratios for comparison with the sea ice zone influenced air (Jones et al., 2006). The sea ice/ snowpack/ atmosphere system at the British Antarctic survey base Halley creates the opportunity to explore the influence of the sea ice zone on the chemistry of the air masses arriving at Halley.

The dataset therefore already existed prior to my involvement in the project. The initial data workup was the first task undertaken (with the help and expertise of Neil Brough) closely followed by the initial data analysis which will be discussed in later chapters. A thorough analysis of the BAS datasets was then conducted, and then a 1-dimensional multiphase chemistry model of the boundary layer (MISTRA) that was recently modified for polar applications (Piot and von Glasow, 2008) was used to test our understanding of processes.

When using the MISTRA model to explore the dataset, a simple 'box' model version was the first step followed by the 1-D and MISTRA-SNOW versions at a later date. The combination of such novel datasets with the MISTRA model provided a powerful opportunity to probe details of chemical processes occurring within a rapidly changing environment. The MISTRA-SNOW model has, to date, only been applied to a single field location – Summit station, in central Greenland, during the Boreal summer. Conditions at Halley during spring are quite different, with considerably lower temperatures, restricted solar radiation, and a significant influence of the sea ice zone on observed atmospheric chemistry. One aim of the project was therefore to test the MISTRA model under Halley springtime conditions, to see if the basic model was able to reasonably reproduce observations. Not only is the dataset presented here the first of its kind, but using MISTRA in versions with varying complexity as a tool in conjunction with this Halley dataset is also a first. The model was then used as a tool to probe the current understanding of bromine explosions (BEs) and ozone depletion events (ODEs) in coastal polar regions from both the meteorology and chemistry viewpoints, with the Halley dataset available for comparison.

1.2. Project design and research methodologies

The MISTRA model (without the SNOW module) has previously been used effectively to investigate the potential role of frost flowers, open leads and recycling on snow in polar tropospheric ozone depletion events (Piot and von Glasow, 2008). Using MISTRA to investigate the CIMS Halley data is a great opportunity to use a numerical model to see what new insights into halogen activation, and chemistry in general; we can gain from the first coastal Antarctic measurements of high resolution Br_2, BrCl and BrO.

The initial focus of the project, as outlined briefly above, had to be changed to include work on a potential CIMS inlet artefact in the form of HOBr as an interferent in the daytime Br_2 and BrCl observations. MISTRA was a suitable platform to explore different contributions of the model output for HOBr to Br_2 and BrCl.

I used back trajectory analyses using the Hybrid Single-Particle Lagrangian Integrated Trajectory (HYSPLIT) model to assess the role of the different source regions (sea ice, open ocean and snowpack). HYSPLIT is available via the NASA ARL READY website (www.ready.noaa.gov/ready/open/hysplit4.html) (Rolph, 2012; Draxler and Rolph, 2012).

The SNOW module recently developed by Thomas et al. (2011, 2012) has been used to give confidence in the community's understanding of chemistry in remote polar regions. It is therefore ideal that it was modified for use at Halley, in conjunction with the novel dataset mentioned previously, to explore an idealised (although realistic and insightful) scenario for Halley.

1.3. Thesis structure

Chapter 2 will look at some background subject matter and discuss related work. Chapter 3 will give an overview of the field observations used for this study. This will include a site description of the CASLab at Halley station, and an overview of the instrumentation used for the chemistry and meteorology measurements. Chapter 4 moves onto a description of the various guises of the MISTRA model, including a description of the new snow photochemistry module (Thomas et al., 2011). In the next chapter (chapter 5) I explore an issue with the CIMS instrument, using the box model version of MISTRA. It is in chapter 6 that the Halley data set is fully introduced, with various comparisons being made (specifically to similar measurements made in the Arctic) and interesting aspects of the data explored. Two interesting events from the Halley data are discussed in chapter 7, and both highlight the importance of the sea ice zone in influencing the chemistry of the atmosphere at Halley. An in-depth description of the model setup for MISTRA-SNOW is given in chapter 8, along with a detailed look at the initial conditions used and changes that were made to make the model representative of the Halley environment. Chapter 9 explores several important aspects of snow-atmosphere interaction and their effects on ozone

depletion and bromine explosions using MISTRA-SNOW. Chapter 10 gives a summary and conclusion of the results from the previous chapters.

2. Background and related work

Synopsis:

Given here is an introduction to halogen chemistry in polar regions, including important chemical mechanisms and some physical properties that play a central role in our understanding of chemistry of the sea ice/ snowpack/ atmosphere system in coastal Antarctica. Also included here is a discussion of ice surfaces as a possible source of reactive halogen species to the atmosphere.

2.1 Review of current understanding: Background and history of Ozone Depletion Events in polar regions

Ozone plays an important, and unique, role in tropospheric chemistry due to its high oxidative capacity, and it is generally accepted that background ozone has at least doubled since pre-industrial times due to human activities (Crutzen and Zimmermann, 1991). The detrimental impact ozone can have on health (Lippmann, 1991) and crop yields (Herstein et al., 1995), has meant that these rises in tropospheric ozone are a cause for concern. That tropospheric ozone has also been recognised as a significant greenhouse gas contributing ~13% of all anthropogenic radiative forcing (IPCC, 2001), it is therefore prudent that our understanding of its transport, formation and loss processes must be better understood. Although it may not seem it, as regions of unusual chemical processes which influence atmospheric and oceanic circulation, the geographically remote Arctic and Antarctic have a significant impact on the global atmosphere (Simpson et al., 2007). Their remote/ unpolluted location (at least in the case of Antarctica) means they are the ideal place to study these ozone related processes which we want to understand. Atmospheric composition histories can be extracted from snow/ icepack of these polar regions by ice coring, and an improved understanding of the polar BL meteorology and chemistry (as discussed in this thesis) will help with the interpretation of these palaeoatmopsheric compositions.

The atmospheric boundary layer (BL) in Antarctica is unique. It is separated from polluted air masses by the Southern Ocean (Simpson et al., 2007) and has been described as very clean

(Wessel et al., 1998). A recent study by Hamilton et al. (2008) has highlighted the presence of a 'chemical equator' near, but not coincident with, the ITCZ (Intertropical Convergence Zone) during the Austral monsoon season. This region of inhibited interhemispheric mixing makes it difficult for polluted air masses from Asia to contaminate the Antarctic troposphere, meaning conditions in Antarctica differ greatly from the Arctic which succumbs to 'Arctic Haze' events (Barrie et al., 1989). The snowpack plays a key role in determining the chemical composition of the polar BL as it is a major source of trace gases (e.g. NO_x, HCHO, H_2O_2) (Grannas et al., 2007). Many snowpack emissions cause an increase in OH radical concentrations thereby enhancing the oxidising capacity of the BL. The sea ice zone is also thought to influence atmospheric chemistry in coastal polar regions (Jones et al., 2006), emitting halogen species which react in the gas phase to destroy ozone (Abbatt et al., 2012).

Antarctica's unusual light conditions (24 hour sunlight and 24 hour darkness for large parts of the year), cold temperatures and stable boundary layer give us a rare opportunity to study atmospheric chemistry in an unpolluted environment. Although the Pacific marine BL can also be seen as unpolluted, coastal polar regions are a prime location to study air masses of different origin (i.e. the sea ice zone, or the continental snowpack).

The term ozone depletion event (ODE) is used to describe the phenomenon when ozone concentrations are depleted from background amounts (typically 30-40ppbv) and can even fall to below instrumental detection limits (roughly a few parts per billion by volume, ppbv) within a few minutes, and remain suppressed for on-the-order of hours to days (Jones et al., 2006).

The first published measurements of ozone depleted air in the polar troposphere were reported from Barrow, Alaska (Oltmans, 1981), followed by a more detailed study in March 1985 at Alert, Nunavut (Bottenheim et al., 1986). A study by Barrie et al. (1988) was the first to link these ODEs to bromine. During the second AGASP campaign (Arctic Gas and Aerosol Sampling Program) in 1986 it was observed that these periods of low ozone coincided with periods of "excess filterable bromine" [f-Br] (Barrie et al., 1988), the source of which could not be determined. Due to this observed anti-correlation between O_3 and [f-Br] Sturges (1990) suggested that a catalytic cycle involving bromoform ($CHBr_3$) photolysis could be the source of Br atoms that subsequently led to the destruction of BL O_3. However, Moortgat et al,(1993) were able to rule out O_3 depletion by $CHBr_3$ photochemistry. The absorption cross section was used to calculate the photolytic lifetime of $CHBr_3$ under polar springtime conditions and was found to be ~ 100 days which is just too long to account for the large observed concentrations of reactive bromine. The Arctic is much easier to access for field campaigns than Antarctica, which has led to many discoveries first being made

in the Arctic and later being "observed to varying degrees in the Antarctic" (Simpson et al, 2007). Since the first observations of boundary layer (BL) ODEs in the Antarctic in the mid-1990s (Kreher et al., 1996; Wessel et al., 1998) and the coincident detection of BrO (Kreher et al., 1997), many more Antarctic field studies have taken place (Rankin et al., 2002; Jones et al., 2006). Roscoe and Roscoe (2006) showed, through analysis of historical ozone data from Halley, that ozone depletion events were evident as far back as 1957/58, thereby showing that they were a natural phenomenon. It is now known that ODEs are present in both polar regions and are extensive, and the current scientific focus is halogen sources and the underlying chemistry.

The chemical destruction of ozone is driven by halogens, especially bromine radicals (e.g. Simpson et al., 2007; Abbatt et al., 2012). It is now widely accepted that bromine catalytic reaction cycles are responsible for surface ozone destruction (Simpson et al., 2007 and references therein), the critical reaction being:

$Br + O_3 \rightarrow BrO + O_2$ (R1)

Catalytic destruction of ozone is achieved if the bromine radicals are re-generated without production of ozone. This can occur in a number of ways, such as:

a) via the BrO self-reaction:

$BrO + BrO \rightarrow 2Br + O_2$ (R2a)

$\rightarrow Br_2 + O_2$ (R2b)

$Br_2 + hv \rightarrow 2Br$ (R3)

b) via reaction with HO_2:

$BrO + HO_2 \rightarrow HOBr + O_2$ (R4)

$HOBr + hv \rightarrow OH + Br$ (R5)

c) via interhalogen reactions, such as:

$BrO + ClO \rightarrow Br + OClO$ (R6a)

$\rightarrow Br + ClOO$ (R6b)

$\rightarrow BrCl + O_2$ (R6c)

$BrCl + hv \rightarrow Br + Cl$ (R7)

There is still much debate over the precise source of atmospheric bromine that drives ODEs, but there is strong observational evidence to suggest a source associated with the sea ice zone (Gilman et al., 2010; Jacobi et al., 2010, Abbatt et al., 2012). Such a source would be consistent with laboratory studies, where heterogeneous reactions have been shown to generate Br_2 and BrCl, via uptake of HOBr onto frozen and dry NaCl/NaBr coated surfaces (Adams et al., 2002; Fickert et al., 1999), via the following multiphase reactions:

$$HOBr + H^+ + Br^- \rightarrow Br_2 + H_2O \quad \text{(R8)}$$

$$HOBr + H^+ + Cl^- \rightarrow BrCl + H_2O \quad \text{(R9)}$$

The term “bromine explosion” (BE; Platt and Janssen, 1995) came about due to the exponential growth of bromine in the BL. The schematic in Figure 2.1 shows the chemical pathways important for both NO_x and reactive bromine cycling at Summit in Greenland. This is unlikely to be very different from the pathways of importance expected at Halley, and is therefore regarded as a good representation of bromine activation in the snowpack in coastal Antarctica. The process which leads to this exponential growth is that one reactive bromine species is consumed by the system (HOBr in Eq. 8), but Br_2 is then produced which creates two Br atoms (Simpson et al., 2007).

Although our knowledge of ODEs and associated chemistry has increased greatly since their discovery, some of the key processes involved (i.e. activation of iodine and chlorine species, and mechanisms of all halogen release from saline surfaces) are not yet fully understood (Simpson et al., 2007; Abbatt et al., 2012), and high temporal resolution observations of inorganic bromine compounds against which to test current theory are sparse.

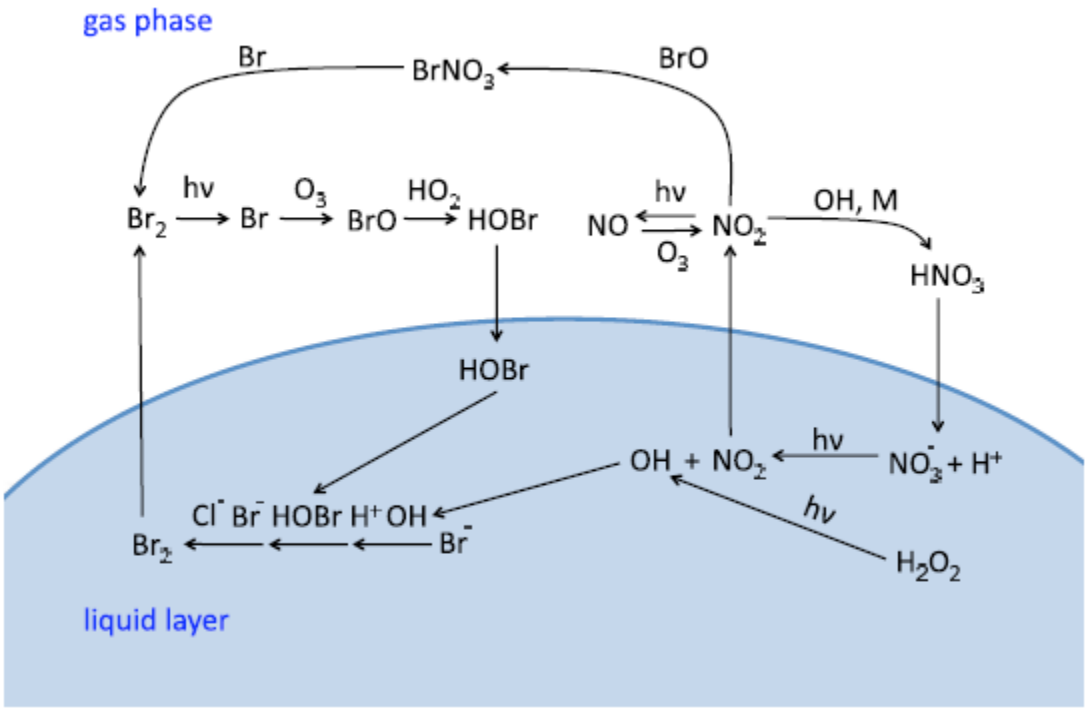

Fig. 2.1: *Schematic of the chemical pathways important for NOx and reactive bromine cycling at Summit, Greenland (taken from Thomas et al., 2011)*

The main processes suspected of supplying condensed phase (a liquid-like surface layer) to initiate the catalytic bromine reaction cycle are shown in Fig.2.2 (taken from Abbatt et al., 2012), and gives a good overview of the suspected halogen sources currently being discussed in the wider literature. As previously mentioned, there is strong observational evidence to suggest a source associated with the sea ice zone and that its surface is saline (Gilman et al., 2010; Jacobi et al., 2010, Abbatt et al., 2012), these are all covered in the literature to some extent. Sea salt deposited to the snowpack adds some salinity (McConnell et al., 1992), and sea ice surfaces/ sea salt aerosol (Frieß et al., 2004)(including acidified sea salt aerosol (Vogt et al., 1996)) are also thought to supply a liquid-like surface layer to the system. Concentrated brines on new sea ice and in frost flowers (Rankin et al., 2002; Kaleschke et al., 2004) links to snow on first year sea ice contaminated with sea salts via 'dunking' and brine 'wicking' (Simpson et al., 2007), and are likely a key halogen source. Of course blowing snow has been shown to significantly effect ODEs and therefore atmospheric halogen concentrations (Yang et al., 2008; Jones et al., 2009), especially if that snow source is snow on first year sea ice contaminated with sea salts as mentioned previously.

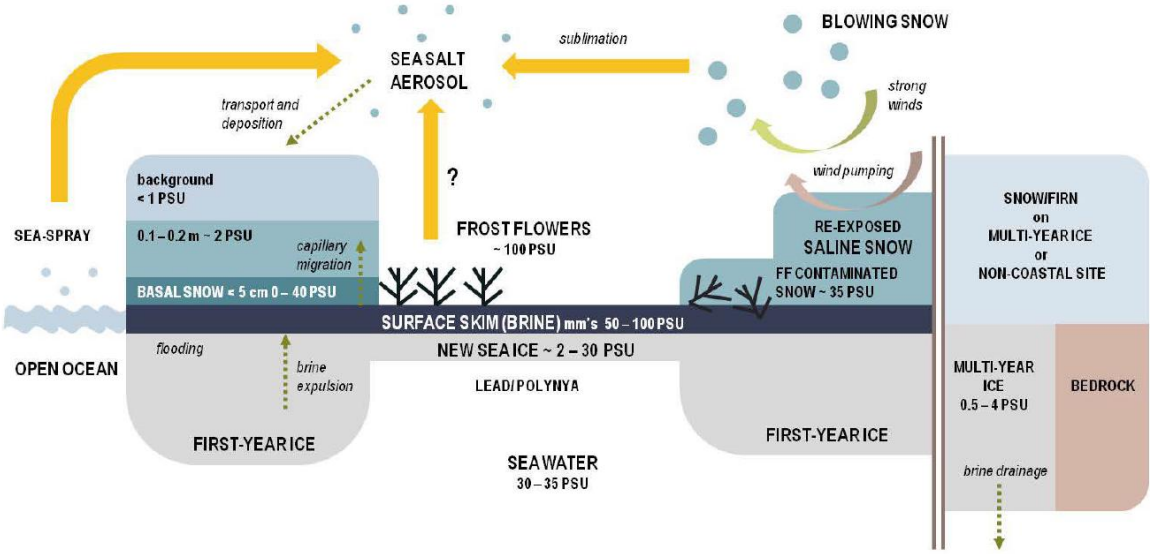

Fig. 2.2: *Sources of halides in the polar boundary layer. A range of salinity values is indicated: frost flowers (Rankin et al., 2002), brine, new ice (Ehn et al., 2007), multi-year ice (Timco and Weeks, 2010), basal snow (Toyota et al., 2011), snow<0.2m (Toyota et al., 2011), background snow (Massom et al., 2001), frost flower (FF) contaminated snow (Obbard et al., 2009) (Diagram and caption taken from Abbatt et al., 2012).*

Of key importance is the ice – atmosphere interface, which is given prominence in the previously mentioned diagram (Fig. 2.2), be it saline sea ice/ frost flowers or lofted sea salt/ blowing snow particles or even the snowpack itself. It is clear that the regions of open water and newly forming sea-ice are key in the BE and OD (Ozone Depletion) process.

Another potentially important halogen species, with regards to polar tropospheric ozone depletion events, is iodine. Atmospheric concentrations of IO near the Weddell Sea are found to be similar to those of BrO whereas bromide is over 1000 times more abundant than iodide in seawater (Saiz-Lopez et al., 2007) meaning that there must be a release mechanism for iodine species which differs from that for bromine species (see Chapter 2.X). The main source for reactive iodine in the marine BL (which is how we would describe the BL at Halley due to its proximity and influence from The Weddel Sea and Precious Bay) is organic compounds which photo degrade to IO and I_2 (Saiz-Lopez et al., 2007; Atkinson et al., 2012). In their study of the Weddel Sea, Atkinson et al. (2012) found that the high mixing ratios of I_2 they measured (up to 31 pptv) were comparable to mid-latitude measurements near macroalgae beds exposed at low tide (Saiz-Lopez and Plane, 2004; Huang et al., 2010a). The measurements of IO and BrO made at Halley by Saiz-Lopez et al. (2007) were obtained by use of a Long Path Doppler Optical Absorption Spectrometer technique (LP-DOAS) looking through the BL. This was the first positive

detection of IO in the polar BL by active DOAS. The peak mixing ratios observed for both these species was ~20 pptv. For BrO this is similar to that found in the Arctic during the spring-time, but this is an order magnitude greater than IO as measured in the Arctic (Saiz-Lopez et al., 2007). However, iodine species are not included in the chemical mechanism of this model study, and are not discussed in later chapters. The many uncertainties in the sources and atmospheric release mechanisms (including the difference between Arctic and Antarctic observations), along with the fact that there were no coincident IO or I_2 measurements made at Halley during the measurement period, were reason enough for us not to include these species in our model calculations.

2.2. Importance of snow and sea ice

A recent review paper by Abbatt et al. (2012) summarises the importance chemical interactions on (and in) environmental snow and ice has on atmospheric composition and halogen activation in particular. Here I will include a concise overview of the key processes (and reactions) of importance in the rest of this thesis. Measurements from field studies and lab work will be discussed and compared, and recent model work on halogen activation will also be included in this section. It is important to note here that saline surfaces have been the focus of recent research in this area, including both sea ice and the snowpack (Abbatt et al., 2012).

2.2.1. Snow: snow grains and other ice surfaces

Thomas et al. (2012) describe a liquid-like layer (LLL) found at ice surfaces to be a combination of the quasi-liquid layer (QLL) and brine layers (BrL), and also mention that these layers form for different reasons (Kuo et al., 2011). The QLL is a nanoscale disordered layer of water molecules found on the surface of pure (or very low impurity) ice (Döppenschmidt and Butt, 2000), whereas the BrL is formed on the surface of impurity-containing ice when sea water freezes (e.g. sea ice) and the impurities are excluded (Thomas et al., 2012; Kuo et al., 2011). Although the QLL and BrL are separate regions, a disordered layer found on pure ice at -30°C has been found to still be present at -80°C when exposed to gas phase HCl (McNeil et al., 2006). It has also been

suggested that the surface of sea ice and sea salt aerosol will still be partially liquid at temperatures down to -30°C (Koop et al., 2000). The LLL described here likely plays an important role in snowpack/ ice/ atmosphere chemistry in polar regions due to its presence at these cold temperatures, and is discussed in detail in the review paper by Abbatt et al. (2012).

The central reactions to the bromine explosion (R8 and R9) have been confirmed by laboratory studies, where Br_2 was produced when frozen NaCl/ NaBr solutions were exposed to gas phase HOBr (Kirschner et al., 1997; Adams et al., 2002; Huff and Abbatt 2002). From reactions (R8 and R9), the BE mechanism implies a need for H^+ (acidity). Interestingly it appears that acidity has little effect on the Br_2 yield in these experiments, and Adams et al. (2002) show that Br_2 and BrCl can be released form an ice surface without any additional acidity being present. These studies suggest that gas phase Br_2 will be formed from reaction on an icy substrate as long as enough surface bromide is present. In contrast, Fickert et al. (1999) conducted studies with aqueous solutions and found that bromine release in this instance required acidity. Huff and Abbatt (2000) also point out that chemical transfer from the atmosphere to the snowpack/ ice surface is likely the rate limiting factor, as the chemical reaction in/ on these mediums is rapid.

Nitrate in the snowpack photo-dissociates to form reactive nitrogen (Honrath et al, 2002; Beine et al., 2008), which then goes onto generate OH (see section 2.4):

$$NO_{3\,aq}^{-} + h\nu(+H^+) \rightarrow NO_{2aq} + OH_{aq} \qquad \text{(R10)}$$

Model results from Thomas et al. (2012) suggest that the presence of an initial oxidant (OH in this case) is almost as important as the presence of bromide, chloride and some acidity to halogen release. Laboratory studies have shown that exposure of gas phase OH to aqueous NaCl/ NaBr solutions formed Br_2 by way of heterogeneous reactions (Frinak and Abbatt, 2006; Sjostedt and Abbatt, 2008). The possible reaction mechanism (adapted from Abbatt et al., 2012) is suggested to be pH independent as there is no proton in the rate determining step, unlike other bulk-phase reactions:

$$OH{\cdot}Br^- + OH{\cdot}Br^- \rightarrow Br_2 + 2OH^- \qquad \text{(R11)}$$

It has also been shown that Br^- has an affinity for the air-aqueous interface, which may also increase the bromide surface enhancement compared with that of chloride (Jungwirth and Tobias, 2001, 2006; Gladich et al., 2011). One study has shown that surface reactions of gas phase ozone with frozen NaCl/NaBr solutions, with composition similar to sea water, dominate over the bulk reactions to form gas phase bromine (Oldridge and Abbatt, 2011). High rates of bromide replenishment from the bulk brine to the surface are also reported, highlighting the

importance of this bromide surface enhancement to the release of gas phase reactive halogen species.

Hydrogen halides such as HBr adsorb rapidly to ice (Abbatt, 2003; Huthwelker et al., 2006), and it has been shown that under lab conditions the ice surface can melt and form a thermodynamically stable solution in which strong acids can fully dissociate (Hanson and Ravishankara, 1992). Reactions (R8 and R9) above suggest that the presence of some acidity is required to sustain the bromine concentrations, and include recycling through the aqueous phase (Sander et al., 2006):

$BrCl \rightarrow BrCl_{aq}$ (R12)

$BrCl_{aq} + Br^- \rightarrow Br_2Cl^-$ (R13)

$Br_2Cl^- \rightarrow Cl^- + Br_{2aq}$ (R14)

$Br_{2aq} \rightarrow Br_2$ (R15)

At first look the source of the acidity required by (R8) and (R9) is unclear, due to the particles involved being derived from alkaline sea water, and created from new sea ice formation. Sander et al. (2006) propose that calcium carbonate precipitation from freezing sea water (newly forming sea ice) may be the trigger for the release of reactive bromine to the atmosphere, as it removes some of this alkalinity and we end up with a brine alkalinity well below that for sea water. Dieckmann et al. (2008, 2010) have identified the dominant calcium carbonate polymorph in the Arctic and Antarctic as ikaite ($CaCO_3.6H_2O$), as it appears to be the kinetically favoured form of calcium carbonate. Morin et al. (2008) predict thermodynamically that ikaite will precipitate at ~268K, which is just below the freezing temperature of sea water (~271K). Bulk acidity of several of these environmental ices (frost flowers, sea ice and non-frost flower snow) have been measured (Kalnajs and Avallone, 2006), but these bulk pH measurements are unlikely to represent the pH of molecules at the surface of these ices prior to melting (Abbatt et al., 2012). All of this (including R12-15) implies that the production of gas phase Br_2 is thermodynamically likely to occur.

The freezing of sea water leads to the exclusion of solutes from the ice matrix. As the temperature decreases ice starts to form, and pressure changes cause this brine to be expelled either upward to the surface or downward to the sea. Chemical fractionation occurs within this brine layer as it cools, for example hydrohalite ($NaCl.2H_2O$) precipitates below 252K and leads to a bromine enrichment (relative to chlorine) in the brine (Koop et al., 2000). When looking at the

rapidly changing climate in the Arctic, studying and understanding the impact temperature can have on halogen chemistry and activation has become important. Pöhler et al. (2010) link the increase they see in daily maximum measured BrO in the Amundsen Gulf with decreasing temperature (starting at 258K and dropping), to the precipitation of hydrohalite as described above. This is consistent with measurements by Tarasick and Bottenheim (2002) made in the Arctic, where they found that temperatures below 253K were the only time severe ODEs were observed. Something that is important to both of these previous studies, and the measurements discussed in this thesis, is that the local ambient temperature coincident at the time the ODE (and enhanced atmospheric halogen) are measured may not correspond to the temperature that was present during the initiation of this BE/ ODE. It may be the case that the chemical depletion occurred upwind of the measurement site, and at a different ambient temperature. However, it is actually the temperature of the chemical system at the snow-air interface that is relevant, not even the ambient temperature of the upwind site.

2.3. Broader influences of meteorology

Although small-scale surface interactions on ice and snow are key for halogen activation and ODEs, meteorology in these coastal polar regions also has an effect on halogen release to the atmosphere and influences on the chemistry.

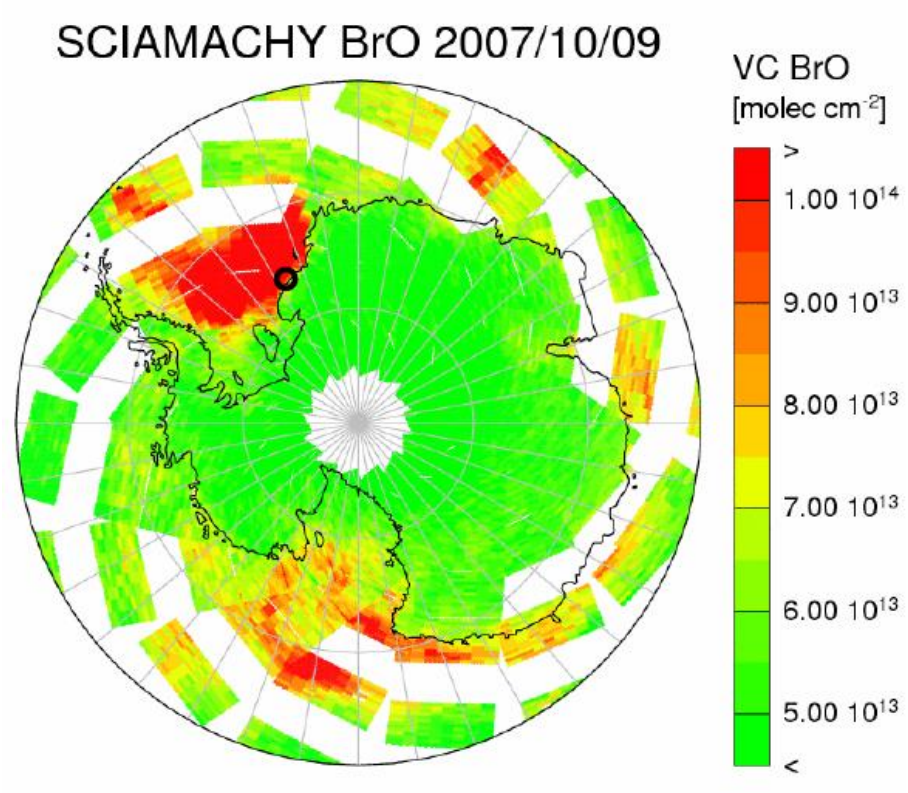

Figure 2.3. *Daily-averaged BrO total-column density on 9 October 2007. The position of Halley is shown by the open circle. (Adapted from Jones et al., 2009).*

The highly saline surface of snow on sea ice is thought to be a region of halogen activation, as supported by recent observations (Foster et al., 2001; Spicer et al., 2002; Pratt et al., 2013). It has also been shown that there is a link between exposure to sea ice and changes in ozone mixing ratios in the Arctic (Gilman et al., 2010; Jacobi et al., 2010). Saline blowing snow (lofted snow on sea ice during high wind events) has been suggested as an alternative to the saline sea ice surface as a surface for halogen activation through both modelling studies (Yang et al., 2008), and measurements linked to satellite observations (Jones et al., 2009). Figure 2.3 shows the spatial extent of enhanced vertical total-column BrO over the Weddel Sea in Antarctica. This enhancement coincides with surface ozone depletion measured at Halley, and during this time of year there is extensive sea ice cover (Figure 2.4). Measurements of a surface ODE made at Halley were observed to coincide with an area of enhanced BrO seen in satellite measurements, which occurred after a blowing snow event. Levels of bromide in the surface layer of the snow after the event were found to be enriched. The source of the blowing saline snow is thought to be lofted snow which has fallen on sea ice, and been salinated through flooding/ upward migration (discussed earlier in section 2.1).

We can see from Fig 2.4 that there is a large seasonality in sea ice extent both in the Arctic and Antarctic, and this change in sea ice extent is one of the reasons that ODEs and enhanced halogen events are only observed in the spring (large areas of first year sea ice which break apart and lead to the creation of regions available for new sea ice formation). The combination of higher salinity of first year/ newly forming sea ice during spring in polar regions, low temperatures, the higher likelihood of more stable BL structure and the presence of a diurnal variation in sunlight may all be factors in the seasonality in ODEs (Wagner et al., 2001). The faster mixing due to a less stable boundary layer at other times of the year, and the presence of continuous (or complete lack of) sunlight make it difficult for the chemical species to build up near the surface. ODEs measured at Halley are not always confined to the surface. Jones et al. (2010) analysed ozone sonde data from 1987 and found that ozone depleted air at height (1-3km altitude) was always associated with blowing snow, high wind speeds and large atmospheric depressions. Blowing snow has also been linked through column BrO satellite observations to halogen activation and ozone loss, during spring in the Arctic (Fig 2.4 shows large areas of first year sea ice; potential halogen activation region) (Begoin et al., 2010).

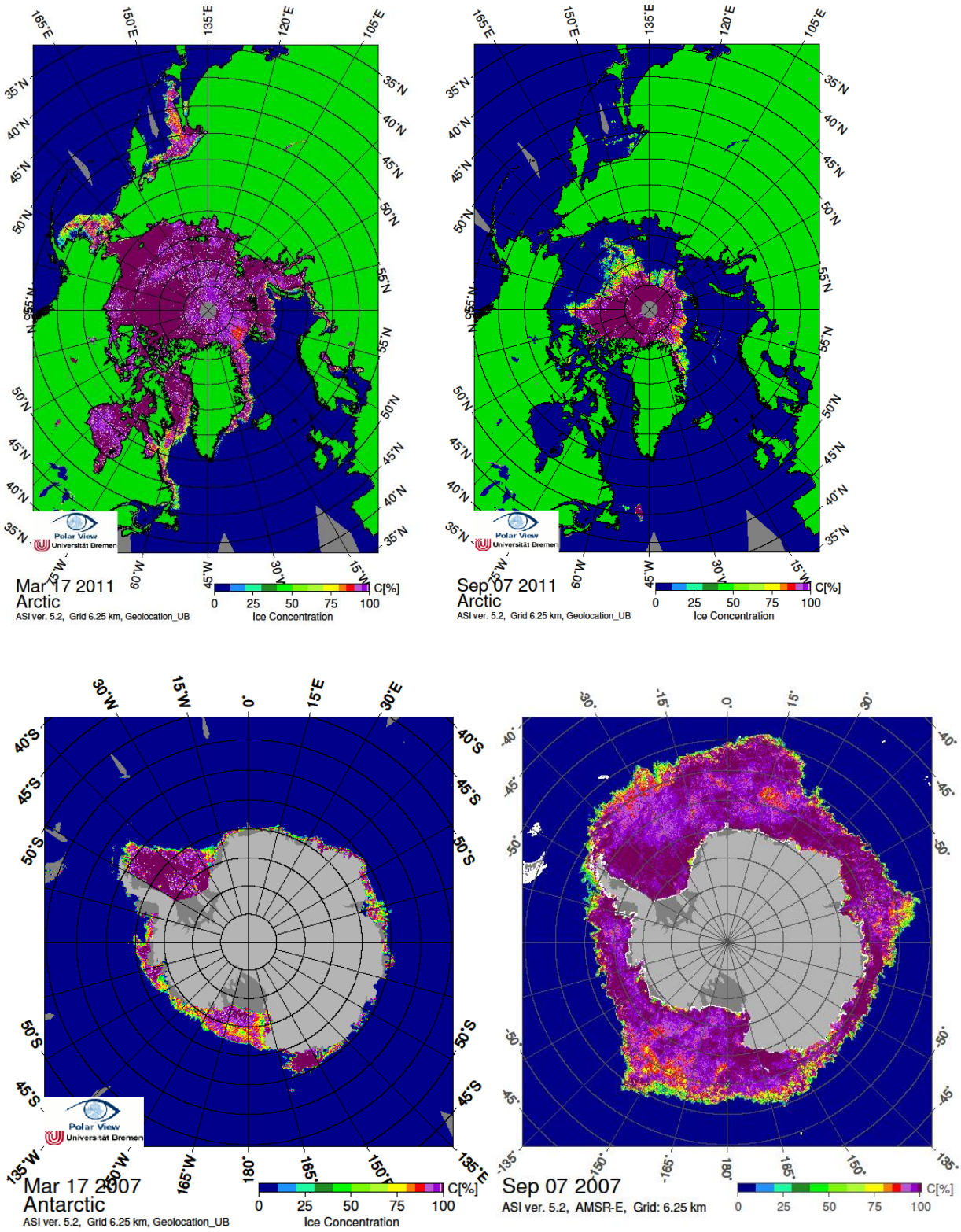

Figure. 2.4: *Top panels show Arctic sea ice maximum and minimum extent (2011), and the two lower panels show Antarctic sea ice maximum and minimum extent (2007 – to correspond with the year of the measurement campaign at Halley).*

Measurements of surface ozone have been made at the Clean Air Sector Laboratory at Halley station in coastal Antarctica (CASLab), as well as coincident meteorological measurements (Jones et al., 2006). They found that on more than one occasion rapid ozone depletion (at one point a loss of 16 ppbv in one minute) was directly correlated to a change in wind direction at Halley, with high winds and associated storm systems. Of note is that two events arrived at Halley at night, meaning the ozone depletion had occurred at some distance from Halley during daylight and had been transported to Halley where it was measured. There are also ODEs shown which were more gradual, and are linked more to stable Boundary Layer (BL) structure, low wind speeds and previous contact with an area of newly forming sea ice. This can lead to a build up of any surface emissions and hence an amplification of any chemical reactions which would occur.

MAXDOAS (Multi Axis Differential Optical Absorption Spectroscopy) measurements from Barrow, Alaska (Frieß et al., 2011) show that bromine activation on aerosol may be important, adding weight to the argument of blowing snow as a possible halogen source related to the sea ice zone.

In a recent study, Yang et al. (2010) consider the production of sea salt aerosol from snow lying on sea ice during blowing snow events. They found that emissions of bromine associated with blowing snow contribute significantly to BrO at mid-latitudes, and Figure 2.5 shows the percentage contribution of blowing snow source to their simulated tropospheric column BrO.

Continental snowpack can also succumb to by wind lofted sea salt aerosol/ blowing snow, and is therefore a potential source of reactive halogen. That polar tropospheric ODEs occur at/ near the surface is in itself indirect evidence of the snowpack as a source of reactive halogen to the atmosphere. A model study by Piot and von Glasow (2008) highlights the importance of halogen recycling on the snowpack, and shows that an ODE could only be reproduced by re-release of bromide deposited to the snowpack in the form of Br_2 and BrCl (see chapters 6 and 7).

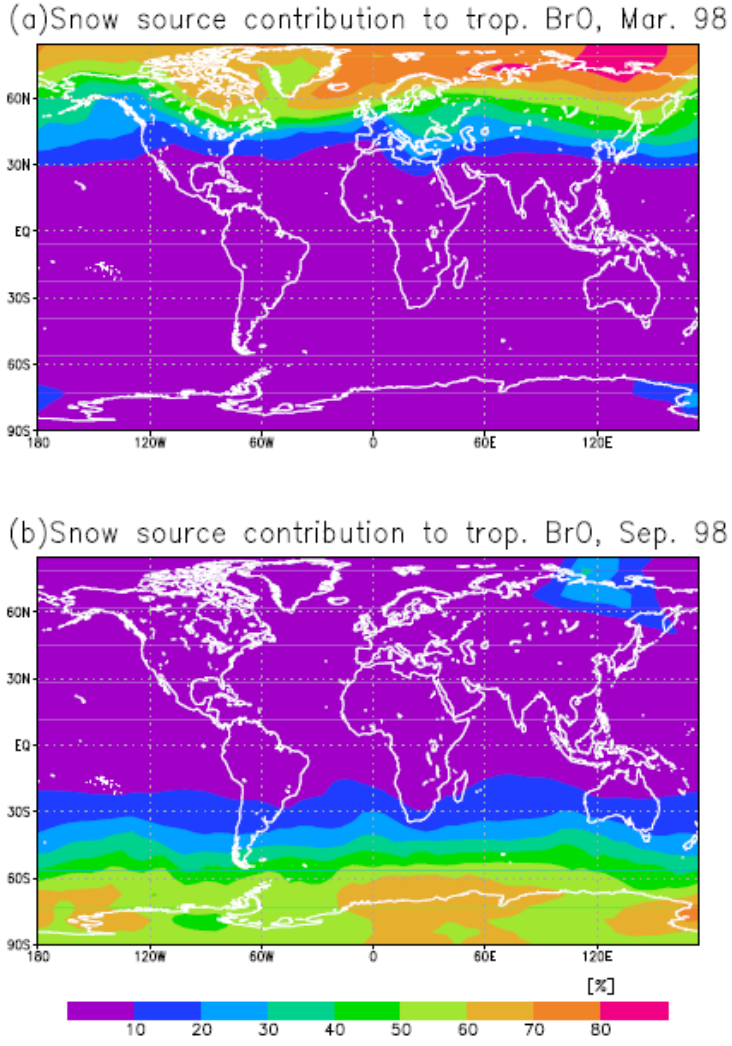

Figure 2.5: *Percentage contribution of blowing snow source to the simulated tropospheric column BrO in* ***(a)*** *March and* ***(b)*** *September of 1998. Values are calculated according to the formula: (BASE run – OCEAN run)/(BASE run)×100%).(taken from Yang et al., 2010)*

2.4. Snowpack photochemistry

Not only are reactions on environmental ice and snow surfaces important, but the interstitial air between the snow grains in the snowpack also has an effect on atmospheric composition above the snowpack (Abbat et al., 2012; Thomas et al., 2011; Helmig et al., 2007; Peterson and Honrath, 2001; Albert et al., 2002). Pratt et al. (2013) show that molecular bromine was only

observed in saline surface snow samples on exposure to sunlight through halogen release to, and reaction in, the interstitial air of the snow samples.

Peterson and Honrath (2001) report the first observations of ozone in the interstitial air of a sunlit snowpack, with measurements made at Summit, Greenland, in July 1999. Ozone was sampled at a depth of 30cm in the snowpack, and alternately measured above the snowpack at a height of no more than 1m. They found that while ozone mixing ratios in the air were relatively constant, there was a diurnal cycle present in the snowpack measurements with amplitude of greater than ~10 ppbv. They conducted an experiment where a $6m^2$ area of the snow surface was shaded, then illuminated. The results indicated that there was a rapid response in the ozone mixing ratios at 30cm depth below the shaded area with a rapid drop of 1 ppbv directly after shading, followed by a steady increase towards ambient background before being illuminated once again. This return to ambient background was attributed to relatively rapid ventilation of the snowpack with ambient air. Once the area was again illuminated, interstitial ozone levels fell rapidly. They go on to suggest that photochemical destruction of ozone in sunlit snowpacks is widespread, and that the presence of ice crystals is important for this process and can lead to ozone depletion in the BL above the snowpack. The importance of ice crystals to this process then brings halogens back into the picture, and as has already been mentioned the importance of snow and ice surfaces in the halogen activation process (see section 2.2)

Soon after Peterson and Honrath (2001) reported ozone depletion with the snowpack at Summit, Albert et al. (2002) showed through both measurements and model studies that ozone can be rapidly depleted in the snowpack of Alert, Nunavut, Canada. They show that ozone is depleted in the snowpack during both daylight and at night, even though air above the surface of the snowpack will be drawn down into the snowpack due to the high flow rate used (2 slpm) and will influence the measurements.

Helmig et al. (2006) conducted similar measurements of ozone in the snowpack, where they sampled at several different depths sequentially for ten minutes at a time. In order to overcome diluting the sampled air with air drawn into the snow from above or below, they sampled at a lower flow rate of 0.6-1.4 slpm (standard litres per minute). From several experiments conducted, including comparison of continuous measurements and intermittent measurements of ozone in the snowpack, they were able to conclude that air flow within the snowpack was natural and that increased air flow from their sample method was not the dominant source of ventilation. Observed ozone gradients in the snowpack are therefore assumed to be indicative of actual chemical gradients. It was found that there was high similarity in ozone levels within the

snowpack and the air above it, even at -90cm ozone was within 1-5ppbv of ambient air ozone. They also found that ozone in the snowpack follows trends in ambient ozone.

Measurements of gas phase species in the snowpack, and in the atmosphere just above it, give an indication of the effectiveness of snow-atmosphere exchange. This is important as halogen species are likely released from the LLL of the snow grains into the snowpack interstitial air, where they will then be influenced by other snow sourced chemical species before being released to the atmosphere above the snowpack. H_2O_2, HONO and HCHO are all emitted from the snowpack, and are known to affect the chemistry of the atmosphere above the snowpack (Thomas et al., 2012). HONO is formed via nitrate photolysis and is an important OH radical precursor, as is H_2O_2 which is formed by the self reaction of HO_2. It is also known that HCHO can play a role in halogen recycling, through formation of HOBr by reaction of HCHO with Br (as shown by Michalowski et al., 2000). All of these species are released from the snowpack to the atmosphere above, and they all affect halogen species mixing ratios either directly (HCHO) or indirectly through increasing OH radical concentrations (HONO and H_2O_2).

3. Methods Part I: Field Observations

Synopsis

This chapter includes descriptions of the measurement site, and the suite of instrumentation used to observe the atmosphere at Halley. Some features of the Halley site will be highlighted, as well as key features of the supporting instruments used, and a short overview of the analysis tool used for the raw data workup will be given.

3.1. Halley research station

Measurements were made at Halley V, an Antarctic coastal research station operated by the British Antarctic Survey (BAS) and situated on the Brunt Ice Shelf, 35 metres above sea level. The surrounding area is snow covered, with the nearest rock outcrops ~200km away (Konig-Langlo et al. 1998). Halley is effectively located on an ellipse of the coastline, a promontory of floating continental ice that extends out into the Weddell Sea, placing it roughly 15 km from the coast to the north, west, and south west (Figure 3.1). During the winter and early spring, the Weddell Sea ice extends up to the edge of the continental ice shelf (Figure 3.2), but of note to the south and west is a large area of polynas and open water with associated newly-forming sea ice kept open by the prevailing easterly winds (referred to as Precious Bay and shown in Figures 3.1 and 3.2). Although the prevailing wind direction throughout the year is easterly, traversing hundreds of kilometres of unbroken snow cover, strong directional changes to westerlies/south-westerlies often occur, especially in the spring and summer months (Figure 3.3). This results in air masses with very different histories arriving at Halley, including air which has traversed Precious Bay. The open water of Precious Bay leads to the formation of new sea ice and gives a great opportunity to study the impact it has on the atmosphere, as observed at Halley.

Figure 3.1: *Map showing the location of Halley on the Brunt Ice Shelf in coastal Antarctica, and also in relation to Precious Bay.*

The instrumentation used for this field campaign was housed in the CASLab (Clean Air Sector Laboratory) which is situated about 1 km south of the main base in an area that is exposed to minimal disturbance by vehicles or base pollution (Jones et al., 2008). The instruments were run, and the measurements made, by Neil Brough of the British Antarctic Survey.

The measurement campaign ran between January 2007 and February 2008. The main instrument of this campaign was a Chemical Ionisation Mass Spectrometer (CIMS), which was capable of measuring halogens as well as other species. During the year, the CIMS operated alternately in two different modes; i) a high pressure mode which measured, separately, OH and RO_2 and ii) a low pressure mode measuring a variety of trace gases including HNO_4, HCl, HNO_3, SO_2. In early spring, BrO, BrCl and Br_2 were added to the suite of low pressure measurements and included over the subsequent low-pressure mode measurement periods. The first direct sunlight at Halley at the end of the polar winter occurs on 13 August, thus the observations reported here almost all fall within the sunlit spring and summer time. The following section is an overview of both the instrument used for this campaign, and the CIMS technique in general.

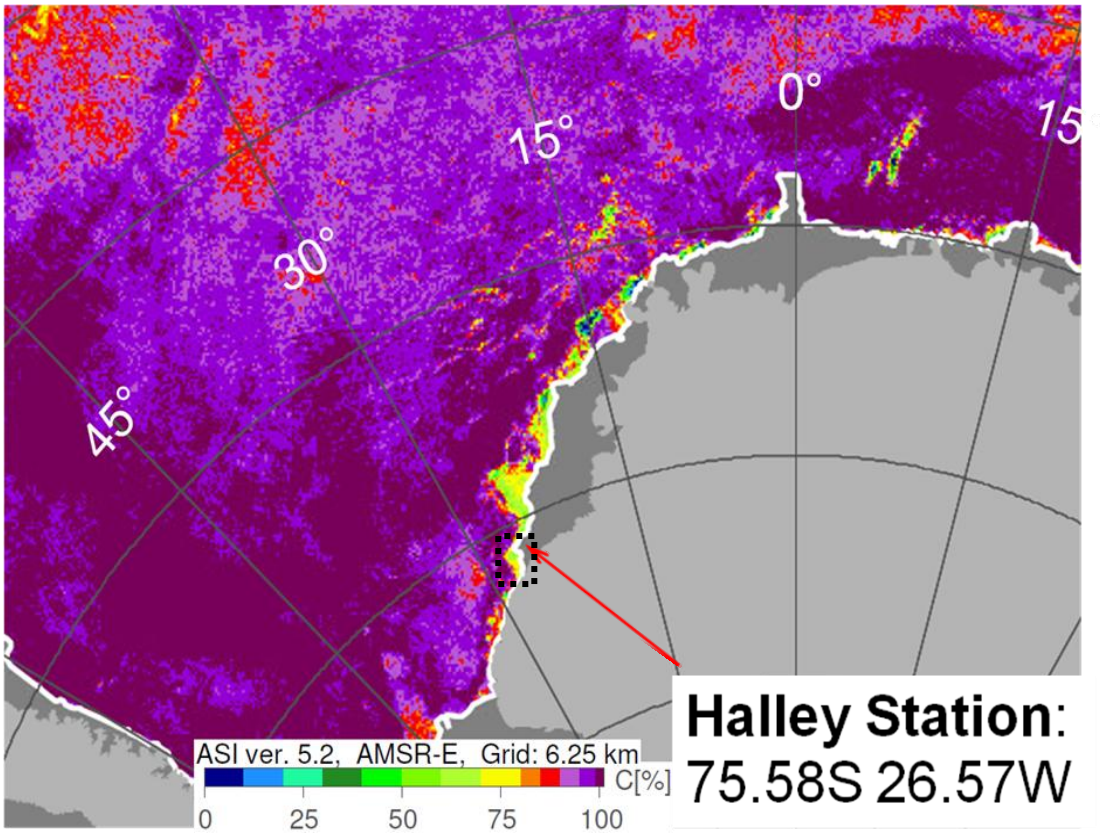

***Figure 3.2**: This is a representative image of % sea ice cover in Antarctica for August to September 2007. The red arrow shows the location of Halley station and the dotted black box shows the location of Precious Bay.*

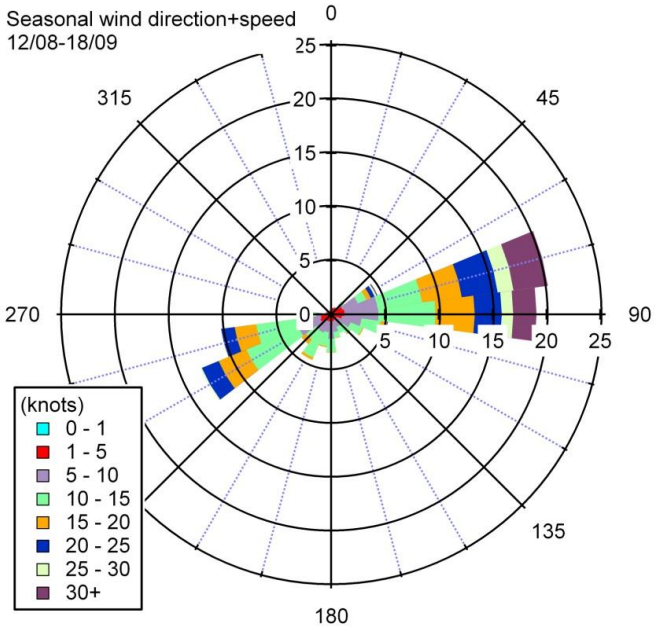

***Figure 3.3**: Wind rose showing seasonal wind direction and speed at Halley for the spring period (12/08/07 – 18/09/07)*

3.2. CIMS instrument description

The CIMS technique has been used to detect many atmospheric trace gases (Huey et al., 1995; Huey et al., 1998; Berresheim et al., 2000; Leibrock and Huey, 2000; Huey et al., 2004; Sjostedt and Abbatt, 2008), but its use as a high mass and temporal-resolution halogen detector is of most importance to this present study. While the CIMS technique is well documented (e.g. Huey et al, 2004; Slusher et al., 2004; Liao et al., 2011b), described here are features that were specific to the configuration at Halley.

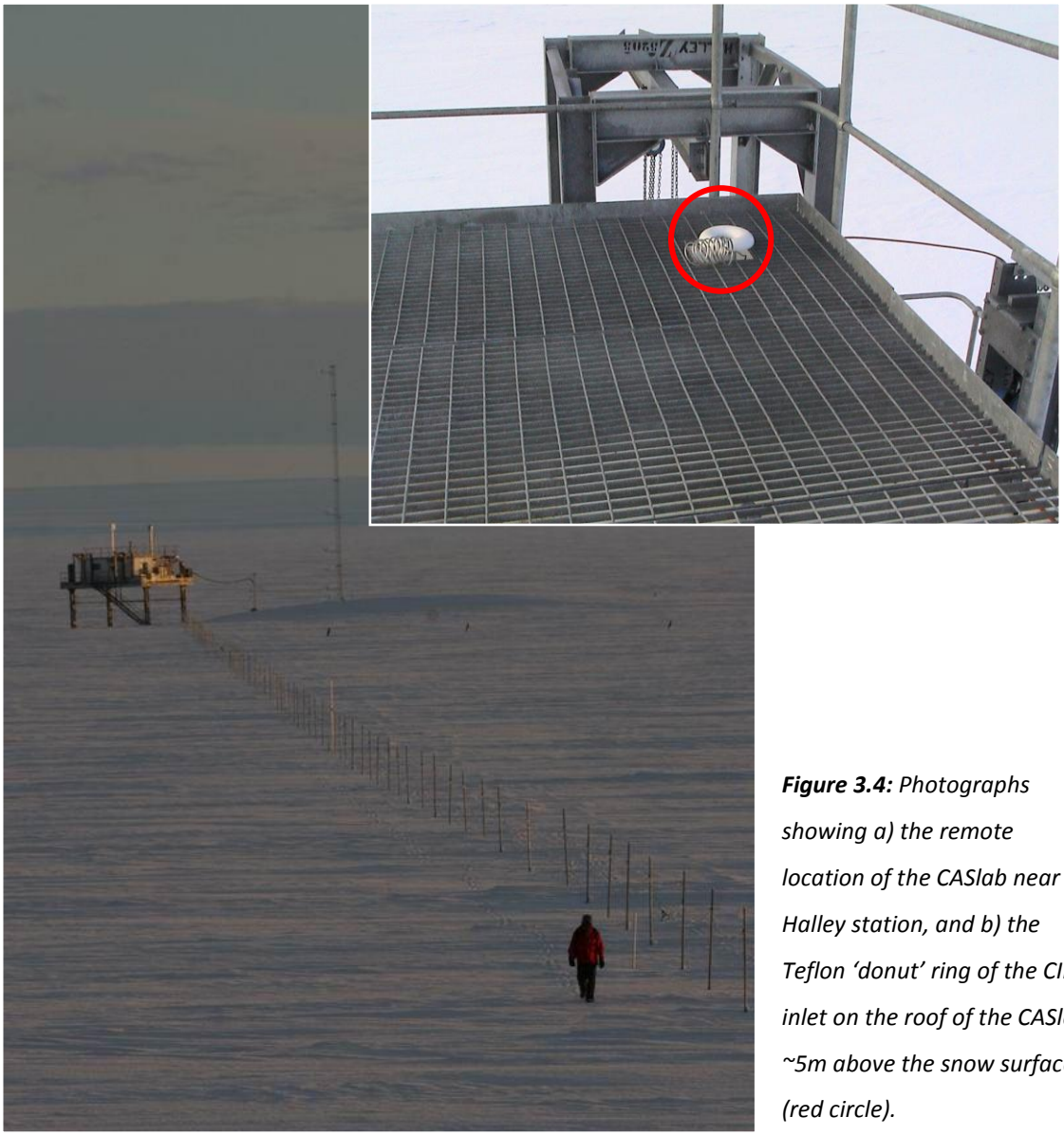

Figure 3.4: *Photographs showing a) the remote location of the CASlab near Halley station, and b) the Teflon 'donut' ring of the CIMS inlet on the roof of the CASlab ~5m above the snow surface (red circle).*

Ambient air was continually sampled at a high flow rate (~2400 slpm) by means of a regenerative blower (Ametek BCDC) into a 40 cm long aluminium pipe of 8 cm inner diameter (i.d.) that protruded 20 cm above the laboratory roof which is roughly 5m above the snowpack. A smoothed Teflon doughnut-shaped cap was secured to the pipe and positioned in the NE corner of the laboratory which allowed the least perturbed flow thereby minimising turbulence as well as shading.

To further reduce problems associated with surface adsorption, air was sampled from the centre of the aluminium pipe at a flowrate ~8 slpm which reduced both the residence and possible wall interaction time ($t < 0.6$ sec). The sampled air was delivered to the CIMS in a heated teflon perfluoroalkoxyalkane (PFA) inlet (i.d.=0.65 cm, length=25 cm) controlled at 40 ± 2°C by a series of thin Kapton (polyimide) heaters. The sampled air then entered the N_2 buffer housing which administered a continual and controlled flow of dry and pure N_2 gas (99.99%) provided by a membrane generator system (Parker Balston N_2-04) at a pressure of 40 psi and a flow rate of 2 slpm by a mass flow controller (MKS 1559A). A 0.015" pinhole on a stainless steel cone inside the buffer housing allowed the air sample to be drawn further into the CIMS at a constant volumetric flow rate and to prevent water clusters forming. This flow was routinely calibrated before and after each measurement period by a bubble flowmeter measuring the pressure as a function of flow rate on the low pressure side of the pinhole and was observed to be 5 +/- 0.2 slpm.

Within the CIMS ionisation region, a mixture of nitrogen doped with a few parts per million by volume (ppmv) of SF_6 was added to the flow tube after passing through a ^{210}Po ion source. This was achieved by way of a stainless steel flow tube reactor coupled at 90° to the sample flow with the ionization source. A controlled amount of 0.2% SF_6 in nitrogen (Air Products, speciality gases) was administered into the ionization. This synthesised the reagent ion SF_6^- in the ion source via associative electron attachment (Huey et al., 2004). The length of the flow tube gives a reaction time of about 50 ms. The usefulness of SF_6^- as a reagent ion can be limited due to its slow second-order reaction with water (Huey et al., 1995; Arnold and Viggiano, 2001), but Slusher et al. (2001) have found that it is viable at dew points below ~-20°C, such as are frequently found in polar regions.

The quadrupole mass filter (Extrel), by exerting an electronic field between the 4 stainless steel rods, allows selective filtering of the ions depending on the pre-selected masses. The selected masses are detected, and the current converted into TTL pulses which are then processed by the computer. The signal is displayed in hz (counts s^{-1}) against the atomic mass number (amu). N_2

collisions with helium dampen the kinetic energy of the ions and serve to quickly focus trajectories towards the ion trap.

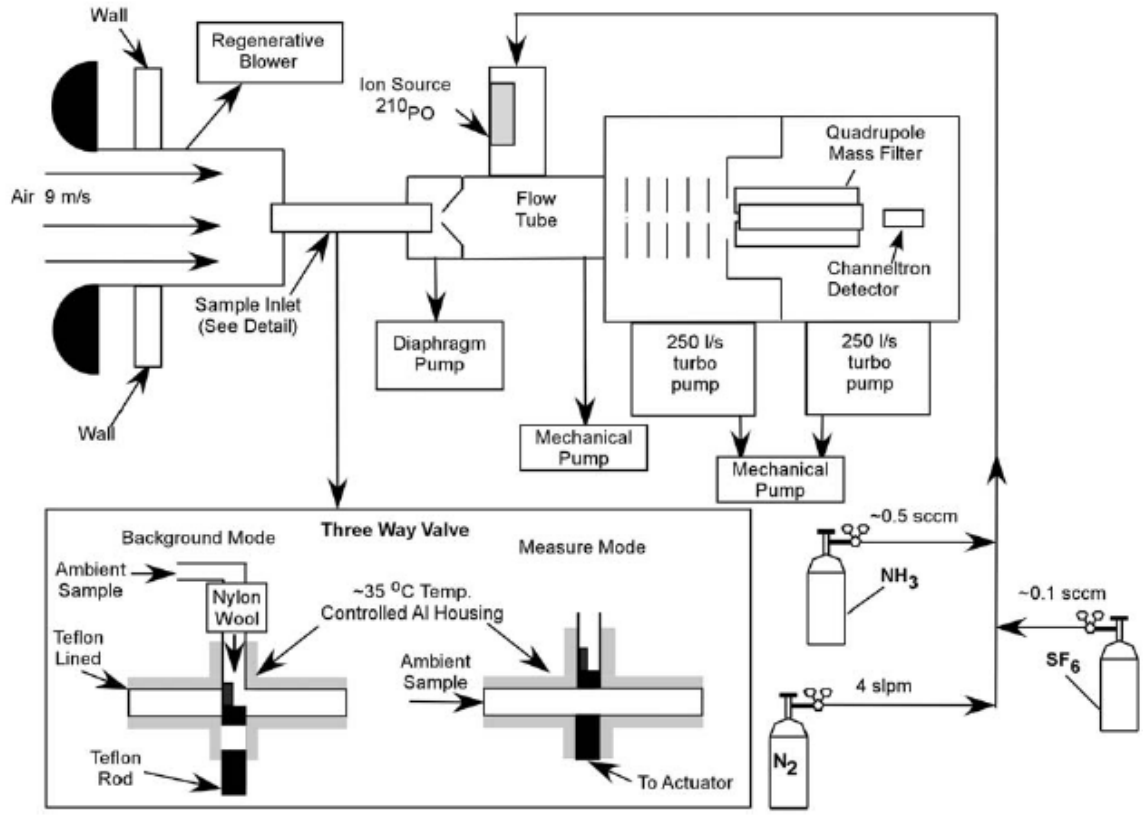

Figure 3.5: *Diagram of the CIMS instrument. The automated three way sampling valve is shown in the inset (diagram taken from Huey et al., 2004).*

From there, sampled air mixed with ions from the ion source such that reactions can occur for the length of the flow tube. A small amount of air from the flow tube is sampled and then electrostatically accelerated by ion optics into the quadrupole mass filter and an ion detector which can detect multiple ion masses on each pass (Huey et al, 2004). Rate coefficients for the reactions of the molecules with SF_6^- have been measured relative to SO_2, as the rate coefficient for reaction (R3.1) has been measured over a wide range of pressures and buffer gases (Slusher et al., 2001). SO_2 is also used as the calibration gas for the instrument.

$$SF_6^- + SO_2 \rightarrow \text{products} \qquad \text{(R3.1)}$$

An automated 3-way sampling valve (Fig 3.5) enabled switching between two flow paths, measurement mode and zero mode, without disrupting the required constant flow (maintained by the diaphragm pump). Background or zero measurements were obtained every 10 minutes by drawing air through a 20 cm x 5 cm i.d. stainless steel filter tube for a 3 minute period. The filter tube contained activated coarse charcoal and nylon glass wool that had been previously soaked and dried in a concentrated $NaHCO_3$ solution. A similar scrubbing method has been successfully employed (Slusher et al., 2004; Liao et al., 2011a), and showed high efficiency for removing HNO_4 and other molecules from the sampled air.

To determine the sensitivity of the CIMS instrument in the field, a mass flow controller (MKS 1479A) provided a continuous 8 sccm (standard cubic centimeters per minute) flow of 0.2% (± 5σ) of a certified standard of our calibration gas (SO_2 in nitrogen, Air Products, speciality gases) to the insulated inlet system every two hours for a 1 minute period. The SO_2 was connected to a 1/8" T-piece Galtek Teflon fitting and was continually removed by vacuum (when not in calibration mode) by a rocking piston pump which, when activated, closed the vacuum valve and allowed SO_2 to flow uninterrupted to the inlet and mix with the sampled air.

At the time of this measurement campaign there was no known direct method of constant Br_2 calibration in the field. As SO_2 was used as our primary calibration gas for the CIMS instrument in the field, it was possible to use the sensitivity ratio of SO_2 to Br_2 (determined in the lab after the fieldwork as a function of dew point temperature) as a proxy to track the sensitivity of Br_2. The ratio of the rate constants for reaction:

$$SO_2 + SF_6^- \rightarrow F_2SO_2^- + SF_4 \quad \text{(R3.2)}$$

and

$$Br_2 + SF^-_6 \rightarrow Br^-_2 + SF_6 \quad \text{(R3.3)}$$

could then be used to calibrate the Br_2 measurements after the campaign. BrCl was calibrated in a similar manner.

BrO calibration was achieved using a similar method to that described in section 2.2 in Liao et al. (2011a). The ratio of the rate constant for the following reaction was used:

$$Br_2 + SF^-_6 \rightarrow Br^-_2 + SF_6 \quad \text{(R3.3)}$$

to reaction

$$BrO + SF^-_6 \rightarrow BrO^- + SF_6 \quad \text{(R3.4)}$$

(determined to be 1.0±25% in the laboratory by Liao et al., 2011a), along with the dew point calculation, to determine the BrO calibration.

The measurements were all corrected for humidity (by taking into account during the calculations of the slow second-order reaction of SF_6^- with H_2O) and converted to mixing ratios.

Limits of detection (LOD) were estimated using 1σ counting precision of the 10 second zero background signal. This approach was assumed to represent the detection limit (Ridley et al., 1994) as there was no suitable invariant ambient data. The standard deviation of the zero data was transformed to pptv using the averaged sensitivity of the instrument to SO_2.

The estimated accuracies were obtained from the uncertainties in the flow meter calibrations for the sample and calibration gas obtained with a bubble flow meter before and after each measurement period and was found to be ~4%. This also includes the uncertainty in the calibration gas standard which the manufacturer provided (5σ). The precision of the instrument to SO_2 was obtained from the scatter (1σ) of the SO_2 sensitivity and found to be <2% (at a dew point of -24°C).

3.3. Supporting observations/ analysis methods

3.3.1. Ozone instrument

Surface ozone was measured at the CASLab, using a Thermo Electron Model 49C. A low pressure mercury vapour lamp emits light at 254nm, and the instrument observes ozone by a UV (Ultra-Violet) absorption technique where ozone molecules absorb UV light at 254nm. The inlet splits the sample into two gas streams, one of which becomes a reference gas and the other the sample gas. The UV light intensities of each cell are measured by detectors, and the Model 49C calculates the ozone concentration for each cell and outputs the average concentration. The instrument has a detection limit of 1 ppbv, and a precision of 1 ppbv. Data were recorded as 1 minute averages of 10 s observations.

3.3.2. Meteorological observations

Measurements of wind speed and wind direction were carried out at the main station, some 1 km from the CASLab. The anemometers and vanes were located at a height roughly 10 meters above the snow surface, and have an accuracy of about 0.5 ms^{-1} for wind speed and 5^{o} for wind direction (König-Langlo et al., 1998). Data are also output every 1 minute.

A sodar instrument was used to map the boundary layer at Halley (Anderson and Neff, 2008). Sodar stands for "SOnic Detection And Ranging" and is a radar working in acoustic frequencies. The Halley Monostatic sodar recorded a time series of turbulence profiles for altitudes ranging from 26m to 1000m. The sodar transmits a pulse of audible frequency sound, and detects the 180°-backscattered signal. Sound can be scattered by eddies in turbulent zones, and the strength of the return signal can be used to determine the boundary layer depth.

3.3.3. Sea ice maps

Information on sea ice concentration was obtained from the satellite-borne AMSR-E instrument (Advanced Microwave Scanning Radiometer-EOS) which provided information at a resolution of 6.25 by 6.25 km until it stopped operations on October 4th 2011. The AMSR-E measured at six different frequencies between 6.9 to 89 GHz at both horizontal and vertical polarization, but only the 89-GHz channels are used to determine the sea ice concentration. These sea ice concentration maps were produced daily by the University of Bremen as part of the GMES project Polar View and of the Arctic Regional Ocean Observing System (Arctic ROOS). The method has been validated in several studies, the most recent being Spreen et al. (2008).

3.3.4. Air mass histories

Back trajectory analyses using the Hybrid Single-Particle Lagrangian Integrated Trajectory (HYSPLIT) model were used to track air mass origins for various cases throughout the

measurement period. HYSPLIT is available via the NASA ARL READY website (www.ready.noaa.gov/ready/open/hysplit4.html) (Rolph, 2012; Draxler and Rolph, 2012). Back trajectories were driven by meteorological fields from the NCEP Global Data Assimilation System (GDAS) model output, and calculated using model vertical velocity at a resolution of 1^{o} by 1^{o}.

The associated errors can be separated into numerical and physical components, and the total error can be estimated to be ~15-30% of the travel distance (www.ready.noaa.gov/ready/open/hysplit4.html). The resolution error can be estimated by starting several trajectories about the initial point (offset in the horizontal and vertical). The divergence of these trajectories will give an estimate of the uncertainty due to divergence in the flow field, and was carried out for several of the longer trajectories (i.e. Chapter 7).

3.3.5. IGOR as a tool: Data work up

IGOR is a powerful scientific graphing, data analysis, image processing and programming software tool for scientists and engineers (http://www.wavemetrics.com/). This software was used as the main direct analysis and work up tool for the measurements taken at Halley.

The CIMS, meteorology and other supporting observation measurements made at Halley during this field campaign were worked up using IGOR. The raw data were processed using macros and other scripts developed for this purpose and, along with other macros and specific scripts which were coded or altered by myself and Neil Brough (colleague) in order to take into account instrument calibrations and missing data points. Examples of scripts that were developed include filtering of data to look at the effects of specific wind directions/ source regions, and averaging of 1 minute data down to 10 minute data.

4. Methods Part II: MISTRA model description

Synopsis

This Chapter describes the MISTRA model in 0-D, 1-D, and 'SNOW' versions. This includes an overview of the model structure (physical grid and chemistry), as well as changes implemented (initial conditions set etc.) to make it representative of Antarctic (and Halley specific) conditions. Results Part I makes use of both MISTRA 0D and 1D, Part II and Part III make use of MISTRA 0D only, while the results chapter Part IV makes use of the new MISTRA-SNOW version. Using numerical models allowed me to be able to probe the cycle of ODEs in their entirety. 0-D box models allowed me to focus on the chemical mechanisms, and 1-D models give an in-depth look at the evolution of the chemistry at play (both in space and time).

To explore features in the CIMS observations I used the 0-D (box-model) and 1-D versions of the Marine Boundary Layer (MBL) chemistry model, MISTRA (von Glasow et al., 2002a,b; Piot and von Glasow, 2008) as well as the newly developed version MISTRA-SNOW (Thomas et al., 2012).

A more detailed model description and evaluation can be found in von Glasow (2000) and von Glasow et al. (2002a, b). However, there have been some more recent model developments including an extension of the sulphur chemistry (von Glasow and Crutzen, 2004) and an improved description of the iodine aqueous phase and of the aqueous phase in general (Pechtl et al., 2007). A new snow-photochemistry module has been developed which includes chemistry which takes place in the quasi-liquid layer/ Liquid Like Layer (LLL) of aerosol (Thomas et al., 2011), which is of great importance to our understanding of the chemistry which initiates a bromine explosion and will be discussed further in section 4.3, and chapter 8. There have been many studies using the MISTRA model, with the most recent model modifications and updates, being discussed in Smoydzin and von Glasow (2009), and Piot and von Glasow (2008), Thomas et al. (2011, 2012) and Buys et al. (2013).

4.1 MISTRA model description

MISTRA is a one-dimensional model of the marine boundary layer (MBL). Originally a microphysical processes only model (Bott et al., 1997), MISTRA was later extended and

developed by von Glasow et al. (2002a,b) to include gas phase, aerosol (sea salt and sulphate particles) and cloud droplet chemistry. MISTRA can also model the evolution of stratiform clouds (von Glasow et al, 2002b), and includes sulphate and cloud droplet chemistry. A polar version of MISTRA was recently developed by Piot and von Glasow (2008), to study chemical reactions in polar regions.

4.1.1 Model resolution, timestep and numerical setup

The model atmosphere in MISTRA 1-D is divided into 150 layers, with the lowest 100 having a constant grid height which can be set in the model and those layers above 100 being spaced logarithmically. Different model grids are used depending on the inversion height chosen, and are stated in this thesis where they are required. The lower most layer in MISTRA 1-D and 0-D (k=1) is represented by an infinitesimally thin layer and is there to allow exchanges between the surface and the air in the overlying layer.

A model timestep of 10s is used for updating temperature, humidity and particle size distribution (along with other meteorological parameters), whereas a 2 minute timestep was initially used for updating photolysis rates.

MISTRA includes descriptions of meteorology, microphysics and thermodynamics as well as a multiphase chemistry module (von Glasow et al., 2002a, b). The chemistry module includes chemical reactions in the gas phase, in and on aerosol particles and takes into account transfer between the gas and aqueous phase. The complete set of chemical reactions incorporated in the multi-phase chemistry module are treated as one set of coupled differential equations and are solved using the kinetic pre-processor (KPP) (Damian et al., 2002) which allows easy changes of the chemical mechanism. The KPP is a software tool used to create code to simulate the chemical system in a computationally efficient manner. A Rosenbrock third-order solver (ROS3) is used to integrate the stiff ordinary differential equations used to describe the set of chemical reactions. This makes use of automatically adjusted timesteps (Sandu et al, 1997) that range from 10^{-10}s for conditions of low liquid water content (LWC) associated with the particles, and 10s if only gas phase reactions are calculated.

4.1.2 Meteorology and microphysics

Meteorology and microphysics are part of the boundary layer model described in detail by Bott et al. (1996). I will start with the following set of prognostic equations describing the horizontal components of the wind speed (u, v), the specific humidity (q), and the potential temperature (θ):

$$\frac{\partial u}{\partial t} = -w\frac{\partial u}{\partial z} + \frac{\partial}{\partial z}\left(K_m \frac{\partial u}{\partial z}\right) + f(v - v_g) \quad \text{(R4.1)}$$

$$\frac{\partial v}{\partial t} = -w\frac{\partial v}{\partial z} + \frac{\partial}{\partial z}\left(K_m \frac{\partial v}{\partial z}\right) - f(u - u_g) \quad \text{(R4.2)}$$

$$\frac{\partial q}{\partial t} = -w\frac{\partial q}{\partial z} + \frac{\partial}{\partial z}\left(K_h \frac{\partial q}{\partial z}\right) + \frac{C}{\rho} \quad \text{(R4.3)}$$

$$\frac{\partial \theta}{\partial t} = -w\frac{\partial \theta}{\partial z} + \frac{\partial}{\partial z}\left(K_h \frac{\partial \theta}{\partial z}\right) - \left(\frac{p_0}{p}\right)^{R/C_p} \frac{1}{C_p \rho}\left(\frac{\partial E_r}{\partial z} + l_{12}C\right) \quad \text{(R4.4)}$$

where u_g and v_g are the geostrophic horizontal wind components in the x and y directions, f is the Coriolis parameter, K_m and K_h are both turbulent exchange coefficients for momentum and humidity respectively and are calculated via dimensionless shear and buoyancy production terms $S_{m,h}$ and $G_{m,h}$ (see 4.5 below). C is the condensation rate, l_{12} is the latent heat of condensation, ρ the density of the air, p the air pressure and p_0 surface air pressure. C_p is the specific heat capacity at constant pressure for dry air, R the gas constant also for dry air, and E_r is the net radiative flux density. The first term of each of the above equations (all include a vertical component of the wind speed; w) describes large scale subsidence, but to conserve mass in the model setup ω tends to zero everywhere. Turbulent vertical transport for each parameter is described by the second term in (R4.1-4.4) above, the Coriolis force is described by the last term in (R4.1 and R4.2) and changes in potential temperature (θ) due to radiation are described by the last term in (R4.4).

Turbulence is parameterised by the level 2.5 model described by Mellor and Yamada (1982) and expanded by Bott et al. (1996), where the following prognostic equation for turbulent kinetic energy e is also discussed in more detail:

$$\frac{\partial e}{\partial t} = -w\frac{\partial e}{\partial z} + \frac{\partial}{\partial z}\left(\overline{e'w'}\right) + \frac{(2e)^{3/2}}{l}\left(S_m G_m + S_h G_h - \epsilon\right) \quad \text{(R4.5)}$$

where the dissipation of turbulent kinetic energy is described by ϵ =1/16.1, and l is the turbulent mixing length.

Microphysics is treated using a two-dimensional particle size distribution function f(a, r). The dry particle radius (a) (the radius the particle would have if there were no water present) and the total particle radius (r) (where some amount of water is contributing to the total particle radius), are used to describe a two-dimensional particle grid (fig. 4.1). The grid is divided into 70 equidistant logarithmically spaced dry aerosol size classes, and 4 different bins. The total range of aerosol radii accounted for in MISTRA is from 0.01µm to 60µm (represented by the crosses in fig. 4.1). This range covers all accumulation mode particles and most of the coarse particles.

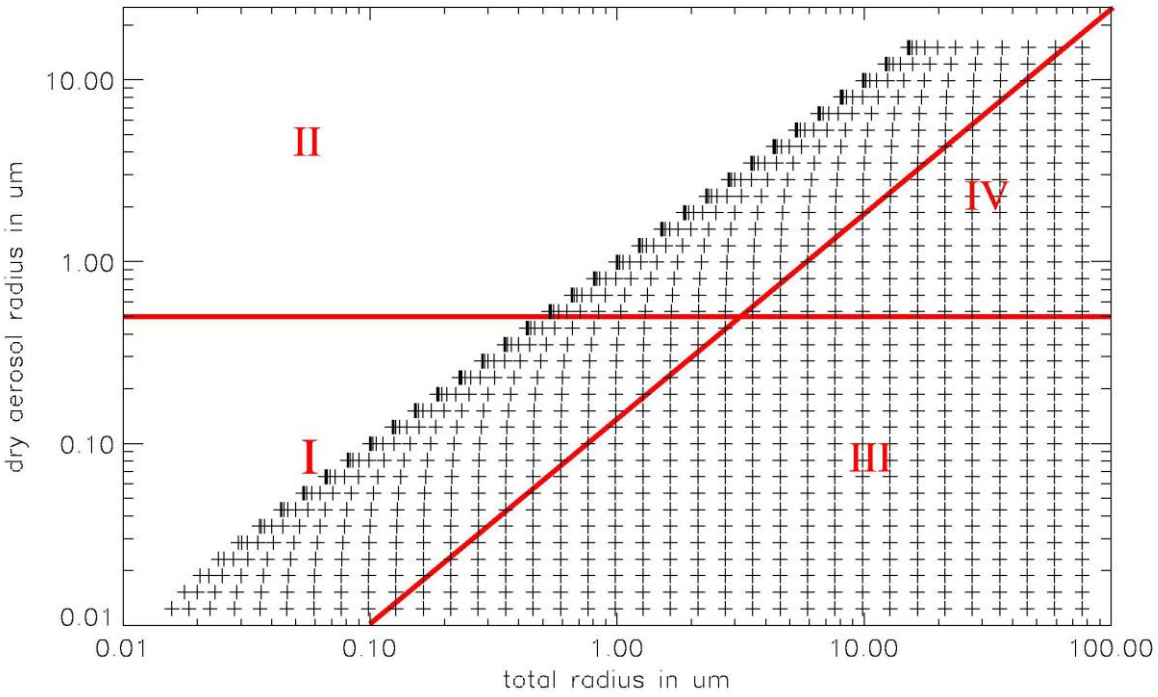

Figure 4.1*: The two-dimensional particle spectrum as function of the dry aerosol radius a and the total particle radius r. Added are the chemical bins. I: sulphate aerosol bin, II: sea salt aerosol bin, III: sulphate cloud droplet bin, IV: sea salt droplet bin. For simplicity a 35 x 35 bin grid is plotted, in the model 70 x 70 bins are used (taken from Piot, 2007).*

The prognostic equation for f(a, r) holds a similar form to those described above (4.1-4.5), where there is again a subsidence term, followed by turbulent mixing and then the final term describes changes to particle growth caused by the coriolis force. Particles are initialised with a water coating according to the equilibrium radius of the dry nucleus at the ambient relative humidity, and their growth including the effects of radiation is calculated explicitly for each bin of the 2D particle spectrum after Davies (1985):

$$r\frac{dr}{dt} = \frac{1}{C_1}\left(C_2\left(\frac{S_a}{S_r} - 1\right) - \frac{F_r(a,r) - m_w(a,r)c_w\frac{dT}{dt}}{4\pi r}\right) \quad \text{(R4.6)}$$

Where the ambient supersaturation S_a, and the droplet surface saturation S_r given by the Kohler equation:

$$S_r = exp\left(\frac{A}{r} - \frac{Ba^3}{r^3 - a^3}\right) \quad \text{(R4.7)}$$

Where the first term $\frac{A}{r}$ defines the particle radius, and the second term $\frac{Ba^3}{r^3-a^3}$ the particle chemical composition. The coefficients C_1 and C_2 are defined by:

$$C_1 = \rho_w l_{21} + \frac{\rho_w C_2}{D_v' S_r \rho_s} \qquad C_2 = kT\left(\frac{l_{21}}{R_v T} - 1\right)^{-1} \quad \text{(R4.8a, b)}$$

The liquid mass of the particle is given by $m_w(a, r)$, c_w and ρ_w are the specific heat capacity and density of water, ρ_s the saturation vapour density, R_v the gas constant for water vapour, k the thermal conductivity and D_v' is the diffusivity of air (both are corrected for gas kinetic effects; see Pruppacher and Klett, 1997). l_{21} is the latent heat of evaporation and T is atmospheric temperature in Kelvin. The net radiative flux at the particles surface is $F_r(a, r)$, and helps determine changes to the particle radius.

Moisture exchange between the surface and the overlying air are calculated via the Clausius-Clapeyron equations (as in Jacobsen, 1999). The model was recently updated to include saturation vapour pressure of water above ice. The saturation vapour pressure of water over the ocean is described by:

$$p_{v,w} = 610.7exp\left(17.5\frac{(T-273.15)}{(T-38.33)}\right) \quad \text{(R4.9)}$$

Whereas the saturation vapour pressure over an ice surface is given as:

$$p_{v,ice} = 6.112exp\left(4648\left(\frac{1}{273.15} - \frac{1}{T}\right) - 11.64ln\left(\frac{273.15}{T}\right) + 0.02265(273.15 - T)\right) \quad \text{(R4.10)}$$

with $T \leq 273.15K$ and $p_{v,w}$ and $p_{v,ice}$ are in millibars. Equation 4.10 is important when discussing the role of sea ice and the snowpack in contributing to atmospheric composition in polar regions.

4.1.3 Chemistry

Chemistry in the model can take place either in the gas phase, or on/in aerosol/ particles. Whereas gas phase chemistry is considered in all model layers, aerosol chemistry is only taken into account in layers where the relative humidity is greater than the crystallisation humidity. Heterogeneous surface reactions as well as exchange between the gas-aqueous phase are included in the chemistry description. The reaction set is based on Sander and Crutzen (1996) but has been expanded and had many stages of updates, so that the complete mechanism consists of 169 gas phase reactions and 150 aqueous, 60 phase change reactions, 13 heterogeneous reactions and 21 equilibria for both sulphate and sea salt aerosols (Piot and von Glasow, 2008). The concentration of a gas phase chemical species c_g (in mol/m_{air}^3) can be expressed by the prognostic equation:

$$\frac{\partial c_g}{\partial t} = \frac{\partial}{\partial z}\left(K_h \rho \frac{\partial c_g/\rho}{\partial z}\right) - D_{dep} + P - Lc_g + E - \sum_{i=1}^{n_{kc}} \overline{k_{t,i}} \left(LWC_i c_g - \frac{c_{a,i}}{k_H^{cc}}\right) \quad \text{(R4.11)}$$

Where the first term is again a turbulence term describing turbulent exchange ($K_h\rho$ is the turbulent exchange coefficient), dry deposition to the open water or snow surface D_{dep} and emission of chemical species E are effective only in the lowermost model layer (von Glasow et al., 2002a), with P and Lc_g being chemical production and loss terms. The last term on the right of the equation describes the bi-directional transport from the aqueous phase into the gas phase and vice-versa, where n_{kc} is the number of aqueous classes considered (n_{kc}=2 for cloud-free runs, and is used throughout this thesis), LWC_i and $c_{a,i}$ are dimensionless liquid water content (in m_{aq}^3/m_{air}^3) and the aqueous concentration of bin i, and k_H^{cc}=k_HRT is the dimensionless Henry constant (where k_H is in mol m^{-3} Pa^{-1}). $\overline{k_t}$ is the mean mass transfer coefficient for a particle population.

Due to computational limitations aqueous phase chemistry is calculated in only the four bins considered in the model, and not in each of the 70x70 microphysical bins. The prognostic equation governing the aqueous concentration of a chemical species in each size class $c_{a,i}$ (in mol m_{air}^{-3}) is as follows:

$$\frac{\partial c_{a,i}}{\partial t} = -w\frac{\partial c_{a,i}}{\partial z} + \frac{\partial}{\partial z}\left(K_h \rho \frac{\partial c_{a,i}/\rho}{\partial z}\right) - D_{dep} + P - Lc_{a,i} + E + P_{pc} - \overline{k_{t,i}}\left(LWC_{l,i} c_{a,i} - \frac{c_{a,i}}{k_H^{cc}}\right)$$

(R4.12)

Again this equation follows a similar form to those mentioned previously, with the new term P_{pc} accounting for the transport of chemical species both from the aerosol to cloud droplet phases and in the other direction. The other terms hold equivalent meanings to those of (R4.11).

Dry deposition of gases onto the sea and snow/ice surface is calculated using the resistance model described by Wesely (1989).

4.1.4 Photolysis calculations

Photolysis rates of photodissociable species are calculated online by the method of Landgraf and Crutzen (1998). The photolysis frequency J_x for a species x is calculated from the spectral actinic flux $F(\lambda)$ via the following integral:

$$J_x = \int_I \sigma_x(\lambda)\, \phi_x(\lambda) F(\lambda) d\lambda \qquad \text{(R4.13)}$$

Where σ_x is the absorption cross section, ϕ_x the quantum yield, λ the wavelength and I is the photochemically active spectral interval. Only 8 spectral bins are used here as suggested by Landgraf and Crutzen (1998), as it is computationally faster to calculate than the ~100 wavelength bins that would otherwise be needed:

$$J_x = \sum_{i=1}^{8} J_{i,x}^{a} \cdot \delta_i \qquad \text{(R4.14)}$$

where $J_{i,x}^{a}$ is the photolysis rate for a purely absorbing atmosphere. The factor δ_i is the ratio between the actual actinic flux $F(\lambda_i)$ and the actinic flux for a purely absorbing atmosphere $F^{a}(\lambda_i)$,and describes the effect of scattering in the atmosphere:

$$\delta_i = \frac{F(\lambda_i)}{F^{a}(\lambda_i)} \qquad \text{(R4.15)}$$

For a more detailed description of these photolysis calculations and the 8 spectral range intervals, see Landgraf and Crutzen (1998) and von Glasow et al. (2002a).

There is a modified 'band approach' for the online calculation of photolysis rates available (Williams and Landgraf, 2006) which could be used to update MISTRA in the future, and implementation of this new method may remove the sharp night to day transition seen for photolysis rates.

4.1.5 Antarctic conditions

The model initially had to be set-up to be representative of the measurement site of Halley station in coastal Antarctica. A prescribed surface albedo was set to be (0.8; Massom et al., 2001), and the solar declination was calculated for Halley (latitude) for the 6th September 2007 at a value of 6.35° (chosen as the base run as the near mid-point of the measurement period, and the test case for exploring the interferent in the CIMS halogen measurements as discussed in Chapter 5). This corresponds to ~ 7 hrs of daylight (sunrise = 0900, Sunset = 1600), which corresponds well with the measurements.

For this work, the MISTRA model runs were initialised using measurements made at Halley station, including: aerosol size distribution and composition (Rankin and Wolff, 2003; Jaenicke., The Landolt-Börnstein Database, 1982), local meteorology (Anderson and Neff, 2008), and measurements of local chemical composition (NO_x, O_3, NMHCs, DMS, HCHO, CO). All emissions from particles and the surface (lowest model layer) result from explicit condensed-phase chemistry, apart from a prescribed flux of Br_2 from the model surface.

The specific initial conditions and model setup used for each simulation will be addressed in the appropriate chapters (5, 6, 7, 8 and 9).

4.2 MISTRA 0-D, box model specific description

MISTRA was initially run in 0D (or 'box-model') mode. This is achieved by simply changing a logical statement from FALSE to TRUE in the "istart" file (used to set restarts, run-time, include chemistry, microphysics and other such parameters as logical switches in the model itself), and defining a box height in m. The box height for these runs was determined using the coincident meteorological measurements made at Halley (outlined in chapter 3), and the meteorological measurements were also used to define the temperature and wind speed to initialise the simulations. In box-model mode the meteorological information is only prescribed and does not evolve throughout the run.

In box-model mode layer k=2 is the only layer in which chemistry is calculated. Layer k=1 has the same features and holds the same function as described in section 4.1.

4.3 MISTRA-SNOW

A description of the new snow module in the coupled snow-atmosphere model (MISTRA-SNOW) is given by Thomas et al. (2011), but I will give an in depth overview here of this new addition. This 1-D coupled model includes descriptions of both chemistry and physics of the atmosphere (sections 4.1 and 4.2) and snowpack, and was initially intended to model conditions at Summit, Greenland (Thomas et al., 2011). By changing the physical properties of the snow and chemical composition of the snowpack and atmosphere to make it more representative of Halley in coastal Antarctica (see section 4.3.2), the goal in using this model was to explore the role of snow chemistry in halogen release from snow covered regions in coastal Antarctica. The aim was to determine whether observed halogen mixing ratios and ozone depletion could be either partly/ or solely due to chemistry in/ on snow. Details of the specific initialisation of both the snowpack and atmosphere chosen for coastal Antarctic conditions (Halley) will be given in chapter 8.

4.3.1 Physical Description of the Snow Module

1D grid and photolysis: The new snow module has a logarithmic one dimensional grid made up of 20 levels, and the snowpack depth is determined and calculated by the depth chosen for the first layer. This logarithmic grid is used to capture the small scale over which chemistry and physics changes within the snowpack. The model grid for the atmosphere is the same as described in section 4.1.1. The snowpack and atmosphere are coupled at the snow surface through gas flux via diffusion and wind pumping. Calculation of gas phase diffusion constants and snow chemistry make use of the temperature and heat flux q_s in the snowpack, which is calculated by:

$$q_s = -k_{eff}\frac{dT}{dz} \qquad \text{(R4.16)}$$

where k_{eff} is the effective thermal conductivity of the snowpack and $\frac{dT}{dz}$ is the temperature gradient. The time dependant temperature variation in the snowpack is calculated using the density of the snowpack ρ_s and the heat capacity C_p:

$$\frac{\partial T}{\partial t} = \frac{\partial}{\partial z}\left(\frac{k_{eff}}{\rho_s C_p}\frac{\partial T}{\partial z}\right) \quad \text{(R4.17)}$$

A diurnal variation in the snow surface temperature is prescribed to drive the temperature variation in the snowpack. This variation forces a diurnal cycle in the atmospheric boundary layer, and this surface temperature T_{surf} is calculated by means of:

$$T_{surf} = T_{amp}\left(1 + sin\left(2\pi\left(\frac{t_h}{24} - \frac{t_{min}+6}{24}\right)\right)\right)/2 \quad \text{(R4.18)}$$

where the amplitude of the surface temperature oscillation T_{amp} is in K, t_h is the hour of day in the model run, and t_{min} is the hour minimum surface temperature is reached.

Gas transport in the snow is the sum of the wind pumping process and molecular diffusion. The vertical wind pumping speed (U_{firn}) calculation used here is described by Cunningham and Waddington (1993):

$$U_{firn} = \frac{6k\rho_{air}}{\pi\mu\lambda_{surf}}\frac{h}{\lambda_{surf}}\frac{\sqrt{\alpha^2+1}}{\alpha}u_{10}^2 exp\left(-\frac{z}{\delta}\right) \quad \text{(R4.19)}$$

with λ_{surf} as the relief wavelength h as the relief amplitude and α is a horizontal aspect ratio of the relief relative to wind direction. k is the permeability of each layer in the snowpack, μ is the dynamic viscosity of air, ρ_{air} is the density of air, z is the depth from the snow surface and the wind speed 10m above the snow surface is included via u_{10}.

As previously stated, molecular diffusion must also be taken into account when discussing gas transport within the snow. It is therefore possible to calculate the effective diffusion constant K (in $m^2\ s^{-1}$) by the sum of the diffusion constant for gases D_g and the vertical wind pumping term (as in equation R4.19):

$$K = \tau D_g + U_{firn}\Delta z \quad \text{(R4.20)}$$

where τ is the tortuosity (a measure of the complexity of the pathway in a porous medium; Albert and Shultz, 2002)) , Δz is the grid spacing and both D_g and U_{firn} are a function of depth.

The physical properties of the snowpack described in the model includes the LLL (liquid like layer; see chapter 2) thickness, snow grain radius (snow grains are assumed to be spherical), density liquid water content and heat capacity (Thomas et al., 2011). These physical parameters are outlined in further detail in Chapter 8 and are based on measurements made in coastal Antarctica collated by Massom et al. (2001).

4.3.2 Chemistry in the snowpack

Figure 2.1 from Chapter 2 shows the chemical pathways important for both NOx and reactive bromine cycling at Summit in Greenland. This is unlikely to be very different from the pathways of importance expected at Halley, and is therefore regarded as a good representation of bromine activation in the snowpack in coastal Antarctica.

The prognostic equation to calculate the concentration of a gas phase chemical species in the SNOW model holds a very similar form to that of reaction (R4.11), where the sum of wind pumping and diffusion k are included in place of the turbulent exchange coefficient$K_{h\rho}$:

$$\frac{\partial c_g}{\partial t} = \frac{\partial}{\partial z}\left(k\rho(z)\frac{\partial c_g/\rho(z)}{\partial z}\right) + P - Lc_g - k_t\left(LWC_i c_g - \frac{c_a}{k_H^{cc}}\right) \quad \text{(R4.21)}$$

where all parameters have the same definition as for reaction (R4.11). However, the mass transfer coefficient k_t is defined for a single snow grain as follows:

$$k_t = \left(\frac{r^2}{3D_g} + \frac{4r}{3\overline{v}\alpha}\right)^{-1} \quad \text{(R4.22)}$$

with r being the radius of the snow grain, $\overline{v}$ is the mean molecular speed and α is the accommodation coefficient. Other parameters hold the same definition as mentioned previously.

Photolysis frequencies calculated in the snowpack take into account decreasing light penetration with depth in the snowpack, and therefore decrease exponentially with depth. An e-folding depth of ϵ_λ = 10cm is used (see Thomas et al., 2011) for all photolysable species to describe their decay with depth in the snowpack. The incident irradiance at the snowpack surface ($E_\lambda(z=0)$) and the e-folding depth ϵ_λ (King and Simpson, 2001) to calculate the photolysis rates in the snowpack:

$$E_\lambda(z) = E_\lambda(z=0)exp(-z/\epsilon_\lambda) \quad \text{(R4.23)}$$

$E_\lambda(z)$ is the actinic flux at depth z. J_{NO2} measured above the snowpack at Halley shows good agreement with model simulated J_{NO2}, although it does appear to slightly under estimate it (see Figure 5.9 in Chapter 5)

5 Results Part I: Investigation of potential interferent in day time CIMS Br_2 and BrCl observations.

Synopsis:

This chapter highlights a CIMS instrument inlet artefact that was apparent when measuring Br_2 (and, as is shown below, likely also when measuring BrCl). Also discussed here are both the 0-D and 1-D MISTRA model setup and preliminary runs used to study the apparent inlet artefact, including initial conditions and the reasons behind these model setups. The chapter ends with a short section which outlines how the data will be dealt with in subsequent chapters, in regards to the daytime interferent in Br_2 and BrCl.

5.1 Brief introduction to data set

The primary interests in the Halley observations are what they can tell us about the sea-ice/ocean/atmosphere system. However, before the data can be explored, it is necessary to address an issue that came to light after the campaign, and that affects observations made during daylight hours.

A surprising feature in the CIMS halogen data from Halley were the above detection limit observations of both Br_2 and BrCl during daytime. This is illustrated in Figure 5.1, which shows observations of Br_2, BrCl, BrO, as well as surface ozone, wind speed and temperature, on 6th and 7th September 2007.

There are only a limited number of ways in which such high mixing ratios of Br_2 and BrCl could be sustained during daylight hours. If real, the data would suggest either an extremely high flux of bromine radicals into the polar boundary layer, or previously unknown chemistry. The alternative, however, is that the data are affected by an artefact caused by the sampling methodology.

The day time Br_2 signal might be explained by low photolysis rates at Halley until the end of September, due to the low angle of the sun in the sky. However, the absorption cross section and quantum yield for photolysis of Br_2 (see Appendix B) indicate that this could not be the case

as the Br_2 cross section closely matches that of NO_2 which is readily photolysed at Halley in spring (N. Brough, pers. comm. 2012)(NO_2 dissociates at λ<420nm). This is discussed further in section 5.4 at the end of the chapter.

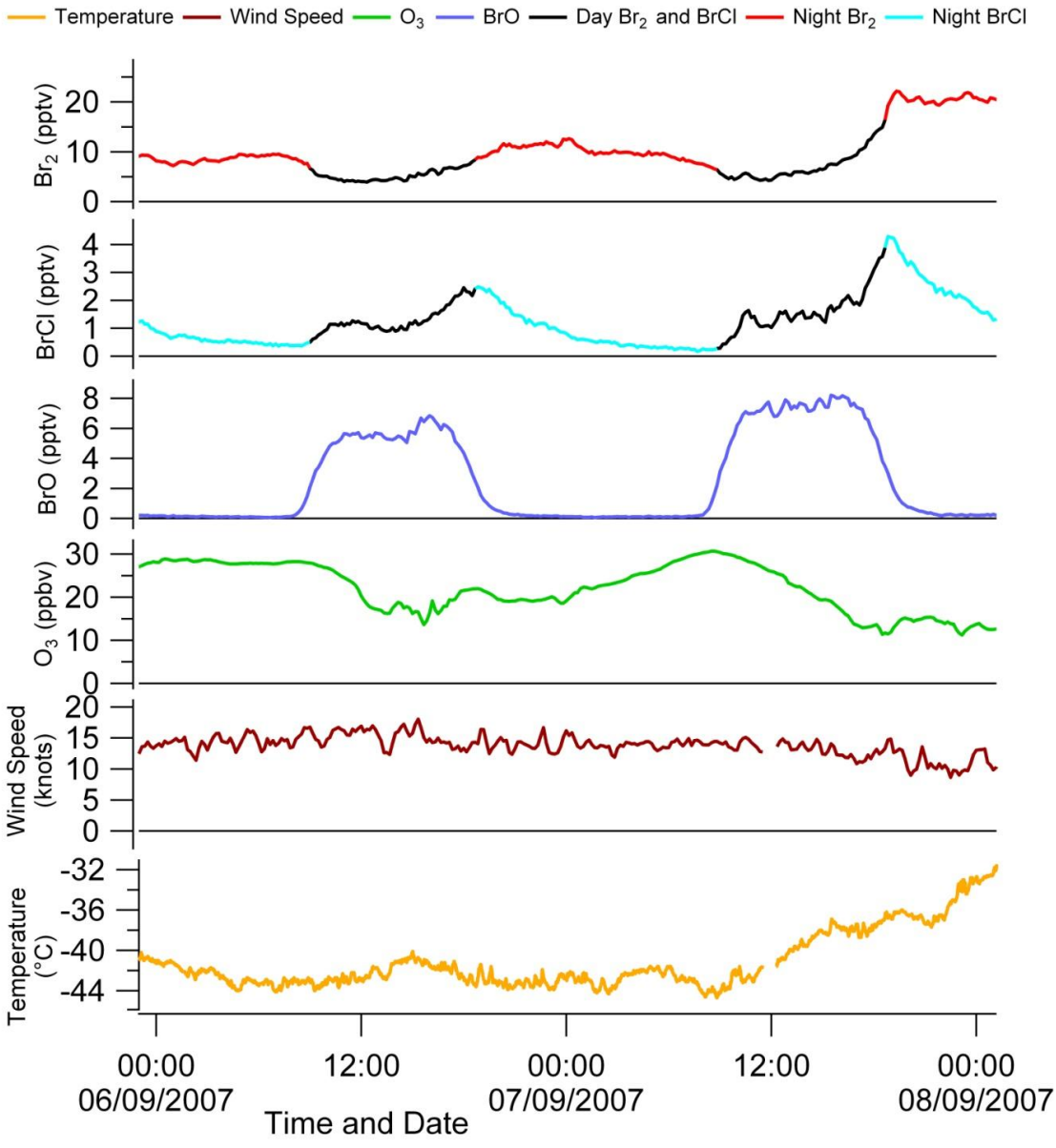

Fig 5.1: *surface wind speed, temperature, O_3, and CIMS Br_2, BrCl and BrO measurements from Halley on 6-7 September 2007. Br_2 and BrCl day time measurements are coloured black. 12:00 is solar noon.*

The potential for CIMS observations of Br_2 to be influenced by an artefact came to light after the campaign. The artefact appears most likely to arise from chemical conversion on the instrument

inlet (Neuman et al., 2010). These authors reported HOBr conversion to Br_2 on a number of different surfaces, both coated with NaBr and uncoated, the latter including the Teflon of the instrument inlet, glass, aluminium, stainless steel, PVDF (Polyvinylidene difluoride; a highly non-reactive and pure thermoplastic fluoropolymer), and several other types of Teflon. Their results are in line with laboratory studies that have shown the rapid generation of Br_2, and to a lesser extent BrCl, on salty surfaces, via uptake of HOBr (Abbatt, 1994; Adams et al., 2002; Kirchner et al., 1997). This is not the first time that measurements of halogens using CIMS have shown daytime concentrations above instrumental detection limits (Spicer et al., 2002), but no mention of an interferent was given. The presence of a CIMS inlet artefact in Br_2 has been acknowledged in subsequent field measurements (e.g. Liao et al., 2012a; Liao et al., 2012b).

Before the CIMS data are discussed further, I will explore two possible reasons for the non-zero daytime Br_2 and BrCl data: i) the presence of a high flux of bromine radicals into the polar boundary layer, and ii) an instrumental artefact. In order to do this I will use the observations from Halley for 6th and 7th September (as shown in Fig 5.1) and results from the MISTRA model.

5.2 MISTRA model initialisation and preliminary runs

5.2.1. 0-D model setup

The chemistry in the model atmosphere was initialised with mixing ratios as laid out in Table 5.1, which consist mainly of local in-situ measurements. Where no local in-situ measurements were available, mixing ratios for spring-time from other studies conducted at coastal Antarctic sites with similar sea-ice influence (e.g. Neumayer station, 800km from Halley) were used. As a small check, a simulation was initially run where the dry deposition was switched off in the model. This run was then compared with previous runs with the deposition switched on. This simply confirmed that the total bromine in the model (Br_{tot}) is conserved when dry deposition is switched off.

The meteorology in the model was initialised using concurrent measurements from Halley of wind speed, wind direction and local ambient temperature as described in Chapter 3 (see Table 5.2).

Chemical species	Initial mixing ratio	Reference
NO	0.002	Pers.comm Neil Brough
NO_2	0.005	Pers.comm Neil Brough
HNO_3	0.001	CHABLIS campaign
SO_2	0.01	Jourdain and Legrand (2002)
O_3	30	Buys et al. (2013)
HCHO	0.1	Reidel et al. (1999); Salmon et al. (2008)
HONO	0.002	Clemitshaw (2006)
PAN	0.01	Mills et al. (2007)
Br_2	0.006	Buys et al. (2013)
C_2H_6	0.3	Rudolph et al. (1989); Rudolph et al. (1992)
DMS	0.05	Read et al. (2008)

Table 5.1, O-D chemistry: *Initial mixing ratios (in nmol mol^{-1}) for gas phase chemical species used to initialise the 0D model*

It was initially unclear what BL/mixed layer height should be used for the model runs. Over the sea-ice zone (where the release of halogen and onset of ozone depletion is thought to occur) the BL height can be on the order of 100m, whereas the BL height at Halley can be as low as 20m. These differences in height are due to the turbulent nature of the air as it passes over the warmer areas of open water in Precious Bay, and passing over the colder ice-shelf surface leads to the creation of an internal boundary layer. Observations from an acoustic sounder (a "sodar") were available for Halley for both the 6th and 7th September, and detailed boundary layer (BL) structure measurements were made using a tethersonde on 7th September. These data clearly showed both the lower and higher boundary layers shown in Fig.5.2. For the model runs, BL structure was initialised so that the higher BL evident in the sodar data was used.

Parameter	Value	Note
Wind speed	6 ms^{-1}	Measured at Halley
Temperature	230K (235K after spin-up)	Measured at Halley
Total column 0_3	225 DU	Measured at Halley
Declination angle	6.35	As for Halley on 06/09/2007
Latitude	75.6	Location of Halley
Box height/ inversion layer	100m – 200m	Measured at Halley

Table 5.2, O-D meteorology: *Initial meteorological input, as well as other input parameters, used to initialise the 0D model*

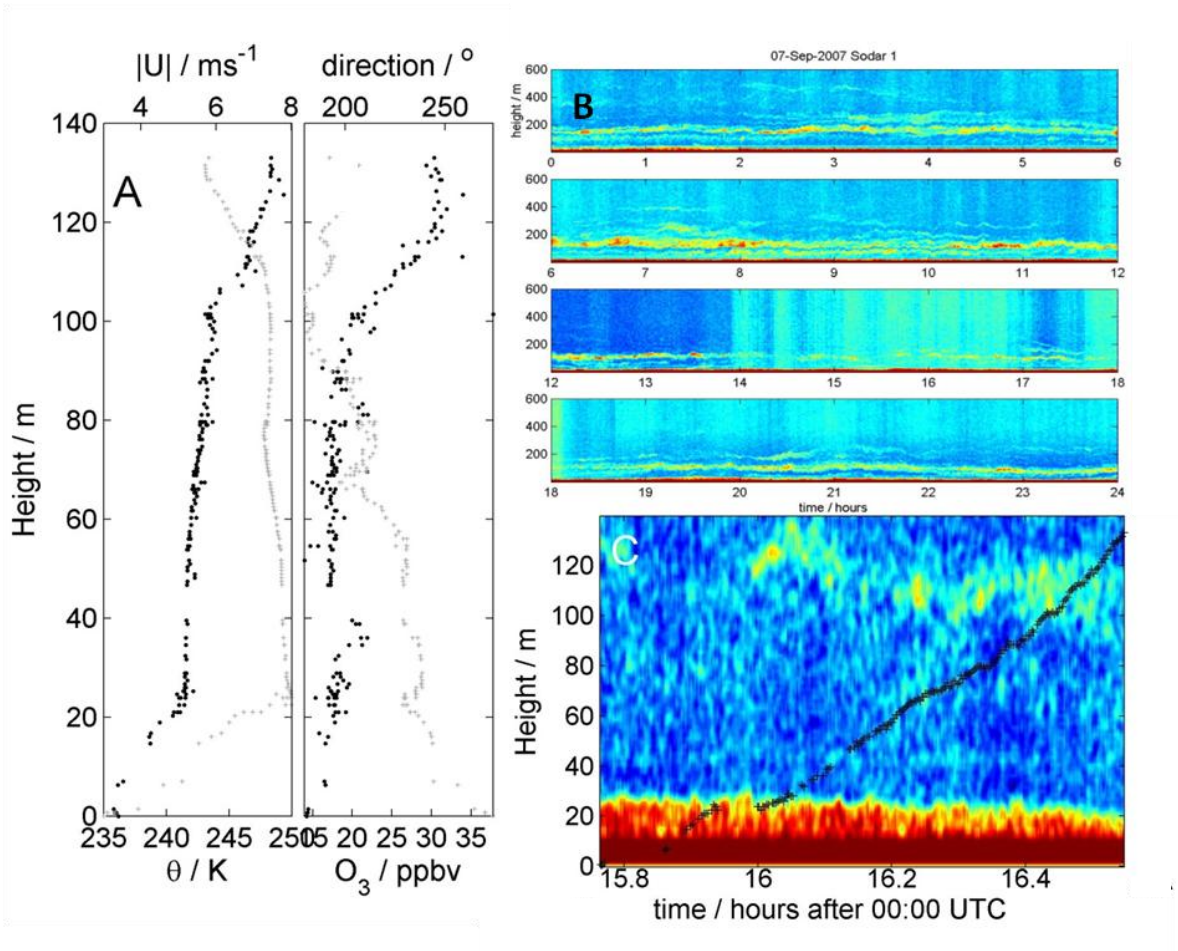

Figure 5.2 *a) tether-balloon sonde data (taken from Jones et al, 2010), and b) and c) are sodar data collected at Halley for 7/09/2007 (see Section 3.3.2). The lower 20m level is shown in a) and c), and the higher 100m level is shown in a), and is also clearly visible as a yellow line in b). The black line visible in c) is the track of the tethered balloon sonde.*

Clear in Figure 5.3a, b, and d is the sharp transition between day and night in the model output. In order to explore this, further model simulations investigated the model sensitivity to the value of the Solar Zenith Angle (SZA) above which photolysis rates are calculated in the model. Initially the SZA value below which photolysis is calculated in the model was chosen as 88° (used by Piot and von Glasow, 2008 and Thomas et al., 2011) as this value was thought to be a good balance between capturing the onset of photolysis without incurring too large errors (Figure 5.3). The method used for calculating photolysis rates in the model works well at lower latitudes (Landgraf and Crutzen, 1998), but increasing errors appear as the latitude increases. The actinic flux and photolysis rates are calculated in 8 wavelength bins, and Br_2 photolysis falls almost entirely into bin 8 ($\lambda \geq 422$nm). This could lead to the sharp transition seen at model sunrise that is seen in figure 5.3a, as Br_2 is photolysed nearly instantly instead of gradually as the SZA decreases and photolysis rates increase. To decrease this sharp transition between night and day SZA values of 89° and 89.99° were used (Figure 5.3 b and c). Unfortunately, Landgraf and Crutzen (1998) go on to state that SZA >80° can lead to large errors which will increase with increasing SZA. In Figure 5.3 the change in photolysis initiation at 88° and 89° is small, while increasing this slightly to 89.99° leads to a large change in the shape of the Br_2 night-day transition caused by changes in photolysis calculation of actual (and perhaps realistic) chemistry. A run using 85° is also shown in Figure 5.3d. However, using a smaller SZA led to the length of the simulated day dropping drastically leading to 4 hours less daylight which would greatly affect the results. Although values >80° can lead to large errors, it was decided that a SZA of 89° would be used for the remainder of the model runs.

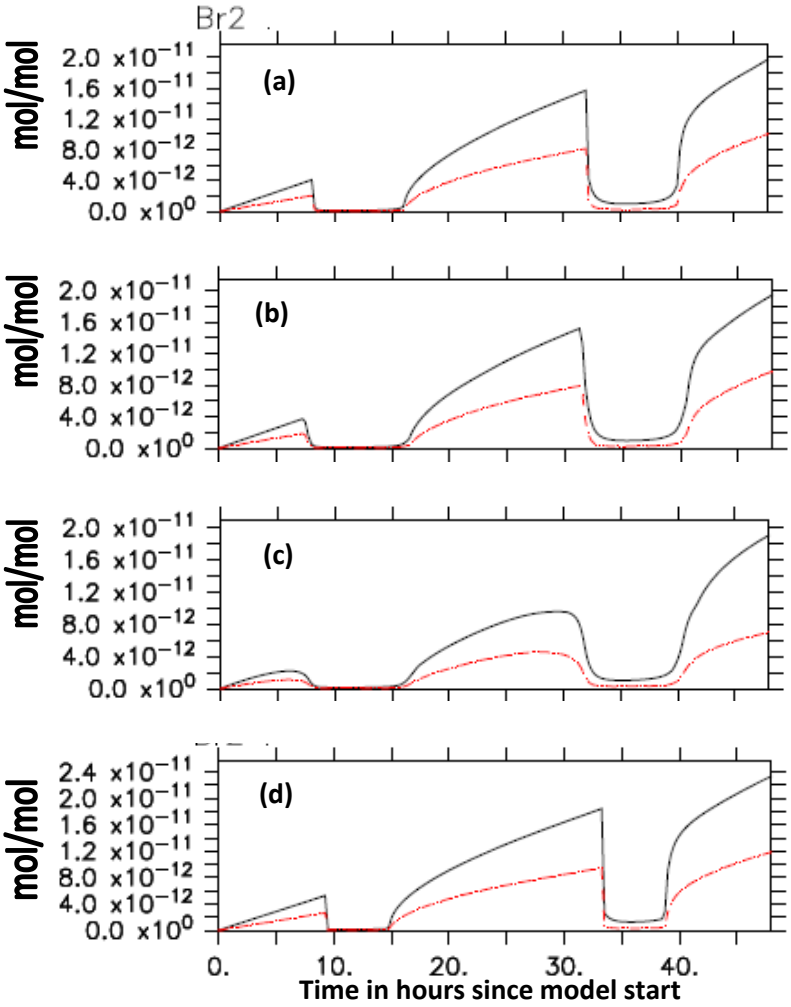

Figure 5.3: *Model results showing Br_2 calculated for photolysis switches of SZA cut offs a) SZA of 88, b) SZA of 89°*, and c) a SZA of 89.99°*, and d) 85°*.

5.2.2. 1-D model setup

The MISTRA 1-D model setup uses the same initial chemistry and meteorology as the 0-D setup (and as shown in tables 5.1, 5.2), but differs in several important ways. The first is the one dimensional nature of this version of the model, which requires more initial input when setting up the model atmosphere. The temperature at the bottom of the model atmosphere is defined, and a temperature gradient (Table 5.3) is imposed in the vertical. The lower boundary condition for the model is re-defined and set up as an "ice" surface, where a diurnally varying temperature is setup (Table 5.3) and saturation specific humidity is calculated with respect to ice.

Parameter	Value	Note
Vertical Resolution	3m	Allows 100 and 200m BL height
Temperature gradient	0.1K/m	Measured at Halley (1-D)
Temperature Amplitude	5K	Measured at Halley (1-D)

Table 5.3, 1-D meteorology: *Additional parameters used to initialise the 1D model*

A 2-day "spin-up" for the model meteorology is required, and used to restart the meteorology for the actual model runs including the full suite of chemistry and microphysics parameters. Table 5.1 contains the initial values for the chemistry input to the model. There is also a chemical flux from the surface in the form of Br_2 release of $6x10^8$ molecules cm^{-2} s^{-1}. This halogen release is discussed further in section 5.3. The temperature gradient and diurnal temperature amplitude (Table 5.3), although based on measurements, were chosen to more accurately represent the atmospheric boundary layer as measured at Halley. The model atmosphere is depicted in Figure 5.4, and the chemistry will be discussed later on in Section 5.3. The vertical profile of potential temperature from the model atmosphere (Figure 5.4a), quite accurately represents the vertical profile of potential temperature measured from the tethered balloon-sonde from Halley on 0709/2007 (Fig 5.2), and the model wind speeds also accurately reproduce both the vertical profile from this balloon-sonde and measurements from a 30m meteorological mast. Model relative humidity also indicates that no clouds formed during this simulation.

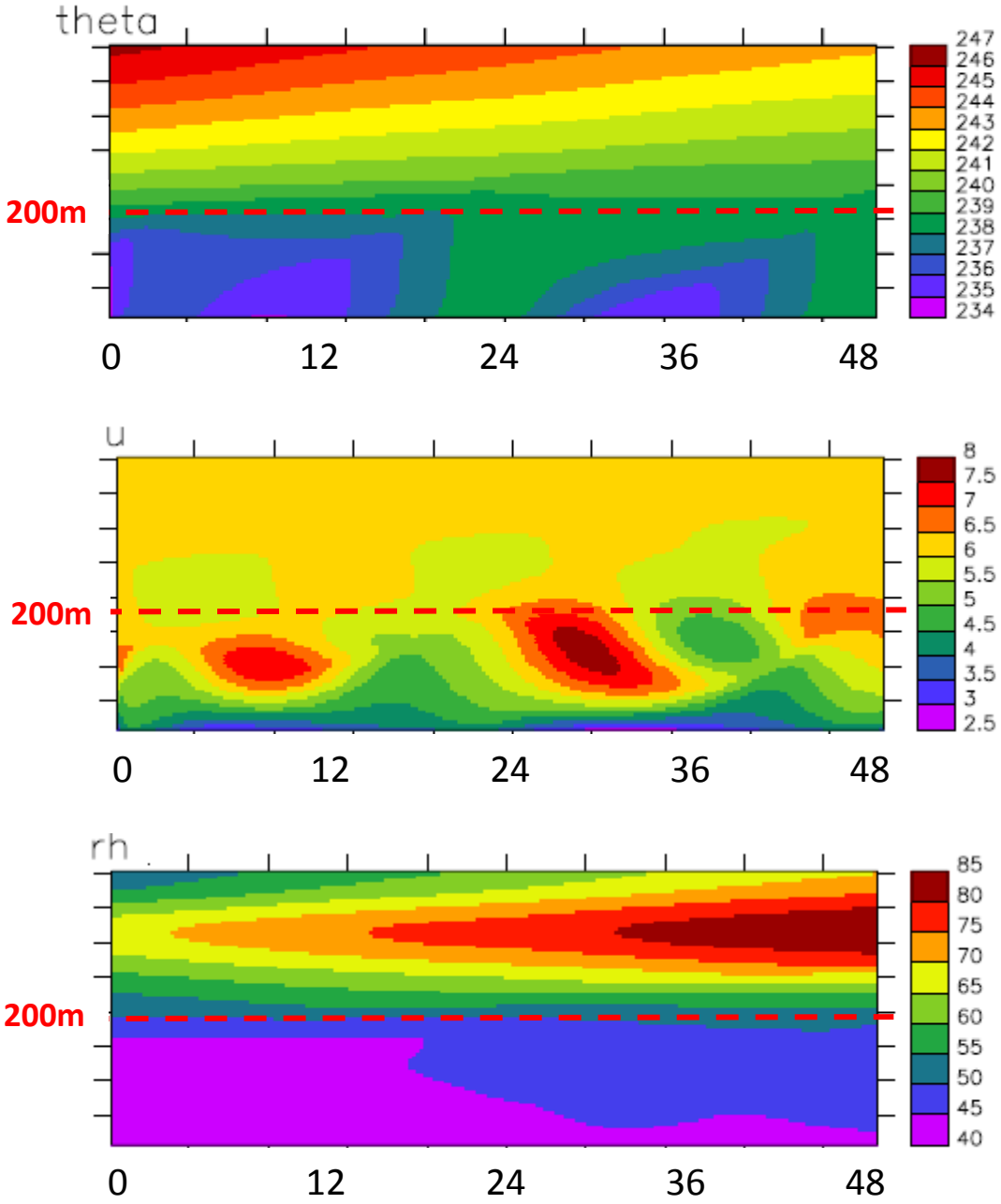

***Figure 5.4**: 1-D MISTRA run model output for a) potential temperature (K), b) horizontal wind speed (ms^{-1}), and c) relative humidity (%). The x-axis shows time since model start (hrs) for a 48hr run with a two day met spin-up (met spin-up not shown), y-axis is height in metres above model surface.*

5.3. Model studies to investigate the detected daytime Br_2 and BrCl

To explore the possible reason for the detection of daytime Br_2 and BrCl in the data, I focus on the 6th and 7th September 2007. The local wind direction throughout this period (~250°) indicates arrival of air at Halley from over Precious Bay, and wind speeds were constant at ~7 ms^{-1}. Temperatures on these days were very low at -40°C although rising to -33 °C during the final 12 hours, and observations from the sodar, which provides information on atmospheric structure, suggest that the top of the inversion layer is at ~200 m on Sept 6th and ~100 m on Sept 7th. Observations of temperature and horizontal wind speed from an adjacent 30 m mast (sensors at 1, 2, 4, 8, 16, and 32m) suggest the BL was well mixed on this day. While a box model can be appropriate to study a well-mixed boundary layer, given that the CIMS inlet was located ~5 m above the snow surface, which is known to affect gradients of many chemical components, I explore the data using both MISTRA-0D and MISTRA-1D.

5.3.1. Bromine radicals flux vs. CIMS interferent in 0D calculations

A suite of model runs were performed employing different halogen flux scenarios in an attempt to simulate observations during this period. All bromine was released as Br_2, and the only parameter changed in the model between the two days was the mixed layer height.

The flux of bromine required to achieve the night-time maximum Br_2 mixing ratio for the 6th September 2007 was calculated assuming constant emission over a 24h period into a well mixed 200m BL/ box. Br_2 was emitted into the model at a fixed rate according to the time the air parcel had spent over newly forming sea ice in Precious Bay, as determined from HYSPLIT back trajectories and sea ice maps (see Figure 5.5). Back trajectories run every 2 hours for the 24 hour period covering the 6th September all show a similar path over the newly forming sea-ice in Precious Bay. A constant emission of Br_2 from the sea-ice zone is assumed, and simulated by release of a constant Br_2 flux over this 24 hour period.

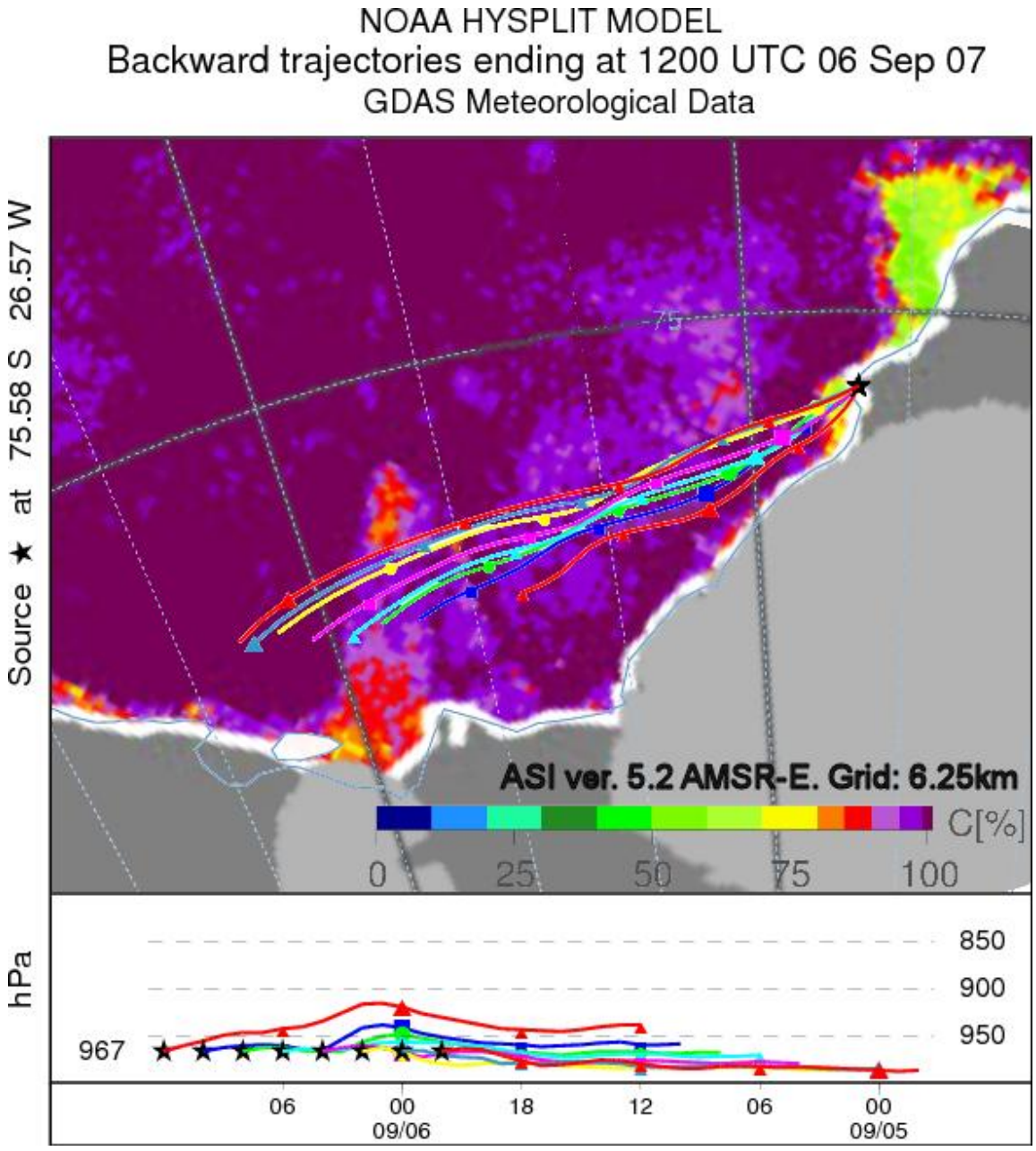

Figure 5.5: *2-day back trajectories showing air parcel history (location and atmospheric pressure) prior to arrival at Halley on 06/09/07 overlaid on an AMSR-E image of percentage sea-ice cover. The star marks the position of Halley, and the symbols mark 6-hourly intervals.*

To compensate photolytic destruction of Br_2, and maintain the observed mixing ratio of ~5pptv around solar noon, would require a Br_2 emission of ~1 x 10^{10} molecules cm^{-2} s^{-1} into a well mixed 100m high boundary layer. This is considerably larger than the release of Br_2 to the atmosphere of ~6 x 10^7 to ~1.8 x 10^8 molecules cm^{-2} s^{-1} simulated by Toyota et al. (2011) for the Arctic spring using a 3D model, and an order of magnitude higher than the 1 x 10^9 molecules cm^{-2} s^{-1} used in a 1D model study of BL halogens in the spring at Halley by Saiz-Lopez et al. (2008). I ran a simulation where this large persistent flux of Br_2 was released over each 24 hour period of the model run, in an attempt to explain the daytime Br_2 and BrCl mixing ratio. Although I was able to reproduce the observed daytime mixing ratio of Br_2 (Figure 5.6a, scaled to higher values), the nighttime values were more than an order of magnitude larger than observed at Halley. The large emission of Br_2 also led to near-complete O_3 destruction immediately after the solar zenith angle (SZA) fell below 88.9° (model "sunrise") on the first day.

I then ran the 0-D model with an imposed diurnally varying Br_2 flux, which was coupled to the SZA (Figure 5.6b). It was set so that there was no flux during the model night time, and the daytime flux varied with SZA. Again I was able to reproduce the daytime Br_2 observations (as well as BrCl) (only on the second and third days of the model run), but even with no emissions at nighttime Br_2 mixing ratios were more than double the observed value at night (See Figure 5.1), and BrCl was an order of magnitude larger than observed). Neither of these model simulations was able to reproduce results comparable to both daytime and nighttime Br_2, or BrCl.

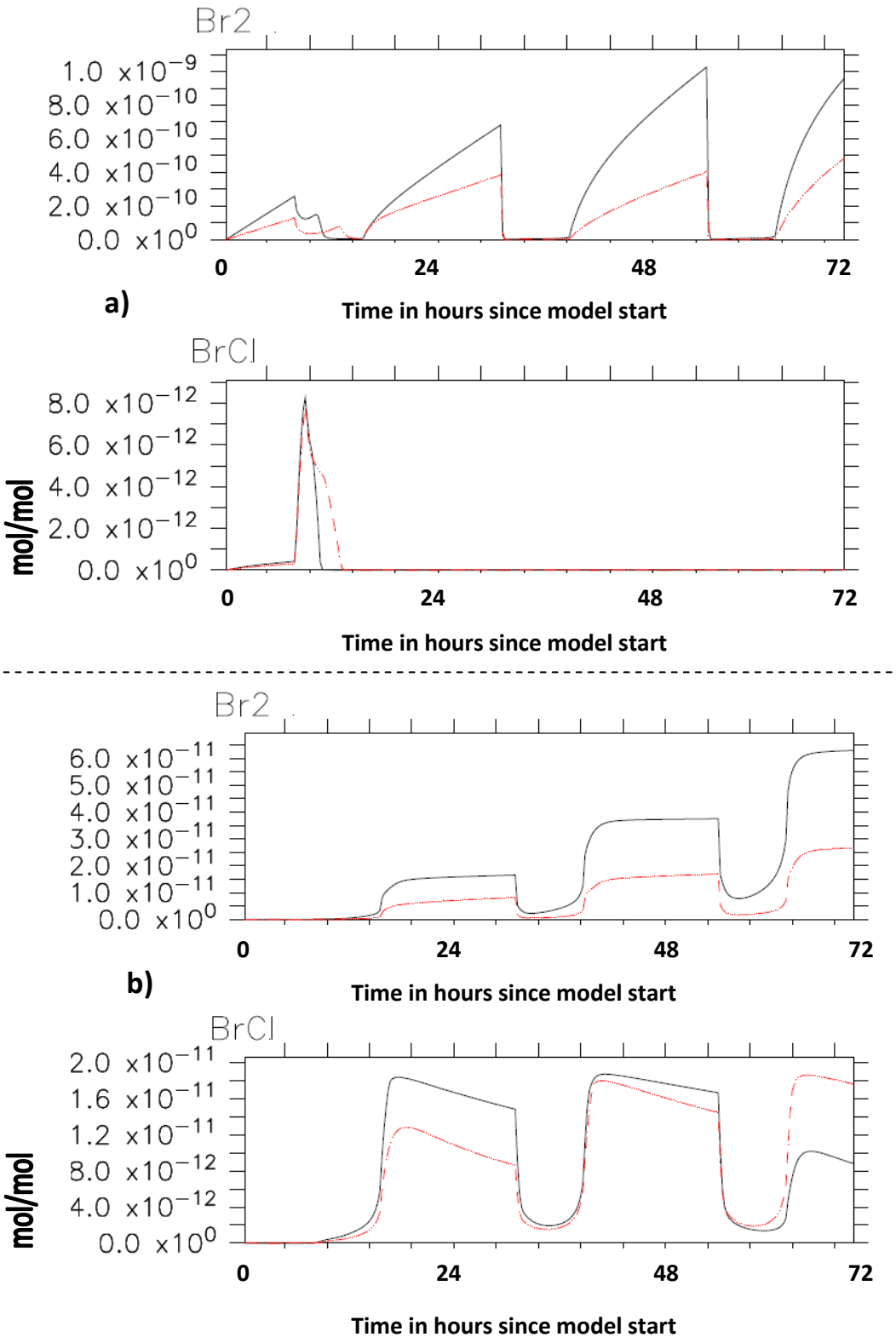

***Figure 5.6**: Time evolution of Br_2 and BrCl simulated with MISTRA 0-D with a) run with constant Br_2 flux of $1x10^{10}$ molecules cm^2 s^{-1}, and b) run with subroutine coupling halogen flux to SZA with a high daytime flux of Br_2. In each case two scenarios are plotted, assuming a BL height of 100m (black lines) and 200m (red lines), respectively. Note the different vertical axis scales in a) and b).*

In the final 0-D model calculation, I derived the flux of bromine required to achieve the nighttime maximum Br_2 mixing ratio for the 6th September 2007 according to the amount of time an air parcel had spent over newly-forming sea ice, which is the expected source region of bromine. Back trajectories run every 2 hours for the 24 hour period covering the 6th September all show a similar path over the newly forming sea-ice in Precious Bay. I assumed a constant emission of Br_2 from the sea-ice zone, and simulated this by release of a constant Br_2 flux over this 24 hour period (similar to the previous runs of high Br_2 flux; Figure 5.6) . A flux of $8x10^7$ molecules cm^{-2} s^{-1} was required to reproduce the nighttime halogen measurements at Halley during this event. This flux is similar to that simulated by Toyota et al. (2011), but much smaller than the flux set by Saiz-Lopez et al. (2008).

The initial Br_2 value (of 6ppt) used for the model runs were chosen to match the CIMS measured Br_2 value for the 6th September 2007, which has a BL height of 200m (SODAR), and a constant Br_2 flux of ($8x10^7$ molecules cm^{-2} s) was calculated to reproduce the night-time Br_2 measurements. The same initial value of Br_2 was used for the run of 7th September 2007, which has a BL height of 100m (SODAR). HYSPLIT back trajectories of air parcel movement highlight that for both the 6th and 7th of September 2007 the air arriving at Halley has spent near equal time (~6hrs) over Precious Bay. This means that the constant Br_2 flux used in the model can be kept the same for both runs so that the only variable is the height of the BL.

Figures 5.7a and 5.7b show both the observations of Br_2 and BrCl and their equivalent modelled output from MISTRA-0D for the latter flux experiment described above. The model lines stop before the data as the model runs are 24hrs long (00:00 – 00:00). It is immediately evident that there are several clear differences between the basic model output and the observations. Firstly, according to the model, daytime mixing ratios of both Br_2 and BrCl should be zero, but the measurements show a clear daytime signal for both Br_2 and BrCl. And secondly, observations of BrCl show a first peak around noon, followed by a second larger peak around 18:00, while the model only simulates a single peak. In light of the potential HOBr interferent, model output was re-plotted, assuming that varying fractions of modelled HOBr are detected by the CIMS as Br2 and BrCl. The results are shown in Figures 5.7c and 5.7d. The initial linear increase in the model run is caused by the constant flux of Br_2 without a significant sink being active. As the model runs start at midnight there is no significant destruction of Br_2 until photolysis starts, at which point the influence of the assumed conversion of HOBr to Br_2 mixing ratio becomes noticeable. Inclusion of this assumed “HOBr interferent” clearly improved agreement between the model and measurements in terms of the daytime mixing ratio amount. Further, for BrCl, inclusion of

the artefact yielded a double peak, as observed in the measurements due to the presence of HOBr during the day and possibly early hours of the night.

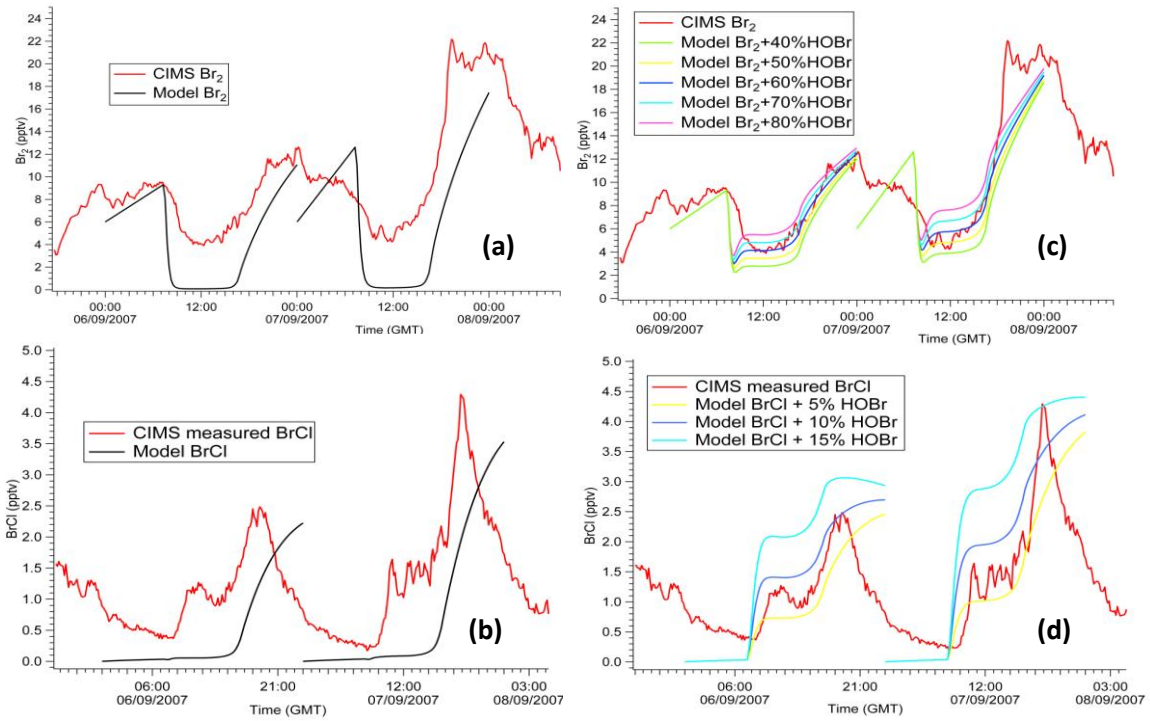

Figure 5.7: *a) comparison between measured (with CIMS) and modelled Br_2 for the 6th and 7th September 2007; b) as for a) but this time showing BrCl ; c) 40%, 50%, 60%, 70%, and 80% of model HOBr added to model Br_2 ; d); 5%, 10% and 15% of model HOBr added to model BrCl*

5.3.2. Calculations with MISTRA 1-D

The initial assumption in the above calculations, regarding the MISTRA 0-D simulations being non height-specific does not take into account vertical gradients such as those introduced by any snowpack emissions. To assess this influence, I used the MISTRA 1-D model to reproduce the BL structure as characterised by the meteorological measurements from Halley. I used the measurements from both the met mast and sodar instrument to initialise the meteorology for these 1-D runs, and initialised the chemistry as for the 0-D simulations. When I used the same Br_2 flux as above, of $8x10^7$ molecules cm^{-2} s^{-1}, the mixing ratios of Br_2 in the model level corresponding to 4.5-7.5m above the snow surface were higher than for the 0-D simulations and did not reproduce the measurements. I found that reducing the Br_2 emission slightly to $6x10^7$ molecules cm^{-2} s^{-1} (the lowest flux derived by Toyota et al., 2011), the model was better able to reproduce the measured Br_2 for the model level representing 4.5-7.5m in height (see Figs 5.8a and 5.8b). This is in line with what I would expect given that in the model Br_2 is emitted from the surface, leading to higher mixing ratios near the surface and dropping off as the distance to the surface increases. While I was not able to reproduce the daytime Br_2 and BrCl measurements in their entirety with the 1D runs, Figs 5.8a and 5.8b again show that inclusion of a proportion of modelled HOBr into both Br_2 and BrCl significantly improved agreement with the daytime observations.

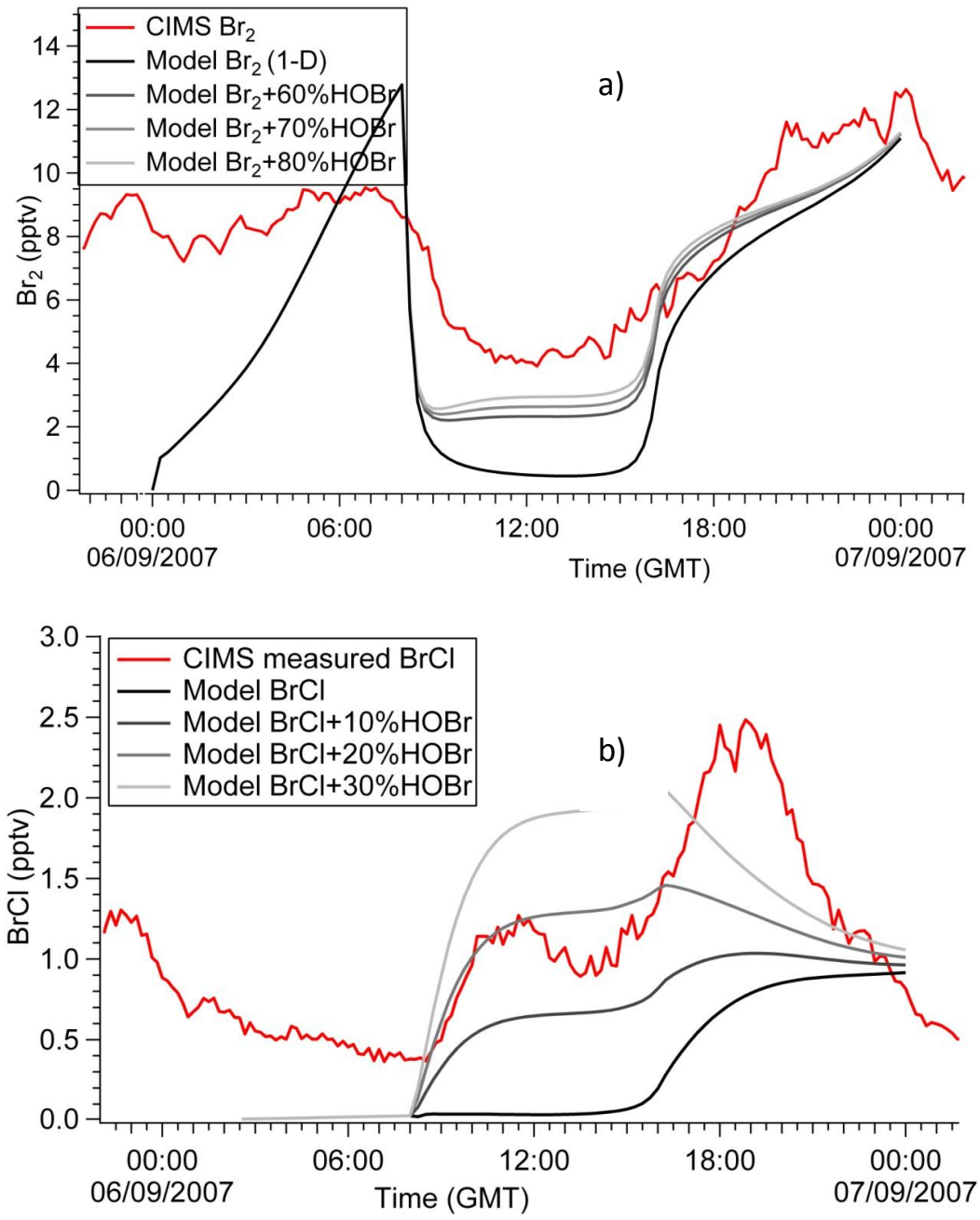

Figure 5.8. *a) comparison between Br_2 measured with CIMS and that modelled with MISTRA-1D, with 60%, 70% and 80% of model HOBr added to model Br_2 ; b) as for a) but with 10%, 20% and 30% of model HOBr added to model BrCl. Both 1D model outputs e) and f) correspond to a height of 4.5-7.5m above the snowpack.*

5.4. Data filtering methodology to address the apparent CIMS artefact

Thus the results from both the 0-D and 1-D MISTRA model simulations are consistent with an artefact representing a conversion of HOBr to Br_2 in the inlet of the CIMS of the order of several tens of percent, with that for HOBr to BrCl being noticeably less but non-negligible. This conclusion is in line with Liao et al. (2012b), who corrected their hourly-averaged diurnal profiles of Br_2 and HOBr observed at Barrow assuming 20% conversion in the inlet.

Although a conversion factor was not mentioned directly by Neuman et al. (2010), it was possible to deduce from their plot of HOBr conversion to Br_2 that 40% of the HOBr was converted to Br_2 when using the 'Teflon Aircraft Inlet' (comparing to the 'Instrument Response'). With the CIMS measurements at Halley likely conducted at much colder temperatures than the laboratory tests, Figures 5.7c, and 5.8a show that a higher % of HOBr converted to Br_2 gives a better fit to the CIMS measurements. Also from the tests in Neuman et al. (2010), I found that the conversion on the Teflon Inlet left 0.5ppb of excess HOBr (20%) which is available for conversion to other compounds such as BrCl. BrCl has a photolytic lifetime of roughly 100s (Mahajan et al., 2009), and is therefore unlikely to be abundant during daylight in the polar BL. Figures 5.7d, and 5.8b show that by adding a fraction of HOBr to the modelled BrCl values it is possible to reproduce the CIMS BrCl measurements. Of the 20%HOBr available for conversion to other species (Neuman et al., 2010), this would appear to be enough which if converted to BrCl gives a better fit.

The temperatures at which the laboratory tests by Neuman et al. (2010) were conducted are not reported in their paper. However, a series of model experiments using MISTRA 0-D were run at different temperatures with the results suggesting the conversion of HOBr to Br_2 and BrCl may be slightly temperature dependant. I should say though, that although the air entering the inlet was at 230-240K, a large part of the inlet tube was warmed to 40°C which would lead to a strong temperature gradient along the inlet possibly affecting the fraction of HOBr conversion.

In order to analyse the data-set to its full extent the day time measurements were removed, and only the nighttime measurements used (unless otherwise mentioned in other chapters). The short photolytic lifetimes of these compounds (on the order of a minute) mean that they are influenced greatly by sunlight.

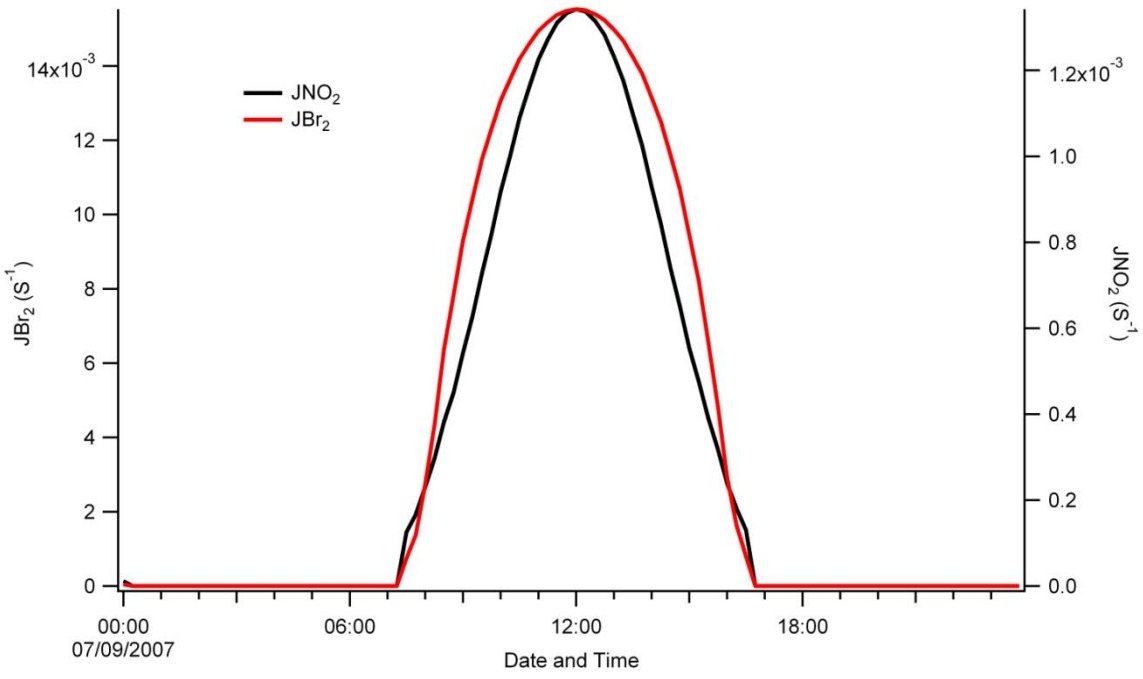

Figure 5.9: *A comparison of MISTRA model output for JNO_2 and JBr_2 for 07/09/2007.*

J_{NO2} was used as a proxy for J_{Br2} only because the J_{Br2} data were not available at the time of the analysis and data filtering. The absorption cross section for Br_2 is very similar to that of NO_2 (DeMoore et al., 1997; Maric et al., 1994). Although the magnitude of the NO_2 cross section differs, they both peak at ~ 410nm. Although the quantum yields differ for these species, they are not completely dissimilar. Of importance here is the timing of photolysis at sunrise and sunset, and as Figure 5.9 shows the timing of photolysis for model output J_{NO2} and J_{Br2} is the same. This therefore allowed me to use the measured j_{NO2} data from Halley as a proxy for the onset/ termination of Br_2 photolysis at this location. The data required a small amount of work prior to filtering the data (removal of negative values etc.), and some modification to an established filtering procedure was needed to allow the daytime values to be removed.

During their field observations at Barrow, Liao et al. (2012b) only observed HOBr above detection limits when $J_{Br2} > 0$. These observations are consistent with theory - no sources of HOBr at night are known for polar regions as all known production pathways require photolytic reactions. Therefore it is reasonable to assume that no HOBr is available for conversion to Br_2 at night. However, as there are no coincident HOBr measurements from Halley, clearly this means that there is still some uncertainty in the influence of HOBr for the Halley case. Nonetheless, for the purposes of this work, and given the evidence for an artefact in CIMS daytime

measurements of Br_2 and BrCl caused by conversion of HOBr in the inlet, all Halley plots are colour coded to differentiate between daytime ($J_{NO2} > 0$) and nighttime ($J_{NO2} = 0$) observations of Br_2 and BrCl, showing all daytime measurements in black.

6. Results Part II: Halley dataset and context

Synopsis:

This chapter will cover the main data results, and put them into context. Firstly I will look for relationships between species within the data, filtered to remove the influence of the interferent in the day-time CIMS Br_2 and BrCl measurements (see chapter 5), then an overview of the most important aspects of the data set will be given.

6.1. Br_2, BrCl, BrO and O_3 timeseries

Although this was a year round measurement campaign at Halley, the CIMS instrument was only configured for detection of Br_2, BrCl and BrO for specific periods. Here I focus on a measurement period in austral spring, from 12th August to 18th September 2007, a time which, according to previous work at Halley (Saiz-Lopez et al., 2007), is likely to have active bromine chemistry.

The CIMS technique has been used to detect halogens in several previous polar field campaigns (Foster et al., 2001; Spicer et al., 2002; Neuman et al., 2010; Liao et al., 2011a; Liao et al., 2011b; Liao et al., 2012b). In contrast to issues with Br_2 and BrCl observations discussed in Section 3.1 and Chapter 5, a recent comparison of Arctic ground-based observations of BrO made using both a CIMS and a long-path DOAS showed good agreement when air masses were well mixed (Liao et al., 2011b). I therefore assume that all BrO observations made at Halley are interferent-free.

6.1.1. Overview of the data

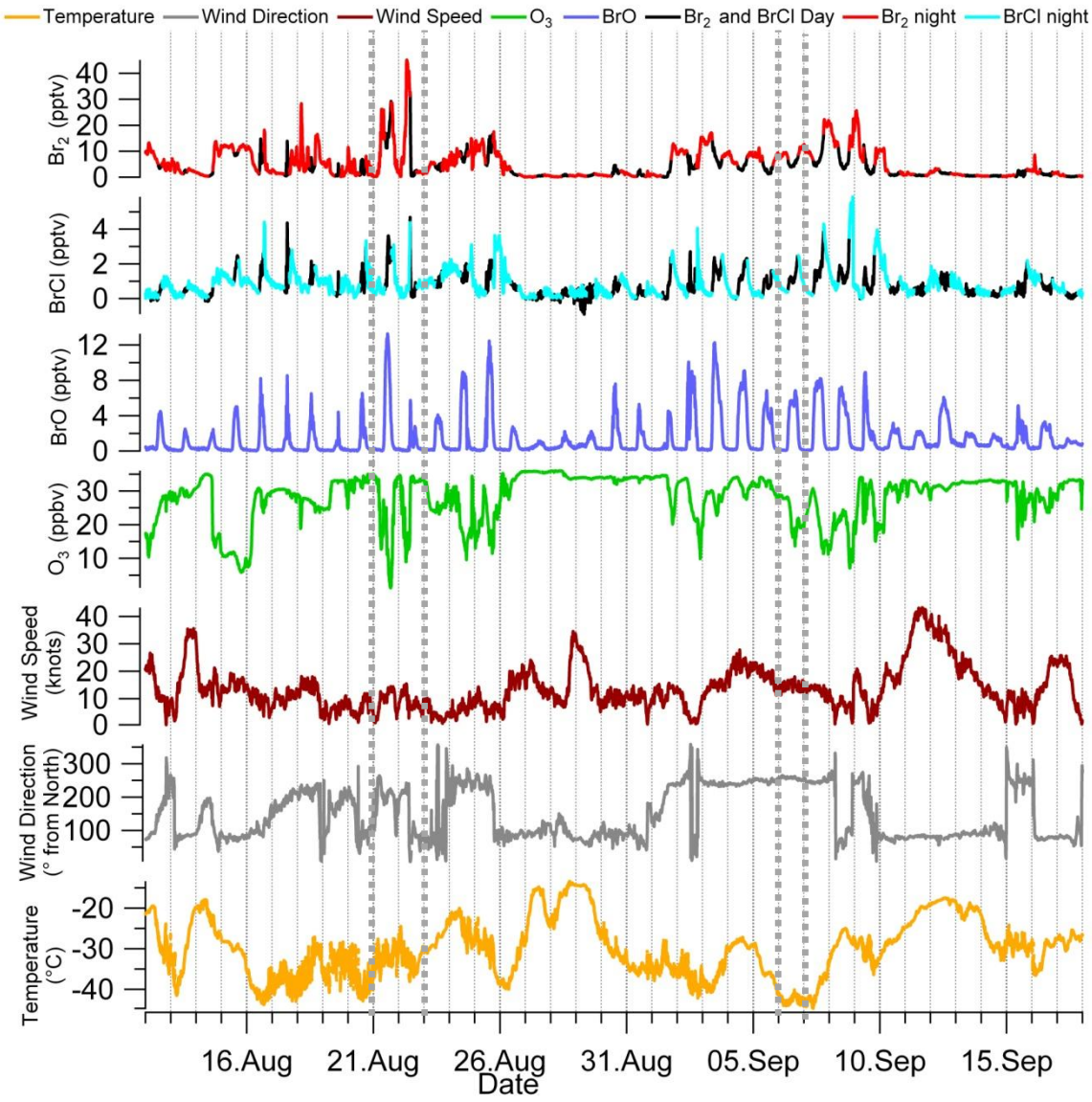

Fig. 6.1: *Overview of measurements at Halley from 12th August to 18th September 2007. Br_2, BrCl and BrO are shown as 10 minute averages; for Br_2 and BrCl, daytime observations are coloured black. Also shown are surface O_3 (10 minute averages), local wind speed and direction, and local temperature. Tick marks on the x-axis denote midnight.*

Figure 6.1 presents the time series of Br_2, BrCl, BrO and surface O_3 together with concurrent meteorological observations of local wind speed/direction and local temperature for the entire measurement period.

	BrO	***Br_2***	***BrCl***
Sensitivity Hz pptv^{-1}	***4.9***	***4.9***	***4.9***
2σ detection limit for 10 min averages (pptv)	***0.6***	***0.4***	***0.1***
Maximum observed (pptv)	***13.3 (Day)***	***45 (Night)***	***5.9 (Night)***
Mean nighttime observation (pptv)	***-***	***5.8***	***1***
Standard deviation of 10 min average (pptv)	***2.2***	***6***	***1***
Measurement uncertainties	***±27%***	***±11%***	***±11%***

Table 6.1, overview: *Instrument parameters and overview of observations for BrO, Br_2 and BrCl for the period 12/08/07-18/09/07. Details of measurements (max, mean, and standard deviation) for Br_2 and BrCl are based on nighttime observations only – see Section 3.2. Minimum values were below detection limits for all three species.*

Br_2 mixing ratios vary from below instrument detection limits (refer to Table 6.1) to a maximum of 45 pptv (observed at night) and BrCl from below detection limits to ~6 pptv (at night). As shown in Fig. 6.1, there is considerable variability in the Br_2 and BrCl observations over the measurement period which is strongly linked to the prevailing meteorology and thus air mass origin. Relatively low and invariant Br_2 and BrCl is generally associated with easterly winds of continental origin with higher mixing ratios in air masses that have passed over sea ice to the west/south west. Surprisingly, the highest measured mixing ratio of Br_2 and the lowest measured surface ozone, appear to be associated with a long-range transport event where air is arriving at Halley from across the continent via the South Pole, with its last sea ice contact somewhere to the west of the Antarctic Peninsula. This is discussed further in Chapter 7.

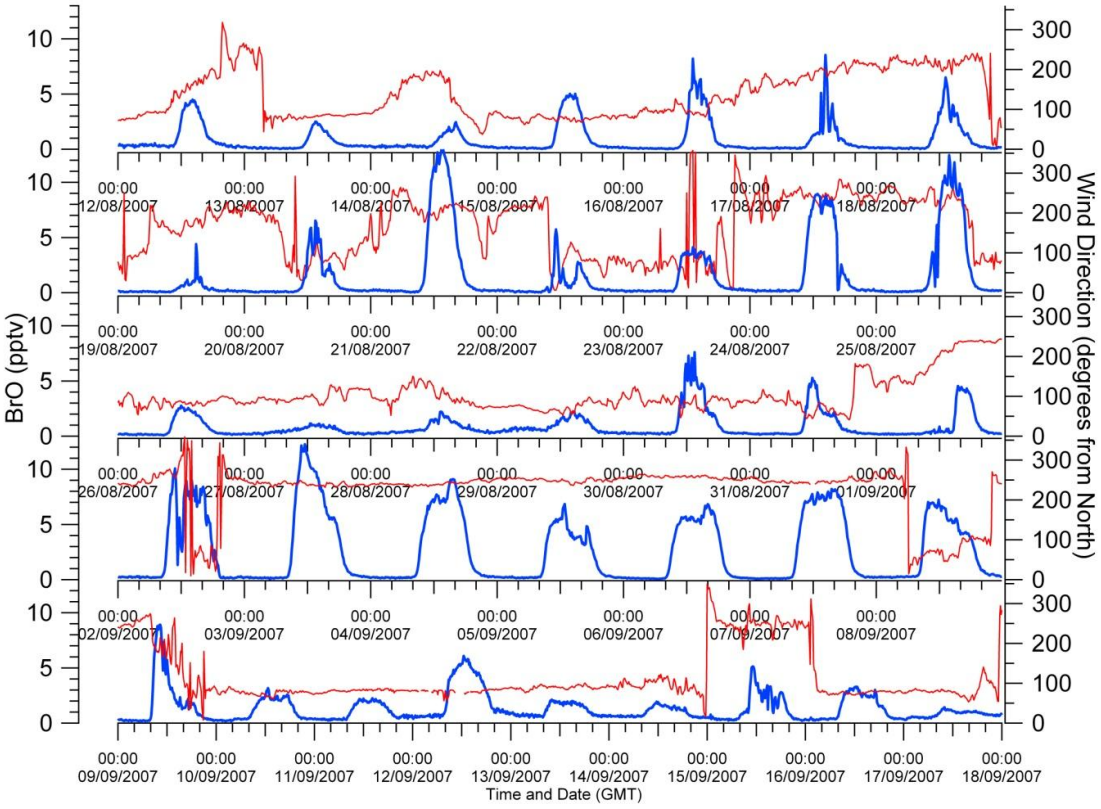

Fig. 6.2: *Time series showing variability of BrO mixing ratio (left y-axis), wind direction (right y-axis) with date and time on the x-axis for the period (12/08/07 – 18/09/07)*

The range of BrO mixing ratios during the measurement period, from instrumental detection limits to ~13 pptv (Fig 6.2), are in line with previous observations at Halley (Saiz-Lopez et al., 2007) made using a long-path DOAS. The BrO maxima at Halley are less obviously correlated with local wind direction than are Br_2 and BrCl. For example, from 27th August until 1st September, while the prevailing wind direction is easterly (implying continental air), Br_2 and BrCl show little variability, and there is no ODE, BrO maintains a diurnal structure with daily maxima ranging from ~2 pptv to ~7 pptv. These values are in line with daytime BrO measured previously at Halley in air of continental origin (Saiz-Lopez et al., 2007). The presence of a diurnal variability in BrO throughout the measurement period suggests that some persistent background bromine/ozone chemistry is active during the day, even when air is not approaching from directly across the sea ice zone (Figure 6.2). This is discussed further in Chapter 7.

Easterly winds which have passed over the continent normally dominate throughout the year but during the austral spring roughly equal (+/-10%) amounts of westerly winds were observed.

Winds from the near coastal regions (200 - 300 degrees) were shown to contribute most (>85%) to Br_2 and BrO concentrations of greater than 5 pptv and 6 pptv respectively.

6.1.2. Period of sustained surface O_3 depletion

Background ozone is 30-35 ppbv (Fig 6.1), with ODEs evident throughout this time period. The most sustained of these (>24 hours) was observed from the 14th to 16th August. O_3 mixing ratios dropped from a background of 33ppbv to 18ppbv (a change of 15ppbv) over a 20 minute period (15:20 – 15:40) on 14 August and continued to decrease to a minimum of 6ppbv in the following 24 hours. This rapid change in [O_3] suggests transport of an ozone depleted air mass to Halley. ECMWF ERA Interim re-analysis plots of mean surface pressure and 10m wind speed vectors indicate that a low pressure system was present over the Weddell Sea sea ice for several days before coming into contact with Halley (Figure 6.3). At noon on 13 August, 10m wind speeds were >12ms^{-1} over the central Weddell Sea and >16ms^{-1} at the northern Weddell Sea near the sea ice edge (Figure 6.3). Wind speeds >12ms^{-1} can create 'blowing snow' conditions (Jones et al., 2009), and Yang et al. (2008) suggest lofted snow on sea ice can give rise to enhanced tropospheric bromine which can then react to destroy ozone. As the low pressure system moved over Halley wind speeds dropped to <4ms^{-1}. This suggests that the high wind speeds (>16ms^{-1}) observed at the northern Weddell Sea sea ice zone on the 13 August could be the driver of the ODE measured at Halley on the 14-16 August. The air mass is first depleted in ozone, then transported to Halley where the wind speeds drop and the ozone depleted air mass resides over Halley for >24 hours. There is then a rise in O_3 from 10 – 25 ppbv from 04:00 – 06:00 on 16 August, signalling the end of the ODE. This replenishment of O_3 may be caused by a shift in the balance of air flow from sea ice zone (low pressure system) and from the continent (orographic flow).

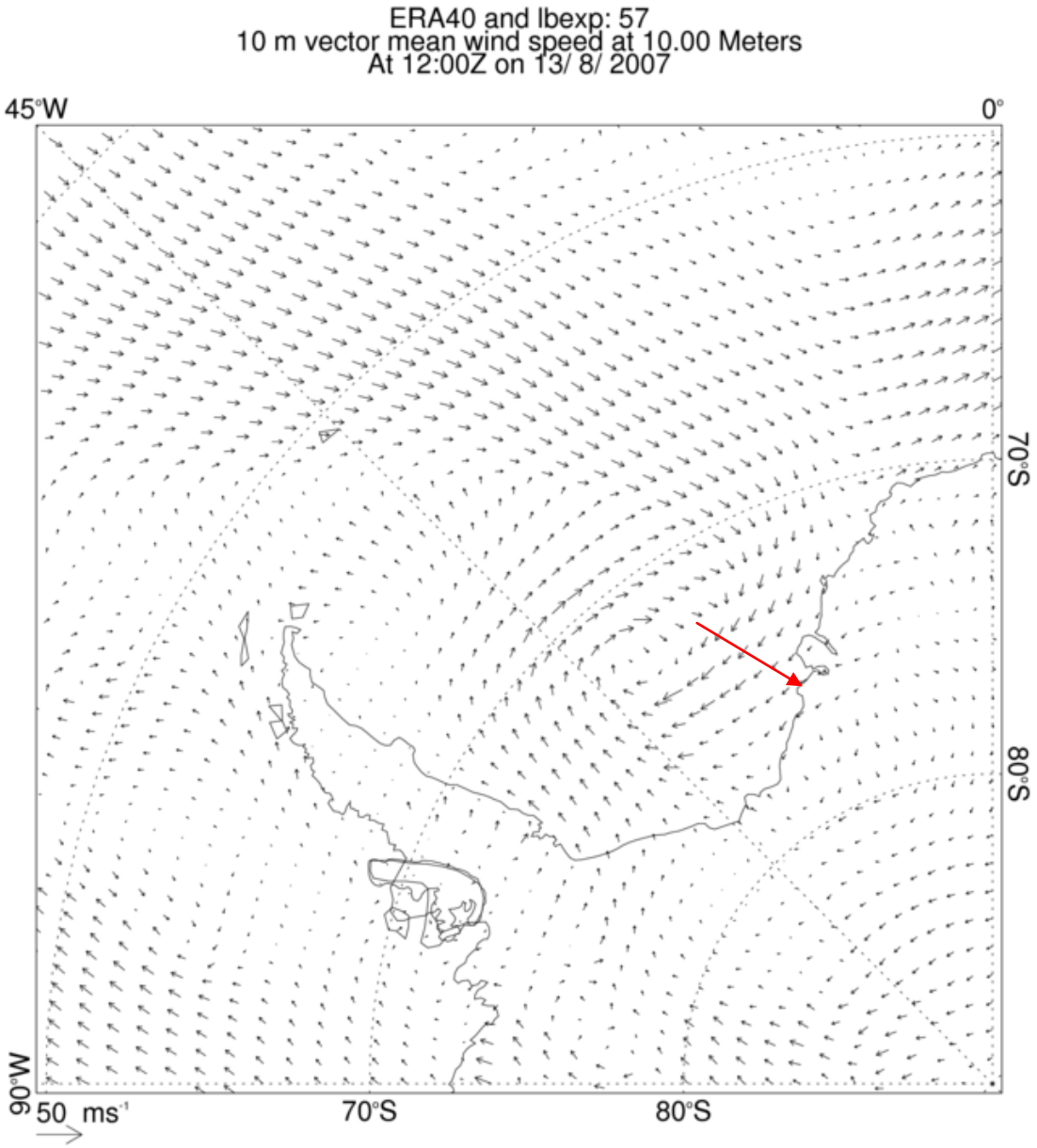

Figure 6.3: *ECMWF analysis output of 10 meter wind vector for the area containing Antarctic Peninsula and Weddell Sea at 1200 hrs on 13/08/2007. The location of Halley is given by the red arrow.*

6.2. Diurnal variability in BrO, Br_2 and BrCl

6.2.1. Diurnal variability in BrO

BrO exhibits a clear diurnal cycle throughout the period of CIMS observations, with nighttime minima around instrumental detection limits (Figure 6.2). The characteristic of the daytime maxima vary from day to day , being either i) a single peak around noon (Figure 6.4a), ii) a broad flat-topped maximum also around noon (Figure 6.4b), or iii) double peaks with maxima shortly after sunrise and shortly before sunset (Figure 6.4c). Such double-peaks were also observed by Pöhler et al. (2010) during springtime measurements in the Amundsen Gulf, and in springtime observations at Barrow, Alaska (Liao et al., 2012b). A model study by von Glasow et al. (2002) also showed this distinct diurnal structure of a BrO minimum around noon, and maxima in the morning and evening. In their model calculations this was caused by differences in the photolysis spectra of O_3 and Br_2, where Br_2 is more rapidly photolysed in twilight than O_3 due to absorption at longer wavelengths.

BrO concentrations are a balance of sources and sinks. The main source of BrO is photolysis of Br_2 followed by reaction of the Br atoms with ozone. The main sink of BrO under polar conditions is reaction with HO_2, highlighted by the following reactions:

$Br_2 + hv \rightarrow 2Br$ (R3, from chapter 2)

$Br + O_3 \rightarrow BrO + O_2$ (R1, from chapter 2)

$BrO + HO_2 \rightarrow HOBr + O_2$ (R4, from chapter 2)

At high solar zenith angles (such as morning and evening) BrO is already produced efficiently, but HO_2 only at lower SZAs. HO_2 itself is photolytically produced by way of O_3 photolysis. Hence the efficiency of the HO_2 sink is highest during the hours around noon causing the dip in BrO mixing ratios around noon in double-peaked profiles or the reduced noon maximum in the flat profiles (Fig 6.5).

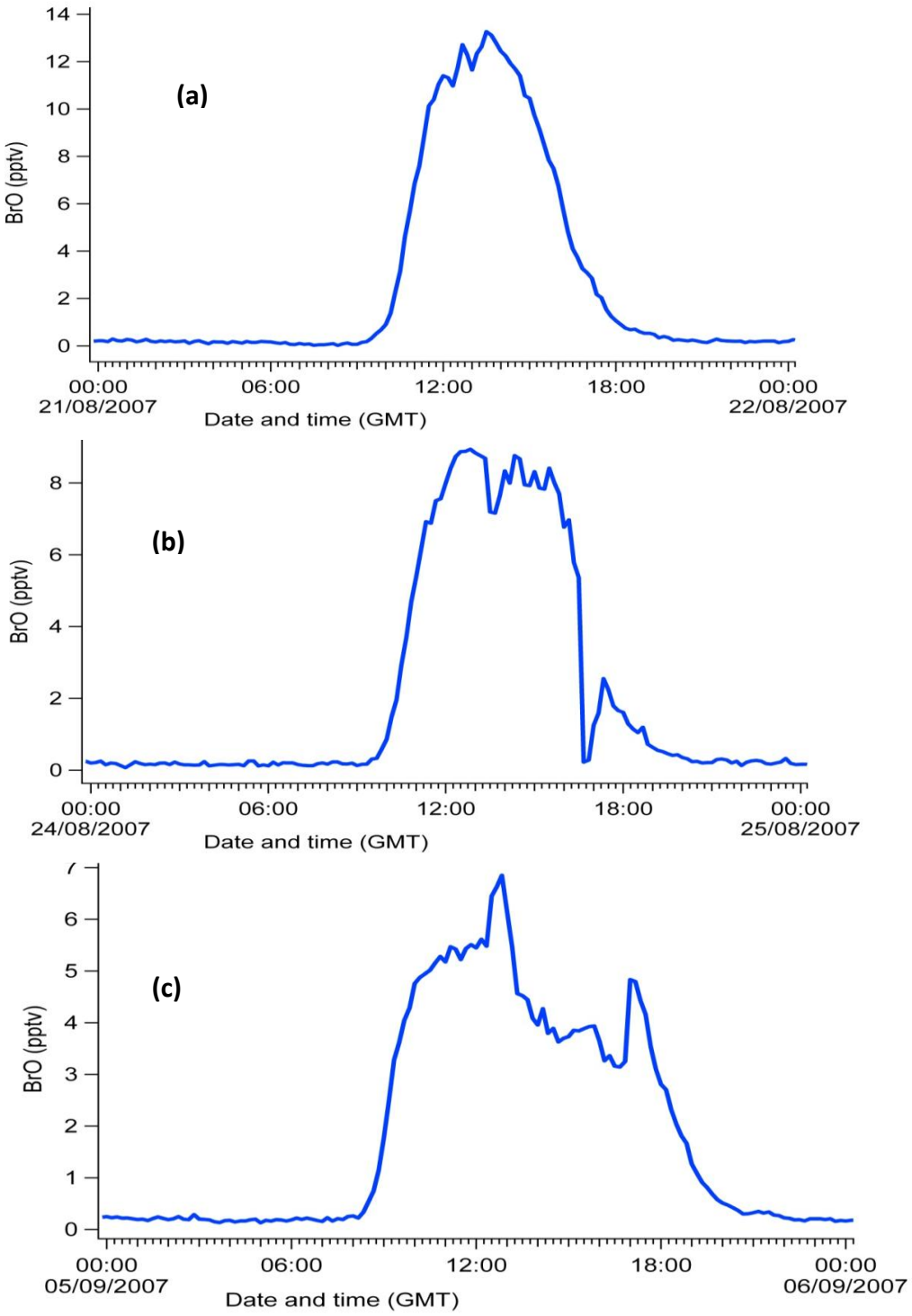

Fig 6.4: *Plots showing diurnal shape of BrO in pptv with time and date on the x-axis. a) a single peak around noon; b) a broad flat-topped maximum also around noon; and c) double peak with maxima shortly after sunrise and shortly before sunset.*

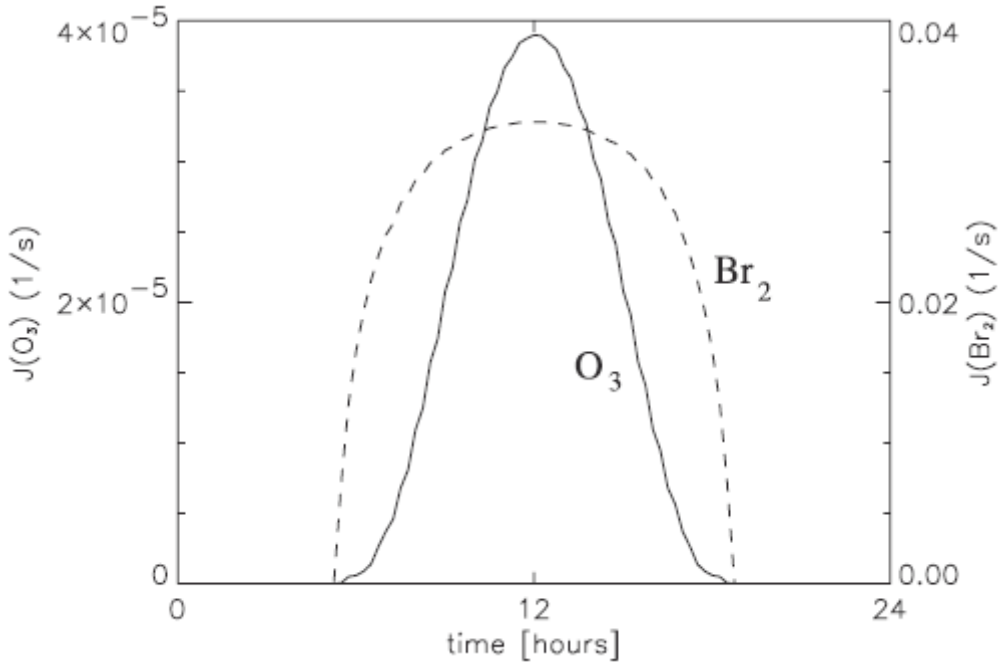

Fig. 6.5: *Diurnal variation of the photolysis frequencies for O_3 and Br_2 (note different units). The difference in the shape of the diurnal variation is the cause for the noon minimum in BrO mixing ratios (taken from von Glasow et al., 2002a).*

The occurrence of flat-topped maxima and double peak BrO increases at Halley as the spring season progresses away from polar night. To explore this changing BrO diurnal shape as the measurement period progressed, two model simulations were run using MISTRA 0-D (Figure 6.6). Figure 6.6a is a model simulation set with a solar declination angle, ϕ, representative of the beginning of the measurement period (13 August, ϕ = 14.5°) and Figure 6.6b with a solar declination representative of the end of the measurement period (18 September, ϕ = 1.9°). Figure 6.6a clearly shows a single BrO peak around noon. At this time of year days are very short, the SZA is very high and O_3 UV photolysis is low, and insufficient HO_2 is produced to reduce BrO mixing ratios significantly to give a noon minimum. The BrO mixing ratios in Figure 6.6b, however, show a clear morning peak followed by a minimum around noon and rising again to a second less-well-defined maximum just prior to sunset. Here days are long enough to allow sufficiently low noon-time SZAs, implying that sufficient HO_2 is produced to reduce BrO mixing ratios leading to a minimum around noon. The BrO+BrO self reaction also removes two molecules of BrOx and introduces a squared dependence.

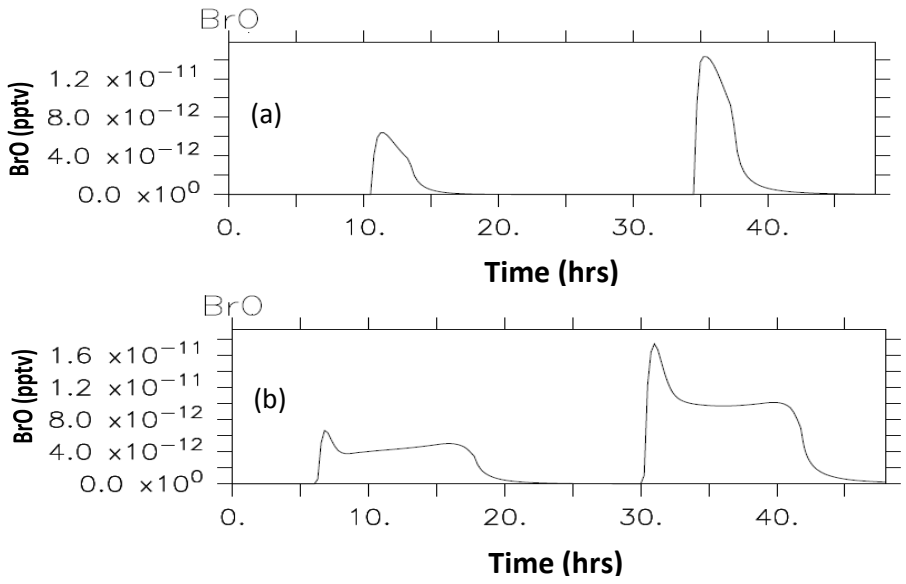

Figure 6.6: *BrO model output from MISTRA 0-D showing a) a single BrO peak around noon when solar declination is set to represent early spring at Halley; and b) a double BrO peak with a maximum in the morning and evening, with a noon time minimum when solar declination is set to represent late spring at Halley.*

6.2.2. Diurnal variability in Br_2 and BrCl

Figure 6.7 shows the hourly mean diurnal variability for the entire measurement period for Br_2 (Figure 6.7a) and BrCl (Figure 6.7b), the three lines on each plot representing i) all data, ii) air with a sea ice zone origin, and iii) air with a continental origin (as determined from local wind direction). Daytime components of Br_2 and BrCl are indicated by black lines, and each species has uncertainties of +/- ~11% associated with them. The data immediately demonstrate the importance of filtering according to air mass origin when calculating averaged diurnal cycles for these halogen species from coastal observations.

Focussing on the hours from midnight to dawn, take note (Fig. 6.6a) that the hourly-averaged Br_2 mixing ratios increase over this time period in air with a sea ice zone origin. The potential for out gassing of Br_2 from sea salt aerosol at night has been demonstrated in modelling calculations by von Glasow et al. (2002a), driven by gas-aqueous partitioning from gas-phase BrCl as shown in reactions below:

$BrCl \rightarrow BrCl_{aq}$ (R12, from chapter 2)

$BrCl_{aq} + Br^- \rightarrow Br_2Cl^-$ (R13, from chapter 2)

$Br_2Cl^- \rightarrow Cl^- + Br_{2aq}$ (R14 from chapter 2)

$Br_{2aq} \rightarrow Br_2$ (R15 from chapter 2)

Such increases in Br_2 are not evident in air with a continental origin (Fig. 6.7a), where the Br_2 mixing ratios decrease between midnight and dawn.

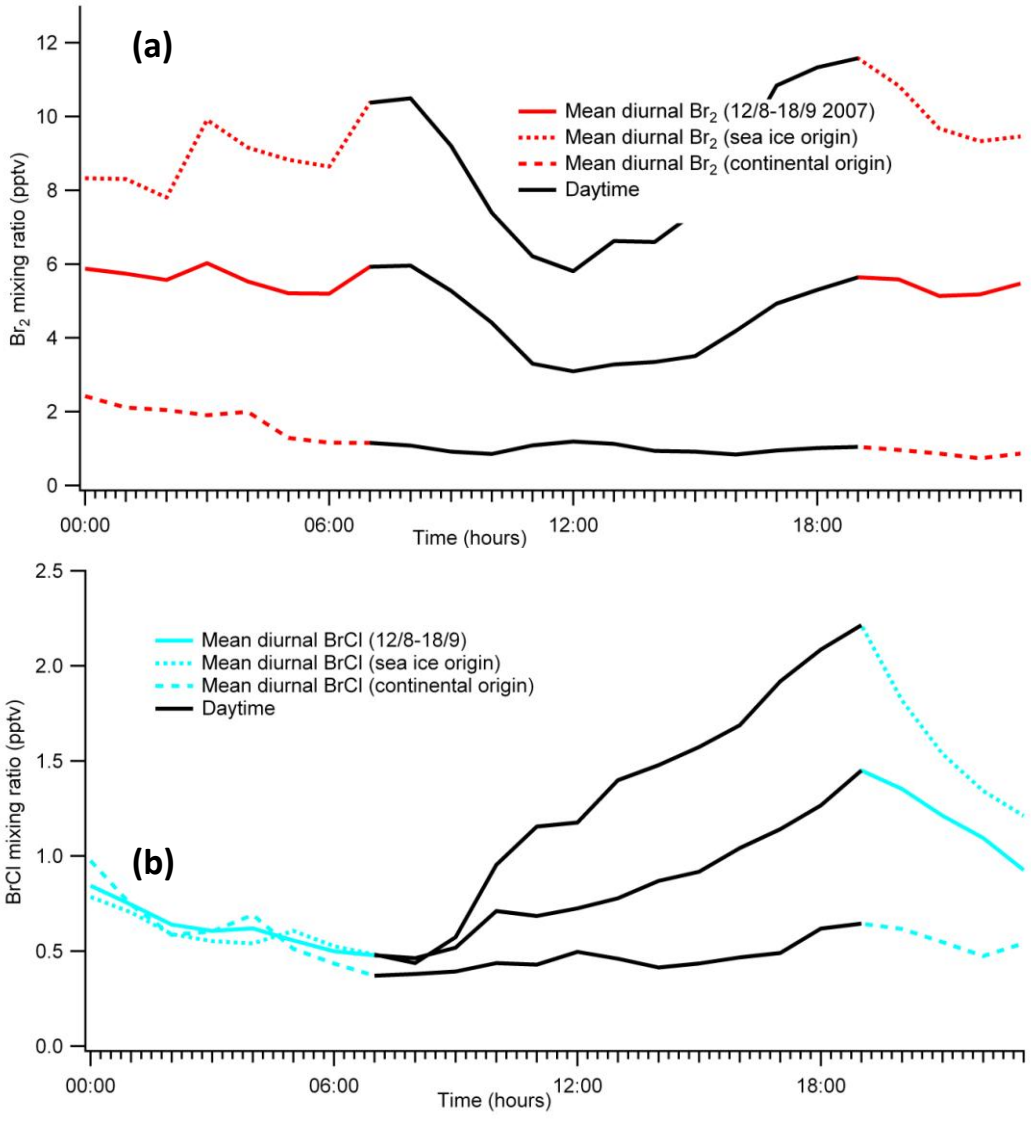

Figure 6.7: *Hourly mean diurnal plots of a) Br_2, and b) BrCl for all the data, and for different source regions (sea-ice zone; continental).*

The reduction in hourly-averaged BrCl between midnight and dawn in sea ice zone air (Fig. 6.7b) is consistent with uptake and re-partitioning to Br_2 (although not sufficient to account for all the observed Br_2 increase). It is somewhat surprising, however, that BrCl mixing ratios are the same regardless of the source region, particularly given that Br_2 mixing ratios in the same air masses change. The observations suggest uptake of both Br_2 and BrCl onto surfaces at night.

6.3. Br_2:BrCl ratios

6.3.1. Source region influence

As discussed previously, air masses arriving at Halley during spring generally have either a continental or a sea ice zone influence. Here I will look at a more detailed picture of the influence the sea ice zone and continental snowpack have on Br_2:BrCl ratios.

Figure 6.8 shows the ratio of Br_2:BrCl derived from the Halley nighttime observations, and colour coded for local wind direction. There is considerable variability in the ratio much of which is clearly associated with wind direction and thereby halogen source region. For example, from 10th September onwards, the ratio is very low, as are the mixing ratios of both Br_2 and BrCl (see Figure 6.1), resulting from air masses with little/no sea ice contact. These air masses have little/no ozone depletion. In contrast, air masses with an origin from the sea ice zone (e.g. 3rd to 8th September) which are depleted in ozone and enhanced in halogens, have a Br_2:BrCl ratio clearly in favour of Br_2 (~2-100). On a very few occasions the Br_2:BrCl ratio drops below 1 (red dashed line in Figure 6.7). Such low ratios can be attributed to the very low (near detection limit) mixing ratios of both Br_2 and BrCl. Use of a 3σ LOD filter rather than a 2σ filter (Table 6.1) would remove these points.

As discussed in section 3.2.1, recycling of bromine deposited on the snowpack can be a source of gas phase bromine. One explanation for this decrease in the Br_2:BrCl ratio could be that the availability of bromine previously deposited to the snowpack reduces over time, leading to less recycling into gas phase bromine.

In laboratory studies of HOBr uptake on frozen NaCl/NaBr surfaces at temperatures between 253K and 233K, Adams et al. (2002) found that the ratio of the products Br_2:BrCl was a strong

function of the reactant Cl^-:Br^- ratio in the condensed phase. They found for a mixed salt surface of similar composition to sea spray that the major product was Br_2, and that BrCl was only produced when Br^- was significantly depleted. The results were, similarly, interpreted as initial formation of BrCl which, given sufficient Br^-, and then reacted further to generate Br_2.

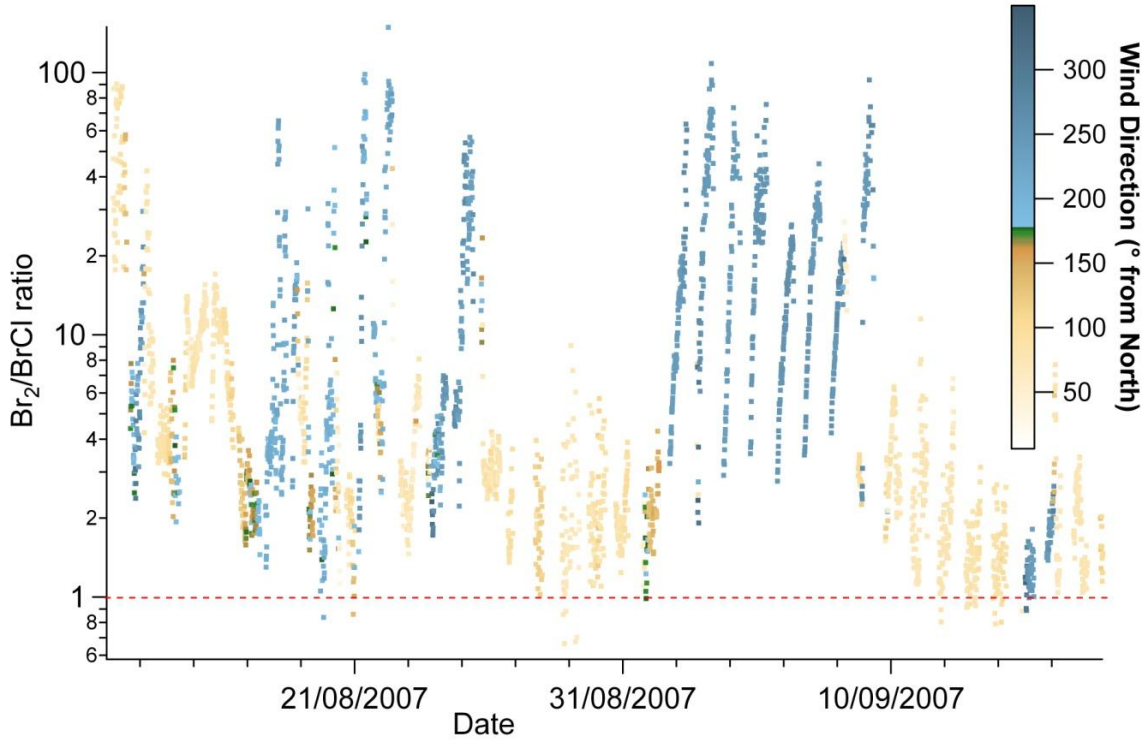

Figure 6.8: *Nighttime ratio of Br_2:BrCl throughout the measurement period on a log scale. The colour coding indicates local wind direction (blues indicate sea ice zone origin; oranges indicate continental origin), emphasising the influence of air mass origin on the calculated ratio. A red dashed line is drawn at a ratio of one to highlight the small number of values found below it.*

6.3.2. Wind speed influence

An initial look at the changes in the ratio of Br_2 to BrCl showed some points of interest (Figure 6.8). It is clear that the ratio leans heavily towards Br_2 when wind is arriving from ~250°, which coincides with the direction of Precious Bay with relation to Halley. There is also a major shift in the ratio at ~ 100° (Figure 6.9a) which is associated with the arrival of air which has skirted the Antarctic coast prior to Arrival at Halley. Air with this origin can also be associated with high

concentrations of halogenated species due to potential contact with sea ice and leads in this area (chapter 7).

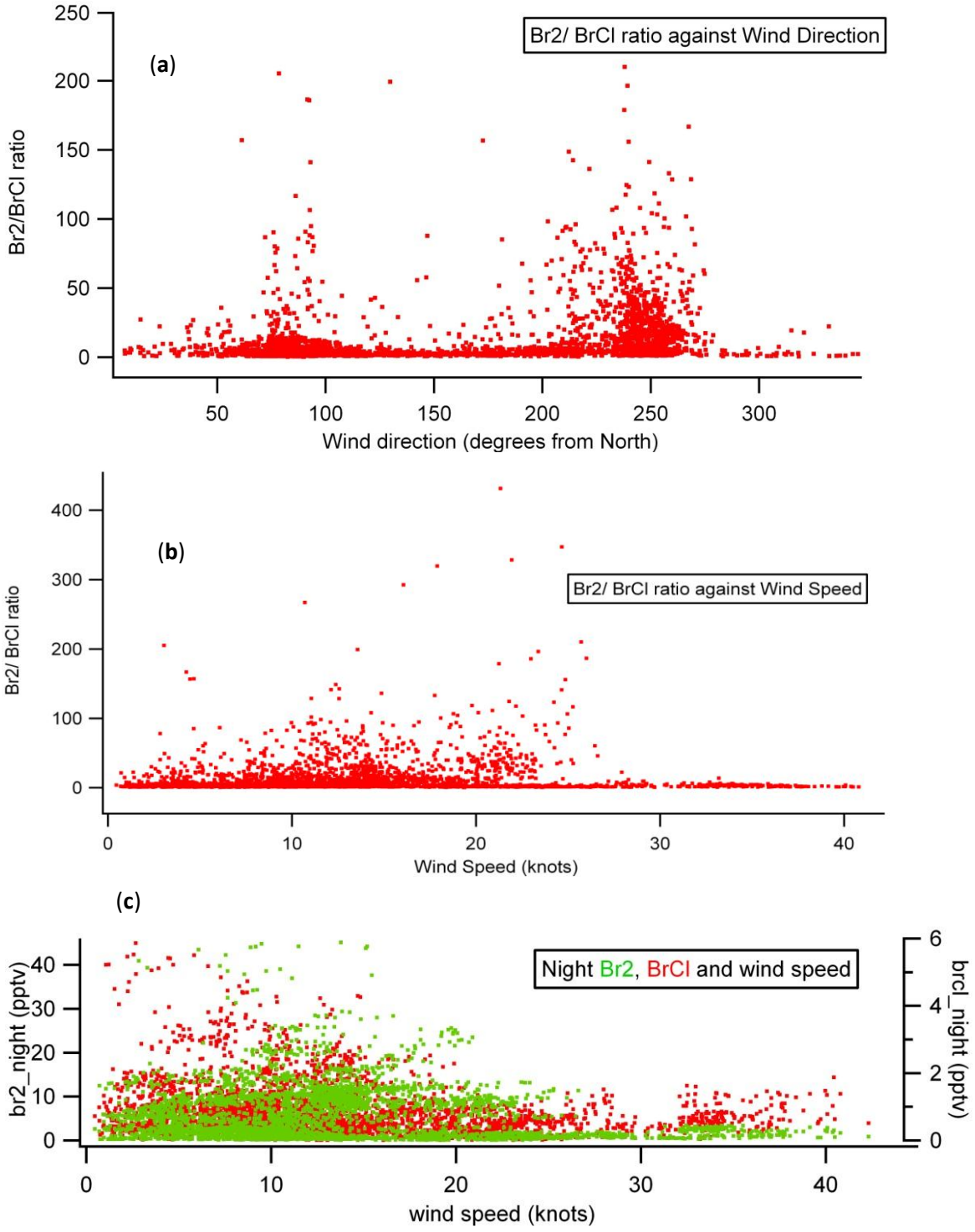

Figure 6.9: *Plots of (**a**) Br_2/BrCl ratio against wind direction, (**b**) Br_2/BrCl ratio against wind speed, and (**c**) night time concentrations of Br_2 and BrCl (pptv) plotted against wind speed at Halley (knots).*

It would appear that high wind speeds are not always associated with high concentrations of halogen. At wind speeds of >20 knots measured at Halley, halogen concentrations decrease rapidly to detection limit levels (Fig 6.9a). The highest concentrations of Br_2 measured are at wind speeds of 5-15 knots. Yang et al. (2008) list u >= 6.75 m/s (~13 knots), and Jones et al. (2009) u =8 m/s (~16 knots) as the threshold for blowing snow, which indicates that the blowing snow hypothesis may not be important for all situations at Halley (Yang et al., 2008 ; Jones et al., 2009). Although it is expected that high Br_2 is seen at the highest wind speeds as well, these observations illustrate that the relationship to wind speed doesn't have to be coincident. High wind speeds on the day before measurements were made would mean that there is no direct correlation with wind speed even though high winds were the source of the high Br_2 mixing ratios (Jones et al. 2010).

Low mixing ratios of ozone (<15ppbv) and low mixing ratios of Br_2 (<2-3pptv) are never measured coincidentally (Fig 6.10). Using the night time only data from Halley, it is clear that ozone concentrations >18ppbv are not measured at Br_2 concentrations > 30pptv.

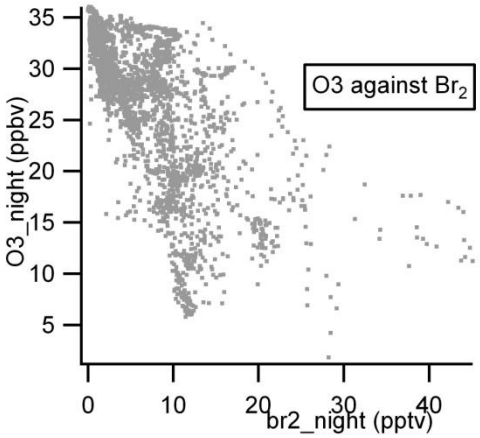

Figure 6.10: *Night time mixing ratios of ozone (ppbv) plotted against night time mixing ratios of Br_2 (pptv).*

6.3.3. Evidence for a temperature dependence in the Br_2:BrCl ratio

The ratio of Br_2:BrCl can be used as an indicator of the chemistry driving release of halogens from the surfaces of salty condensed phase substrates (brine slush, frost flowers, sea salt aerosol etc.). Various factors have been suggested to influence the ratio of Br_2:BrCl in the air. Foster et al. (2001), attribute their reported ratio to differences in Henry's Law coefficients, which at the

temperatures of Arctic spring, render Br_2 less soluble (and therefore more easily lost to the atmosphere) than BrCl. The latter, by remaining in the liquid like layer of the snow/ ice, would also be more likely to decompose through secondary reactions. These conclusions are in line with estimates by Sander et al. (2006), based on thermodynamic data, that at low temperatures (in the region 240K) the equilibrium reaction $BrCl + Br^- \leftrightarrow Br_2Cl^-$ shifts to the right, enhancing the proportion of Br_2Cl^- in the system which then dissociates to release Br_2 (see reactions above).

A further possible factor affecting the ratio of Cl^-:Br^- in sea ice surfaces is the precipitation of hydrohalite ($NaCl.2H_2O$) once surface temperatures drop below ~-21°C (Koop et al., 2000).

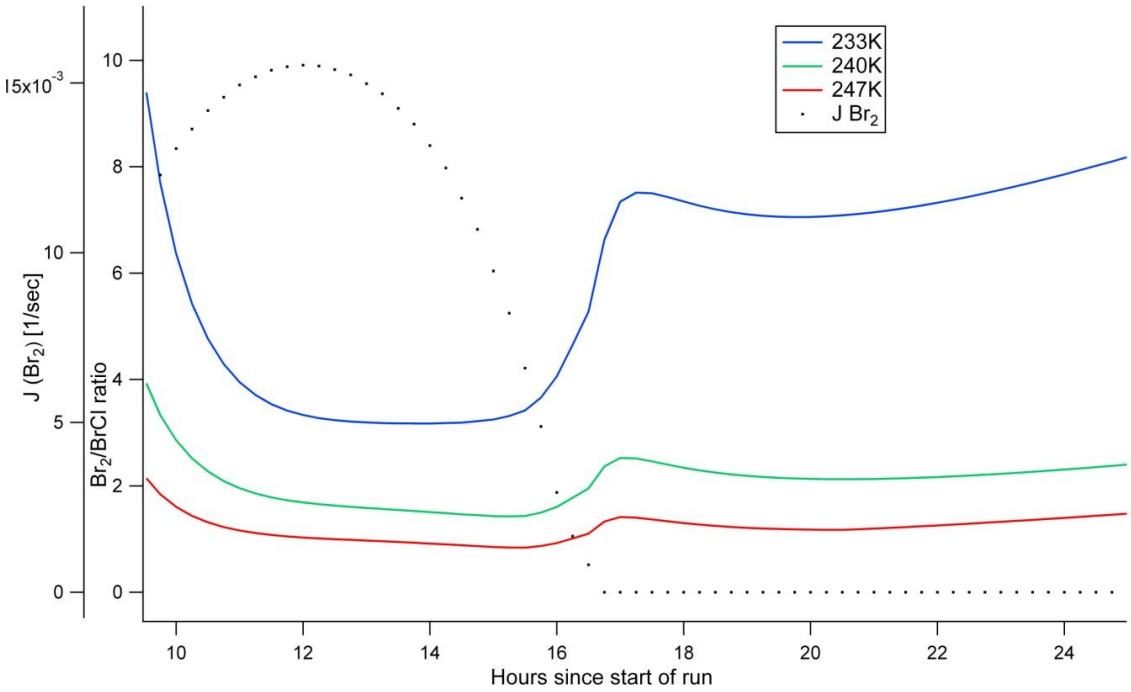

Figure 6.11: *Modelled variation in Br_2:BrCl ratio at three temperatures relevant to polar spring. The black dots indicate J(Br_2).*

To explore the sensitivity of the Br_2:BrCl ratio to variations in temperature, I ran the MISTRA model at a range of polar spring temperatures, -40°C, -33°C and -26°C. The model chemistry includes the temperature-dependent reactions and Henry's Law coefficients described above, but does not include a description of hydrohalite precipitation. However, the temperature dependencies of the underlying equations are estimated and not measured. The calculated Br_2:BrCl ratios for each 24 hour run are shown in Figure 6.11. The modelled ratio is clearly highly temperature-dependent, progressively shifting towards Br_2 as modelled temperatures are

reduced. Note also that the calculated ratio is non-linear over this temperature-range, and that for all three temperature scenarios considered here, the ratio of gas-phase Br_2:BrCl remains greater than or equal to 1.

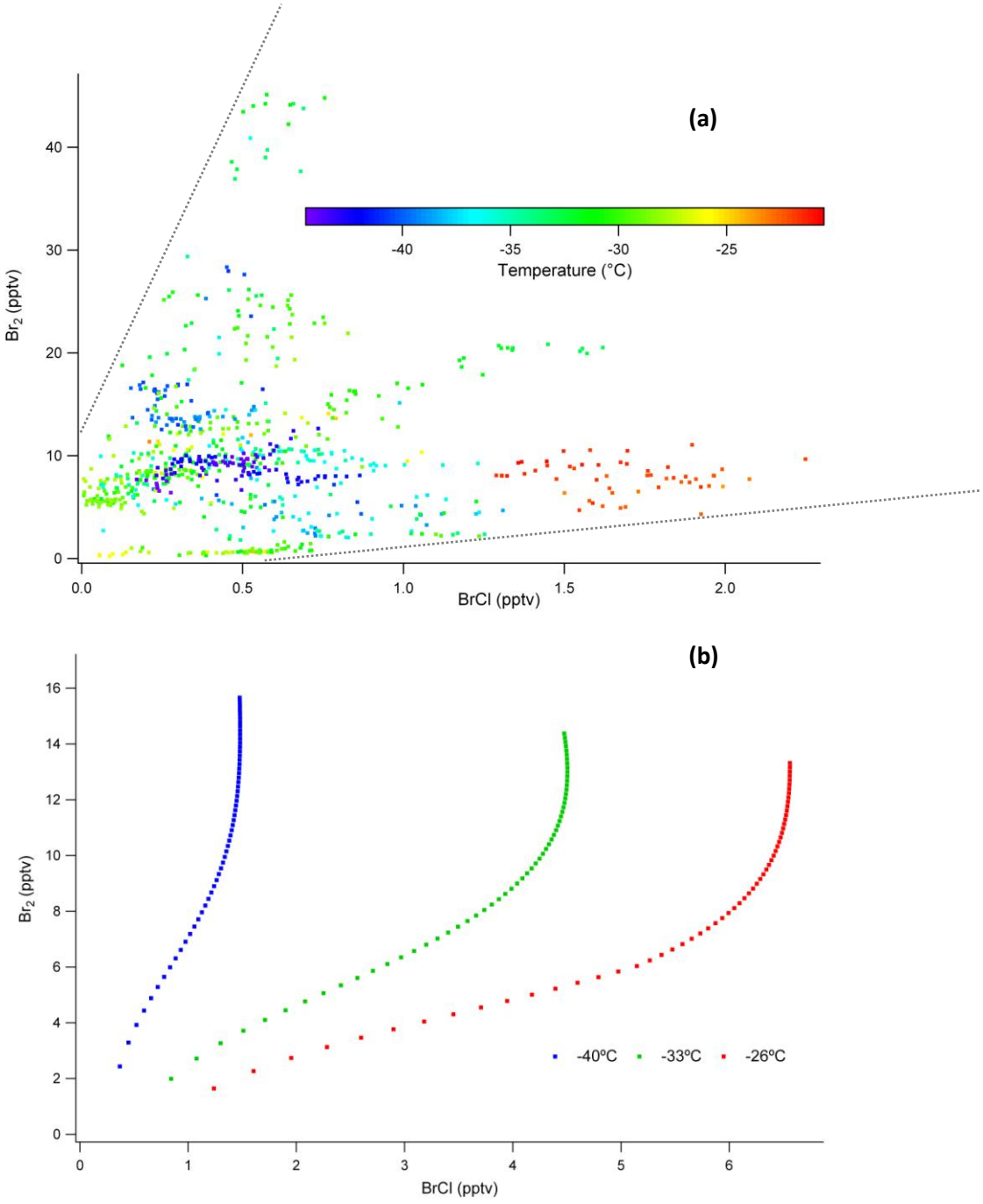

Figure 6.12: *a) Observed Br_2 vs BrCl, colour coded for temperature, for air arriving at Halley from directly across the sea ice zone (200° - 300°) at night. b) Modelled Br_2 vs BrCl, colour coded for temperature. Please note differing scales on axis.*

The question then arises: is it possible to see any signal of temperature-dependence in the Br_2:BrCl ratio in the observations? To consider this, the Halley observations were filtered according to local wind direction to include only data with a direct sea ice zone origin (200^o to 300^o); to account for the HOBr interferent, only night time data were considered. Figure 6.12a shows, for this filtered dataset, the observed Br_2 plotted against observed BrCl and colour coded according to local temperature at Halley. There are clearly boundaries to the data population, marked by the grey dashed lines on the figure. Some relationships between Br_2 and BrCl appear to hold within certain temperature ranges, for example observed Br_2 are clustered at both the coldest temperatures (blue dots) and warmest temperatures (red dots). However, Figure 6.12b shows the equivalent plot using output from the MISTRA model runs described above (again, limited to night time results) to show the "expected" relationship between Br_2 and BrCl as determined by chemical thermodynamics. The clear association between Br_2 and BrCl at the different temperatures of the model runs are not apparent in the observations. An obvious limitation to such an analysis is the use of local ambient temperature at the observation site, rather than the temperature at the sea ice surface where the reactions are occurring. It appears that even during the night, there is sufficient mixing within/between air masses to disguise any influence on Br_2:BrCl arising from equilibrium reactions within the condensed phase and exchange with the air.

While temperature changes would be expected to drive a chemical thermodynamic response in the data in a relatively smooth manner, precipitation of hydrohalite ($NaCl.2H_2O$) would result in a discontinuity. Within the filtered dataset (including only sea-ice zone and night time data) there was only one event during which ambient temperatures were above -25^{o}C. These data are shown in red in Figure 6.13a. While at temperatures below roughly -24^{o}C the Br_2:BrCl ratio is highly scattered, and persistently spans the range ~1 to ~70 (and above, off the scale of the plot), at temperatures warmer than roughly -24^{o}C, the ratio remains below ~7. Figure 6.13b shows the evolution of this event with time, as a function of temperature. At the warmer temperatures during the early part of 24th August, the Br_2:BrCl ratio remains below ~7. Once temperatures drop, around 21:00 on 24th August, the Br_2:BrCl ratio rapidly increases. Throughout this period of observations both the local wind speed and direction at Halley are constant. It would also appear that air that has passed over the sea-ice zone prior to the temperature drop does not show evidence of increase in the Br_2:BrCl ratio (see Figure 6.13c). This is likely due to the air having descended from height, and therefore having no direct BL influence. While this is certainly not explicit proof of the role played by hydrohalite precipitation in determining the

Br_2:BrCl ratio, and thereby participating in the "bromine explosion" reactions, these data are nonetheless consistent with this mechanism .

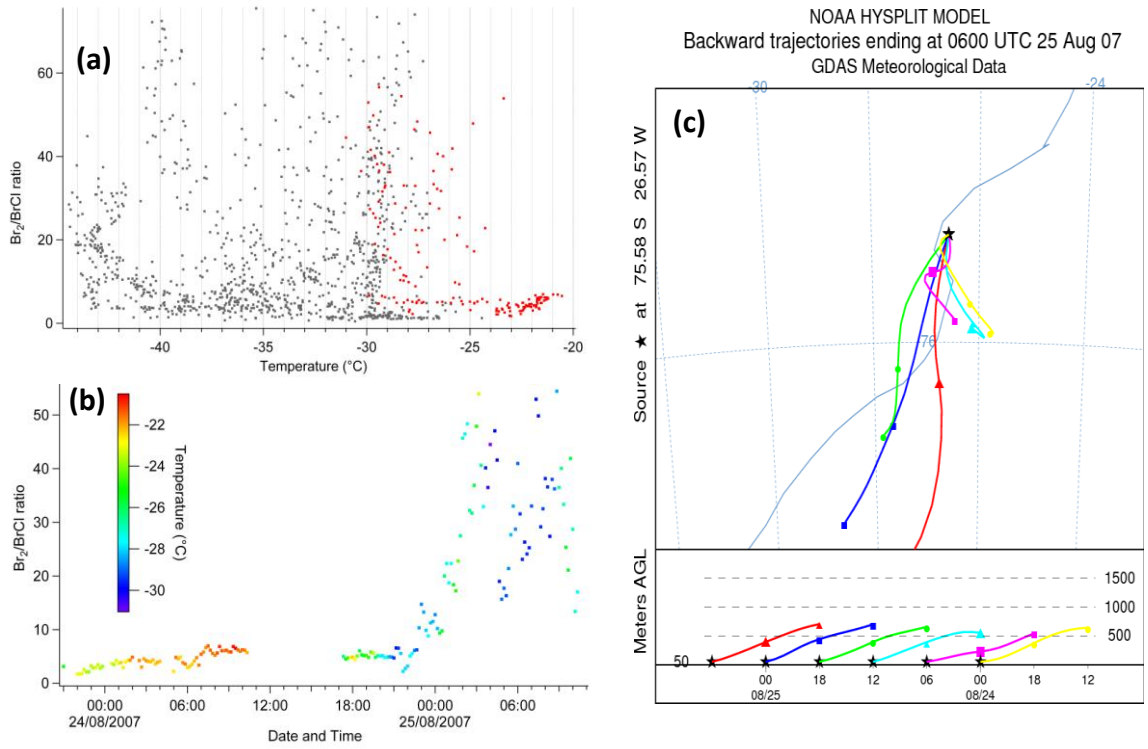

Figure 6.13: *a) Measured Br_2:BrCl ratio versus ambient temperature for observations filtered to include only air arriving directly from the sea ice zone (200° to 300°), and including only night time observations. The data in red are for a 2 day period (24th – 25th August) which is the only time in these filtered data when ambient temperatures were above -25°C; b) time series of Br_2:BrCl ratio, colour coded for temperature, for the 24th-25th August; c) 12-hour back trajectories arriving at Halley on 24th-25th August. Air masses arriving at Halley during the early part of the period, when temperatures were ~ -20°C, had also passed over Precious Bay, the region of open water/newly forming sea ice, to the south west of Halley.*

6.4. Comparison with Arctic Br_2, BrCl and BrO observations

High resolution ground-based measurements of Br_2 and BrCl were previously made in the Arctic as part of the Alert Polar Sunrise Experiment (PSE) (Foster et al., 2001; Spicer et al., 2002). These measurements were conducted prior to first direct sunlight, and continued for a further two weeks after polar sunrise. In the period following first direct sunlight, Spicer et al. (2002) reported Br_2 mixing ratios at Alert that ranged from instrumental detection limits to 27 pptv (which was measured when solar irradiance was 0 $W.m^{-2}$, i.e. nighttime observations). For the

same period at Alert, Foster et al., (2001) reported BrCl mixing ratios ranging from detection limits to ~35 pptv, although without showing whether this was daytime or nighttime data. However, Spicer et al. (2002) measured daytime (i.e. solar irradiance > 0 $W.m^{-2}$) BrCl up to ~25 pptv, and nighttime (i.e. solar irradiance = 0 $W.m^{-2}$) BrCl up to ~18 pptv. Their nighttime BrCl is considerably larger than was observed at Halley, where nighttime BrCl mixing ratios were never greater than 6 pptv. The data from Spicer et al. (2002) therefore suggest that BrCl in the Arctic can reach considerably greater mixing ratios than were measured at Halley. Furthermore, when 18pptv of BrCl were measured at Alert, the coincident Br_2 measured was only ~4 pptv, i.e. a Br_2:BrCl ratio of ~0.2 – considerably less than observed at Halley. In general Foster et al. (2001) describe the measured ratio of Br_2 to BrCl in the air to be ~1, whereas at Halley, the ratio was almost always significantly greater than 1 (see section above). The measurements at Alert were made using a similar CIMS technique to that at Halley, but with a ~9m long teflon inlet (J. Bottenheim, pers. comm., 2012), which raises the question of whether they were also subject to an inlet artefact in daytime Br_2 and BrCl observations discussed in section 3.1. If so, this would likely affect both the recorded ratios and mixing ratios.

A more recent study by Liao et al. (2012b), reports measurements of BrO, Br_2 and HOBr made using a modified CIMS technique at Barrow, Alaska, in spring 2009. Their observations show a BrO maximum of > 30pptv, more than double the observed maximum at Halley of 13pptv. Maxima in Br_2 at the two stations are very similar, with 46 pptv at Barrow and 45 pptv observed at Halley.

Overall it is clear there is considerable variability in the Br_2 and BrCl observations, where low and invariant Br_2 and BrCl is associated with winds of continental origin and higher mixing ratios with air masses that have passed over the sea ice zone.

Background ozone is 30-35 ppbv with ODEs evident throughout the observation period. The most sustained ODE lasted for more than 24 hours with ozone dropping to a minimum of 6ppbv during that event.

BrO exhibits a clear diurnal cycle throughout the period of CIMS observations, with nighttime minima around instrumental detection limits. The daytime measurements show a distinct diurnal structure of a BrO minimum around noon, and maxima in the morning and evening, which tends to evolve throughout the measurement period. From this it is clear that BrO concentrations are a balance of sources and sinks. BrO mixing ratios observed are in line with

previous observations at Halley (Saiz-Lopez et al., 2007), and it is clear the BrO maxima at Halley are less obviously correlated with local wind direction than are Br_2 and BrCl.

The observed Br_2:BrCl ratio at Halley varies under many different conditions, and shows sensitivity and correlation with, air mass source region, temperature and wind speed. It would also appear that there are significant differences in this ratio, as well as mixing ratios of the separate bromine species, between measurements made in the Arctic and Antarctic.

7. Results Part III: Exploring processes

Synopsis:

Here I will explore some of the more unusual cases that were found in the CIMS measurements discussed previously (Chapters 5 and 6). The processes involved in these specific cases have led to the measurement of interesting bromine and ozone-related chemistry at Halley.

First I will address the question of bromine recycling on continental snowpack, which has been discussed previously by Piot and von Glasow (2008) in a modelling paper. Their findings suggested that to reproduce ODE, recycling of bromine deposited to the snowpack and re-emitted from the snow surface back into the atmosphere is required. However, it is key to note that the model used was the 1-D version of MISTRA prior to the implementation of the snow-photochemistry module (Thomas et al., 2011). Although no model runs were conducted here, a thorough analysis of the measurements made at Halley (both meteorology and chemistry) is included to represent this case.

I will then go on to discuss an unusual long range transport event which may have been the precursor to both the strongest ODE, and the highest Br_2 measured at Halley throughout the period 12/08/2007 – 18/09/2007. Although storms and blowing snow (Yang et al., 2008; Jones et al., 2009) have been found to play an integral role in some ODEs measured at Halley, and their large scale structure has been identified (Jones et al., 2010), the case identified in these CIMS measurements (Figure 7.4) creates a different picture of potential halogen source regions which can influence chemistry at Halley.

7.1 Recycling on continental snowpack, or a sea ice source of halogens?

It has previously been proposed that the coastal snowpack could be a direct source of bromine compounds (Simpson et al., 2007). For this to be the case, the snow would need to have an increased salinity, for example from sea salt aerosol deposition (see Chapter 8). At Halley, easterly airflow generally has a continental origin, occasionally skirting close to the sea ice edge. Such conditions provide a good test case for the snowpack source hypothesis. Recent work by Pratt et al. (2013) indicates that the coastal continental snowpack may even be a greater source

of halogens than snow on sea ice itself, and therefore influence ODEs and other such chemistry in such coastal polar regions.

7.1.1 Continental Background

Easterly winds of continental origin normally dominate throughout the year at Halley, but during spring winds from coastal regions to the west also play a prominent role by contributing most to Br_2 and BrCl concentrations of greater than 5pptv and 2pptv respectively. Enhanced halogen concentrations at Halley are closely linked to the air mass source region Precious Bay. Although ozone depleted air is measured from both continental air and sea-ice air (O_3 = 5-10ppbv), the strongest ozone depletion (O_3<5ppbv) is only measured when air has arrived at Halley from over Precious Bay.

Thinking about wind direction, from the 27th August until 1st September, while the prevailing wind direction is easterly (implying continental air; Figure 6.1 and 6.2 from chapter 6), Br_2 and BrCl show little variability, and there is no ODE, yet BrO maintains a diurnal structure with daily maxima ranging from ~2 pptv to ~7 pptv. The presence several pptv of BrO during the day throughout the measurement period suggests that some persistent background bromine/ozone chemistry is active during the day, even when air is not approaching from directly across the sea ice zone.

This time period above is a clear example of such background chemistry, specifically the 30th August when ~7 pptv of BrO was measured in air arriving at Halley, the highest BrO mixing ratios measured during a period of sustained continental origin (Figure 7.1) There is little O_3 depletion on this day, but the ~3-4 pptv of "Br_2" measured during daylight is indicative of active bromine chemistry (possibly as HOBr) (see Chapter 5). Wind speeds were low (~5ms^{-1}) and local ambient temperature was around -30°C. The importance of halogen recycling in/on the snowpack is discussed in a model study by Piot and von Glasow (2008), where they varied the percentage re-emission of Br_2 and BrCl in their runs from 0 – 100%. They found that major ODEs could only be reproduced in their model simulations when the recycling of bromine deposited on snow into gas phase bromine was included. If we therefore assume that recycling of bromine deposited on (or present in) snow is generally occurring at all times in coastal polar regions, the measurements discussed here (30th August 2007) suggest that a cold, stable/stratified BL has led to this build up of several pptv of BrO. Under the same meteorological conditions on the

following day (31st August 2007), up to 5pptv of BrO was measured. These enhanced BrO mixing ratios measured in air of sustained continental origin suggest release of halogens directly from the snowpack, and their detection at the several pptv level may be dependent on these very specific meteorological conditions.

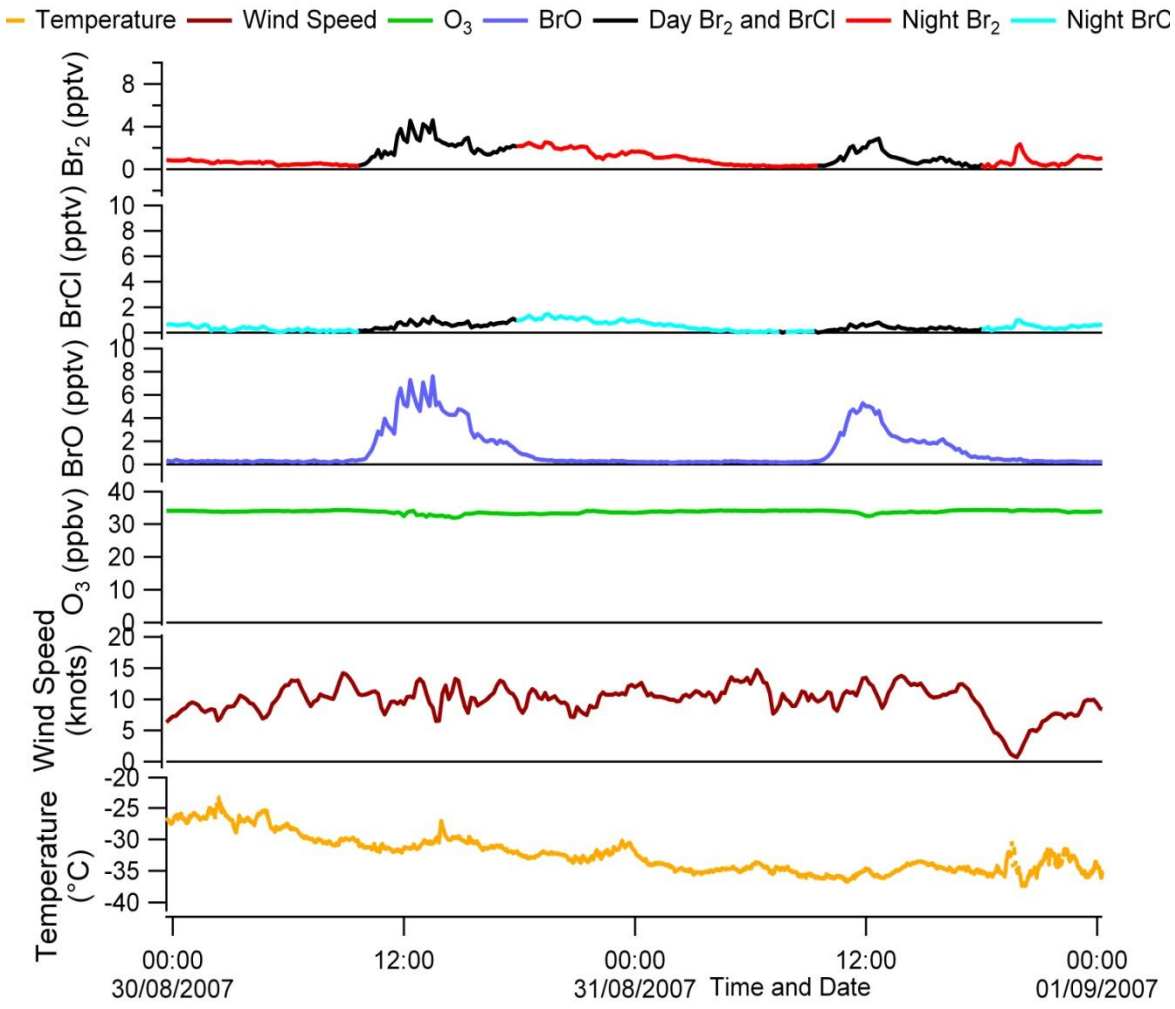

Figure 7.1: *Wind speed, temperature, surface O_3 and CIMS Br_2, BrCl and BrO measurements from Halley on 30-31 August 2007. Br_2, BrCl and BrO all have the same scale on the y-axis.*

7.1.2 Snowpack recycling or a sea ice source?

For a 4 day period in September, from 11th-14th (Fig 7.2), air arrived at Halley from the east. Unusually for this wind direction there also appeared to be higher than background BrO mixing ratios, slightly higher Br_2 and BrCl mixing ratios on several of these days, and some evidence of ozone depletion, associated with this 'continental air'. Looking at air mass pressure from HYSPLIT back trajectories (Fig 7.4) reveals that air arriving at Halley on the 11th and 12th had been in the BL since the previous day. In contrast, air arriving on the 13th and 14th had skirted the coast and had no direct contact with the snow surface or with sea ice.

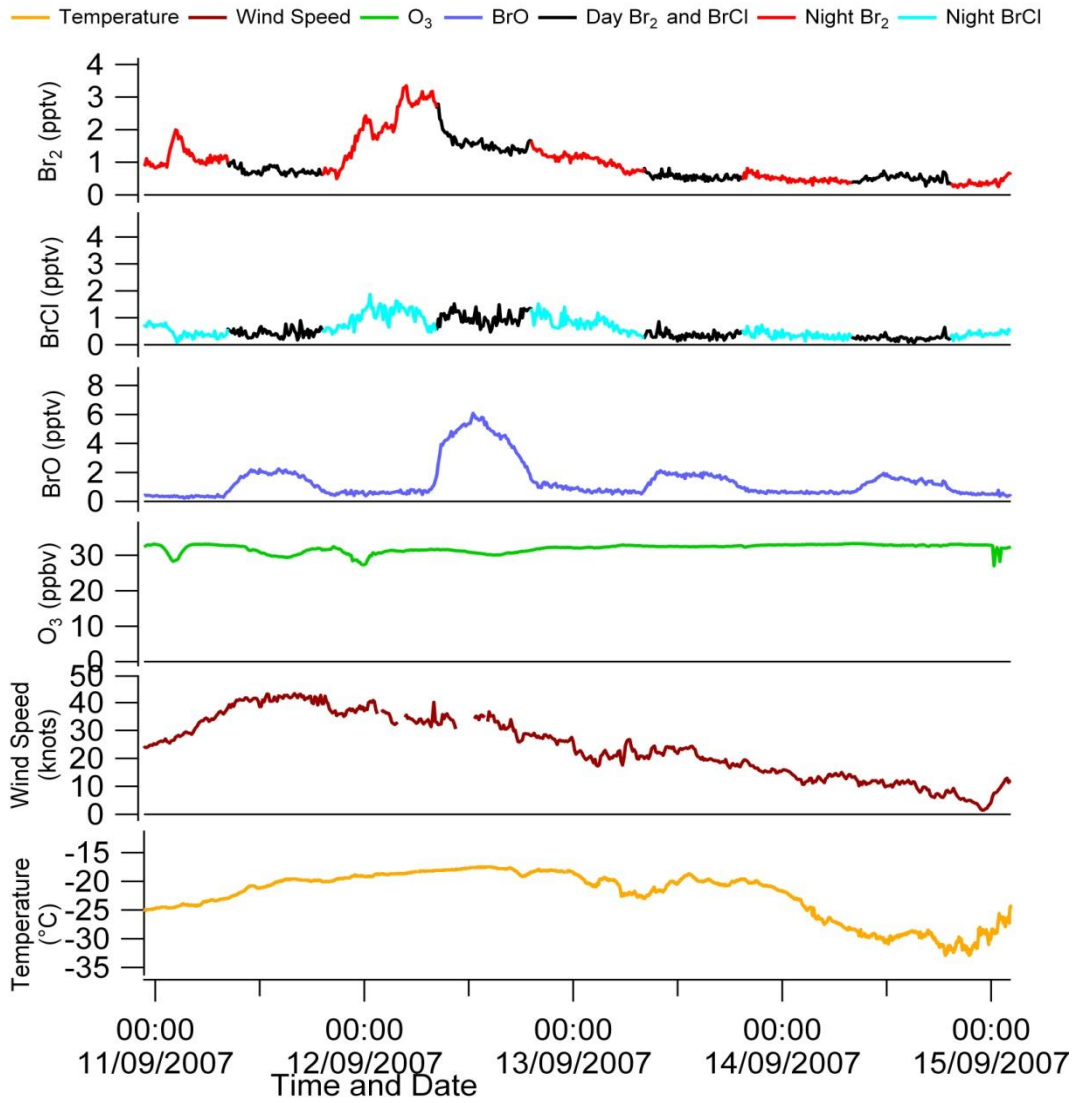

Figure 7.2: *Wind speed, temperature, surface O_3 and CIMS Br_2, BrCl and BrO measurements from Halley on 11-14 September 2007*

Some key characteristics for this 4 day period are high wind speeds of 20-40 knots (10-20 ms^{-1}) converging at the coast, with temperatures consistently around -20°C (only dropping on the last day). Looking at ECMWF Interim reanalysis data (Figure 7.3) it is clear that there is a large storm system present over the Weddell Sea on the 11th and 12th. On the night of the 11th there is a small amount of ozone depletion around midnight, and Br_2 (~4pptv) is high for continental influenced air. As this is observed at night (in the dark) it is safe to assume that this mildly ozone depleted/ Br_2 enriched air is a transported remnant air mass from the high winds further out in the Weddell Sea earlier that day. The day of the 12th is associated with direct sea-ice contact (Fig 7.4), and higher BrO (~7pptv) was observed on this day than on the 11th, 13th and 14th. This high BrO on the day after the enhanced nighttime Br_2 could be due to local chemistry. These conditions of high winds associated with a storm in the Weddell Sea have previously been associated with blowing snow (Jones et al., 2009). It has been suggested that salty blowing snow could act as bromine source (Yang et al., 2008), subsequently triggering the onset of ODEs. The evidence suggests that could be what is observed on these two days.

As the wind speeds drop on the 13th and 14th there is a signal of 2-3pptv of BrO present. It is possible that during the storm on the previous days, bromide was deposited on the continental snow (as discussed by Piot and von Glasow, 2008). This could account for the BrO signal of ~2pptv which is observed on the 13th and 14th. The air mass pressure (from the HYSPLIT back trajectories in Fig 7.4) indicates that the air mass was much higher above the snowpack on the 13th and 14th than on the previous days. This combined with the drop in wind speed and likely reduction in aerosol loading aloft, is another indication that bromine recycling on the snow pack might be occurring.

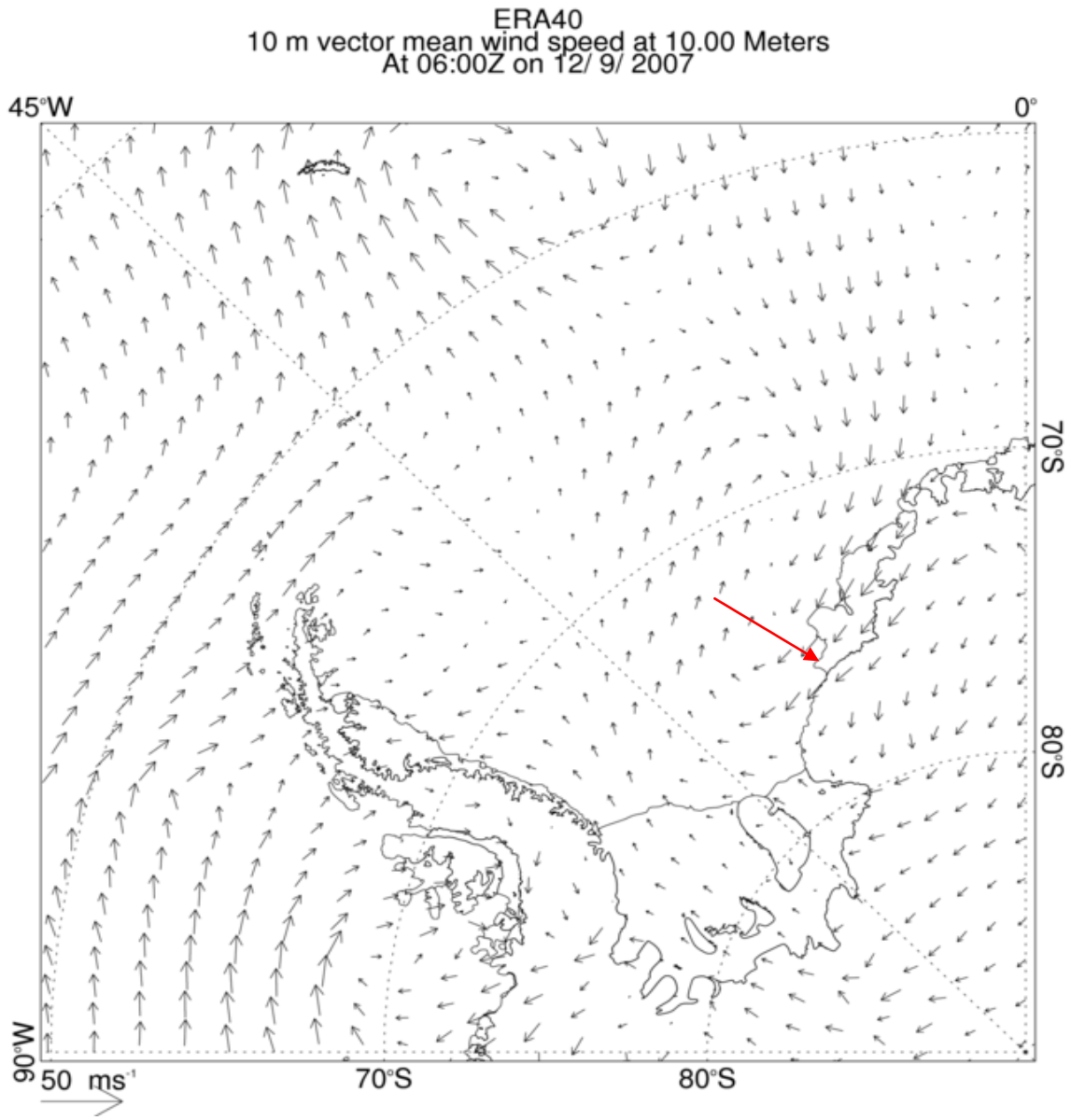

Figure 7.3: *ECMWF analysis output of 10 meter wind vector for the area containing Antarctic Peninsula and Weddell Sea at 0600 hrs on 12/09/2007. The location of Halley is given by the red arrow.*

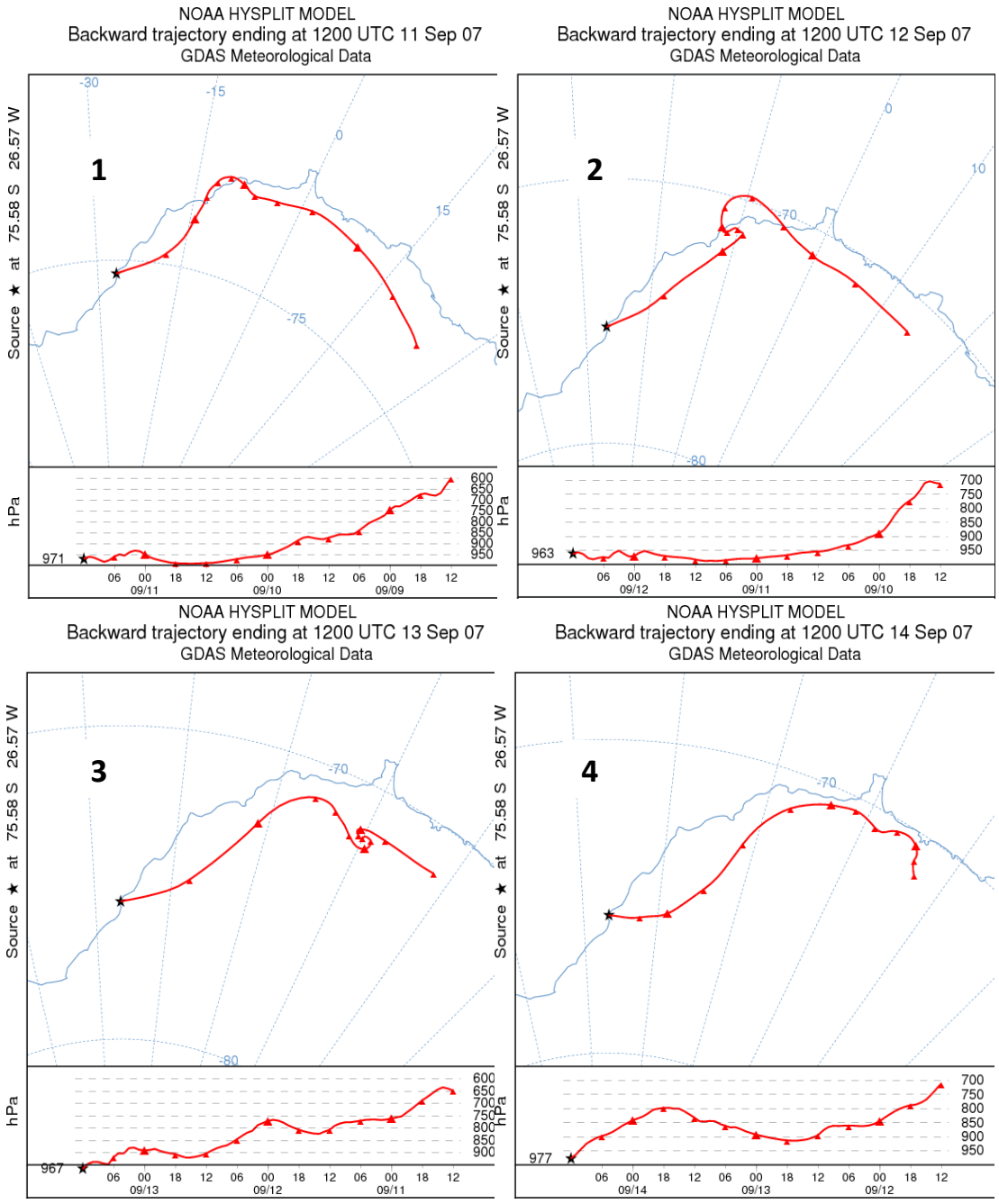

Figure 7.4: *HYSPLIT 3-day back trajectories from 1200hrs on 11-14 September 2007, with pressure as an indicator of height of the air mass*

7.2 Long range transport (in darkness) of a halogen enriched, ozone depleted, air mass: Br_2 as a night-time Br reservoir

Over a two day period from 21st – 22nd August an intriguing event was observed at Halley, with the lowest measured [O_3] throughout the entire period of observations and the highest measured [Br_2] and [BrO] (Figure 7.5).

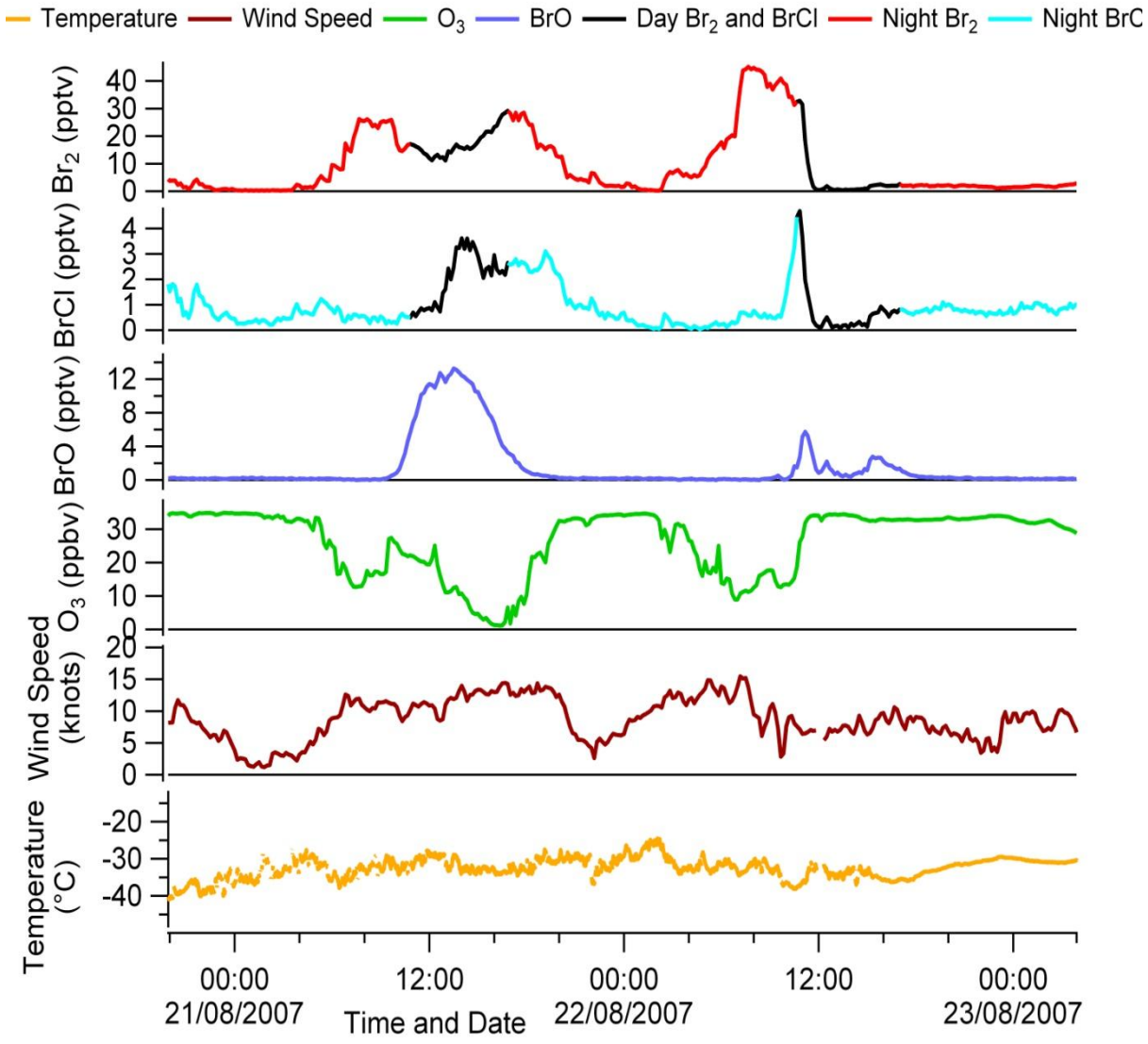

Figure 7.5: *Wind speed, temperature, surface O_3 and CIMS Br_2, BrCl and BrO measurements from Halley on 21st and 22nd August 2007*

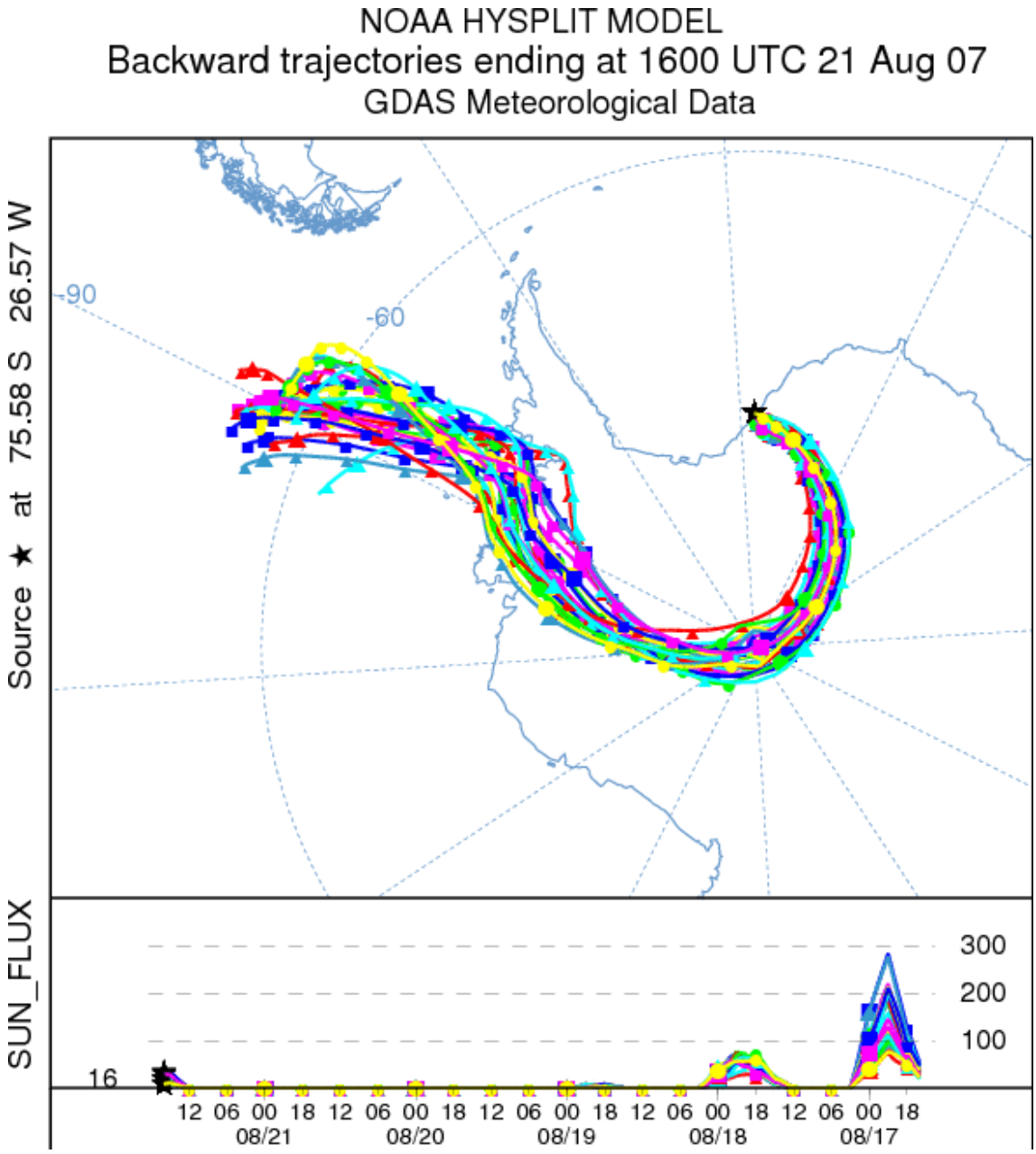

Figure 7.6: *5-day HYSPLIT Ensemble back trajectory from Halley. Included is a measure of 'Downward Solar Radiation Flux (W.m^{-2})' to indicate when the air parcel last saw light.*

The highest measured [Br_2] of the whole spring period occurred after midnight on 22nd August, so is not likely to be influenced by the HOBr interferent (discussed in Chapter 5). Ensemble HYSPLIT back trajectories suggest that this ozone depleted air mass had arrived at Halley having travelled across the continent of Antarctica from the Bellingshausen Sea, to the west of the Antarctic Peninsula (Figure 7.6). As shown by the lower panel of Figure 7.6, the air mass had

travelled in darkness for the previous 3 ½ days with no possibility of photochemical reactions taking place. AMSR-E maps (Figure 7.7) show open water leads, with associated sea-ice formation processes, at the coastal edge of the Bellingshausen in the region of the air mass trajectories. This area could be seen as the main source of halogen for the air mass, but it could also be argued that the furthest edge of the sea-ice is the greatest halogen source. A third possibility is that these source regions may have some influence, but what is seen is also the result of chemistry in the near-coastal environment at Halley.

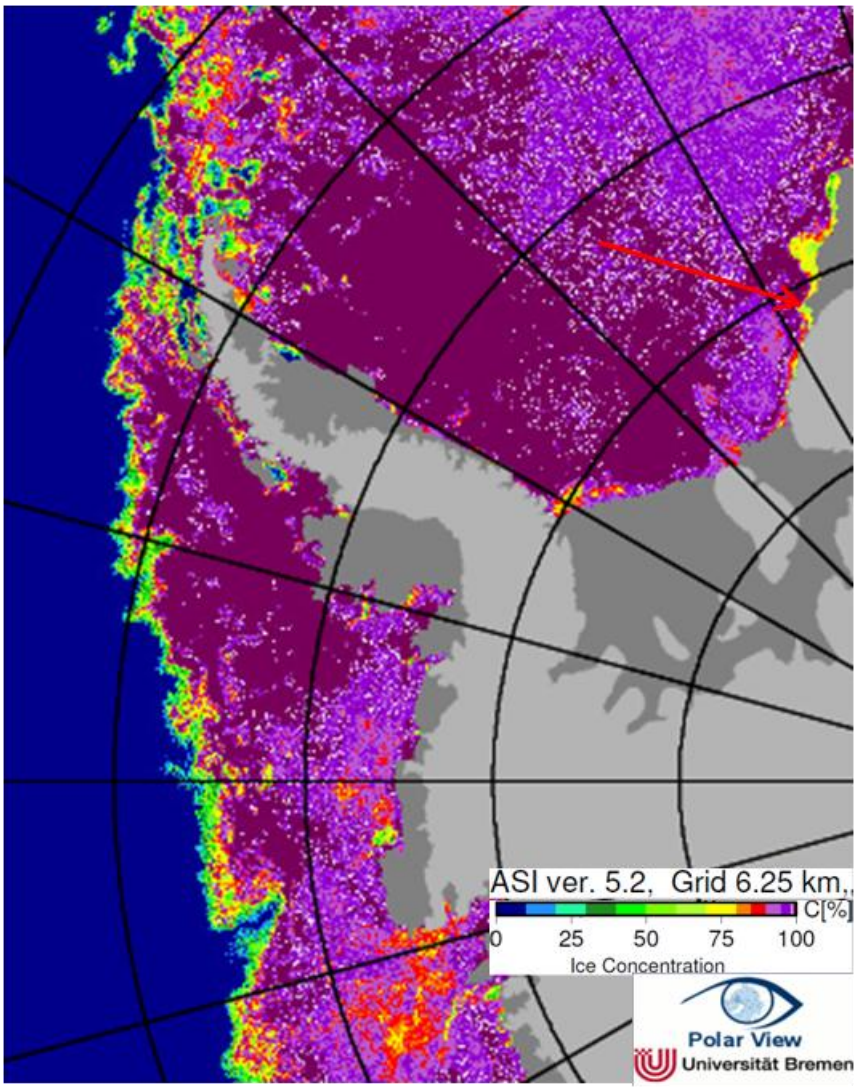

Figure. 7.7: *AMSR-E sea ice map for Antarctica corresponding to the potential source region of this long-range transport event. Daily average for 18/08/2007. Location of Halley is shown by red arrow.*

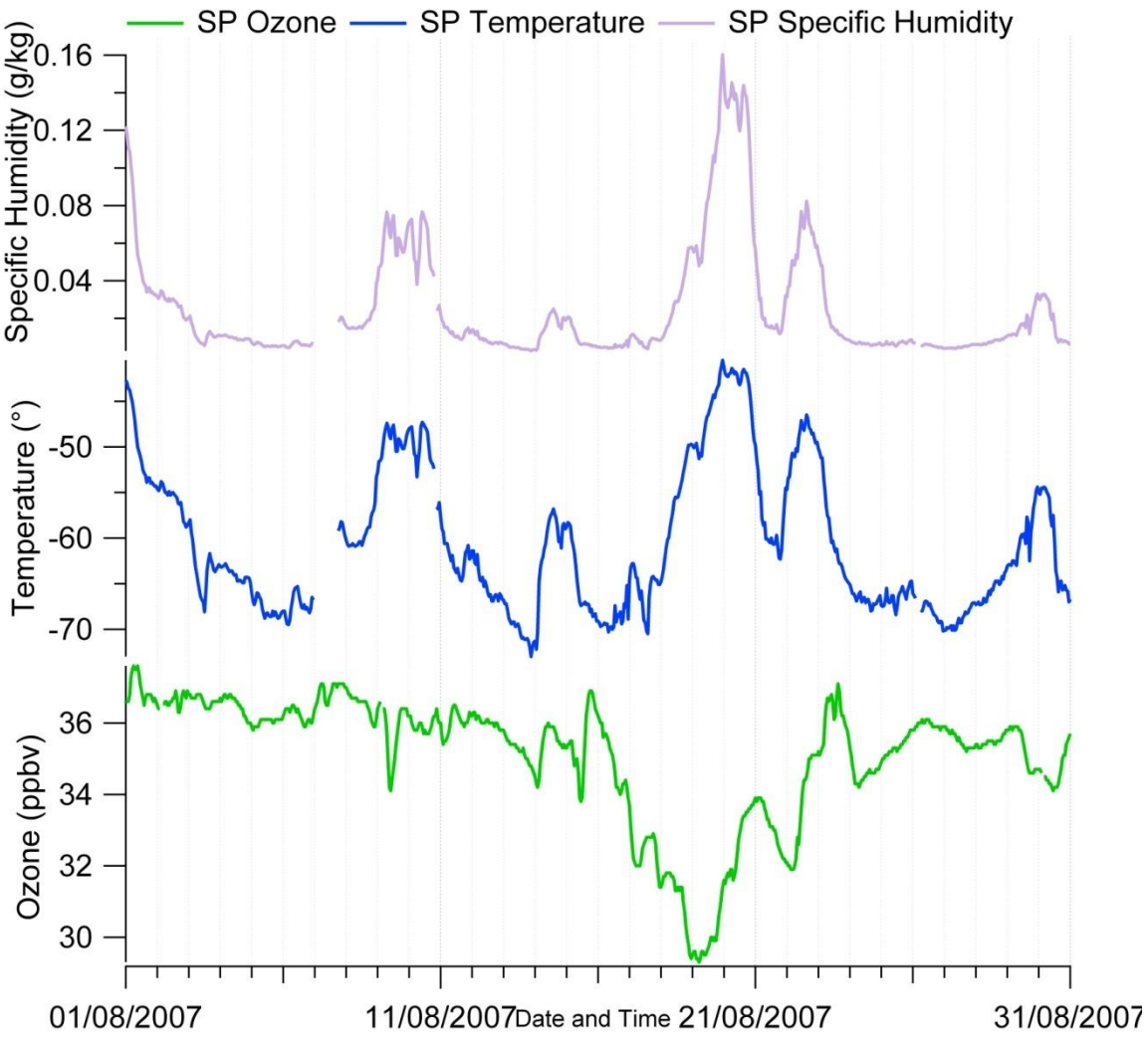

Figure 7.8: *South Pole surface ozone, temperature and specific humidity, from 1-31 August 2007.*

Figure 7.8 shows surface ozone measurements from South Pole from the 1st – 31st August 2007. The outstanding feature is the drop in ozone that occurs on 19th – 20th August. The back trajectories shown on Figure 7.6 indicate that the low-ozone air arriving at Halley on August 21st had passed over South Pole on August 19th – 20th .While the drop in ozone at South Pole is modest compared with the Halley observations, the HYSPLIT trajectories suggest that the Halley air mass did not contact the South Pole surface, but travelled at some height (>1000 metres) over South Pole. The drop in surface ozone of 7-8ppb on 19th August is consistent with an ozone depleted air mass following this trajectory over South Pole with only a small influence being evident at the surface. Unfortunately no ozone sonde was launched from South Pole on this day, from which the profile of ozone could be seen. However, data from South Pole of temperature and specific humidity both show significant increases, consistent with passage of marine air.

Further, Bromwich et al. (1996) suggest that passage of air across the continent along this route is not uncommon.

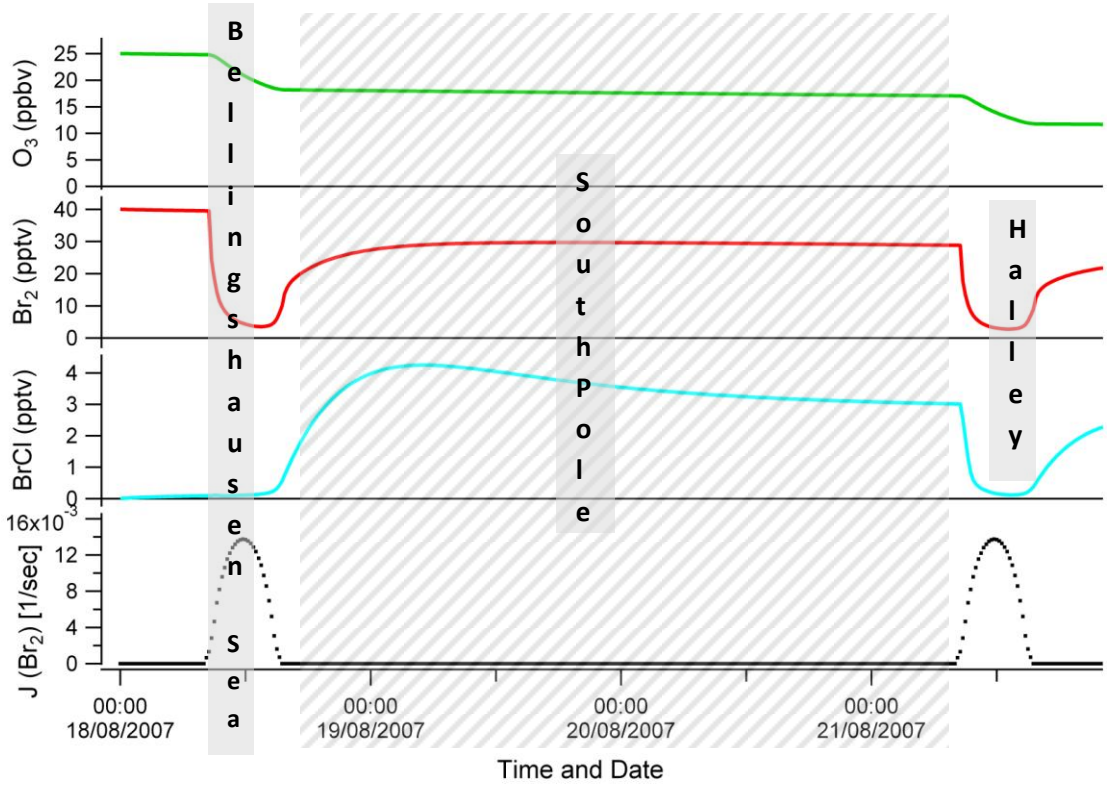

Figure 7.9: *MISTRA 0-D run 4 days in length showing [Br_2], [BrCl], [O_3] and J(Br_2) model output. Only the first and last of those days under the influence of sunlight (darkness is highlighted with the gray box). Mixing ratio on the left axis, and time in hours since the start of the run along the bottom. The location of the air mass is highlighted at key stages of its transcontinental path.*

In an attempt to understand the halogen chemistry occurring during this period of darkness as the air mass traversed the continent, a box model run in MISTRA was set up to recreate the conditions the air mass would see (Figure 7.9). An initial mixing ratio for Br_2 was set at 40 pptv, with the majority of the remaining parameters set for a typical Halley model run. HYSPLIT trajectories were used to determine the length of run required, and the influence of light on the air mass. The result is shown in Figure 7.9. It is clear that the initial influence of sunlight is of vital importance in the partitioning of halogen species between Br_2 and BrCl, but it appears that the lack of photolysis thereafter effectively 'stalls' the ozone depleting reactions. This implies that the majority of ozone depletion would have to occur prior to the period of darkness, although

there is some photolytic influence near the end of the run. Although the model run does not show complete ozone depletion as observed at Halley, the run does highlight the transport of the depleted air mass in the dark. The final [Br_2] and [BrCl] output from the model run is comparable to the halogen observations from Halley on the 21st August 2007 (see Figure 7.9).

Several pptv of BrO was consistently observed during the day even when air is not approaching from directly across the sea ice zone suggesting some persistent background bromine/ozone chemistry is active during the day. Enhanced BrO mixing ratios measured in air of sustained continental origin suggest release of halogens directly from the snowpack, and their detection at the several pptv level may be dependent on a very specific set meteorological conditions characterised by a cold, stable/stratified BL.

The lowest measured [O3] and the highest measured [Br_2] and [BrO] appear to be associated with a long-range transport event. Ensemble HYSPLIT back trajectories suggest that this ozone depleted air mass had arrived at Halley having travelled across the continent of Antarctica from the Bellingshausen Sea, to the west of the Antarctic Peninsula. Chemical and meteorological observations from both South Pole and Halley give strong evidence for this being the path the air mass has travelled.

8. MISTRA-SNOW I: Model setup and initialisation

Synopsis:

A new snow-photochemistry module had been developed for MISTRA (MISTRA-SNOW), which includes chemistry which takes place in the quasi-liquid layer on frozen surfaces (Thomas et al., 2011). This newly-developed version of MISTRA was used here to examine BL chemistry at Halley. An outline of the model setup used, and the basic initial conditions, are given here for MISTRA-SNOW. A more in-depth description of the SNOW module has already been given in Chapter 4. The runs presented here are initialised using measurements made at Halley station (and other coastal Antarctic or polar sites where required), with the main aim to explore both the chemical and meteorological conditions involved in halogen release and ozone depletion (snow – atmosphere interaction) in this coastal polar environment. The model setup for snow on sea ice is first looked at, and is followed by a description of the changes made to make the snow-module representative of the continental snowpack. Only a brief description of the model results will be made here, with the aim of understanding the results from the basic simulations representing each snow type. A more in-depth discussion of model results will take place in Chapter 9, where a broad set of idealised simulations (inspired by the open issues as described in section 7 of Abbatt et al., 2012) will be explored.

8.1. Motivation

The MISTRA-SNOW model has, to date, only been applied to a single field location – Summit station, in central Greenland, during the Boreal summer. Conditions at Halley during spring are quite different, with considerably lower temperatures, restricted solar radiation, and a significant influence of the sea ice zone on observed atmospheric chemistry. The initial aim was therefore to test the MISTRA-SNOW model under Halley springtime conditions, to see if the basic model was able to reasonably reproduce observations. This ‘proof of concept’ is what will be described in this chapter.

8.1.1. Model setup and initialisation overview

The two cases looked at in Chapter 7 both bring to light the potential importance of contact with the sea ice zone for halogen release. The ultimate goal of using this newly-developed SNOW module was highlighted by Piot and von Glasow (2008), who discussed the effects of leads/ open water and halogen recycling on the snowpack for ozone depletion in the atmosphere above the snow surface. The aim here is to use MISTRA-SNOW to "create" snow on sea ice (along with associated characteristics as discussed in section 8.2), and a continental snowpack which can then influence, and interact with, the model atmosphere. The two types of runs discussed here will be defined as "snow on sea ice", and "continental snowpack" runs. The importance of air mass contact with the sea ice zone prior to arrival at Halley has been discussed in depth in previous chapters (2, 6 and 7), and these model simulations using MISTRA-SNOW were the culmination of these discussions. The model output will be tested against Halley data, so typical trajectories of air masses arriving at Halley are used. This led to the inclusion of open water to simulate the lead/polynas system found in Precious Bay, near Halley.

Only the individual 'base' runs for snow on sea ice and continental snowpack will be discussed here (as well as a short description of "spinups" and restarts used in these runs), the wider range of snow-on-sea ice/ continental snowpack runs are explored in detail in Chapter 9.3. The model is parameterised using physical observations of snow on sea ice (Massom et al., 2001; P. Anderson, pers. comm. 2012) in order to be insightful.

8.1.2. Physical characteristics of the snow in MISTRA-SNOW

The first physical snow property that will be discussed is the LLL (liquid like layer) thickness. There is a lot of controversy around the discussion of this LLL or QLL (quasi-liquid layer) (Abbatt et al., 2012), but since this SNOW module has already been used for polar work, it made sense to choose the LLL thickness based on that used by Thomas et al. (2011). Based on this previous work by Thomas et al. (2011), the LLL thickness used for the Halley continental snowpack was 10nm, and the snow grain radius is 1mm. From this I was able to calculate the liquid water volume (LWV) of the LLL of the individual snow grains, and was found to be $1.26e^{-13}$ m^3. The LLL thickness used for the snow on sea ice was 20nm, and the snow grain radius was 1.5mm (based

on observations from Massom et al., 2001). These values were used to convey the wetter, warmer, environment of the snow on sea ice in comparison with the continental snowpack which is colder and drier. The LWV calculated for each grain of snow on sea ice was found to be $5.65e^{-13}$ g m^{-3}. When comparing the LWV for grains of snow on sea ice with that calculated for grains in the continental snowpack, although the snow on sea ice snow grains are nearly twice the size of those used on the continental snow, and the LLL thickness is twice that used in the continental snow, the LWC is just under 5x greater (not even 1 order of magnitude).

The physical snow grid is outlined in Table 8.1, showing that the thickness of the top layer of the snowpack is only 2.4cm, and the total depth of the snowpack is 2.87m. When I discuss the continental snowpack 'base' run the entirety of the snowpack depth was used as the continental snowpack itself is many metres thick. The sharp temperature change in the continental snowpack is due in part to the resolution of the available temperature measurements. For the snow on sea ice runs the model depth was changed to ~40cm by setting an impermeable layer at layer 10 (see 8.1.3). Snowpack density for these runs was chosen from observations of snow on the sea ice zone (Massom et al., 2001), as was the snow permeability.

The physical properties discussed in this section are set out in Table 8.2 for snow on sea ice and continental snowpack.

layer no.	depth from snow surface (m)	depth of snow layer (m)	Initial temperature of snow on sea ice snow (K)	Initial temperature of continental snowpack(K)
1	0	0.02359	253.15	233.15
2	0.02359	0.0278	253.15	233.15
3	0.05139	0.03277	253.15	233.15
4	0.08416	0.03863	254.15	233.15
5	0.12278	0.04553	255.15	233.15
6	0.16831	0.05366	256.15	233.15
7	0.22197	0.06325	257.15	233.15
8	0.28522	0.07455	258.15	233.15
9	0.35977	0.08787	259.15	233.15
10	0.44764	0.10357	260.15	233.15
11	0.55121	0.12208	261.15	233.15
12	0.67329	0.14389	262.15	233.15
13	0.81718	0.1696	263.15	233.15
14	0.98678	0.1999	264.15	233.15
15	1.18669	0.23562	266.15	233.15
16	1.42231	0.27772	267.15	243.15
17	1.70003	0.32735	267.15	243.15
18	2.02738	0.38584	267.15	243.15
19	2.41321	0.45478	267.15	243.15
20	2.86799	0.45478	267.15	243.15

Table 8.1, Snow Grid: *The snow module consists of 20 layers, included here are the depth of the bottom of each layer beneath the snow surface and the depth of each individual snow layer. Initial temperature for snow on sea ice snow is interpolated from observations by Massom et al. (2001), and the initial temperature for the continental snowpack is adapted from data collected at Halley from buried snow temperature probes (P. Anderson, pers. comm. 2012)*

snow type	LL thickness (m)	snow grain radius (m)	snow density (kg/m^3)	snow permeability as a function of depth (m^2)
Snow on sea ice	$2.0x10^{-8}$	$1.5x10^{-3}$	$3.5x10^{2}$	$8.0x10^{-10}$
Continental	$1.0x10^{-8}$	$1.0x10^{-3}$	$3.0x10^{2}$	$8.0x10^{-10}$

Table 8.2, snow parameters: *The snow module consists of 20 layers, here are the physical properties used to initialise the snow on sea ice. All measurements are taken from Massom et al. (2001).*

8.1.3. Chemistry initialisation in the snowpack

The model is initialised with gas and aqueous phase concentrations, the values used are measurements from a snow pit excavated at Halley. During the measurement period discussed in the previous chapters (12/08 – 18/09 2007), no snow pits were dug at Halley so there was no gas and aqueous phase chemistry available from this period with which to initialise the snowpack in the MISTRA-SNOW model. However, later on in the spring season on 19/10/2007 a snow pit was dug and measurements of ionic and aqueous content were made at varying depths from the surface down to several metres. This snow pit was dug in response to a storm and potential blowing snow situation, so the measurements were made a day after the storm was observed. These measurements gave me the opportunity to run MISTRA-SNOW initialised with actual measurements of snowpack composition at Halley. Measurement data collected on the physical properties of snow in coastal Antarctica (Massom et al., 2001) were also used to initialise the new snow module. The model atmosphere was setup using the coincident meteorological measurements made at the Halley site (as for the 1D model simulations in Chapter 5).

Although the measurements were not made at a time coincident with the main chemistry and meteorology data set being used here, the measurements still fall within the spring time period and are made only one month after the last observations from Halley (Chapters 5 and 6). All samples were stored frozen and returned to the British Antarctic Survey in the UK, where they were analysed using an ion chromatograph (IC) (Jones et al., 2009).

The partitioning of volatile aqueous species are determined by Henry's law equilibrium (Thomas et al., 2011), but ions are dealt with in a different manner. The concentration in melted snow is multiplied by an enhancement factor:

$$C_{LLL} = ø \times C_{snow} \quad \text{(R 8.1)}$$

The above equation (R8.1) describes the distribution/ partitioning of ions within the snow grain. C_{snow} is the concentration in melted snow, C_{LLL} is the concentration in the LLL and ø is the enhancement factor mentioned above. This enhancement factor describes the distribution of the ions between the LLL and the ice-like core of each snow grain (Thomas et al., 2011), by taking the measured (bulk) concentration in the melted snow sample and moving some (or all) of this measured concentration to the LLL at the surface of the model snow grain. The formation of liquid brine during freezing of water, and exclusion of non-volatile species from the ice-matrix during this process is well known (Thomas et al., 2011).

Surface ion concentrations should also increase due to gas deposition and dissociation in the LLL, when compared to the bulk concentration. When looking at frozen NaCl solutions it has been suggested by experiment that chloride is concentrated in quasi-brine layers (Cho et al., 2002), and there is also evidence from molecular dynamics simulations that chloride is excluded from the ice matrix upon freezing (Vrbka and Jungworth, 2005). To link this to bromide as well, at ambient temperatures lab studies show that chloride and bromide are found to be more concentrated on the surface of liquid water solutions than nitrate (Jungworth and Tobias, 2001, 2002; Thomas et al., 2007). In the absence of ions, it is also found that anisotropy at the ice-air interface leads to a LLL at the surface of pure ice (summarized by Rosenberg, 2005). The difference between the quasi-brine layer and the LLL at the surface of ice is discussed in Chapter 4.

In MISTRA-SNOW the enhancement factor of 3.3×10^4 used by Thomas et al. (2011) to represent the distribution of bromide and chloride was chosen using the knowledge that there is a liquid layer on pure ice and that chloride is concentrated in a liquid layer on freezing. Using this knowledge, bromide and chloride were placed entirely within the LLL on the surface of the snow grain, and nothing was initialised in the bulk. This re-distribution was achieved using the enhancement factor mentioned above. A key point to note is that the only bromine of any kind initialised in the model is in the form of bromide in the LLL of the snow grains in the snow.

	initial mixing ratio in nmol mol^{-1} (ppb)		
species	bottom of atmosphere	top of troposphere	Reference
NO	0.005	0.001	pers. comm. Neil Brough
NO_2	0.005	0.001	pers. comm. Neil Brough
HNO_3	0.01	0.05	Jones et al. (2007)
O_3	30	30	Buys et al. (2013)
HCHO	0.3	0.3	Reidel et al. (1999); Salmon et al. (2008)
H_2O_2	0.6	0.6	de Serves (1994); Snow et al. (2002);
PAN	0.01	0.1	Mills et al. (2007)
DMS	0.006	0.006	Read et al. (2008)

Table 8.3, snow atmosphere chemistry: *Initial mixing ratios (in nmol mol^{-1}) for gas phase chemical species used to initialise the atmosphere of the snow on sea ice run.*

species	initial mixing ratio in nmol mol^{-1} (ppb)	Reference
NO	0.005	pers comm Neil Brough
NO_2	0.005	pers comm Neil Brough
HNO_3	0.01	Jones et al. (2007)
O_3	30	Buys et al. (2013)
HCHO	0.3	Reidel et al. (1999); Salmon et al. (2008)
H_2O_2	0.6	de Serves (1994); Snow et al. (2002)
PAN	0.01	Mills et al. (2007)
DMS	0.006	Read et al. (2008)

Table 8.4, snow gas-phase: *Initial mixing ratios (in nmol mol^{-1}) for gas phase and chemical species used to initialise the snow of the "snow on sea ice" run.*

species	measured (melted snow) M	ø	Reference	LLL (initial) M
H+	3.5×10^{-6}	2.5×10^{3}	As for Thomas et al. (2011)	8.8×10^{-3}
SO_4^-	5.3×10^{-7}	2.5×10^{3}	Halley snow pit data	1.3×10^{-3}
NO_3^-	8.0×10^{-7}	2.5×10^{3}	Halley snow pit data	2.0×10^{-3}
CL^-	3.1×10^{-6}	3.3×10^{4}	Halley snow pit data	1.0×10^{-1}
Na^+	2.4×10^{-5}	3.3×10^{4}	Halley snow pit data	8.3×10^{-1}
Br^-	5.0×10^{-8}	3.3×10^{4}	Halley snow pit data	1.7×10^{-3}
MSA	$2.0 X10^{-8}$	2.5×10^{3}	Halley snow pit data	5.0×10^{-5}

Table 8.5, snow aqueous phase: *Concentrations of LLL chemical species used to initialise the snow of the "snow on sea ice" run. The only change between this setup and that for the continental snowpack is that the initialised Br^- changes from 5.0×10^{-8} mol/l to 0 mol/l.*

Initialisation of the chemistry of the atmosphere and snowpack in MISTRA-SNOW are given in Tables 8.3, 8.4, 8.5 and 8.6 for both the snow on sea ice and continental snowpack. As will be discussed in Section 8.3., the atmosphere of the continental snowpack run uses a restart file from the end of the snow on sea ice run as the initialisation.

Model meteorological parameters are shown in Table 8.6.

Run	Surface temperature (K)	Temperature gradient (K/m)	Horizontal wind speed (m/s)	Surface temperature amplitude (K)	Time of minimum surface temperature (hrs)
ice1	248	0.1	5	4	0900
snow1	240	0.1	5	4	0900

Table 8.6, snow meteorology: *Meteorological parameters used in the snow on sea ice, and continental snowpack runs. These value are based on measurements and observations made at Halley.*

8.2. Snow on sea ice run

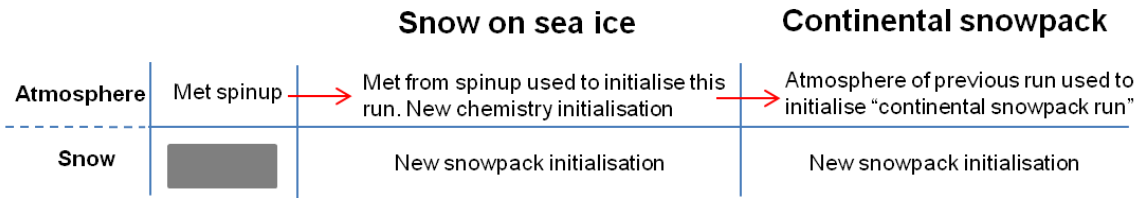

Figure 8.1: *Schematic of "snow on sea ice" and "continental snowpack" runs and setup, highlighting where each initialisation comes from.*

The meteorological conditions in polar regions are known to play a key role in our understanding of ODEs in some situations. However, the meteorological observations used for this study were only collected on site at Halley station ~14km from the edge of the sea ice zone. This means that only a 'best-guess' at the met conditions out over the sea ice can be given. We can, however, deduce that the air is likely to be wetter and warmer than that found over the continent due to the influence of sea ice and open water/ leads. The meteorological conditions that the model reproduces over the continental snowpack are of more interest here, so the model meteorological output will be discussed in detail in section 8.3 where the continental snowpack model simulation is discussed. The chemistry output from this snow on sea ice run will be considered here. A schematic highlighting the initialisations for these runs is shown in Figure 8.1 (details see below).

The first parameter that had to be initialised as it differs between the snow on sea ice and the continental snowpack was the snow depth. It was decided that a depth of 40-50cm would be used, as that is close to what is measured for snow depth on sea ice (Table 8.5) in the Weddell Sea (Massom et al., 2001). In order to keep the two model versions (snow on sea ice and continental snowpack) as similar as possible, this was achieved by setting a layer within the snowpack to be impermeable. This meant that although the model would still run for the full snowpack depth (discussed in section 8.3.), there would be no transport of properties between the adjoining layers.

As discussed in section 8.1.1., several of the physical parameters of the snowpack were changed between the continental snowpack and snow on sea ice model initialisations. Of key importance

is the initial temperature in the air above the snow, and in the snow itself. Although the temperatures measured at Halley itself can get as low as 230K, the air temperature over the sea ice zone will be much warmer (at least 10 to 20°C). The temperature of the snow-atmosphere interface as layed out in Massom et al. (2001) was used to define the sea ice zone air temperature used in these runs (248K). There were also measurements of the temperature of the snow-ice interface at the bottom of the snowpack in Massom et al. (2001). In order to get the temperature profile in the modelled snow on sea ice snowpack, the measured temperature at the air-snow and snow-ice interfaces were used to linearly interpolate for the layers in between.

The initialisation of the chemistry in the snowpack has already been discussed in section 8.1.3. An important difference between this snow on sea ice and the continental snow runs is the salinity of the snowpack. Surface salinity of young sea ice can be as much as 2-4 times that of old sea ice in the Weddell Sea (Eicken et al., 1992). From this, it was assumed that the bromide concentrations found in snow on sea ice in Precious Bay would be twice that measured in the continental snow at Halley. A value of 50×10^{-9} mol/l was used for the bromide concentration in the snow on sea ice (Table 8.4), but we used zero for the continental snow. This value was use to explore an extreme case of zero bromide content prior to contamination.

A short overview of the run setup is as follows: snow on sea ice run was initialised with the physical parameters and chemistry defined in tables (8.1, 8.2 and 8.3 and 8.4); the atmosphere was initialised with the chemistry in Table 8.3, and a 2-day meteorological spin-up (as described in Chapter 5 for the 1-D model initialisation) but with an initial atmosphere temperature of 248K. The model was run for a 24hr period starting and ending at midnight, the surface was changed from the snow on sea ice to open water for the last 15 minutes before midnight.

An open water surface was used in the model in order to replicate the lead/polynas system found in Precious Bay which is an area air masses often cross prior to arrival at Halley. This was achieved by changing the surface layer of the SNOW module so that the atmosphere doesn't interact with the snow layers beneath it, as well as changing the physical properties of the surface. To make this area of open water the surface temperature was set to 271K (to simulate water cold enough to freeze) and the saturation humidity was set to represent that over open water rather than over snow or ice. Now that the model setup and initialisation for this snow on sea ice run has been described in detail, it is possible to discuss some of the results.

Figure 8.2 shows several species which can be used to explore this run with regards to initialisation chemistry, ODEs and halogen release from the snow. When looking at the Br_2 and BrCl in the snow, it is clear that there is a model artefact as instantaneous Br_2 and BrCl production of that magnitude is unlikely to occur in the real snowpack. In the model it is due to Henrys law equilibrating and repartitioning between the aqueous and gas phase in the snow pack within one model timesteps. However, when looking at the atmospheric mixing ratios for Br_2 (10-20 pptv) and BrCl (1-3 pptv) they are not dissimilar to those measured at Halley (see Chapter 6). BrO is also produced during daylight hours both in the snowpack (up to 100 pptv) and the atmosphere (10-20 pptv). Much higher concentrations are formed in the snowpack, likely due to there being more Br_2 found there. Associated with the BrO production, there looks to be a small amount of ozone depletion in the atmosphere, and there is ~10 ppbv of ozone depleted within the snowpack. From these initial observations it is clear that there is interaction and mixing of air between the interstitial air of the snowpack, and the atmosphere above. This is caused by the wind pumping parameterisation (Cunningham and Waddington, 1993), which is the main source of gas transport in the snow and between the snowpack and atmosphere.

During the very first time-step of the model run, NO is entirely repartitioned to NO_2 both in the snowpack and the atmosphere by reaction with O_3. This is realistic as there is very little NO and no photolysis and no NO source (at least not in the model). Again the mixing ratios observed at Halley for NO and NO_2 (N. Brough, pers. comm. 2012) match well with those from the model, with similar NO_2 values compared with NO. There is a clear diurnal shape in both these species, with a minimum at 1800hrs for atmospheric NO_2, a maximum for NO_2 in the snowpack at noon, and a maximum above the boundary layer at ~ 140m during daytime for NO.

OH and HO_2 give an indication of daylight hours. HO_2 values output by the model of 1-2 pptv near the surface (up to 100m) match well with those calculated by Bloss et al. (2007) for the same time of year (0.76pptv – 1.5 pptv) for coastal Antarctica.

The atmosphere of this “snow on sea ice” run is used to initialise the atmosphere of the “continental snowpack” run, which I discuss in the next section.

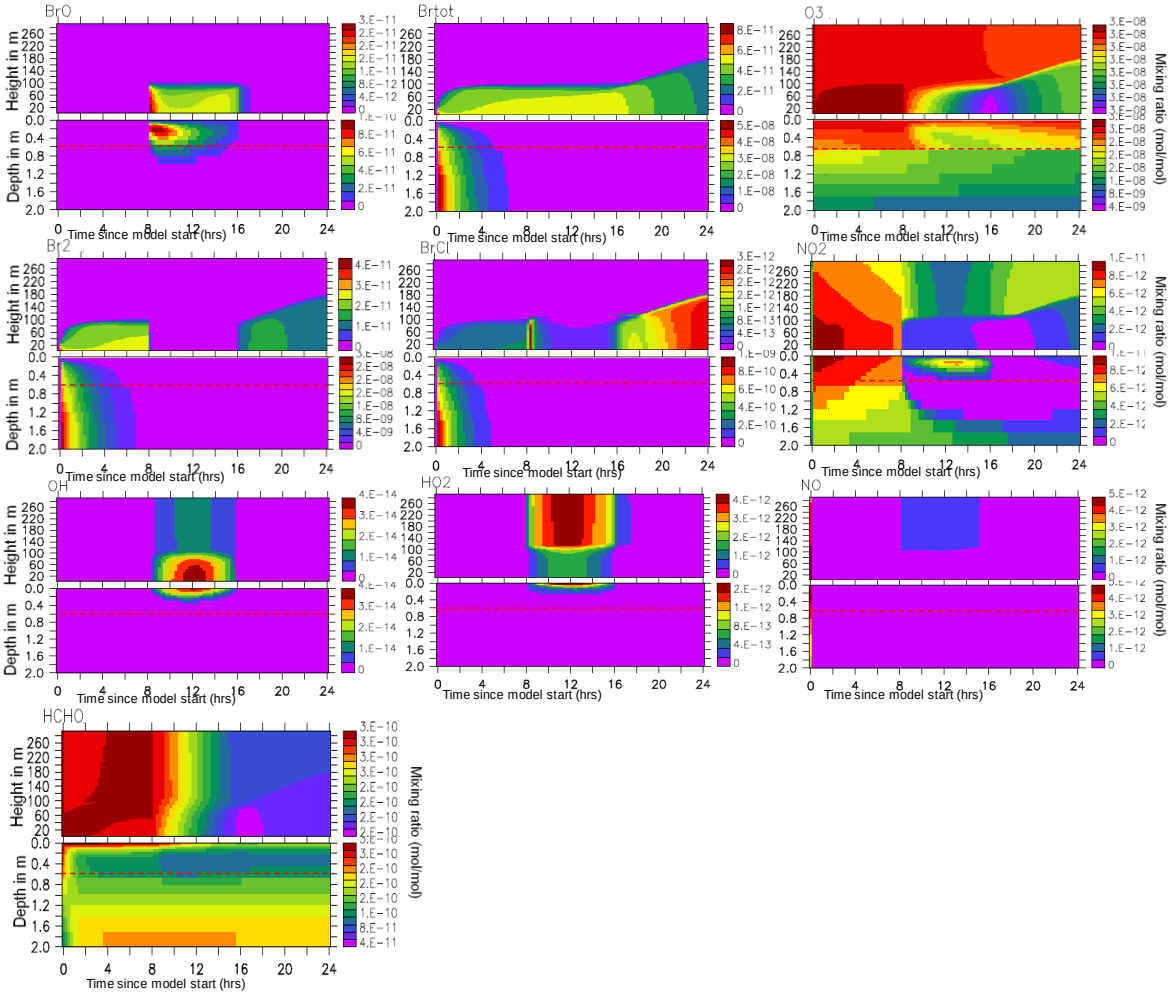

F***igure 8.2:*** *Model output of several chemical species from the snow on sea ice run; NO, NO_2, O_3, HCHO, OH, HO_2, Br_2, BrCl, BrO and total Br (all modelled gas phase Br-compounds). The upper panel for each species represents the atmosphere, with the lower representing the snow. The colour code on the right hand side is mixing ratios for each species, Time in hrs running along the bottom of the x-axis, and height in m (either above the snowpack for the atmosphere, or below the snow surface for the snow) on the left hand y-axis. The red line in the snow plot for each species emphasizes the depth at which the snow stops interacting with the layers above.*

8.3. Continental snowpack run

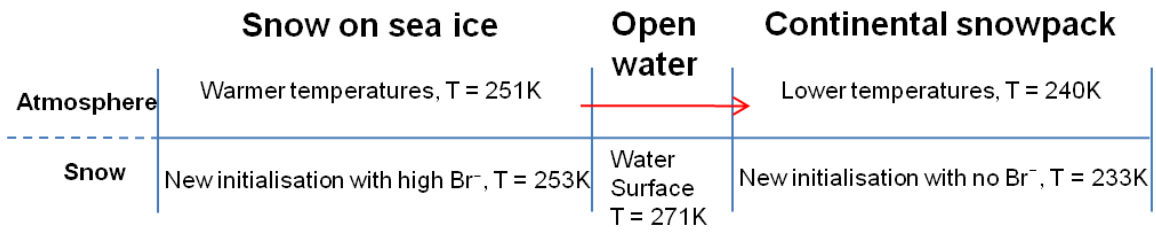

Figure 8.3: *Schematic for "snow on sea ice" and "continental snowpack" runs, showing some major features for the various stages of these runs.*

The model setup for the continental snowpack run was very similar to that described in section 8.3. for the snow on sea ice run, but there are some major differences (Figure 8.3). The main differences in the physical and chemical parameters of the snow have already been mentioned in section 8.1.2., so I will therefore go into detail regarding the changes made to the initial conditions for the atmosphere. It is possible to compare this run with observations from Halley.

The atmosphere for this run is initialised using a restart file that consists of the output from the final time step of the snow on sea-ice run. This restart includes both the meteorology and chemistry of the atmosphere. The snowpack, however, has a new initialisation which follows that laid out in Tables 8.1, 8.2, 8.4 and 8.5. The only three differences in the snowpack initialisation are the snow depth, snow temperature profile, and that the Br^- in the snowpack is set to 0. In the continental snowpack run it is assumed that all the bromine chemistry originates from Br^- in the snow on sea ice run, and is passed over to the continental snowpack run. For the continental snowpack the snow depth was not limited to ~40cm, but allowed its full depth of 2.87m as calculated based on the depth of the first snow layer. This was the same snow depth as used in previous studies with a similar model setup for continental snowpack (Thomas et al., 2011; 2012). This run is also 48 hrs in length instead of 24.

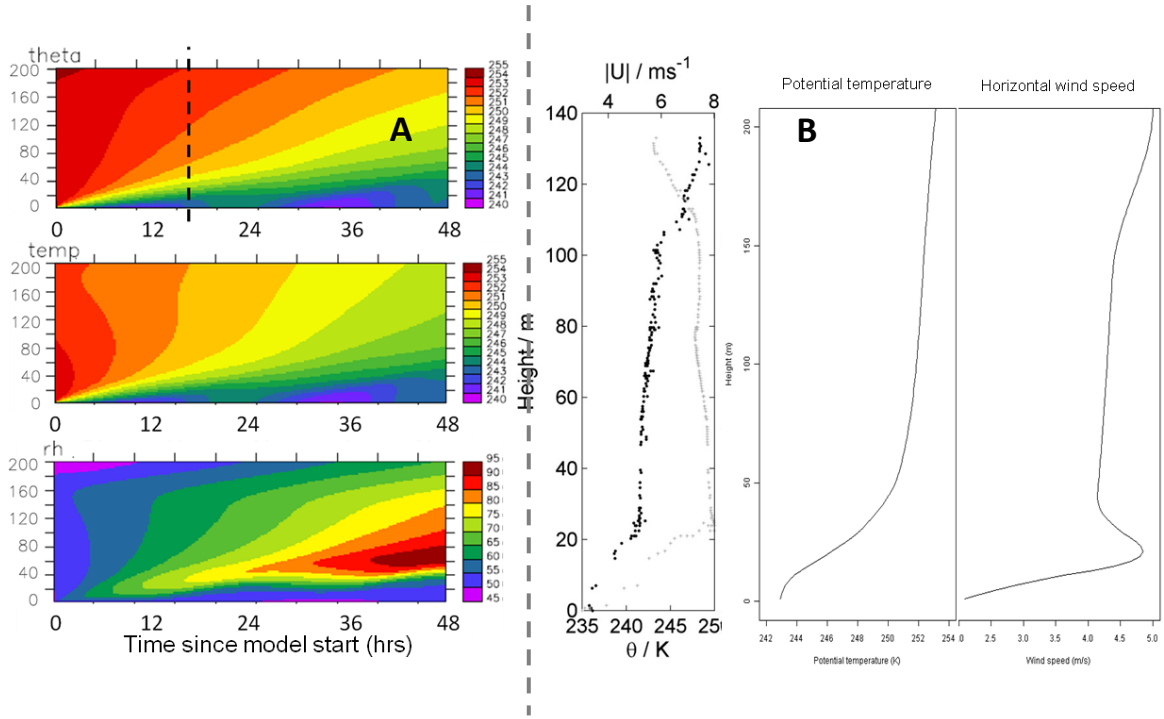

Figure 8.4: *Meteorological output from MISTRA-SNOW run for continental snowpack. a) contour plots with height (m) on the y-axis, and time since model run start (hrs) on the x-axis. Shown are potential temperature (theta) where the black dotted line indicates the time corresponding to the tethersonde flight (~1600 hrs), temperature and relative humidity (rh), and b) shows a tethersonde profile on the left from Halley (discussed previously in chapter 5), and a vertical profile of potential temperature and horizontal wind speed output from the continental snowpack MISTRA-SNOW run at 1600 hrs.*

In order to fully understand any results from these Halley based snowpack model simulations, the first task is to understand what the model is doing and see how representative it is of the 'real world'. Although this run (as well as the previous snow on sea ice run) represents an idealised case and is not representative of any specific event, it is still important to see how it compares to measurements made at Halley. The meteorology of the model atmosphere is the first thing to look at, and how it compares to the atmosphere as measured at Halley (Figure 8.4).

On September 7th 2007 a tethersonde was released at Halley which measured potential temperature (θ), horizontal wind speed (u) at different vertical heights in the atmosphere. In Figure 8.4a it is clear that the model creates a shallow, cold surface layer when looking at the temperature and potential temperature (theta). This is because the continental snowpack and surface temperatures used to initialise the run are much colder than the atmosphere from the restart of the previous run (Figure 8.3). This shallow stable BL is often seen at Halley (Jones et al.,

2010). The relative humidity increases throughout the model run, a consequence of the heat and moisture flux from the open water at the end of the snow on sea ice run.

When a vertical profile of the potential temperature and wind speed is plotted for 1600 hours of the first day of the model simulation (that is the same time as the tethersonde flight) the model captures the lower inversion level (although at ~40m instead of 20m, and it is not as sharp), but doesn't show a clear inversion above that (Figure 8.4b). The surface change in the model to open water during the last 15 minutes of the snow on sea ice run led to heat and moisture being input to the atmosphere, and increased the vertical mixing. This heat input and increased mixing are the reasons that the model doesn't clearly show an upper layer inversion, along with the fact that vertical mixing in the MISTRA model is faster than the real atmosphere (von Glasow, 2000). Other parameters from the model output when plotted as a vertical profile for the same time of 1600 hrs (horizontal and vertical wind speeds, liquid water content and relative humidity) do show two inversion layers at ~40m and ~160m.

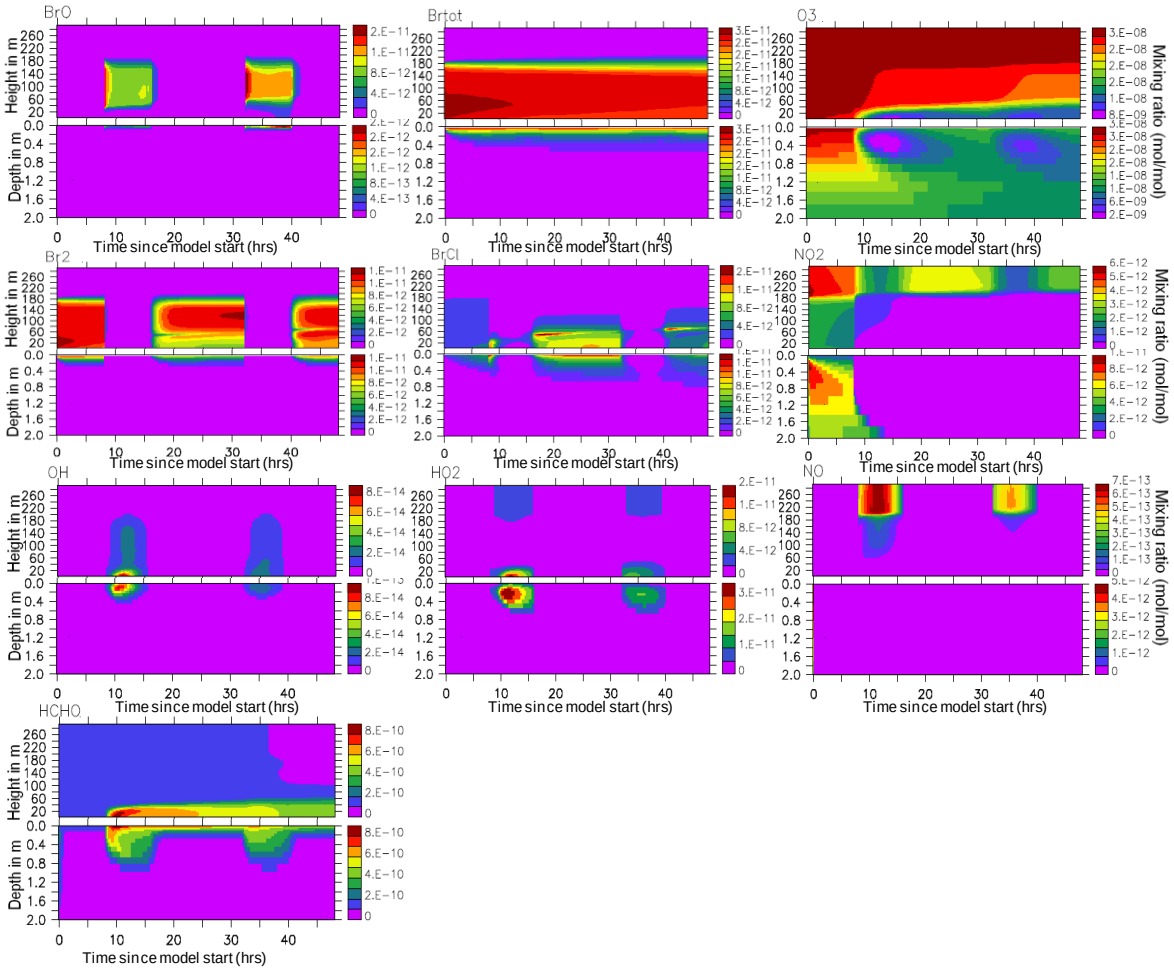

Figure 8.5: *Model output of several chemical species in the gas phase from the continental snowpack run; NO, NO_2, O_3, HCHO, OH, HO_2, Br_2, BrCl, BrO and total Br (all modelled gas phase Br-compounds). The upper panel for each species represents the atmosphere, with the lower representing the snow. The colour code on the right hand side is mixing ratios for each species, Time in hrs running along the bottom of the x-axis, and height in m (either above the snowpack for the atmosphere, or below the snow surface for the snow) on the left hand y-axis.*

The same chemical species as for the snow on sea ice run are plotted here for the continental snowpack run (Figure 8.5). Looking at Br_2 and BrCl in the snowpack it is immediately clear that the 'artificial' jump at the start of the run is not present, as there is no bromide initialised in the snowpack for this run. However, there is some mixing of these species down into the surface layers of the snowpack from the atmosphere. Br_2 and BrCl are present at mixing ratios not untypical compared to measurements at Halley; in the model they are caused by inflow from the

sea ice as modelled by using the “snow on sea ice” run as initialisation for this run With the onset of daylight Br_2 is completely photolysed both in the snowpack and in the atmosphere, with subsequent BrO production in both the atmosphere and the snowpack. Coincidentally there is near immediate BrO production of ~20pptv at sunrise. The creation of the shallow, cold surface layer clearly plays an important role in the extent of the ozone depletion that takes place in the model run. There is strong depletion of up to 22ppbv within the shallow surface mixed layer, and only mild depletion of ~10ppbv above it in the residual layer. The ozone depletion may be bromide limited as there is no BrO in the atmosphere of the shallow surface layer at all, yet the ozone is not completely depleted. The ozone depletion is even stronger in the surface layers of the snowpack, where 28ppbv (93%) is depleted within ~1 hr.

It is clear that the model does a good job of representing both the physical structure and chemistry of the atmosphere as observed at Halley. Something to note is that the only source of bromine chemistry in this continental snowpack run is the bromide initialised in the snow on sea ice, with only the bromine present in the atmosphere at the end of that run able to influence this run. Yet the mixing ratios for all bromine species follow the observations at Halley (see Chapter 6), and there is ozone depletion both in the snowpack and the atmosphere. It is apparent that the presence of this shallow surface mixed layer, which is observed at Halley (and reproduced by the MISTRA-SNOW model), plays a central role in determining the extent of ozone depletion as the bromine species are ‘trapped’ in a shallow layer where chemistry can progress without too much replenishment of the depleted ozone.

9. MISTRA-SNOW II: Exploring snow physical properties and snow-atmosphere interaction

Synopsis:

For this chapter, the MISTRA-SNOW model (as described in Chapter 8) is used to explore several important aspects of snow-atmosphere interaction and their effects on ozone depletion and bromine explosions. The first set of experiments stem from some questions and aims for future work as discussed in the final section of Abbatt et al. (2012). The discussion begins with the statement "First-year sea ice is a potentially important source of reactive halogens due to its highly saline surface", which is something that I have highlighted and discussed several times in previous Chapters (2, 6 and 7). The discussion then moves onto improving our understanding of the physical properties of snow and their effects on the snow-atmosphere exchange, as well as meteorological conditions. In this chapter both meteorological and snowpack properties will be explored, and their effects on snowpack/atmosphere exchange analysed.

9.1. Atmosphere – snowpack interaction

9.1.1. Physical properties

The physical properties of the snowpack are thought to play a key role in the transfer of gaseous species from the snowpack to the atmosphere, and vice-versa (Helmig et al., 2007). The MISTRA-SNOW model was used to explore changing several physical properties of the snowpack and their effect on atmospheric mixing ratios of gaseous species known to be released from the snowpack, and the effect on some species within the snowpack itself. The parameters which were looked at are the wind speed 10m above the snow surface (m s^{-1}), snow grain size (mm), and snow density (kg m^{-3}). The parameters used for each run are laid out in Table 9.1. Take note that changing the snow grain size will also change the LLL volume, even if the LLL thickness is not also changed. The LLL thickness was not changed for these runs, so when discussing changes in snow grain size we have to remember that the LLL volume is also changing. This will be discussed

in more detail below. Other associated wind pumping parameters (see section 9.1.2.) are as mentioned in Thomas et al. (2011). The model was set up for continental snowpack, initialised with 30 x 10^{-9} mol/l of bromide to have a bromine source, and was run for 5 days (120 hours).

run	wind speed (m s^{-1})	grain size (mm)	snow density (kg m^{-3})
1	**4**	**1**	**200**
2	**4**	**1**	**400**
3	**4**	**3**	**200**
4	**4**	**3**	**400**
5	**8**	**1**	**200**
6	**8**	**1**	**400**
7	**8**	**3**	**200**
8	**8**	**3**	**400**
9	**12**	**1**	**200**
10	**12**	**1**	**400**
11	**12**	**3**	**200**
12	**12**	**3**	**400**

Table 9.1, snow properties runs: *Outline of runs and changes made to physical properties of the snowpack. Wind speed was based on measurements made at Halley from 12/08/07 to 18/09/07, and chosen to represent high, low, and medium speed situations. Snow grain size and density were chosen from high and low values for the Weddell Sea from table 5 of Massom et al. (2001). Not all runs are explicitly described here.*

First I will look at the effect wind speed has on snowpack/ atmosphere interaction. This will be done by comparing runs 1, 5 and 9, keeping snow grain size and snow density constant and varying the model wind speed. BrO shows this change in the model runs clearly, and both the atmosphere and snowpack are shown in Figure 9.1 for each of runs 1, 5 and 9.

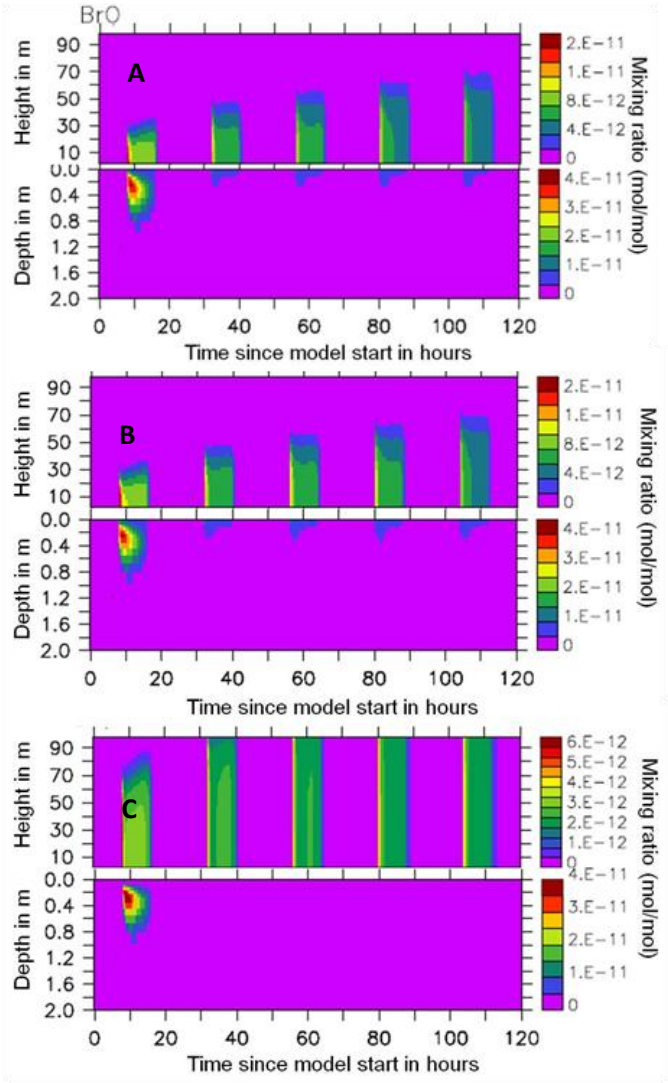

Figure 9.1: *Figure of model BrO in the atmosphere and snowpack interstitial air for a) 4ms^{-1} run, b) 8ms^{-1} run, c) 12ms^{-1} run. Top panel is atmosphere, bottom is snow. Note that BrO in the atmosphere of plot c) is on a different mixing ratio scale.*

Increasing the wind speed has led to greater vertical mixing in the atmosphere above the snowpack, highlighted by the increased vertical extent of BrO in Figure 9.1c compared with 9.1a and 9.1b. There is a change in snowpack interstitial air (near surface) BrO between Figure 9.1a and 9.1c. This is caused by increased ventilation from the snowpack as well as a reduction in surface deposition. The reduction in mixing ratios in Figure 9.1c, compared with 9.1a and b, is caused by the increased height of the BL which BrO has to mix into. Total column BrO for these runs is similar, but it is spread over a larger area.

What happens if the density of the model snowpack is changed? At low wind speeds (in this case 4ms^{-1}), snow density change does not have a big effect on snow/ atmosphere exchange. However at higher wind speeds (8ms^{-1} and 12ms^{-1}) the effect is more pronounced. Figure 9.2 shows again BrO for a constant wind speed of 8ms^{-1}, constant snow grain size of 1mm, but changing the snowpack density from 200kg m^{-3} (Figure 9.2a) to 400kg m^{-3} (Figure 9.2b).

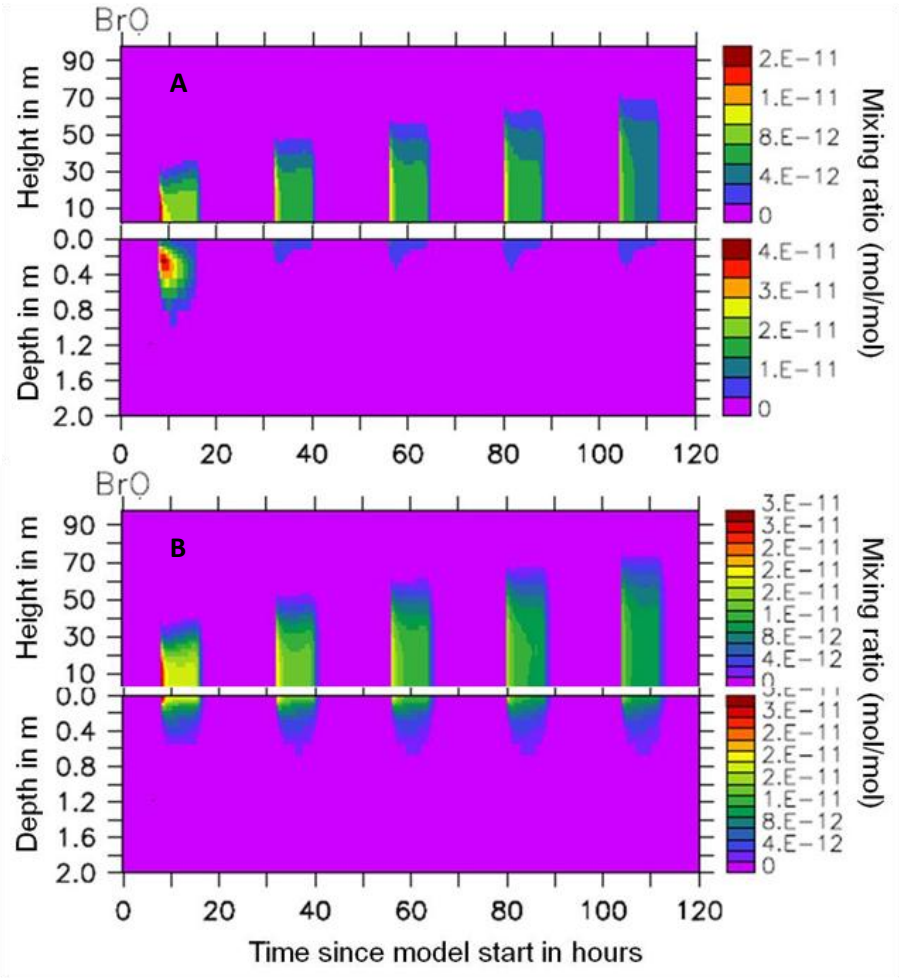

Figure 9.2: *Figure of model BrO in the atmosphere and snowpack interstitial air for a) 200kg m^{-3} snowpack density run (run 5), b) 400kg m^{-3} snowpack density run (run 6).*

The difference between these model runs is that the denser snowpack run (Figure 9.2b) has ~2x more Br^- in the snowpack caused by the difference in density. The denser snowpack means there is more snow, more LLL and therefore more initial bromide. There is an increase in atmospheric

bromine species mixing ratios due to the increased snowpack bromide (Figure 9.2b), indicating that snow-atmosphere exchange is also greater in this run. This increased snowpack density has also increased the LLL-interstitial air exchange.

Changing the snow grain size again had little to no effect on snow-atmosphere exchange at low wind speeds, but at $8ms^{-1}$ it is clear that there are some large differences between these runs. For these runs (run 5 and run 7) a constant wind speed of $8ms^{-1}$ was used, a constant snowpack density of 200kg m^{-3}, the snow grain size was changed from 1mm to 3mm. It is key here to remember that although the thickness of the LLL (liquid like layer) found on the surface of each snow grain was not changed, due to changing the size of the snow grain its volume will have changed.

There are some notable differences in the model output of runs 5 and 7 (Table 9.1). Bromine and chlorine species have much lower mixing ratios in both the snowpack and atmosphere for run 7 (3mm snow grain) compared with run 5 (1mm snow grain). The reason for this becomes clear when exploring the model output for the snowpack aqueous phase, as there is ⅓ of the NO_3^-, ¼ of the Cl^-, and ¼ of the Br^- found in run 7 compared with run 5. The relative change is not the same in the initialisation as the enhancement factor (see chapter 8), although the same for bromide and chloride, is different for nitrate.

As discussed in Section 8.1.3., Thomas et al. (2011) use specific enhancement factors for Cl^-, Br^- and NO_3^-. The value of the enhancement factors was not changed prior to these runs. The enhancement factor describes how ions are distributed between the LLL and the ice-like core of the snow grain, and was a fitted parameter in their model runs (Thomas et al., 2011). Unfortunately this change in enhancement factor was not taken into account for these runs, so the enhancement factor used is not fitted for these snow grain properties. By changing the snow grain size by this much, the enhancement factors employed no longer do what they were intended to do, i.e. place all the bromide and chloride in the LLL near the surface of the snow grain so that there is none left in the ice-like core of the snow grain.

9.1.2. Wind pumping parameters

In this section I make a comparison of model output for the wind pumping (mixing of air above the snowpack with the interstitial air near the surface) parameters used by Thomas et al. (2011),

and a new set of observations for wind pumping made for the new Halley VI site. This is to check the influence (and importance) of the different wind pumping parameters used in the MISTRA-SNOW model (namely amplitude and wavelength).

run	amplitude (cm)	wavelength (m)
base	**1.5**	**0.03**
hw1	**4**	**4**
hw2	**4**	**6**
hw3	**5**	**4**
hw4	**5**	**6**
hw5	**6**	**4**
hw6	**6**	**6**
hw7	**-**	**-**

Table 9.2, wind pumping runs: *Parameters to explore the importance of wind pumping to halogen release to the atmosphere. Values are a range as measured at Halley (Neil Brough, pers. comm., 2013).*

These parameters correspond to the amplitude and wavelength of the crests and dips of the snowpack created by the winds influence. Up to this point (and including the runs in section 9.2 – 9.3) the wind pumping parameters used by Thomas et al. (2011) were also used for the Halley runs, as no measurements of snowpack wave amplitude or wavelength were made at Halley at the same time as the other measurements discussed in previous chapters (5,6 and 7). During the 2012-2013 summer season Neil Brough, a member of BAS staff at Halley working to set up the newly re-opened CASLab, was contacted and asked to take this set of measurements of the snowpack at the Halley site. Although the Halley site had moved since the original measurements were made (CASLab moved to the new Halley VI site), it was still located on the Brunt Ice-shelf so would be affected by similar meteorological conditions. The observed values are shown in Table 9.2, and were input to the model and used to parameterise wind pumping at Halley in these model runs. These 5 day long model runs are compared with a 5-day base run using the Summit wind pumping parameters (Thomas et al., 2011), and there is also a run where the wind pumping is switched off in the model (Table 9.2.).

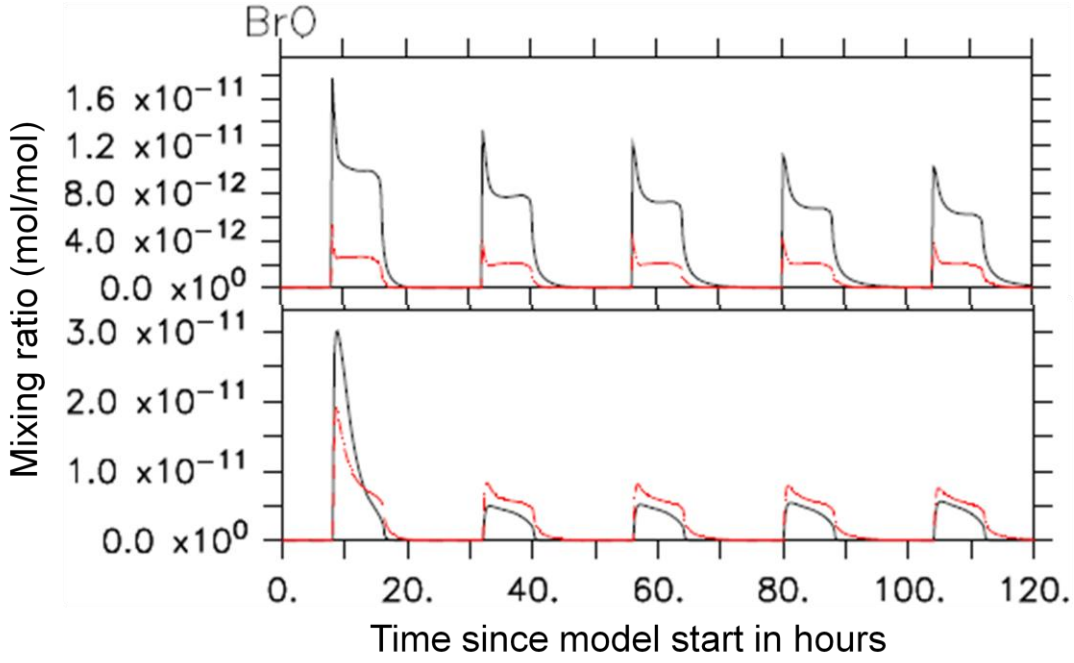

Figure 9.3: *Plot of model output for BrO in the atmosphere (4.5-6.5m above snow) and the snow (8-12cm depth), with a comparison between the Summit base run (black line) and hw1 (red line).*

BrO was chosen to be plotted here for the reasons outlined in the previous section (and discussed further in section 9.3). It is clear from figure 9.3 that changing the wind pumping parameters do have some effect on snow atmosphere exchange. In this case there is ~20% more BrO in the 'Halley' snowpack (run hw1 from Table 9.2) than in the "Summit base run" using the Summit wind pumping parameters (Thomas et al., 2011), and lower BrO mixing ratios (~70% less) in the atmosphere of run hw1. This indicates that there was less transfer between the snowpack and atmosphere in run hw1, than in the base run using the Summit parameters.

The next parameter tested was the effect changing the amplitude of the wave in the snowpack at Halley has on wind pumping/ snow-atmosphere exchange. These three values of 4, 5 and 6cm (runs hw1, hw3 and hw5) represent 3 different measurements made at Halley.

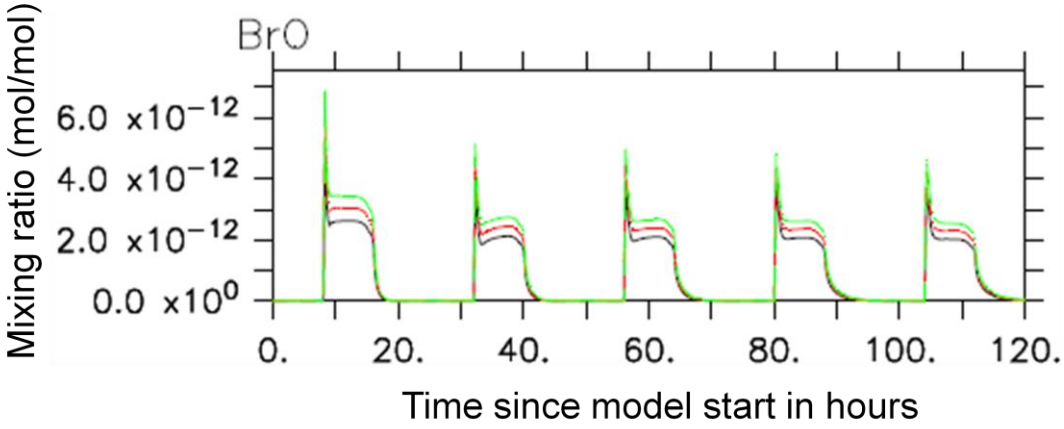

Figure 9.4: *Plot of model output for BrO in the atmosphere (4.5-6.5m above snow) with wavelength kept constant at 4m, and changing amplitude from 4cm (black line),to 5cm (red line) and 6cm (green line).*

Only the model atmospheric mixing ratio of BrO is shown in Figure 9.4, as the snowpack mixing ratios in the model were very similar for each amplitude (4-6cm) to that found in run hw1 (Figure 9.3). There is only a difference of ~1pptv between all three of these runs, with the 4cm amplitude showing the lowest snow atmosphere exchange (lowest BrO mixing ratio) and the 6cm amplitude showing the highest BrO in these simulations. Although the range of these amplitudes is very small, it is clear that changing the amplitude of the snow crests within Halley observed values has a small effect on air exchange from the snowpack to the atmosphere.

But what effect does changing the wavelength of the snowpack wave structure have on snow/atmosphere air exchange? To explore, the wavelength was varied from 4m to 6m, and the wave amplitude was kept constant at 5cm.

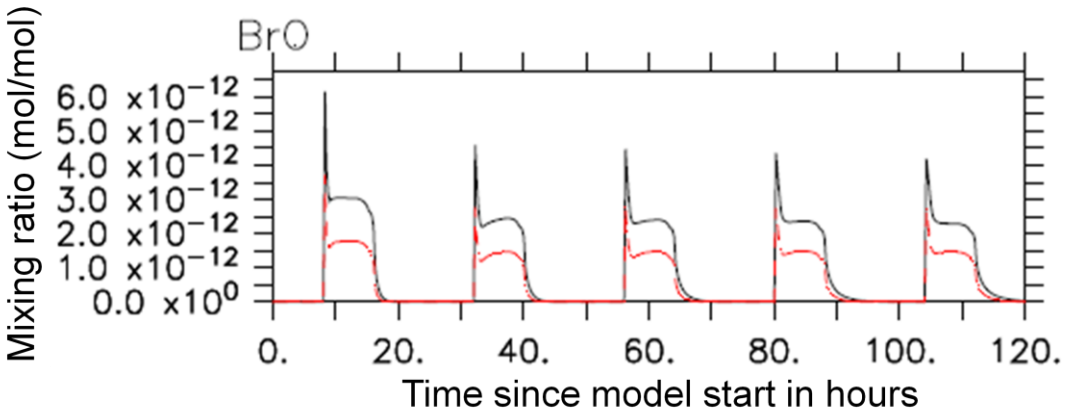

Figure 9.5: *Plot of model output for BrO in the atmosphere (4.5-6.5m above snow) with amplitude kept constant at 5cm, and changing wavelength from 4m (black line), to 6m (red line).*

Again only the model atmospheric mixing ratio of BrO is shown in Figure 9.5, as the snowpack mixing ratios in the model differed only slightly for each wavelength from what they were for run hw1 (Figure 9.3). The longer 6m wavelength run has ~40% less BrO in the atmosphere ~5m above the snowpack than the shorter 4m wavelength run. Other bromine species follow a similar trend with smaller mixing ratios in run hw4 compared with hw3. From this it is possible to conclude that changes in wavelength (within the limits set by observations at Halley) have a greater effect on snowpack/atmosphere exchange than does amplitude of the snow waves.

As a final test, the wind pumping mechanism was switched off in the model.

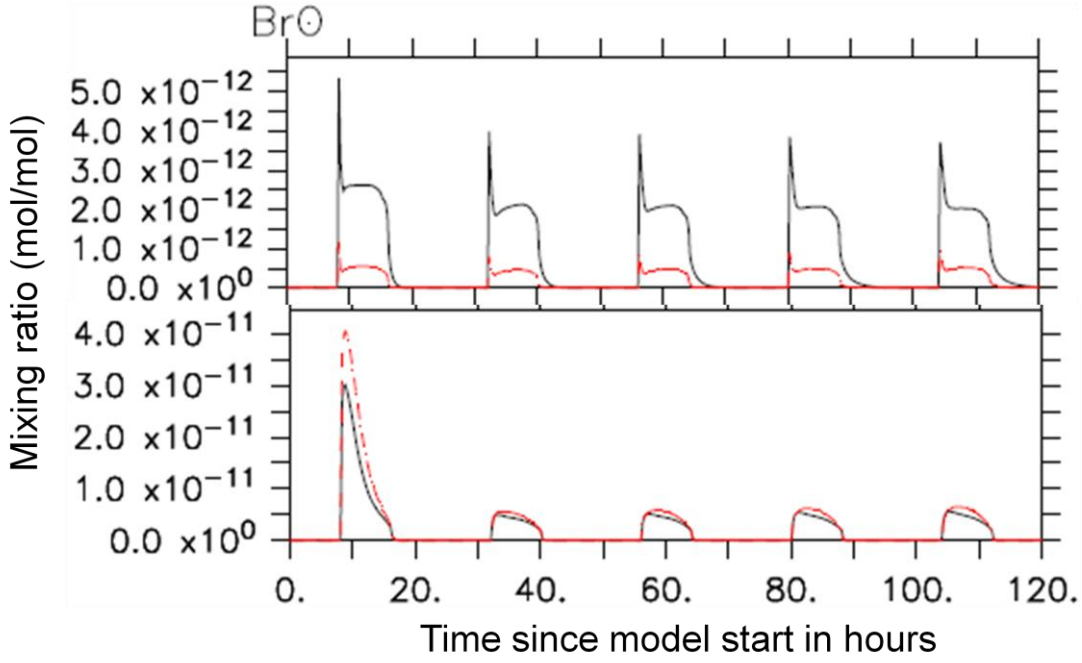

Figure 9.6: *Plot of model output for BrO in the atmosphere (4.5-6.5m above snow) and in the snow (8-12cm depth), with wind pumping switched off in the model run hw7 (red line), compared with run hw1 (black line).*

As expected, switching off the wind pumping mechanism (Figure 9.6) has the most dramatic effect on bromine in the atmosphere (proxy for snowpack/atmosphere exchange). Not only that, but there is even slightly more BrO present in the snowpack for this run. All the other runs (hw1-hw6) showed very little change in their snowpack mixing ratios for any species, but there is clearly more BrO in run hw7 compared with run hw1 in Figure 9.6.

These runs were sensitivity studies to see what impact changing the wind pumping physical parameters to those observed at Halley would have on snow/ atmosphere exchange. Unfortunately the data for the amplitude and wavelength for Halley were only used in the model after the runs discussed in section 9.3. For the other the SNOW runs discussed in this Chapter, wind pumping parameters used are the same as used in Thomas et al. (2011).

9.2. Snowpack salinity sensitivity studies (LGM + present)

Snowpack salinity is a concept discussed by Abbatt et al. (2012), as previously mentioned at the start of this chapter. To explore this feature, the MISTRA-SNOW model (Thomas et al., 2011; 2012) was used to explore the salinity required to initiate an ozone depletion event (ODE). ~3 $x10^{-8}$ mol/l of bromide was a value measured in the snow at Halley (see Chapter 8) and was used to initialise the model for the first of the runs presented in this section. This is then compared with model simulations of 0.5x, 1x, 1.5x, 2x, 4x, and 10x this "base" bromide. Model output is representative of a height of 5-7m above the snowpack, and 10-15cm below the snow surface (Figures 9.7 and 9.8). These runs also contain the model initialisation artefact (introduced in chapter 8)

The bromide values used are all within observed concentrations either in situ at Halley (present day scenario, Figure 9.7a and 9.8a), or found in ice core records dating back to the LGM (last glacial maximum, Figure 9.7b and 9.8b) (Spolaor et al., 2013). Due to wind pumping action model mixing ratios are similar at a depth of 10-15cm in the snowpack, to those in the atmosphere above.

Figure 9.7 shows model results for Br_2 and BrCl. Looking at 9.7a, Br_2 production steadily increases in both the snowpack and the atmosphere as the snowpack bromide is increased. However, when looking at BrCl, the lowest bromide concentration initially (first 2 days of run) shows a larger mixing ratio in the atmosphere than for the 1x 'base' run. This is also apparent in the snowpack, which can be explained by a bromide limited snowpack leading to production of BrCl over Br_2.

For the higher initial bromide concentration runs (Figure 9.7b), as the bromide increases so does Br_2 in the atmosphere and snowpack. It looks to be a simple relationship of both bromide and Br_2 increase by a factor of 2. Again, looking at Fig 9.7b) BrCl also continues to increase with increasing bromide on the first 2 days of the run, but once the bromide gets to 4x and 10x there is no BrCl in the atmosphere after the 3rd and 1st days respectively. Br_2 also looks different for the 10x run when compared with the previous runs. The reason for the lack of Br_2 and BrCl in the 4x and 10x runs is that all of the ozone is depleted in both the snowpack and atmosphere, meaning a different oxidation pathway comes into play and the bromine is ending up in reservoir species (hence the coincident drop in BrO as seen in Figure 9.8b and discussed further below).

There looks to be non-linearity in the effect the bromide increase in the LLL has on BrO production, and also on ozone depletion rates (Figure 9.8), with depletion increasing rapidly as bromide is increasing. BrO production in both the atmosphere and the snowpack interstitial air falls off rapidly with time in the higher bromide runs (Figure 9.8b). Ozone has near complete depletion by the 3rd day for the 4x run, and by the 2nd day for the 10x run (Figure 9.8b). No ozone means no BrO can be produced, hence the drop in BrO on these days. The “10x bromide” run is using a bromide concentration found in ice cores dating back to the LGM (Spolaor et al., 2013). Model simulations suggest that the high bromide content would have meant much less ozone in the polar lower troposphere during the spring months in coastal polar regions. Quite simply more bromide in the snowpack leads to more gas phase bromine species and more ozone depletion, both in the snowpack and the atmosphere above it.

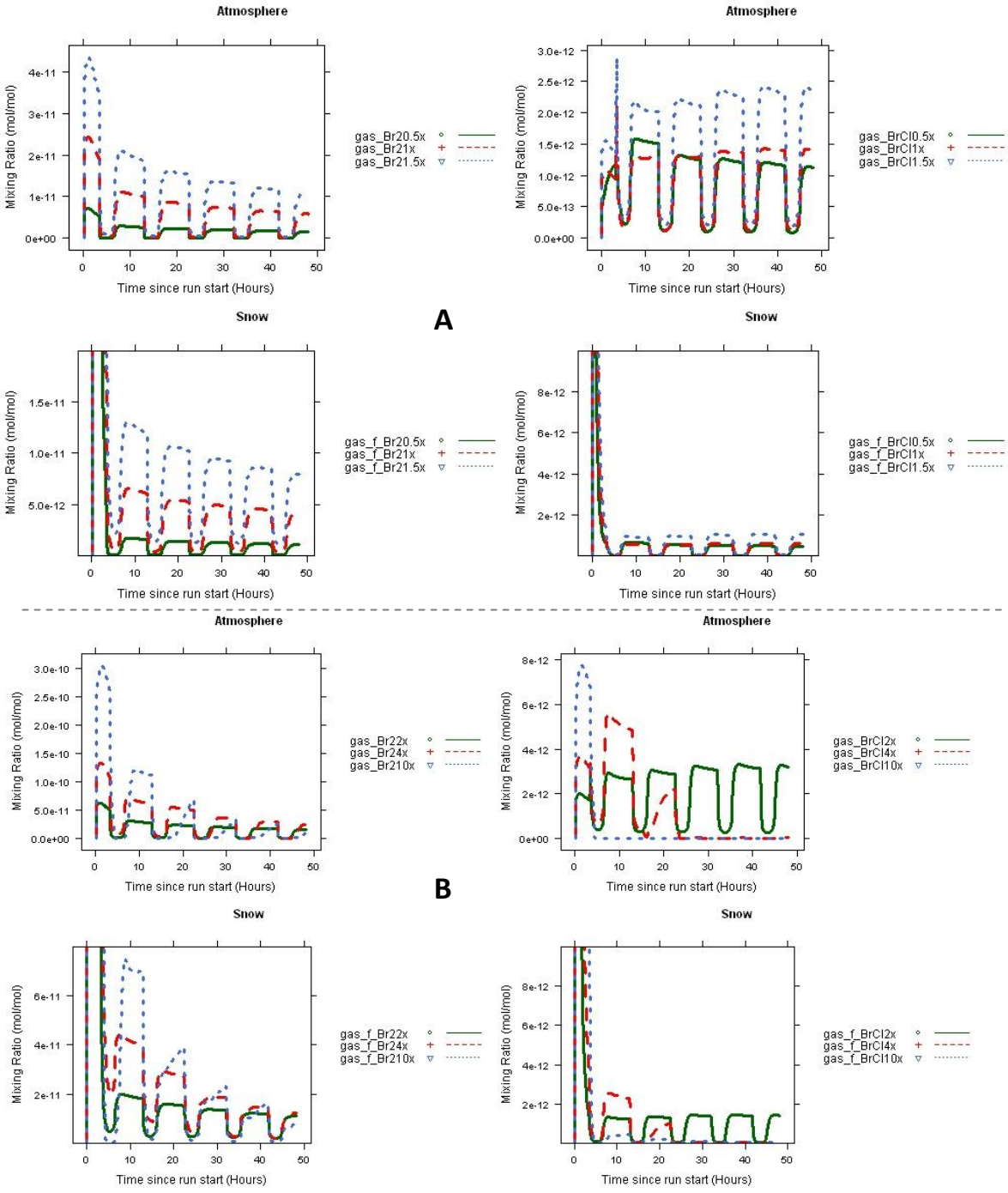

Figure 9.7: *a) Br_2 and BrCl with 0.5x to 1.5x "base" bromide in the liquid like layer (LLL), b), as for a) but with 2x to 10x "base" bromide.*

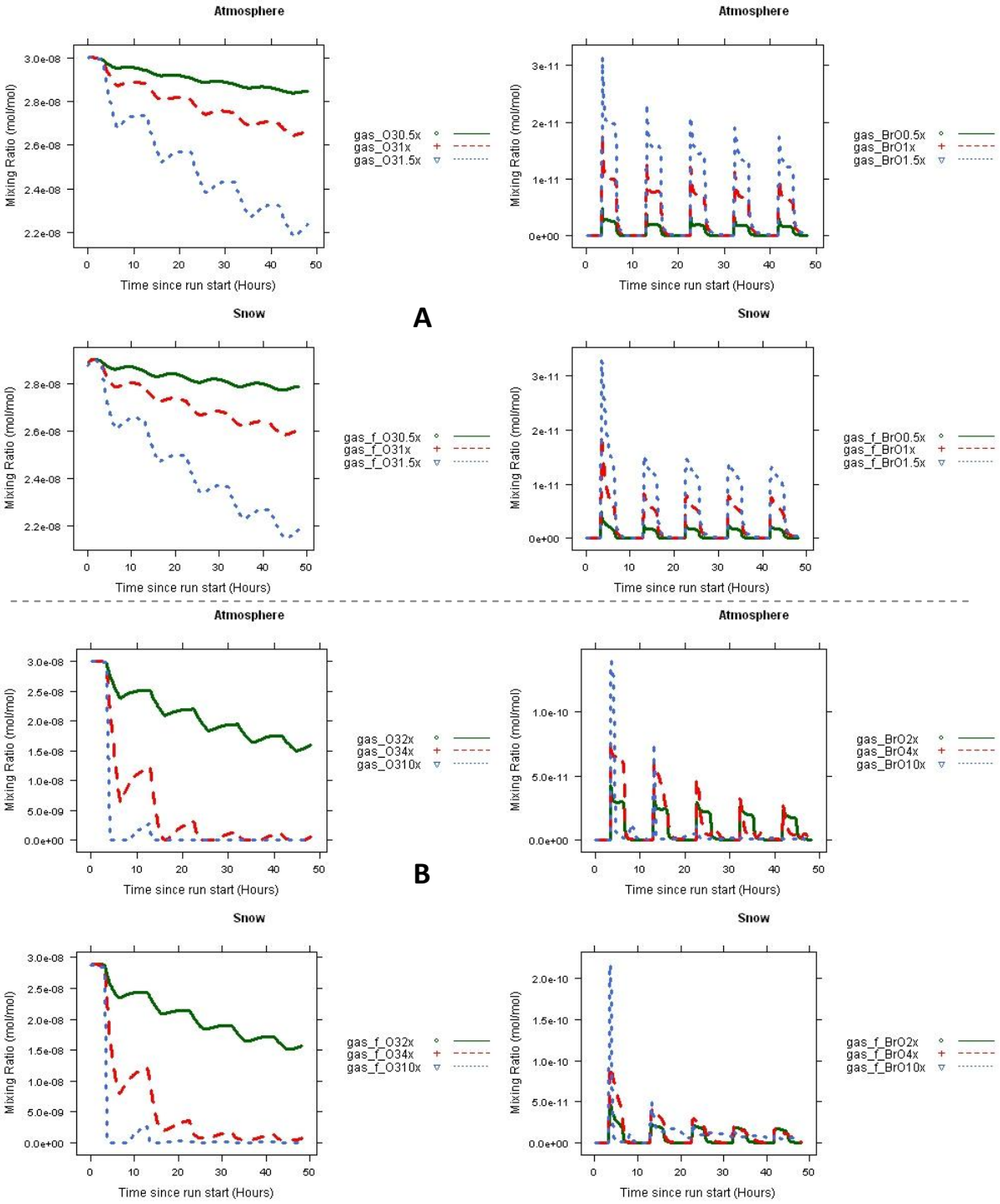

Figure 9.8: *a) O_3 and BrO with 0.5x to 1.5x "base" bromide in the liquid like layer (LLL), b) as for a) but with 2x to 10x "base" bromide.*

This is a good point at which to highlight that the only source of bromine to the atmosphere and the snowpack interstitial air in these runs was Br^- in the snowpack. You can generate a complete ODE within 2 model days when snowpack Br^- is 4x present day. Note the discontinuity between 2x and 4x bromide runs. This suggests real sensitivity to Br^-, which is relevant given our lack of

knowledge of Br^- concentrations in the snow on sea ice zone, and how heterogeneous its distribution is both spatially and with depth (and time through the year).

9.3. Surface changes – coupled snow on sea ice/ continental snowpack runs

This section carries on from the initial 'base' runs discussed in sections 8.1.2 and 8.1.3., where the initial model setup for snow on sea ice and continental snowpack was discussed. The aim here is to explore the importance of snow on sea ice as a precursor to the observation of elevated mixing ratios of brominated species and ODEs seen over the continental snowpack at Halley. This experiment has been performed previously using the MISTRA model (Piot and von Glasow, 2008), but the new SNOW module was not developed at that time. This means that the model simulations discussed here are a logical next step forward from the runs of Piot and von Glasow (2008), where we can now use the snow as both a source and a potential recycling mechanism for Br_2 and BrCl deposited to the snow. As discussed in Thomas et al. (2011), and in Chapter 8, the SNOW module is fully coupled with the previously-used MISTRA model so there is exchange of chemical species between the snow and atmosphere as is seen in the field.

There are 2 sets of runs discussed in this section both of which include snow on sea ice, and continental snowpack. The first set will use the model setup and initialisations mentioned in chapter 8 where a 2 day meteorological spin up is used to initialise the meteorology of the snow on sea ice run (the entire snowpack, and chemistry of the atmosphere, are initialised for the first time here), and the atmosphere just continues to run as the surface changes from snow on sea ice to continental snowpack (which has a new initialisation) (Section 9.3.1.). The second set of runs are similar, but are setup/ initialised in a different way to rid the model output of the initialisation artefact discussed in Chapter 8 (see Section 9.3.2.).

9.3.1. Surface change runs 1

The model setup is best described with an illustration which links these model simulations and physical parameters with those of the idealised (yet realistic) situation which we assume to be occurring at the Halley site (Figure 9.9). The situation of air passing over the Weddell Sea sea ice

zone and Precious Bay prior to arrival at Halley has been highlighted previously (sections 2, 3, 6, and 7), and is what was used to base these model simulations on.

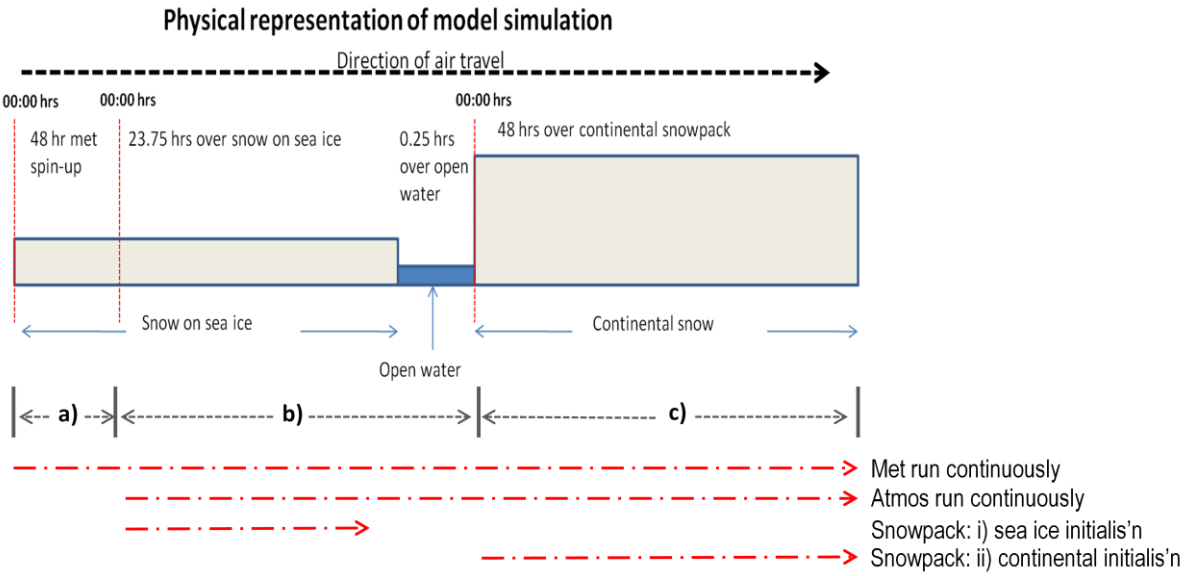

Figure 9.9*: Diagram of the basic physical representation of the model setup and subsequent simulations run using the setup. a) here is an initial 2-day meteorological spinup, followed by b) a 24 hour run with snow on sea ice as the surface and the meteorology from the spinup as a restart (including the final 15 minutes of the run over open water, representative of a lead in the real environment) but with a new initialisation for chemistry in the atmosphere and the snowpack, and finally c) a 48 hour run over the continental snowpack where the atmosphere in its entirety (chemistry and meteorology) from the previous snow on sea ice run are used as a restart, but the snow has a new intitialisation.*

The suite of runs are shown in Tables 9.4 and 9.5, for snow on sea ice and continental snowpack respectively. The main differences in the snow on sea ice runs (Table 9.4) are the presence of a lead/ open water for the last 15 minutes of the model run, and whether the atmosphere was initialised with any Br_2. This lead is a feature often seen at Precious Bay, and the duration the air would take to pass over a typical lead travelling from the sea ice zone to Halley was calculated to be ~15 minutes using sea ice maps overlaid with HYSPLIT back trajectories. It is possible that the atmosphere is slightly chemically 'processed' prior to arrival at Precious Bay (e.g. bromine rich from passing over another source area), hence the runs with Br_2 initialisation in the atmosphere.

Run no.	Open Water	Time of run start (24hr run)	Atmos Br_2 Init (pptv)
ice1	Y	00:00	0
ice2	Y	00:00	10
ice3	Y	12:00	0
ice4	Y	12:00	10
ice5	N	00:00	0
ice6	N	00:00	10

Table 9.3, snow ice runs 1: *Parameters changed between the different snow on sea ice runs, including the presence of a lead/ open water for the last 15 minutes of the run, the model start time (either midday or midnight) and the run being initialised with/ without any Br_2 in the atmosphere.*

Run no.	Atmos restart	Snow Br^- (mol/l)
snow1	ice1	0
snow2	ice2	0
snow3	ice1	25×10^{-9}
snow4	ice2	25×10^{-9}
snow5	ice3	0
snow6	ice4	0
snow7	ice3	25×10^{-9}
snow8	ice4	25×10^{-9}
snow9	ice5	0
snow10	ice6	0
snow11	ice5	25×10^{-9}
snow12	ice6	25×10^{-9}

Table 9.4, continental snow runs 1: *Parameters changed between the different continental snowpack runs, including which snow on sea ice atmospheres were used, and whether the run was initialised with/ without any Br^- in the continental snowpack.*

The runs ice1 and snow1 have already been discussed/ outlined in the previous chapter, and were used as the base case for comparison with the other runs shown in Tables 9.3 and 9.4.

The measurement site discussed throughout this thesis is situated over the continental snowpack at Halley, ~14km from the sea ice zone (see Chapter 3). For this reason, and following the model setup described in Chapter 8, these snow on sea ice runs (Table 9.4) are used as a spinup for the atmosphere to restart the continental snowpack runs.

I will first look at the runs which have a lead included in the snow on sea ice runs (ice1-4, and snow1-8). The initial jump in Br^- and Br_2 obvious in the model output of the snowpack is mentioned previously in Chapter 8. This repartitioning and re-equilibrating at model initialisation is dealt with in a different manner in the next section (9.3.2.) so will not be discussed in detail here.

Looking at the continental snowpack runs, by keeping the atmosphere restart the same (in this case using ice1), it is possible to look at the influence of including bromide in the continental snow at model initialisation (snow3). The pH of the LLL on the snow grains (see chapter 2) is the same for these runs (~pH2). Comparing snow1 (no bromide initialised, shown in Figure 8.5 in Chapter 8) and snow3 (Figure 9.10) there is clearly less ozone depletion and less chlorine in the atmosphere of snow3, which looked to play a role in the ODEs of the run snow1 due to the chloride dominated snowpack. Other than an initial jump in the atmosphere Br_2 and BrCl at the start of the run (caused by the snowpack repartitioning mentioned in Chapter 8), bromine compound mixing ratios are very similar.

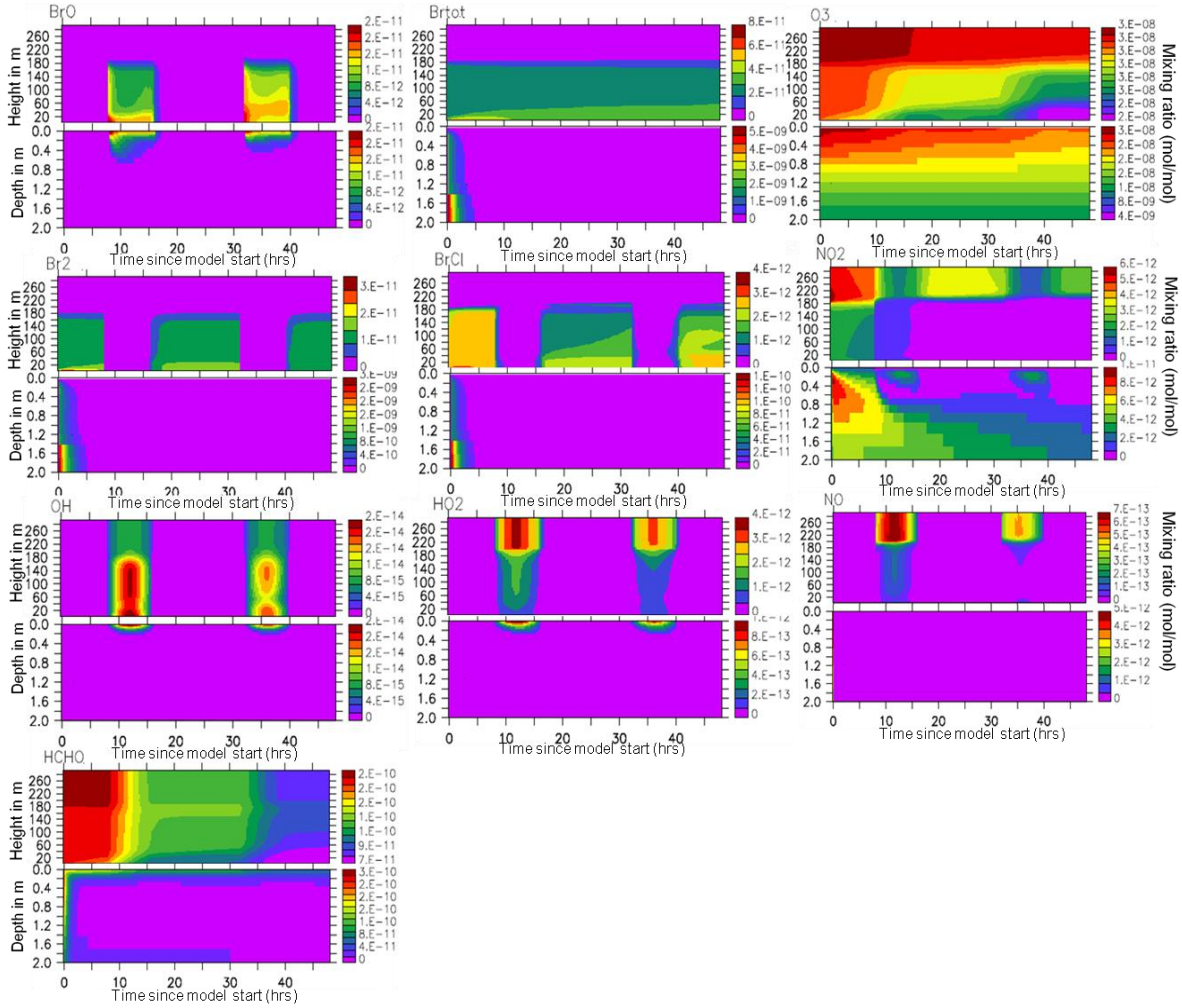

***Figure 9.10**: Model output of several chemical species from the continental snowpack run snow3; NO, NO_2, O_3, HCHO, OH, HO_2, Br_2, BrCl, BrO and total Br. The upper panel for each species represents the atmosphere, with the lower representing the snow. The colour code on the right hand side is mixing ratios for each species, Time in hrs on the x-axis, and height in m (either above the snowpack for the atmosphere, or below the snow surface for the snow) on the left hand y-axis.*

However, there is a very different picture unveiled when exploring the snowpack from these runs. In snow1 (Figure 8.5) there is clearly extreme ozone depletion starting at the first model sunrise from 30ppbv down to 0.2 ppbv (>99% depletion), which is also apparent to a similar extent (~97% depletion) in the atmosphere. Depletion of ~30-40% is seen in the snowpack of snow3, and there is clearly a similar proportion of depletion in the atmosphere but not to the same extent seen in snow1.

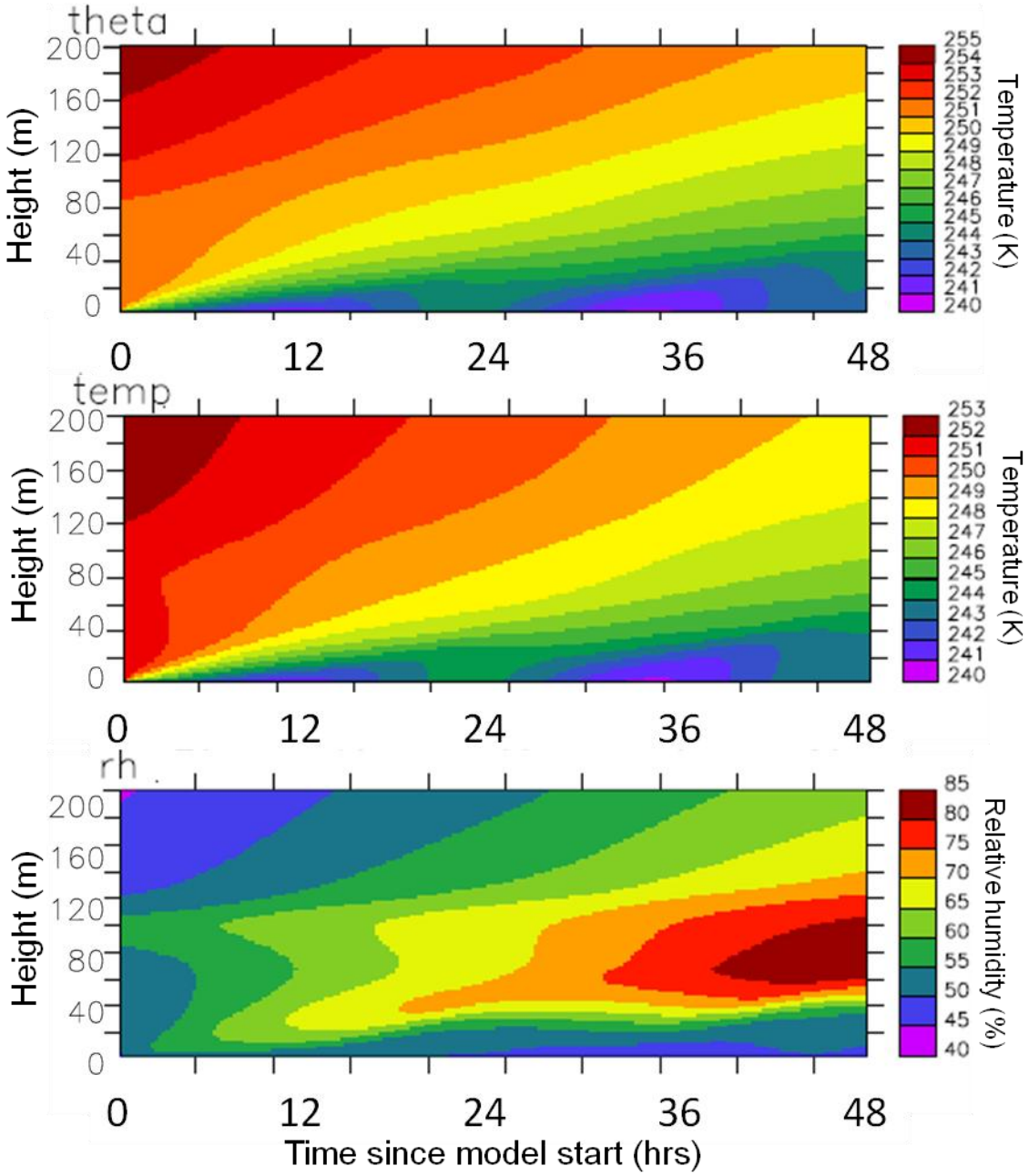

Figure 9.11: *Model output of run snow5 showing, from top to bottom, potential temperature, temperature and relative humidity of the model atmosphere for the 48hr run over the continental snowpack. X-axis shows hours since start of the run, the y-axis shows metres above the model snow surface, and the legend is in Kelvin for the top 2 plots, and the 3rd shows %RH.*

Snow1 has a chlorine dominated snowpack (no Br^- initialised), but snow3 has a bromine dominated snowpack. The chlorine in snow3 is mostly found in Cl- and BrCl, due to the high Br^- initialised in LLL in snow3. This feature is also present in runs snow5 and snow 7 respectively, which are discussed further below.

When using an atmosphere restart initialised with 10pptv of Br_2 during the snow on sea ice run (run ice2; Table 9.3), runs snow2 and snow4 showed little to no difference with snow1 and snow3. There is no change in ozone depletion in the snowpack or atmosphere, and the only change of note is that the nighttime mixing ratio of Br_2 is ~7-10pptv higher, and that daytime mixing ratios of BrO and HOBr are each ~7-10pptv higher for the runs using ice2 rather than ice1.

The runs Snow5 and Snow7 used ice3 as the atmosphere initialisation, and have a run time of 48 hours with a start time of midday rather than midnight. Looking at the model meteorology for these runs, it is immediately clear that the BL structure is very different to that found in the base runs discussed above (and in chapter 8) where the runs started at midnight rather than midday (Figure 9.11). The BL height in run snow5 is ~80-100m, whereas this was nearer to 160-180m in snow1 (Figure 8.4 in Chapter 8). The relative humidity of the run is also less, reaching only around 85% in comparison with the 95% seen in snow1. The reason for this change in BL structure is caused by several reasons. Key among them is the fact that the snow on sea ice run used to restart the atmosphere (ice3) was itself restarted at midday (i.e. after only 36 hours of initial met spinup), rather than midnight (the 48 hours after initial met spinup) used for ice1. Therefore no deep, stable, nighttime boundary layer was present at the start of run ice3. As model run snow5 was initialised from ice3, the prescribed diurnal temperature did not initially have the same effect as for snow1 (minimum temperature was chosen to occur at 9am, which does not happen until well into the runs ice3 and snow5) and therefore led to run ice3 and snow5 having a different BL structure to runs ice1 and snow1 (Chapter 8).

When comparing the chemistry of these runs snow5 and snow7 (Figure 9.12), the only setup difference between them is that the continental snowpack in snow7 is initialised with bromide (see Table 9.4). Other than the change of timing (midnight start to midday start) which affected the meteorology quite dramatically, many of the prevalent features in runs snow5 and snow7 are very similar to their equivalent runs (snow1 and snow3 respectively). The enhanced snowpack bromide in snow7 leads to complete ozone depletion in the surface layers of the snowpack interstitial air by the end of the run, which is mirrored by total depletion in the atmosphere for the entire second day of the run up to a height of 100m. For experiment snow5, there is complete ozone depletion in the top layers of the snowpack interstitial air almost immediately after the run start removing the oxidant for chloride in the snowpack. However, unlike for snow7 the depletion in the snowpack on the second day of the run is not complete (86% depleted compared with the background value of 30ppbv). Ozone depletion in the atmosphere of snow5, very near the surface on day 1 of the run, is very similar to that of snow7

(both being due to the newly forming low, cold, stable BL created by the cold snow surface temperature in the model). Ozone depletion is also evident up to 100m on day 2 of run snow 5, when the cold and stable BL is fully formed. Similar to run snow1, chemistry in the snowpack interstitial air of snow5 is also dominated by chlorine chemistry, due to the lack of bromine, and is likely the source of the snowpack depletion of ozone on the first day of the run, over bromine initiated chemistry (as there is no bromine initialised in the snowpack). The snowpack of snow7 however is again bromine dominated (as for snow3), due to being initialised with some bromide (Table 9.4). Although atmospheric BrCl mixing ratios are reasonable for snow7 when compared to Halley observations (5-6pptv), Br_2 mixing ratios are at least 20pptv higher than those observed at Halley. However when looking at the atmosphere of snow5, although Br_2 is again ~10-20pptv above that observed at Halley, BrCl is almost an order of magnitude greater than that observed at Halley. This change in the Br_2:BrCl ratio is discussed in Chapter 6, but briefly: Br_2 is less soluble than BrCl (Bartlett and Margerum, 1999), meaning BrCl is more likely to undergo secondary reactions in the LLL forming and releasing Br_2 to the atmosphere. However, in snow5 there is no bromide initialised in the snowpack and the only source of bromine in the run is from the atmosphere which is passed over from run ice3. Therefore BrCl is unable to undergo reaction with Br^- in the snowpack and suppress BrCl/ Cl_2 production, leading to the chlorine rich snowpack.

Runs snow9 – snow12 all use snow on sea ice restart runs without the open water/ lead present (ice5 and ice6), starting at midnight for a 48 hour run. There is very little difference between the previous runs using snow on sea ice runs as restarts which had the open water, and those without. This is likely due to the timing of the runs. Snow9-snow12 start at midnight, so there is no immediate reactive photochemistry occurring at the start of the run. These runs will not be discussed further.

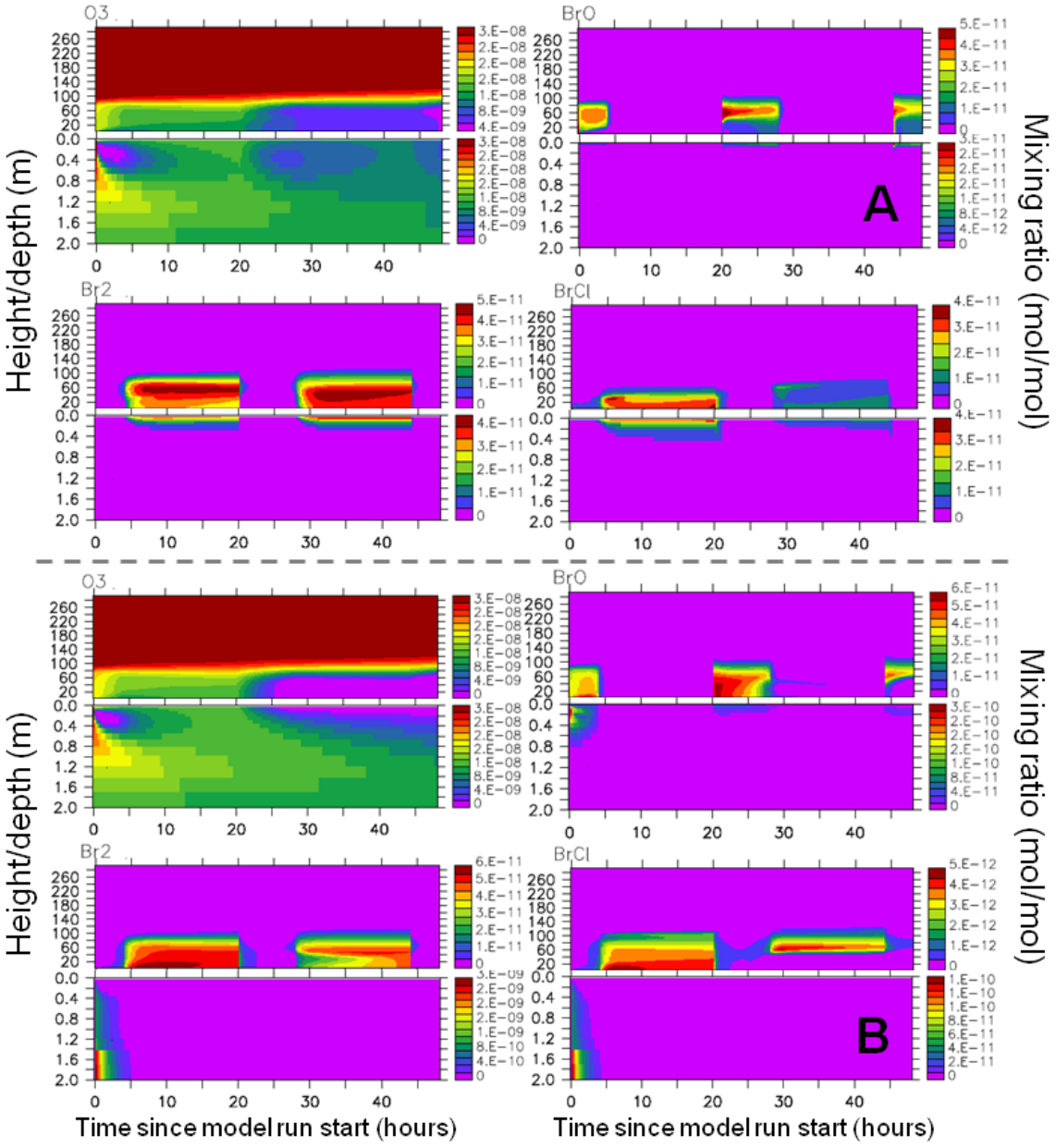

Figure 9.12: *Comparison of model output for runs snow5 (A) and snow7 (B), showing O_3, BrO, Br_2 and BrCl.*

9.3.2. Surface change runs 2

In order to address the initial 'jump' in Br_2 in the snow, caused by Henry's Law equilibration and re-partitioning, it was suggested that the runs mentioned in section 9.3.1. be re-run with a new initialisation for the snowpacks. A 2-day atmosphere spinup was used for the meteorology initialisation as before, but a 1 day spinup of the whole model was also run (including the chemistry) to use as initialisation of both the snow on sea ice and continental snowpack runs.

What this achieved is a chemically pre-processed snowpack (Henrys Law equilibration has occurred already, so no large initial 'jump'), but this was only used to initialise the snowpack as the atmosphere was still started with a fresh chemistry initialisation (Figure 9.13). The similarities to the runs from the previous section (9.3.1.) are clear in Tables 9.5 and 9.6. Although the chemistry of the continental snowpack was also initialised using this new chemistry spinup, the bromine species were set to zero by hand (over-written) in the model to keep the focus of the runs on the sea ice zone as the only bromine source (unless Br^- was initialised in the continental snow as in several of the runs laid out in Table 9.6).

What is immediately clear when looking at this set of runs (both snow on sea ice, and continental snowpack) is that none show as strong an ODE/bromine explosion as the 'old' runs even if they were initialised with Br_2 in the atmosphere to begin with (Figures 9.14 and 9.15).

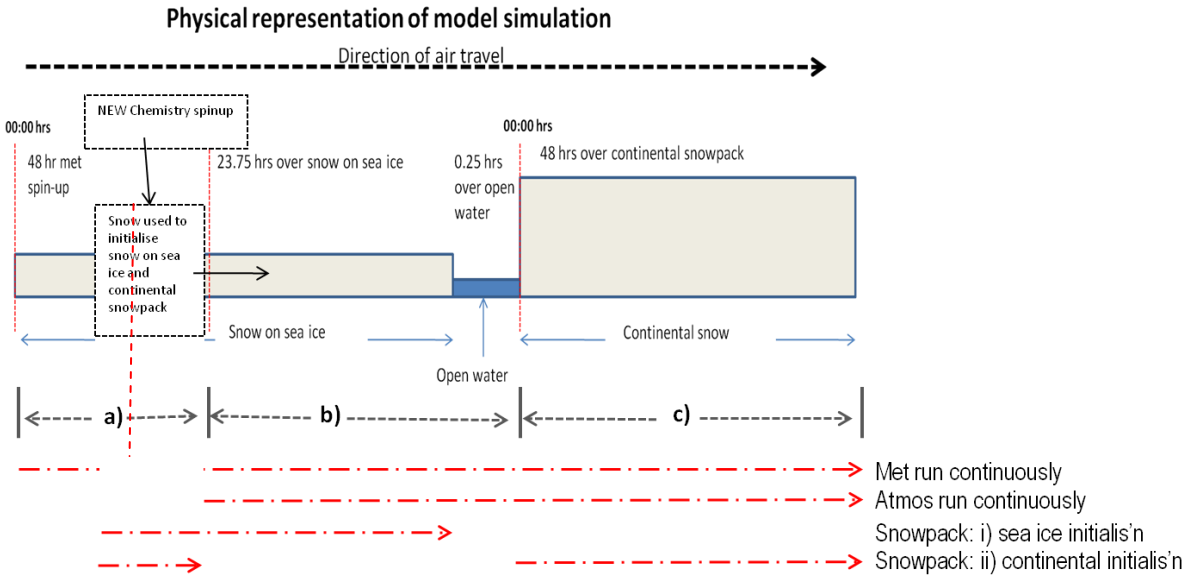

***Figure 9.13**: Similar to Figure 9.9, but shows the new chemistry spinup used to initialise the snowpack of both the snow on sea ice, and continental snowpack runs.*

Comparing ozone and other gas phase bromine species in Figures 9.14 (snow on sea ice; run icea) and 9.15 (continental snowpack; run snowa), with those of ice1 and snow1 discussed in Chapter 8, it would appear that the bromine explosion seen there was caused by the redistribution of Br^- to other bromine compounds in the snow pack at model start. No run showed any bromine explosion or an ODE without initialising the atmosphere with bromine

(even then the result was minimal). The pH in the liquid like layer in the snow pack in runs such as icea, and snowa, is 2, i.e. low enough for the chemistry to work. Looking at OH precursors in the snow (H_2O_2 and NO_3^- for example), the values are similar to those used by Thomas et al. (2011), suggesting that the BE and subsequent ODE chemistry is not OH or NO_3^- limited. The problem here is that there is simply not enough Br^- available in these runs for a bromine explosion to occur (such as bromine activation similar to that seen in Chapter 8 or even section 9.3.1.). This is due to the model setup and initialisation for this set of runs.

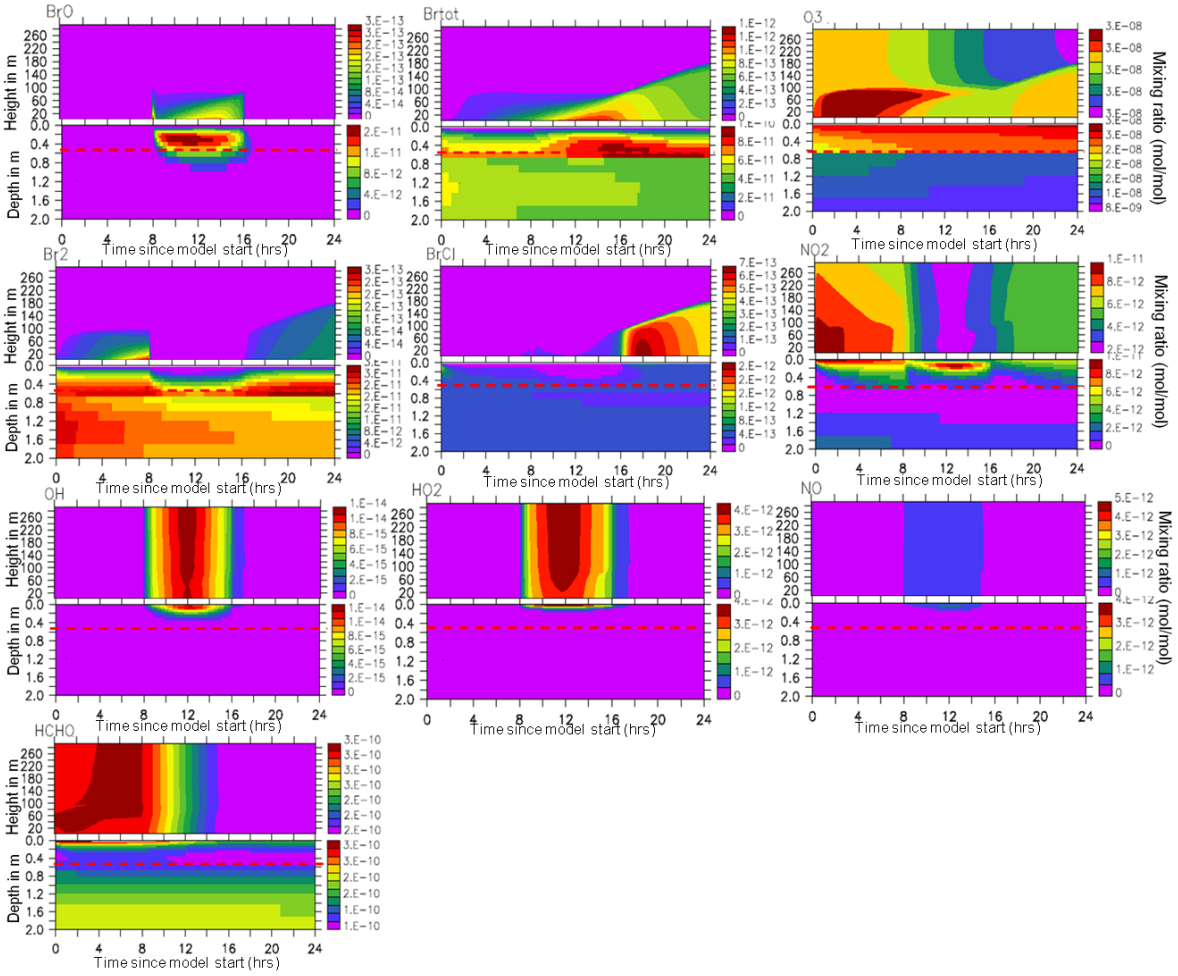

Figure 9.14: *Model output of several chemical species from the snow on sea ice run icea; NO, NO_2, O_3, HCHO, OH, HO_2, Br_2, BrCl, BrO and total Br. The upper panel for each species represents the atmosphere, with the lower representing the snow. The colour code on the right hand side is mixing ratios for each species (mol/mol), Time in hrs running along the bottom of the x-axis, and height in m (either above the snowpack for the atmosphere, or below the snow surface for the snow) on the left hand y-axis. The red line in the snow plot for each species emphasises the depth at which the snow stops interacting with the layers above.*

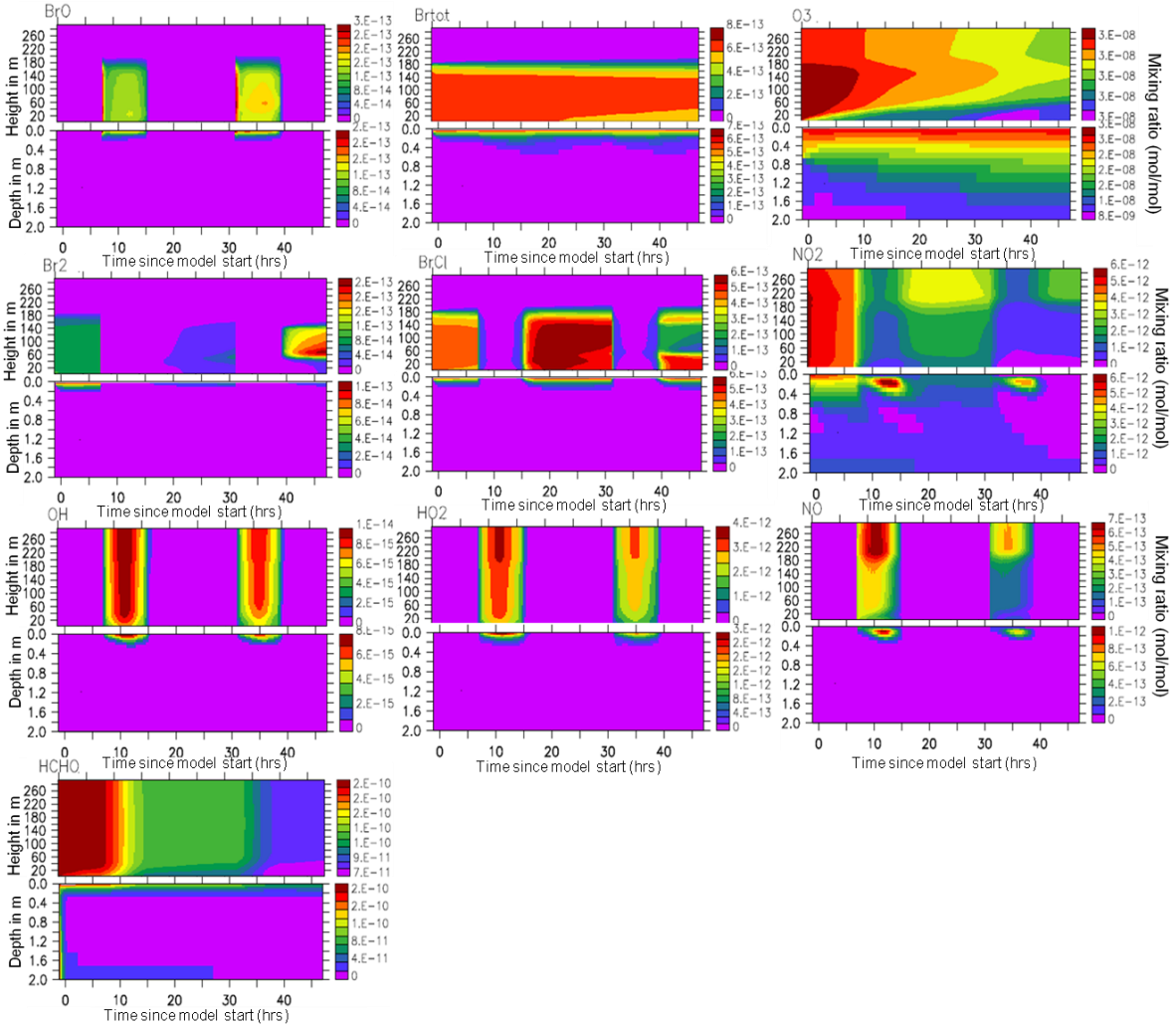

Figure 9.15.: *Model output of several chemical species from the continental snowpack run snowa; NO, NO_2, O_3, HCHO, OH, HO_2, Br_2, BrCl, BrO and total Br. The upper panel for each species represents the atmosphere, with the lower representing the snow. The colour code on the right hand side is mixing ratios for each species, Time in hrs running along the bottom of the x-axis, and height in m (either above the snowpack for the atmosphere, or below the snow surface for the snow) on the left hand y-axis.*

Run no.	Open Water	Time of run start (24hr run)	Atmos Br_2 Init (pptv)
icea	Y	00:00	0
iceb	Y	00:00	10
icec	Y	12:00	0
iced	Y	12:00	10

Table 9.5, snow ice runs 2: *Parameters changed between the new snow on sea ice runs, including the presence of a lead/ open water for the last 15 minutes of the run, the time the run was start at (either midday or midnight) and the run being initialised with/ without any Br_2 in the atmosphere.*

Run no.	Atmos restart	Snow Br^- (mol/l)
snowa	icea	0
snowb	iceb	0
snowc	icea	25×10^{-9}
snowd	iceb	25×10^{-9}
snowe	icec	0
snowf	iced	0
snowg	icec	25×10^{-9}
snowh	iced	25×10^{-9}

Table 9.6, continental snow runs 2: *Parameters changed between the new snow on sea ice runs, including which snow on sea ice runs was used to initialise the atmosphere and the run being initialised with/ without any Br^- in the snowpack.*

Although there is initially more Br^- in my runs (Tables 9.6 and 9.7) than those of Thomas et al. (2011), the use of a 1 day spin up of chemistry for the snowpack initialisation, and not the chemistry for the atmosphere initialisation, has led to the removal and redistribution of a large portion of the bromine available in the model. The large mixing ratios of Br_2 and BrCl in the atmosphere after this spinup are not passed over to the initial snow on sea ice run, and there is also less Br- in the snowpack to initiate a bromine explosion. One possible way to reconcile these new runs with measurements (see Chapter 6) is by suggesting that the air has been previously

processed by another sea ice source region and background ozone has been mixed back into the air-mass prior to it being measured at Halley. There are periods in the measurements from Halley that high ozone and slightly enhanced bromine species are observed simultaneously, although this is more usually associated with air of continental origin (see Chapter 7).

In the model runs discussed in section 9.3.1, although the initial jump in interstitial Br_2 looks unrealistic, we could see the sea ice 1 day run as a spinup of the atmospheric chemistry for the continental snow run which uses the atmosphere chemistry as a restart (so we get the high atmosphere Br_2 and BrCl passed over, and that is the only source of Br for the continental snow run and we get ODEs). Although this is not what was originally proposed as an ODE from first principles, these simulations may still represent an idealised situation of an air mass arriving at Halley (discussed below). Although the bromine explosion might not be this fast in real life, if there is precipitation of bromine enriched snow, or the snow on sea ice is submerged and the snow is infused with sea water, the equilibration would still need to occur. It may not be instantaneous like the model but the Henry's Law constant for Br_2 leads to very fast release to the gas phase so it could happen over the course of an hour or two. The amount of bromine released to the atmosphere could therefore still be large enough over the course of a day to achieve an ODE. Section 6.3 looks at the Br_2:BrCl ratio and gives a possible explanation for not entirely dismissing this rapid bromine release from the aqueous to the gas phase.

This model simulation does not entirely reproduce ODEs under the conditions employed through this model setup and initialisation. For these new runs, the ozone depletion will have to have happened elsewhere out over the sea ice zone and in-mixing of ozone rich air will have happened en-route to Halley where it is measured. This doesn't remove Precious Bay as being a halogen source region, but it is unlikely that there is enough bromine left in the snow of the snow on sea ice run after the 1 day chemistry spin up for ODEs to occur in either these runs or the following continental snowpack runs. With regards to the model calculations, the presence of Br^- plays a key role in determining the amount of OD. The discrepancy in ODE reproduction in these simulations could possibly be accounted for by the absence of iodine chemistry in the model calculations. The presence of both IO and BrO together can greatly increase the OD efficiency of a system (Saiz-Lopez, 2007), and could account for the missing OD here.

MISTRA-SNOW was used to explore changing several physical properties of the snowpack and their effect on atmospheric mixing ratios of gaseous species known to be released from the snowpack. Wind speed 10m above the snow surface (m s-1), snow grain size (mm), and snow

density (kg m-3) were altered, where increasing the snowpack density led to the greatest impact by increasing mixing ratios of bromine species in the atmosphere by ~50%.

Wind pumping parameters were also explored, and it was found that increasing the snowpack wavelength led to less snowpack-atmosphere exchange, and increasing the snowpack amplitude led to a higher snowpack-atmosphere exchange.

Changes in initial snowpack bromide concentrations were explored, where the bromide values used are all within observed concentrations either in situ at Halley (present day scenario), or found in ice core records dating back to the LGM (last glacial maximum; Spolaor et al., 2013). The only source of bromine to the atmosphere and the snowpack interstitial air in these runs was Br- in the snowpack. A complete ODE was generated within 2 model days when snowpack Br- is 4x present day. A discontinuity between the 2x and 4x bromide runs suggests real sensitivity to Br-, which is relevant given our lack of knowledge of Br- concentrations in the snow on sea ice zone, and how heterogeneous its distribution is both spatially and with depth (and time through the year).

Changing the surfaces in MISTRA-SNOW was explored, where snow-on-sea-ice was simulated, followed by open-water, and continental-snowpack. This was thought to represent a typical air mass path prior to arrival at Halley, and was able to reproduce an ODE as observed at Halley. However, the sharp transition found in some snowpack species, caused by re-partitioning to the gas phase, appeared unnatural. Therefore the snowpack initialisation was updated and some more simulations were run.

The final runs with a chemically pre-processed snowpack, led to the removal and redistribution of a large portion of the bromine available in the model. The large mixing ratios of Br_2 and BrCl in the atmosphere after this spinup are not passed over to the initial snow on sea ice run, and there is also less Br^- in the snowpack to initiate a bromine explosion. An air mass previously processed by another sea ice source region could reconcile these new runs with measurements.

10. Conclusions and further work

10.1. Summary and conclusions

Reported here are the first high temporal resolution measurements of BrO, Br_2 and BrCl in coastal Antarctica, made during spring 2007 using a CIMS instrument. The inclusion of coincident ozone and meteorology measurements created a great opportunity to explore the chemistry of the atmosphere in this environment, and the effects of different chemical source regions and meteorological regimes on atmospheric composition. The use of a numerical model (MISTRA) facilitated this work greatly. Soon after the start of this project, it was reported by Neuman et al. (2010) that there may be an interferent in daytime CIMS Br_2 measurements using a technique similar to that used at Halley. This is not, however, a fundamental instrument restriction and refers more to the specific sampling methodology. It was therefore likely that this interferent, in the form of HOBr conversion on the Teflon inlet of the instrument, may also be present in the data from this study. Daytime mixing ratios of several pptv of Br_2 were evident in the observations from Halley, which was surprising as this compound has a photolytic lifetime on the order of 20 seconds. To explore this, the MISTRA model was set up to represent the Halley environment, and then used to quantify the extent of this artefact in the observations. Results from the MISTRA 0-D and 1-D model runs indicate that the artefact likely represents a conversion of HOBr to Br_2 of the order of several tens of percent. It was also evident from the Halley observations that there was also a daytime signal in the BrCl observations of a few pptv. Comparison of the model output and observations from Halley suggest that conversion of HOBr to BrCl on the Teflon inlet is less efficient but non-negligible. It was then clear that the daytime observations of these species would be problematic (as there were no coincident measurements of HOBr), but conclusions could be drawn about the Br_2 and BrCl observations by restricting focus to their nighttime results only.

Mixing ratios of BrO, Br_2 and BrCl ranged from instrumental detection limits to 13 pptv (daytime), 45 pptv (nighttime), and 6 pptv (nighttime), respectively. As the spring season progressed, the diurnal shape of BrO changed from a sharp single peak, to a broad/ flat-topped peak and finally to a double peak with BrO maxima in the morning and evening along with noon time minima. This behaviour, which was reproduced with the MISTRA model, is the result of differences in the photolysis spectra of O_3 and Br_2, where Br_2 is more rapidly photolysed in twilight than O_3 due to absorption at longer wavelengths.

This suite of Antarctic data also provides the first analogue to similar measurements made in the Arctic. Previously-reported nighttime maxima for Br_2 (46 pptv at Barrow, Liao et al., 2012b and 27 pptv at Alert, Spicer et al., 2002) are in line with the Halley observations. Arctic nighttime BrCl mixing ratios up to 18 pptv (Spicer et al., 2002), however, are considerably larger than observed at Halley. Further, the Br_2 : BrCl ratio at Alert was found to be about 1. The ratios as observed at Halley are often much higher than this, where air masses with an origin from the sea ice zone have a ratio in favour of Br_2 and are never less than 1 if filtered using a 3σ LOD.

An exploration of two interesting events highlighted the effect of air mass contact with the sea ice zone on enhanced halogen mixing ratios (from background) and ODEs. Exploration of higher than background halogen mixing ratios associated with air supposedly of continental origin (11-14/09/2007), brought to light an air mass that had skirted the Halley coast and possibly had contacted the sea ice zone prior to arrival at Halley. From HYSPLIT air mass back trajectories, it was clear that on the day prior to measurement of highest halogen mixing ratios for this time period, the air mass had looped out from the continent edge and been in contact with the sea ice zone. This was consistent with the sea ice zone being an important halogen source region.

An unusual event of trans-continental air mass transport in darkness was associated with severe surface ozone depletion observed at Halley. Trajectory model analysis (HYSPLIT back trajectories) indicated that the air mass had traversed the Antarctic continent, from west of the Antarctic Peninsula. Model calculations, using MISTRA 0-D, were consistent with the halogen source region being to the west of the Antarctic Peninsula, with the air mass having spent 3 1/2 days in complete darkness crossing the continent prior to arrival at Halley. Not only was this air mass strongly depleted in O_3, it was also the source of both the highest measured [Br_2] and [BrO] for the whole measurement period.

Although it is clear that the sea ice zone is a major source of halogens for this coastal polar region, there is halogen chemistry evident even in air of continental origin. On the 30th and 31st of August 2007, 7-8pptv of BrO and ~3-4 pptv of "Br_2" measured during daylight is indicative of active bromine chemistry (possibly as HOBr). This is the highest BrO mixing ratio observed during a period of air masses with sustained continental origin. Piot and von Glasow (2008) explore the importance of bromine recycling on the snowpack to sustained halogen mixing ratios in the atmosphere above the snow and producing an ODE. If one assumes that bromine is deposited on (or present in) snow and being recycled at all times in coastal polar regions, the coincident meteorology observations for this period suggest that the source of bromine was the continental snowpack as opposed to the sea ice zone, and that a cold, stable/stratified BL has led to this

build up of several pptv of BrO. This fits well with recent measurements made by Pratt et al. (2013) in snow near Barrow, where high mixing ratios of Br_2 released from the continental Tundra snowpack were observed.

MISTRA-SNOW was initially used to explore the influence of changing the physical properties of the model snow on snow-atmosphere interaction. Properties such as snow grain size, snowpack density, and various wind pumping parameters were studied, as well as changing the snowpack bromide content. Increasing the snowpack density led to the presence of more initial bromide in the snowpack, leading to an increase in model BrO in the atmosphere above the snowpack. When altering the snow grain size, changing the enhancement factors (calculated for particular snowpack properties; chapter 3) was not taken into account. This led to there being much less bromide and chloride available at the surface of the 3mm snow grains when compared to the 1mm snow grain runs, leading to lower gas phase mixing ratios of bromine and chlorine containing species in the snowpack. When investigating the model wind pumping parameters, it was found that changing the wavelength (distance between snow crests) had the greatest effect, of the parameters looked at, on snow-atmosphere exchange. Changing this parameter in the model from 4m to 6m halved the model BrO at 5 m above the snowpack.

Changing the bromide content of the snowpack was also explored. The bromide values used are all within observed concentrations either in situ at Halley (present day scenario), or found in ice core records dating back to the LGM (Spolaor et al., 2013). Br_2 production steadily increases in both the snowpack and the atmosphere as the snowpack bromide is increased, but for the 4x and 10x bromide runs there is no BrCl in the atmosphere after the 3rd and 1st days respectively. It is key to note that the only source of bromine to the atmosphere and the snowpack interstitial air was Br^- in the snowpack. It was possible to generate a complete ODE within 2 model days when snowpack Br^- is 4x present day. The discontinuity in O_3 between the 2x (no complete depletion) and 4x (complete depletion in 2 days) runs suggests real sensitivity to Br^-, which is relevant given our lack of knowledge of Br^- concentrations in the snow on sea ice zone, and how heterogeneous its distribution is both spatially and with depth (and time through the year).

The newly-developed MISTRA-SNOW model was then used to examine BL chemistry at Halley. The physical environment at Halley created the opportunity to explore the influence of snow on sea ice, and continental snowpack, on halogen release and ODEs as observed over the continental snowpack at the Halley site. The runs presented were initialised using measurements made at Halley station (and other coastal Antarctic or polar sites where required), with the main aim to explore both the chemical and meteorological conditions involved in halogen release and

ozone depletion (snow – atmosphere interaction) in this coastal polar environment. Two runs were set up. The first used measurements from Massom et al. (2001) to initialise snow on sea ice representative of that found in the Weddell Sea sea ice zone near Halley, and the second used measurements from Massom et al. (2001) and Halley to represent the continental snowpack found at Halley itself. A period of open water was included at the end of the snow on sea ice run to represent a lead/ polyna, a feature often present in Precious Bay. The atmospheric conditions of the snow on sea ice run were used to initialise a run over the continental snowpack, only the surface influence of the model was changed; effectively this amounts to a continuous trajectory of an air mass from the sea ice over a lead and then continental snow pack.

When the snow was initialised with bromide (based on measurements of snow pit data from Halley), there was found to be a sharp transition in the snowpack Br^-, Br_2 and BrCl. This is due to Henrys law equilibrating and repartitioning between the aqueous and gas phase in the snow pack in the first model timestep. This artefact in the model snowpack may not be a realistic feature, but it does represent a natural equilibration which could be reproduced by real world scenarios such as flooding of snow on sea ice by sea water creating a high salinity snowpack which will need to undergo a similar process to that described by the model.

The initial goal was to reproduce an ODE from “first principles” using MISTRA-SNOW. To some extent this was achieved, as all of the initial runs show ozone depletion to some extent with some even showing complete depletion. This was quite surprising considering the only bromine influencing the continental snowpack run was that passed over from the atmosphere of the snow on sea ice run, in turn only initialised with bromide in the snow. Initialising the atmosphere of the snow on sea ice run with bromine in the form of 10 pptv of Br_2, as well as the bromide in the snowpack, had little effect on the OD seen in the continental snowpack run.

The start time of the runs had a big effect on both the meteorology and chemistry of the model. The atmosphere has a much lower BL for the midday start runs than for the midnight start runs (~100m compared with ~200m), and the relative humidity of the run is also less. The lower BL is due to the lack of build up of a deep stable nighttime BL at both the end of the snow on sea ice run, and the start of the continental snowpack run. The runs starting at midday and running for 48hrs over the continental snowpack (using the atmosphere from the snow on sea ice run) also show stronger OD than for the continental snowpack runs starting at midnight. When there was no bromide initialised in the continental snow, ozone was depleted in the atmosphere by up to 86%. However, when the continental snow was initialised with some bromide, there was

complete ozone depletion for the entirety of the second model day in the atmosphere, and the surface layers of the snowpack.

To remove the model artefact of the initial rapid Henry's law equilibrating and repartitioning between the aqueous and gas phase in the snow, a snowpack chemistry spinup was run and used to initialise the snowpack. The snow on sea ice runs used this "as is", and the continental snowpack runs used this spinup with all of the bromine species manually set to zero. Unfortunately by changing the initialisation of the snowpack for both the snow on sea ice and continental snowpack runs, the model no longer achieved a strong ODE or bromine explosion. The reason for this is likely that there is simply not enough bromine in the model snowpack after the initial snowpack chemistry spinup due to loss from the atmosphere or redistribution of the bromine to other compounds.

Although there is initially more Br^- in my runs than those of Thomas et al. (2011), the use of a 1 day spin up of chemistry for the snowpack initialisation, and not chemistry for the atmosphere initialisation, has led to the removal and redistribution of a large portion of the bromine available in the model. What this means is that the large mixing ratios of Br_2 and BrCl in the atmosphere after this spinup are not passed over to the initial snow on sea ice run, and there is also less Br^- in the snowpack to initiate a bromine explosion. This in turn leads to less bromine being passed over to the continental snowpack atmosphere.

Although iodine species were not included in the model calculations presented and discussed here, Saiz-Lopez et al. (2007) have shown through a model study that their presence can contribute greatly to ODEs. Their model calculations were the first to include iodine chemistry, and the results indicated that there was a fourfold increase in the ozone depletion rate when considering both bromine and iodine chemistry, over bromine alone. However, other results from the same field campaign suggest an anti-correlation of IO with ozone in the Antarctic troposphere. Although there is evidence that iodine chemistry can effect ozone depletion in coastal polar regions, we felt the uncertainties were too great to include it in our model calculations.

10.2. Further work/ research needs

With regards to improving our understanding of ozone and halogen chemistry in coastal polar regions, such as Halley, the following future measurements/ observations would be beneficial.

- Measurements including vertical distribution of halogen species above the snowpack, starting at the snow surface (for example different inlet heights on a mast)
- Measurements of gaseous halogen species at varying depths within the snowpack, for comparison with measurements in the atmosphere above the snow surface.
- Measurement of bromide and chloride content of snow on sea ice under different meteorological conditions (e.g. varying wind speeds, before and after a high precipitation event)
- Measurement of bromide/ chloride content of the LLL on the surface of the ice/ snow grain (possibly by an optical absorption technique)
- Meteorology measurements over the sea ice zone (especially wind speed – blowing snow, and ambient temperature – better indication of ice surface temperature
- Accurate measurement of the temperature of the snow surface over the sea ice zone
- pH measurements of the LLL at the snow/ ice surface

In terms of future modelling work, although the final model runs (chapter 9.3.2) using an extra chemistry spinup for the snowpack did not respond as expected, they have definitely highlighted some areas for improvement in future model studies. The bromide content measured in the snow at Halley is actually going to be the bromide content of a "processed" snowpack, so it would be interesting to initialise the snow with some bromide again after the snow chemistry spinup. As there will already be gas phase bromine species in the snowpack there will likely be less re-partitioning and therefore a less artificial looking jump in the snowpack bromide and gas phase Br_2 and BrCl. This would potentially give a more realistic representation of the bromide content of the snowpack, and allow more transfer of halogen species to the atmosphere. Looking at the total bromine atmosphere: snow ratio, it is clear that the 48hr continental snowpack run is not long enough to fully analyse this effect. Therefore, running this simulation for an extended period of time would give a better grasp on the bromine recycling efficiency of the model snowpack.

Of course the MISTRA-SNOW model used here has now been applied to situations in both the Arctic (Thomas et al., 2011; 2012) and Antarctic (chapters 8 and 9), but the time of year differs between these studies. A “next-step” might be to run MISTRA-SNOW in the spring-time Arctic (e.g. different chemistry, pollution, aerosol loading) to get a good comparison with the results from the spring-time Halley environment. It would also be interesting to “scale-up” the MISTRA-SNOW model (like in the proposed POLAR-WRF-CHEM-SNOW model), to represent the whole of the Antarctic coastal/ sea ice zone, or the Arctic coastal/ sea ice zone, and include a full representation of large scale meteorological effects in the model. This would allow an exploration of the effects of halogen release from the sea ice zone and continental snowpack on the chemistry of these different polar regions (i.e. under very different meteorological conditions).

Some questions that could be addressed by this “scaled-up” MISTRA-SNOW model would be: What effect will changing/ increasing first year sea ice in the Arctic have on the oxidising capacity of the atmosphere in the northern hemisphere, especially in spring? An update of the work by Voulgarakis et al. (2009) to include chemistry in/ on snow would be ‘what happens to the chemistry if there is no summer sea ice in the Arctic at all?’. If a model similar to MISTRA-SNOW is scaled-up to represent a larger area, what are the differences in halogen release and transport in a sea ice covered ocean surrounded by land (Arctic), and land surrounded by sea ice (Antarctica)?

Addressing questions such as these with models like MISTRA-SNOW, could give us a clearer indication of the future effects the ever changing polar regions will have on the chemistry of the rest of our planet.

Appendix

Appendix A

Table of abbreviations used throughout thesis

Abbreviation	Corresponding meaning
BL	Boundary Layer
CIMS	Chemical Ionisation Mass Spectroscopy
CASLab	Clean Air Sector Laboratory
ODE	Ozone Depletion Event
OD	Ozone Depletion
BE	Bromine Explosion
MBL	Marine Boundary Layer
LWC	Liquid Water Content
DOAS	Doppler Optical Absorption Spectroscopy
MAXDOAS	Multi Axis Differential Optical Absorption Spectroscopy
LPDOAS	Long Path Differential Optical Absorption Spectroscopy
LGM	Last Glacial Maximum
KPP	Kinetic Pre-Processor
MISTRA	MIcrophysical STRAtus model
IC	Ion Chromatograph
LWV	Liquid Water Volume

Table A.1

Appendix B

The absorption cross section for Br_2 is very similar to that of NO_2 (DeMoore et al., 1997; Maric et al., 1994). Although the magnitude of the NO_2 cross section differs, they both peak at ~ 410nm. The quantum yield for NO_2 is also given here (Br_2 was not available). These cross sections and quantum yield come from the MISTRA manual but the artificial spikes in the cross sections have been corrected.

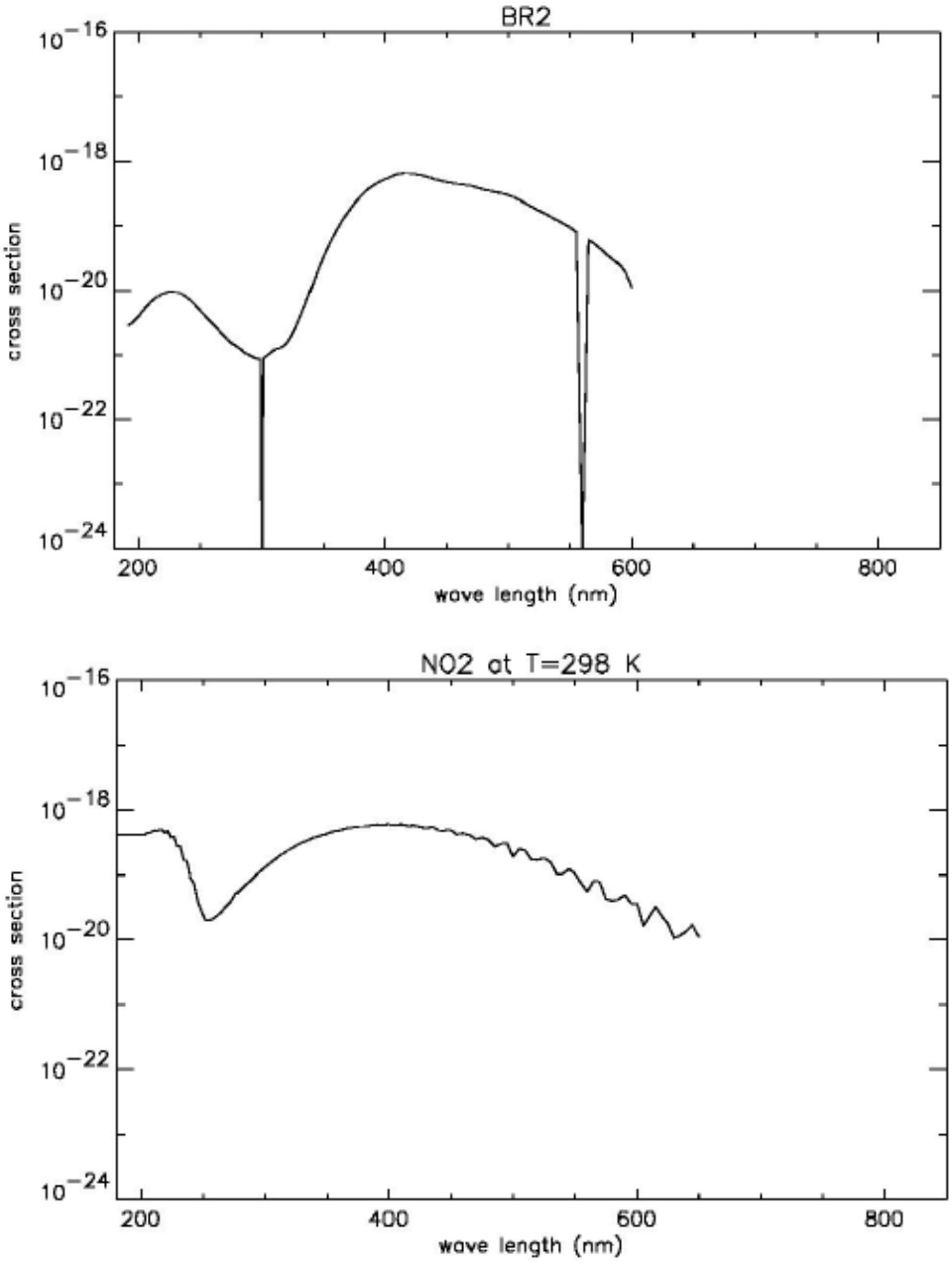

Figure B.1

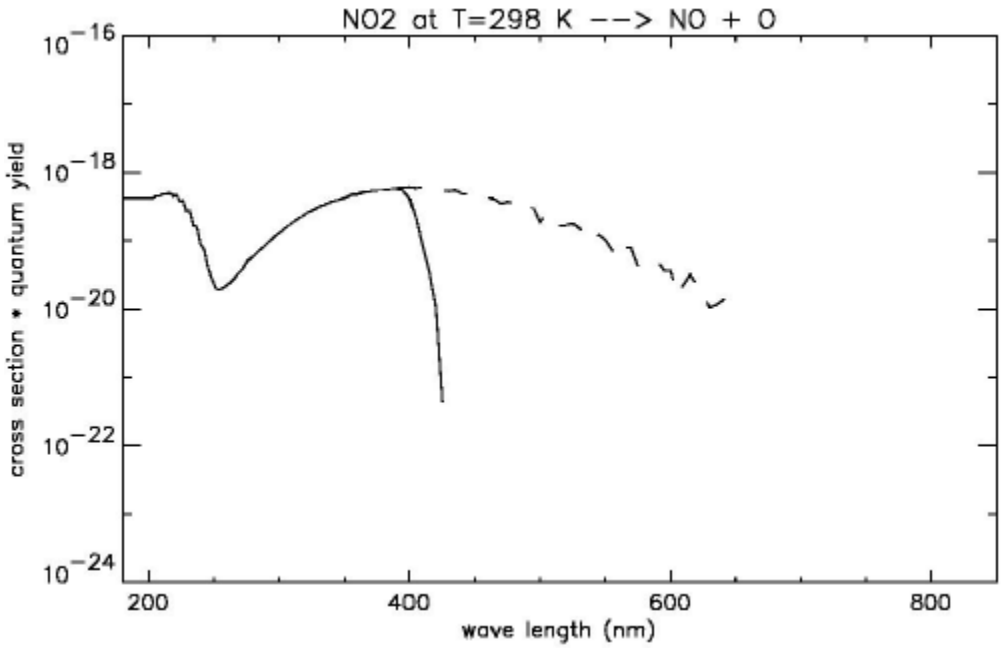
NO2 at T=298 K --> NO + O
cross section * quantum yield
10^{-16}
10^{-18}
10^{-20}
10^{-22}
10^{-24}
200
400
600
800
wave length (nm)

Figure B.2

Appendix C

First author paper – Buys, Z., Brough, N., Huey, L. G., Tanner, D. J., von Glasow, R., and Jones, A. E.: High temporal resolution Br_2, BrCl and BrO observations in coastal Antarctica, Atmos. Chem. Phys., 13, 1329-1343, doi:10.5194/acp-13-1329-2013, 2013.

Chapters 5, 6 and 7 each includes some material from this piece of published work, but have been re-formatted/ re-written to ensure integration with the rest of the thesis. All included work is directly attributable to me.

Atmos. Chem. Phys., 13, 1329–1343, 2013
www.atmos-chem-phys.net/13/1329/2013/
doi:10.5194/acp-13-1329-2013
© Author(s) 2013. CC Attribution 3.0 License.

Atmospheric Chemistry and Physics Open Access

High temporal resolution Br_2, BrCl and BrO observations in coastal Antarctica

Z. Buys[1,2], N. Brough[1], L. G. Huey[3], D. J. Tanner[3], R. von Glasow[2], and A. E. Jones[1]

[1]British Antarctic Survey, NERC, High Cross, Madingley Road, Cambridge, UK
[2]University of East Anglia, School of Environmental Sciences, Norwich, UK
[3]Georgia Institute of Technology, School of Earth and Atmospheric Sciences, Atlanta, USA

Correspondence to: Z. Buys (zakysa@bas.ac.uk)

Received: 23 March 2012 – Published in Atmos. Chem. Phys. Discuss.: 27 April 2012
Revised: 15 January 2013 – Accepted: 23 January 2013 – Published: 1 February 2013

Abstract. There are few observations of speciated inorganic bromine in polar regions against which to test current theory. Here we report the first high temporal resolution measurements of Br_2, BrCl and BrO in coastal Antarctica, made at Halley during spring 2007 using a Chemical Ionisation Mass Spectrometer (CIMS). We find indications for an artefact in daytime BrCl measurements arising from conversion of HOBr, similar to that already identified for observations of Br_2 made using a similar CIMS method. Using the MISTRA model, we estimate that the artefact represents a conversion of HOBr to Br_2 of the order of several tens of percent, while that for HOBr to BrCl is less but non-negligible. If the artefact is indeed due to HOBr conversion, then nighttime observations were unaffected. It also appears that all daytime BrO observations were artefact-free. Mixing ratios of BrO, Br_2 and BrCl ranged from instrumental detection limits to 13 pptv (daytime), 45 pptv (nighttime), and 6 pptv (nighttime), respectively. We see considerable variability in the Br_2 and BrCl observations over the measurement period which is strongly linked to the prevailing meteorology, and thus air mass origin. Higher mixing ratios of these species were generally observed when air had passed over the sea-ice zone prior to arrival at Halley, than from over the continent. Variation in the diurnal structure of BrO is linked to previous model work where differences in the photolysis spectra of Br_2 and O_3 is suggested to lead to a BrO maximum at sunrise and sunset, rather than a noon-time maxima. This suite of Antarctic data provides the first analogue to similar measurements made in the Arctic, and of note is that our maximum measured BrCl (nighttime) is less than half of the maximum measured during a similar period (spring-time) in the Arctic (also nighttime). This difference in maximum measured BrCl may also be the cause of a difference in the Br_2 : BrCl ratio between the Arctic and Antarctic. An unusual event of transcontinental air mass transport appears to have been responsible for severe surface ozone depletion observed at Halley over a 2-day period. The halogen source region appears to be the Bellingshausen Sea, to the west of the Antarctic Peninsula, with the air mass having spent 3 1/2 days in complete darkness crossing the continent prior to arrival at Halley.

1 Introduction

The first published measurements of tropospheric ozone depletion events (ODEs) were reported from Barrow, Alaska (Oltmans, 1981), followed by a more detailed study in March 1985 at Alert, Nunavut (Bottenheim et al., 1986). A study by Barrie et al. (1988) was the first to link these ODEs to bromine. Since the first observations of boundary layer (BL) ODEs in the Antarctic in the mid-1990s (Kreher et al., 1996; Wessel et al., 1998) and the coincident detection of BrO (Kreher et al., 1997), many more Antarctic field studies have taken place (Rankin et al., 2002; Jones et al., 2006). Roscoe and Roscoe (2006) showed, through analysis of historical ozone data from Halley, that ozone depletion events were evident as far back as 1957/58.

During ozone depletion events, ozone mixing ratios can fall from background amounts (typically 30–40 ppbv) to below instrumental detection limits (roughly a few parts per billion by volume, ppbv) within a few minutes and remain suppressed for on the order of hours to days.

Published by Copernicus Publications on behalf of the European Geosciences Union.

The chemical destruction of ozone is driven by halogens, especially bromine radicals (e.g. Simpson et al., 2007; Abbatt et al., 2012), the critical reaction being:

$$Br + O_3 \rightarrow BrO + O_2 \quad (R1)$$

Catalytic destruction of ozone is achieved if the bromine radicals are re-generated without production of ozone. This can occur in a number of ways, such as:
(a) via the BrO self-reaction:

$$BrO + BrO \rightarrow 2Br + O_2 \quad (R2a)$$

$$\rightarrow Br_2 + O_2 \quad (R2b)$$

$$Br_2 + h\nu \rightarrow 2Br \quad (R3)$$

(b) via reaction with HO_2:

$$BrO + HO_2 \rightarrow HOBr + O_2 \quad (R4)$$

$$HOBr + h\nu \rightarrow OH + Br \quad (R5)$$

(c) via interhalogen reactions, such as:

$$BrO + ClO \rightarrow Br + OClO \quad (R6a)$$

$$\rightarrow Br + ClOO \quad (R6b)$$

$$\rightarrow BrCl + O_2 \quad (R6c)$$

$$BrCl + h\nu \rightarrow Br + Cl \quad (R7)$$

There is still much debate over the precise source of atmospheric bromine that drives ODEs, but there is strong observational evidence to suggest a source associated with the sea ice zone (Gilman et al., 2010; Jacobi et al., 2010; Abbatt et al., 2012). Such a source would be consistent with laboratory studies, where heterogeneous reactions have been shown to generate Br_2 and BrCl, via uptake of HOBr onto frozen and dry NaCl/NaBr coated surfaces (Adams et al., 2002; Fickert et al., 1999), via the following multiphase reactions:

$$HOBr + H^+ + Br^- \rightarrow Br_2 + H_2O \quad (R8)$$

$$HOBr + H^+ + Cl^- \rightarrow BrCl + H_2O \quad (R9)$$

Although our knowledge of ODEs and associated chemistry has increased greatly since their discovery, some of the key processes involved are not yet fully understood (Simpson et al., 2007), and high temporal resolution observations of inorganic bromine compounds against which to test current theory are sparse. In 2007, year round measurements were made at the British Antarctic Survey station Halley (75°35′ S, 26°19′ W), in coastal Antarctica, using a Chemical Ionisation Mass Spectrometer (CIMS). During the austral spring and summer, the CIMS was configured to perform high resolution measurements of BrO, Br_2 and BrCl. In addition, concurrent measurements of surface ozone and local meteorology were made. Although such observations have been made in the Arctic (Neuman et al., 2010; Liao et al., 2011a, b, 2012b), this is the first such suite of measurements made in Antarctica.

Here we present an analysis of the springtime data. However, we first explore the issue of an apparent CIMS inlet artefact (Neuman et al., 2010) that arises from conversion of HOBr on surfaces, and appears, in our data, to affect both Br_2 and BrCl observations (although not BrO) during sunlit hours. We use the MISTRA model to make an estimate of the influence of this artefact on Br_2 and BrCl, and restrict subsequent discussions of Br_2 and BrCl to nighttime data only. We discuss BrO observations in terms of changes in the diurnal shape throughout the measurement period, and the chemistry responsible for these changes. We, further, explore the influence of air masses passing over different source regions prior to arrival at Halley. As these are the first suite of Antarctic data to provide an analogue to similar measurements made in the Arctic, we compare our observations in the south with those in the north, including differences in the Br_2 : BrCl ratio. Finally we present an unusual event of air mass transport, where the halogen source region associated with severe ozone depletion and the highest measured Br_2 mixing ratio, appears to be to the west of the Antarctic Peninsula.

2 Experimental methods

2.1 Halley research station

Measurements were made at Halley, an Antarctic coastal research station operated by the British Antarctic Survey (BAS) and situated on the Brunt Ice Shelf, 35 m above sea level. Halley is effectively located on a promontory that extends out into the Weddell Sea and of note, to the south and west is a large area of open water with associated newly-forming sea ice (referred to as Precious Bay). Although the prevailing wind direction at Halley throughout the year is easterly, traversing hundreds of kilometres of undisturbed snow, strong directional changes to westerlies/southwesterlies often occur, especially in the spring and summer months. This results in air masses with very different histories arriving at Halley.

The instruments used for this field campaign were housed in the CASLab (Clean Air Sector Laboratory) which is situated about 1 km south of the main base in an area that is exposed to minimal disturbance by vehicles or base pollution (Jones et al., 2008).

The measurement campaign ran between January 2007 and February 2008. During the year, the CIMS operated alternately in two different modes; (i) a high pressure mode which measured, separately, OH and (HO_2+ RO_2) and (ii) a low pressure mode measuring a variety of trace gases including HNO_4, HCl, HNO_3, SO_2. In early spring, BrO, BrCl and Br_2 were added to the suite of low pressure measurements

and included over the subsequent low-pressure mode measurement periods. The first direct sunlight at Halley at the end of the polar winter occurs on 13 August, thus the observations reported here almost all fall within the sunlit spring time.

2.2 CIMS instrument description

The CIMS technique has been used to detect many atmospheric trace gases (Huey et al., 1995, 1998; Berresheim et al., 2000; Leibrock and Huey, 2000; Huey et al., 2004; Sjostedt and Abbatt, 2008), but its use as a high mass and temporal-resolution halogen detector is of most importance to this present study. While the CIMS technique is well documented (e.g. Huey et al., 2004; Slusher et al., 2004; Liao et al., 2011b), we describe here features that were specific to the configuration at Halley.

Within the CIMS ionisation region, a mixture of nitrogen doped with a few parts per million by volume (ppmv) of SF_6 was added to the flow tube after passing through a ^{210}Po ion source. This synthesised the reagent ion SF_6^- in the ion source via associative electron attachment (Huey et al., 2004). The use of SF_6^- as a reagent ion can be limited due to its slow second-order reaction with water (Huey et al., 1995; Arnold and Viggiano, 2001), but Slusher et al. (2001) have found that it is viable at dew points below $\sim -20\,^{\circ}C$, such as are frequently found in polar regions.

Ambient air was continually sampled at a high flow rate (~ 2400 slpm) by means of a regenerative blower (Ametek BCDC) into a 40 cm long aluminium pipe of 8 cm inner diameter (i.d.) that protruded 20 cm above the laboratory roof which is roughly 5 m above the snowpack. A smoothed Teflon doughnut-shaped cap was secured to the pipe and positioned in the NE corner of the laboratory which allowed the least perturbed flow thereby minimising turbulence as well as shading.

To further reduce problems associated with surface adsorption, air was sampled from the centre of the aluminium pipe at a flowrate ~ 8 slpm which reduced both the residence and possible wall interaction time ($t < 0.6$ s). The sampled air was delivered to the CIMS in a heated teflon perfluoroalkoxyalkane (PFA) inlet (i.d. $= 0.65$ cm, length $= 25$ cm) controlled at $40 \pm 2\,^{\circ}C$ by a series of thin Kapton heaters. From there, sampled air mixed with ions from the ion source where reactions can occur for the length of the flow tube. A small amount of air from the flow tube is sampled and then electrostatically accelerated by ion optics into the quadrupole mass filter and an ion detector which can detect multiple ion masses on each pass (Huey et al, 2004). Rate coefficients for the reactions of the molecules with SF_6^- were measured relative to SO_2, as the rate coefficient for Reaction (R10) has been measured over a wide range of pressures and buffer gases (Slusher et al., 2001). SO_2 is also used as the calibration gas for the instrument.

$$SF_6^- + SO_2 \rightarrow \text{products} \quad \text{(R10)}$$

An automated 3-way sampling valve enabled switching between two flow paths, measurement mode and zero mode, without disrupting the required constant flow (maintained by the diaphragm pump). Background or zero measurements were obtained every 10 min by drawing air through a 20 cm $\times$ 5 cm i.d. stainless steel filter tube for a 3 min period. The filter tube contained activated coarse charcoal and nylon glass wool that had been previously soaked and dried in a concentrated $NaHCO_3$ solution. A similar scrubbing method had previously been successfully employed (Slusher et al., 2004; Liao et al., 2011a).

To determine the sensitivity of the CIMS instrument in the field, a mass flow controller (MKS 1479A) provided a continuous 8 sccm (standard cubic centimeters per minute) flow of 0.2 % ($\pm 5\sigma$) of a certified standard of our calibration gas (SO_2 in nitrogen) (Air Products, speciality gases) to the insulated inlet system every two hours for a 1 min period.

As SO_2 was used as our primary calibration gas for the CIMS instrument in the field, we were able to use the sensitivity ratio of SO_2 to Br_2 (determined in the lab after the fieldwork as a function of dew point temperature) as a proxy to track the sensitivity of Br_2. The ratio of the rate constants for reaction $SO_2 + SF_6^- \rightarrow F_2SO_2^- + SF_4$ and $Br_2 + SF_6^- \rightarrow Br_2^- + SF_6$ could then be used to calibrate the Br_2 measurements after the campaign.

BrO calibration was achieved using a similar method to that described in Sect. 2.2 in Liao et al. (2011a). We use the ratio of the rate constant for the reaction $Br_2 + SF_6^- \rightarrow Br_2^- + SF_6$ to the reaction $BrO + SF_6^- \rightarrow BrO^- + SF_6$ (determined to be 1.0 ± 25 % in the laboratory by Liao et al., 2011a), along with the dew point calculation, to determine the BrO calibration.

The measurements were all corrected for humidity (to account for any influence of the slow second-order reaction of SF_6^- with H_2O) and converted to mixing ratios.

Limits of detection (LOD) were estimated using 1σ counting precision of the 10 s zero background signal. This approach was used (Ridley et al., 1994) as there was no suitable invariant ambient data. The standard deviation of the zero data was transformed to pptv using the averaged sensitivity of the instrument to SO_2.

Table 1 gives details of instrument performance, and associated uncertainties in the halogen measurements. The estimated accuracies were obtained from the uncertainties in the flow meter calibrations for the sample and calibration gas obtained with a bubble flow meter before and after each measurement period and was found to be ~ 4 %. This also includes the uncertainty in the calibration gas standard which the manufacturer provided (5σ). The precision of the instrument to SO_2 was obtained from the scatter (1σ) of the SO_2 sensitivity and found to be < 2 % (at a dew point of $-24\,^{\circ}C$).

Table 1. Instrument parameters and overview of observations for BrO, Br_2 and BrCl for the period 12 August–18 September 2007. Details of measurements (max, mean, and standard deviation) for Br_2 and BrCl are based on nighttime observations only – see Sect. 3.2. Minimum values were below detection limits for all three species.

	BrO	Br_2	BrCl
Sensitivity Hz pptv^{-1}	4.9	4.9	4.9
2σ detection limit for 10 min averages (pptv)	0.6	0.4	0.1
Maximum observed (pptv)	13.3 (Day)	45 (Night)	5.9 (Night)
Mean nighttime observation (pptv)	–	5.8	1
Standard deviation of 10 min average (pptv)	2.2	6	1
Measurement uncertainties	±27 %	±11 %	±11 %

2.3 Supporting observations

Surface ozone was measured at the CASLab, using a UV absorption technique (Wilson and Birks, 2006). The instrument used was a Thermo Electron model 49C, which has a detection limit of 1 ppbv, and a precision of 1 ppbv. Data were recorded as 1 min averages of 10 s observations. Measurements of wind speed and wind direction were carried out at the main station, some 1 km from the CASLab. The anemometers and vanes were located at a height roughly 10 m above the snow surface, and have an accuracy of about 0.5 m s^{-1} for wind speed and 5° for wind direction (König-Langlo et al., 1998). Data are also output every 1 min. Information on sea ice concentration was obtained from the satellite-borne AMSR-E instrument (Spreen et al., 2008) which provides information at a resolution of 6.25 by 6.25 km.

2.4 MISTRA, model description

To explore features in the CIMS observations, we use both the 0-D (box-model) and 1-D versions of the Marine Boundary Layer (MBL) chemistry model, MISTRA (von Glasow et al., 2002).

MISTRA includes descriptions of meteorology, microphysics and thermodynamics as well as a multiphase chemistry module (von Glasow et al., 2002). The chemistry module includes chemical reactions in the gas phase, in and on aerosol particles and takes into account transfer between the gas and aqueous phase. The complete set of chemical reactions incorporated in the multi-phase chemistry module are solved using the kinetic pre-processor (KPP) (Damian et al., 2002) which allows easy changes of the chemical mechanism.

The model atmosphere in MISTRA 1-D is divided into 150 layers, with the lowest 100 having a constant grid height which can be set in the model (here chosen to be $\Delta z = 3$ m), and those layers above 100 being spaced logarithmically. Whereas gas phase chemistry is considered in all model layers, aerosol chemistry is only taken into account in layers where the relative humidity is greater than the crystallisation humidity. Dry deposition of gases onto the sea and snow surface is calculated using the resistance model described by Wesely (1989), and photolysis rates are calculated online by the method of Landgraf and Crutzen (1998).

For our work, we initialised the MISTRA model runs using measurements made at Halley station, including: aerosol size distribution and composition (Rankin and Wolff, 2003), local meteorology (Anderson and Neff, 2008), and measurements of local chemical composition (NO_x, O_3, NMHCs, DMS, HCHO, CO). All emissions from particles and the surface (lowest model layer) result from explicit condensed-phase chemistry, apart from a prescribed flux of Br_2 from the model surface.

2.5 Air mass history

Back trajectory analyses using the Hybrid Single-Particle Lagrangian Integrated Trajectory (HYSPLIT) model were used to track air mass origins. HYSPLIT is available via the NOAA ARL READY website (www.arl.noaa.gov/ready.php) (Rolph, 2012; Draxler and Rolph, 2012). Back trajectories were driven by meteorological fields from the NCEP Global Data Assimilation System (GDAS) model output, and calculated using model vertical velocity at a resolution of 1° by 1°.

3 Results and discussion

3.1 Investigation of potential interferent in daytime CIMS Br_2 and BrCl observations

A surprising feature in the CIMS halogen data from Halley were the above detection limit observations of both Br_2 and BrCl during daytime (e.g. Fig. 1). If real, the data would suggest either an extremely high flux of bromine radicals into the polar boundary layer, or previously-unknown chemistry. The alternative, however, is that the data are affected by an artefact caused by the sampling methodology.

It has recently been demonstrated that CIMS observations of Br_2 can suffer from an artefact, most likely arising from chemical conversion on the instrument inlet (Neuman et al., 2010). The authors reported HOBr conversion to Br_2 on a number of different surfaces, both coated with NaBr and uncoated, the latter including the Teflon of the instrument inlet, glass, aluminium, stainless steel, PVDF (Polyvinylidene difluoride; a highly non-reactive and pure thermoplastic

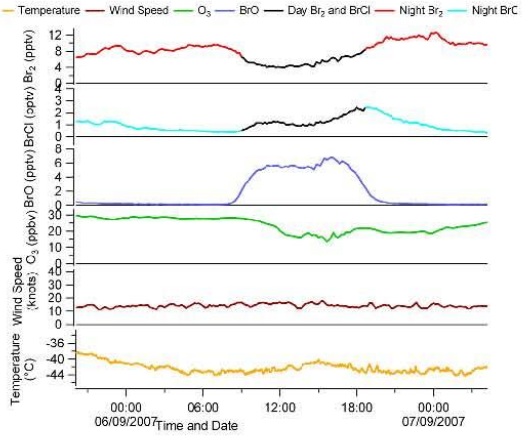

Fig. 1. Wind speed, temperature , surface O_3, and CIMS Br_2, BrCl and BrO measurements from Halley on 6–7 September 2007. Br_2 and BrCl daytime measurements are coloured black.

fluoropolymer), and several other types of Teflon. Their results are in line with laboratory studies that have shown the rapid generation of Br_2, and to a lesser extent BrCl, on salty surfaces, via uptake of HOBr (Abbatt, 1994; Adams et al., 2002; Kirchner et al., 1997). The presence of a CIMS inlet artefact in Br_2 has been acknowledged in subsequent field measurements (e.g. Liao et al., 2012a, b).

Before we discuss the data further, we will explore these hypotheses.

To explore the possible presence of a CIMS inlet artefact in our data, we focus on a few days in September during which meteorological conditions were roughly constant (Fig. 1). The local wind direction throughout this period ($\sim$250°) indicates arrival of air at Halley from over Precious Bay, and wind speeds were constant at $\sim 7\,m\,s^{-1}$. Temperatures were very low at $-40\,°C$ and observations from an acoustic sounder (a "sodar"), which provides information on atmospheric structure, suggest that there was a well-defined boundary layer (BL) (at $\sim 200\,m$ on 6 September). Observations of temperature and horizontal wind speed from an adjacent 30 m mast (sensors at 1, 2, 4, 8, 16, and 32 m) suggest the BL was well mixed on this day. While a box model can be appropriate to study a well-mixed boundary layer, given that the CIMS inlet was located $\sim 5\,m$ above the snow surface, which is known to affect gradients of many chemical components, we explore the data using both MISTRA-0D and MISTRA-1D.

A suite of model runs were performed using the MISTRA 0-D model employing different halogen flux parameterisations in an attempt to simulate observations on this day, with all bromine released as a surface flux of Br_2.

To overcome photolytic destruction of Br_2, and maintain the observed mixing ratio of ~ 5 pptv around solar noon, would require a Br_2 emission of $\sim 1 \times 10^{10}$ molecules $cm^{-2}\,s^{-1}$ into a well mixed 200 m high boundary layer. This is considerably larger than the release of Br_2 to the atmosphere of $\sim 6 \times 10^7$ to $\sim 1.8 \times 10^8$ molecules $cm^{-2}\,s^{-1}$ simulated by Toyota et al. (2011) for the Arctic spring using a 3-D model, and an order of magnitude higher than the 1×10^9 molecules $cm^{-2}\,s^{-1}$ used in a 1-D model study of BL halogens in the spring at Halley by Saiz-Lopez et al. (2008). We ran a simulation where this large persistent flux of Br_2 was released over each 24 h period of the model run, in an attempt to explain the daytime Br_2 and BrCl mixing ratio. Although we were able to reproduce the observed daytime mixing ratio of Br_2, the nighttime values were more than an order of magnitude larger than observed at Halley. The large emission of Br_2 also led to near complete O_3 destruction immediately after the solar zenith angle (SZA) fell below 88.9° (model "sunrise") on the first day. We then ran the 0-D model with an imposed diurnally varying Br_2 flux, which we coupled to the SZA. Again we were able to reproduce the daytime Br_2 observations (as well as BrCl), but even with no emissions at nighttime Br_2 mixing ratios were more than double the observed value (and BrCl was an order of magnitude larger than observed). Neither of these model simulations was able to reproduce results comparable to both daytime and nighttime Br_2, BrCl or BrO observations.

In the final 0-D model calculation, we derived the flux of bromine required to achieve the nighttime maximum Br_2 mixing ratio for 6 September 2007 according to the amount of time an air parcel had spent over newly-forming sea ice, which is the expected source region of bromine. This was determined from HYSPLIT back trajectories and sea ice maps (see Fig. 2). Back trajectories run every 2 h for the 24 h period covering 6 September all show a similar path over the newly forming sea-ice in Precious Bay. We assumed a constant emission of Br_2 from the sea-ice zone, and simulated this by release of a steady Br_2 flux over this 24 h period. A flux of 8×10^7 molecules $cm^{-2}\,s^{-1}$ was required to reproduce the nighttime halogen measurements at Halley during this event. This flux is in line with that simulated by Toyota et al. (2011), but much smaller than the flux set by Saiz-Lopez et al. (2008).

Figure 3a and b show both the observations of Br_2 and BrCl and their equivalent modelled output from MISTRA-0D for the latter flux experiment described above. It is immediately evident that there are several clear differences between the basic model output and the observations. Firstly, according to the model, daytime mixing ratios of both Br_2 and BrCl should be zero, but the measurements show a clear daytime signal for both Br_2 and BrCl. And secondly, observations of BrCl show a first peak around noon, followed by a second peak around 18:00, while the model only simulates a single peak. In light of the potential HOBr interferent,

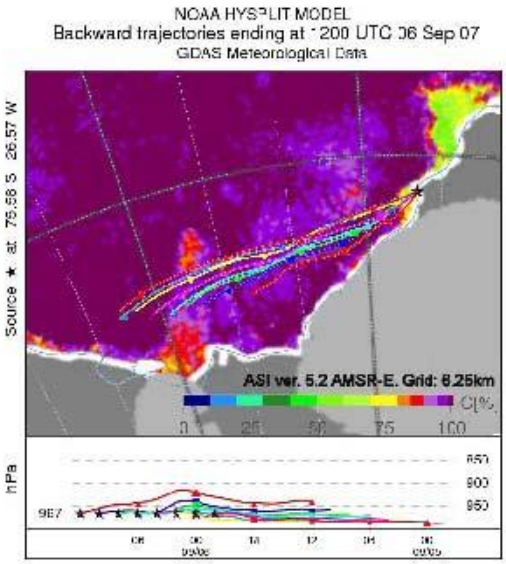

Fig. 2. 2-day back trajectories showing air parcel history (location and atmospheric pressure) prior to arrival at Halley on 6 September 2007 overlaid on an AMSR-E image of percentage sea-ice cover. The star marks the position of Halley, and the symbols mark 6-hourly intervals.

model output was re-plotted, incorporating a proportion of modelled HOBr into both modelled Br_2 and modelled BrCl. The results are shown in Fig. 3c and d. Inclusion of this assumed "HOBr interferent" clearly improved agreement between the model and measurements in terms of the daytime mixing ratio amount. Further, for BrCl, inclusion of the artefact yielded a double peak, as observed in the measurements due to the presence of HOBr during the day and possibly early hours of the night.

The initial assumption in the above calculations, regarding the MISTRA 0-D simulations being non height-specific does not take into account vertical gradients such as those introduced by any snowpack emissions. To assess this influence, we used the MISTRA 1-D model to reproduce the BL structure as characterised by the meteorological measurements from Halley. We used the measurements from both the met mast and sodar instrument to initialise the meteorology for these 1-D runs, and initialised the chemistry as for the 0-D simulations. When we used the same Br_2 flux as above, of 8×10^7 molecules $cm^{-2}\,s^{-1}$, the mixing ratios of Br_2 in the model level corresponding to 4.5–7.5 m above the snow surface were higher than for the 0-D simulations and did not reproduce the measurements. We found that reducing the Br_2 emission slightly to 6×10^7 molecules $cm^{-2}\,s^{-1}$ (the lowest flux derived by Toyota et al., 2011), the model was better able to reproduce the measured Br_2 for the model level representing 4.5–7.5 m in height (see Fig. 3e and f). This is in line with what we would expect given that in the model Br_2 is emitted from the surface, leading to higher mixing ratios near the surface and dropping off as the distance to the surface increases. While we were not able to reproduce the daytime Br_2 and BrCl measurements in their entirety with the 1-D runs, Fig. 3e and f again show that inclusion of a proportion of modelled HOBr into both Br_2 and BrCl significantly improved agreement with the daytime observations.

Thus the results from both the 0-D and 1-D MISTRA model simulations are consistent with an artefact representing a conversion of HOBr to Br_2 of the order of several tens of percent, with that for HOBr to BrCl being noticeably less but non-negligible. This conclusion is in line with Liao et al. (2012b), who corrected their hourly-averaged diurnal profiles of Br_2 and HOBr observed at Barrow assuming 20 % conversion in the inlet.

During their field observations at Barrow, Liao et al. (2012b) only observed HOBr above detection limits when $J_{Br_2} > 0$. These observations are consistent with theory – no sources of HOBr at night are known for polar regions as all known production pathways require photolytic reactions. Therefore it is reasonable to assume that no HOBr is available for conversion to Br_2 at night. However, as there are no coincident HOBr measurements from Halley, clearly this means that there is still some uncertainty in the influence of HOBr for the Halley case. Nonetheless, for the purposes of this work, and given the evidence for an artefact in CIMS daytime measurements of Br_2 and BrCl caused by conversion of HOBr on the inlet, all Halley plots (Figs. 1, 4, 7, and 9) are colour coded to differentiate between daytime ($J_{NO_2} > 0$) and nighttime ($J_{NO_2} = 0$) observations of Br_2 and BrCl, showing all daytime measurements in black.

3.2 Br_2, BrCl and BrO timeseries

Although this was a year round measurement campaign at Halley, the CIMS instrument was only configured for detection of Br_2, BrCl and BrO for specific periods. Here we focus on a measurement period in austral spring, from 12 August to 18 September 2007, a time which, according to previous work at Halley (Saiz-Lopez et al., 2007), is likely to have active bromine chemistry.

The CIMS technique has been used to detect halogens in several previous polar field campaigns (Foster et al., 2001; Spicer et al., 2002; Neuman et al., 2010; Liao et al., 2011a, b, 2012b). In contrast to issues with Br_2 and BrCl observations discussed in Sect. 3.1, a recent comparison of Arctic ground-based observations of BrO made using both a CIMS and a long-path DOAS showed good agreement when air masses were well mixed (Liao et al., 2011b). We therefore assume that all BrO observations made at Halley are interferent-free.

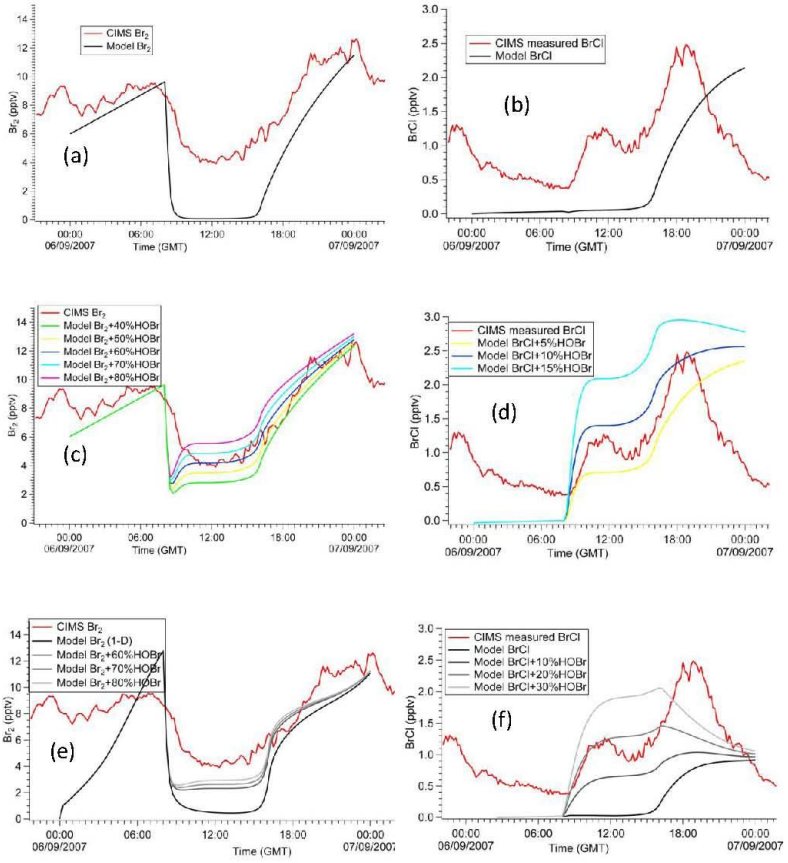

Fig. 3. **(a)** comparison between Br_2 measured with CIMS and that modelled with MISTRA-0D for 6 and 7 September 2007; **(b)** as for **(a)** but this time showing BrCl; **(c)** comparison between Br_2 measured with CIMS, and that modelled with MISTRA-0D, but now with 40 %, 50 %, 60 %, 70 %, and 80 % of model HOBr added to model Br_2; **(d)** as for **(c)** but with 5 %, 10 % and 15 % of model HOBr added to model BrCl; **(e)** comparison between Br_2 measured with CIMS and that modelled with MISTRA-1D, with 60 %, 70 % and 80 % of model HOBr added to model Br_2; **(f)** as for **(e)** but with 10 %, 20 % and 30 % of model HOBr added to model BrCl. Both 1-D model outputs **(e)** and **(f)** correspond to a height of 4.5–7.5 m above the snowpack.

3.2.1 Overview of the data

Figure 4 presents the time series of Br_2, BrCl, BrO and surface O_3 together with concurrent meteorological observations of local wind speed/direction and local temperature for the entire measurement period.

Br_2 mixing ratios vary from below instrument detection limits (refer to Table 1) to a maximum of 45 pptv (observed at night) and BrCl from below detection limits to $\sim$ 6 pptv (at night). As shown in Fig. 4, there is considerable variability in the Br_2 and BrCl observations over the measurement period which is strongly linked to the prevailing meteorology and thus air mass origin. Relatively low and invariant Br_2 and BrCl is generally associated with easterly winds of continental origin with higher mixing ratios in air masses that have passed over sea ice to the west/south west. Surprisingly, the highest measured mixing ratio of Br_2 and the lowest measured surface ozone, appear to be associated with a long-range transport event where air is arriving at Halley from across the continent via the South Pole, with its last sea ice contact somewhere to the west of the Antarctic Peninsula (discussed in Sect. 3.5)

The range of BrO mixing ratios during the measurement period, from instrumental detection limits to $\sim$ 13 pptv, are in line with previous observations at Halley (Saiz-Lopez et

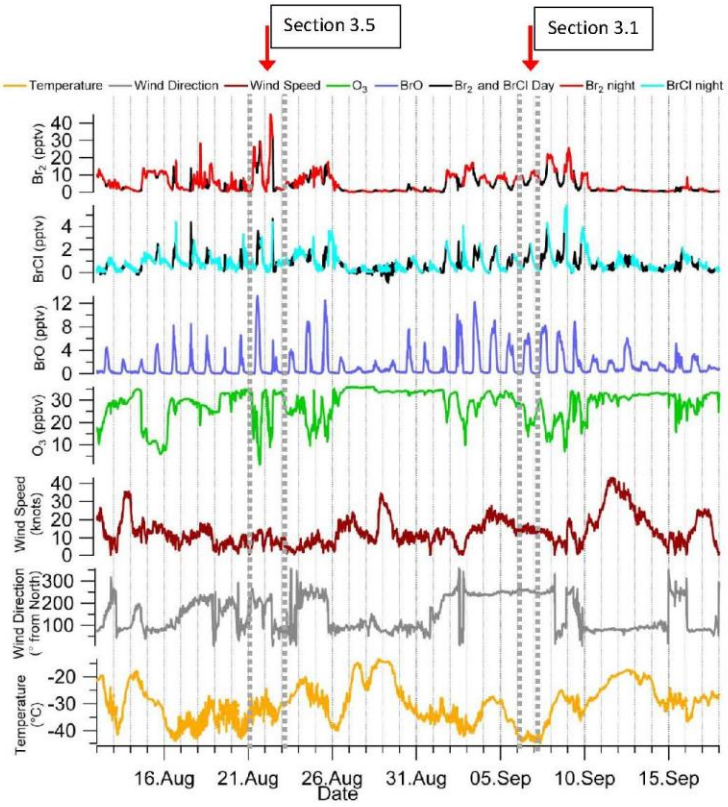

Fig. 4. Overview of measurements at Halley from 12 August to 18 September 2007. Br_2, BrCl and BrO are shown as 10 min averages; for Br_2 and BrCl, daytime observations are coloured black. Also shown are surface O_3 (10 min averages), local wind speed and direction, and local temperature.

al., 2007) made using a long-path DOAS. The BrO maxima at Halley are less obviously correlated with local wind direction than are Br_2 and BrCl. For example, from 27 August until 1 September, while the prevailing wind direction is easterly (implying continental air), Br_2 and BrCl show little variability, and there is no ODE, BrO maintains a diurnal structure with daily maxima ranging from $\sim$2 pptv to $\sim$7 pptv. These values are in line with daytime BrO measured previously at Halley in air of continental origin (Saiz-Lopez et al., 2007). The presence of a diurnal variability in BrO throughout the measurement period suggests that some persistent background bromine/ozone chemistry is active during the day, even when air is not approaching from directly across the sea ice zone.

A clear example of such background chemistry occurs on 30 August when $\sim$7 pptv of BrO was measured in air arriving at Halley, the highest BrO mixing ratios measured during a period of sustained continental origin (Fig. 4). There is little O_3 depletion on this day, but the $\sim$3–4 pptv of "Br_2" measured during daylight is indicative of active bromine chemistry (possibly as HOBr) (see Sect. 3.1). Wind speeds were low ($\sim 5\,m\,s^{-1}$) and local ambient temperature was around $-30\,^{\circ}C$. The importance of halogen recycling in/on the snowpack is discussed in a model study by Piot and von Glasow (2008), where they varied the percentage re-emission of Br_2/BrCl in their runs from 0–100 %. They found that major ODEs could only be reproduced in their model simulations when the recycling of bromine deposited on snow into gas phase bromine was included. If we therefore assume that recycling of bromine deposited on (or present in) snow is generally occurring at all times in coastal polar regions, the measurements discussed here (30 August 2007) suggest that a cold, stable/stratified BL has led to this build up of several pptv of BrO. Under the same meteorological conditions

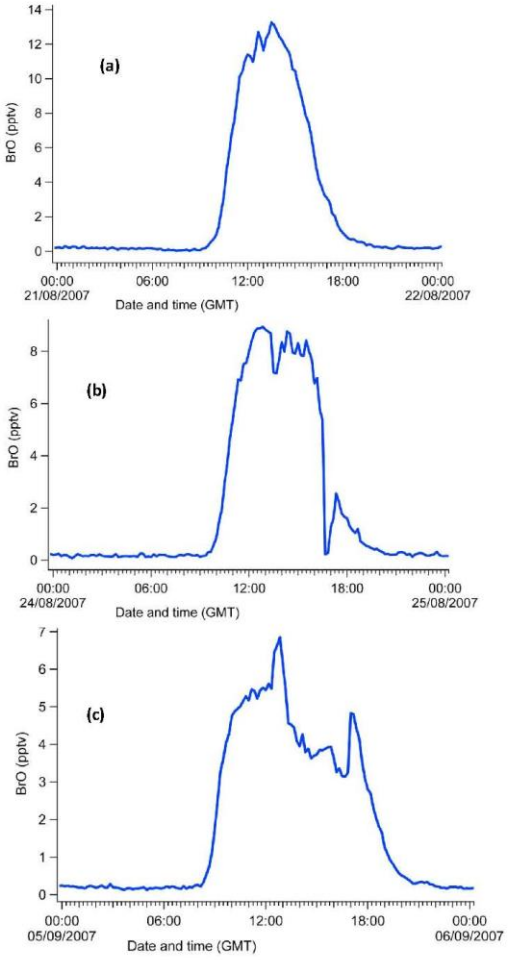

Fig. 5. Plots showing diurnal shape of BrO in pptv with time and date on the x-axis. **(a)** a single peak around noon; **(b)** a broad flat-topped maximum also around noon; and **(c)** double peak with maxima shortly after sunrise and shortly before sunset.

on the following day (31 August 2007), we measure up to 5pptv of BrO. These enhanced BrO mixing ratios measured in air of sustained continental origin suggest release of halogens directly from the snowpack, and their detection at the several pptv level may be dependent on these very specific meteorological conditions.

3.2.2 Diurnal variability in BrO, Br_2 and BrCl

BrO exhibits a clear diurnal cycle throughout the period of CIMS observations, with nighttime minima around instrumental detection limits (Fig. 4). The characteristic of the daytime maxima vary from day to day, being either (i) a single peak around noon (Fig. 5a), (ii) a broad flat-topped maximum also around noon (Fig. 5b), or (iii) double peaks with maxima shortly after sunrise and shortly before sunset (Fig. 5c). Such double-peaks were also observed by Pöhler et al. (2010) during springtime measurements in the Amundsen Gulf, and in springtime observations at Barrow, Alaska (Liao et al., 2012b). A model study by von Glasow et al. (2002) also showed this distinct diurnal structure of a BrO minimum around noon, and maxima in the morning and evening. In their model calculations this was caused by differences in the photolysis spectra of O_3 and Br_2, where Br_2 is more rapidly photolysed in twilight than O_3 due to absorption at longer wavelengths. BrO concentrations are a balance of sources and sinks. The main source of BrO is photolysis of Br_2 followed by reaction of the Br atoms with ozone. The main sink of BrO under polar conditions is reaction with HO_2. HO_2 itself is photolytically produced by way of O_3 photolysis. At high solar zenith angles (such as morning and evening) BrO is already produced efficiently but the HO_2 only at lower SZAs. Hence the efficiency of the HO_2 sink is highest during the hours around noon causing the dip in BrO mixing ratios around noon in double-peaked profiles or the reduced noon maximum in the flat profiles.

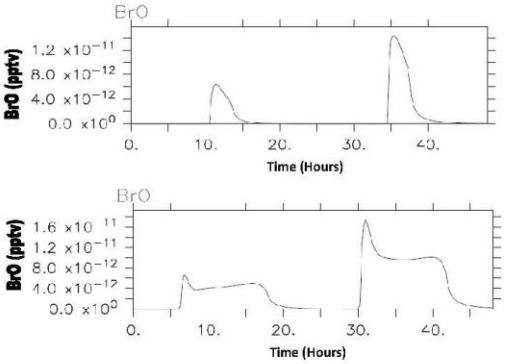

Fig. 6. BrO model output from MISTRA 0-D showing **(a)** a single BrO peak around noon when solar declination is set to represent early spring at Halley; and **(b)** a double BrO peak with a maximum in the morning and evening, with a noon time minimum when solar declination is set to represent late spring at Halley.

The occurrence of flat-topped maxima and double peak BrO increases at Halley as the spring season progresses away from polar night. To explore this changing BrO diurnal shape as the measurement period progressed, two model simulations were run using MISTRA 0-D (Fig. 6). Figure 6a is a model simulation set with a solar declination angle, φ, representative of the beginning of the measurement period (13 August, $\varphi = 14.5°$) and Fig. 6b with a solar declination

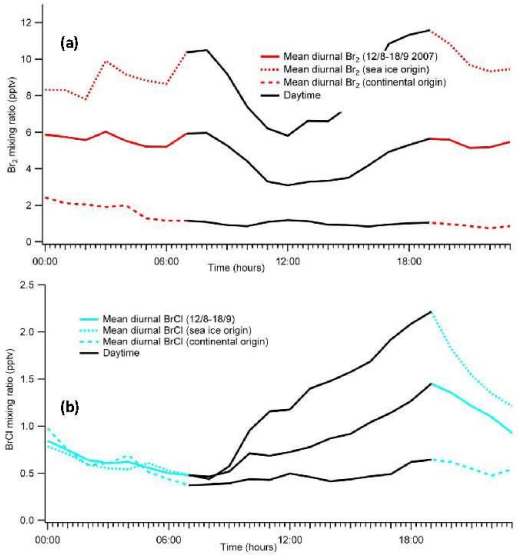

Fig. 7. Hourly mean diurnal plots of **(a)** Br_2, and **(b)** BrCl for all the data, and for different source regions (sea-ice zone; continental).

representative of the end of the measurement period (18 September, $\varphi = 1.9°$). Figure 6a clearly shows a single BrO peak around noon. At this time of year days are very short, the SZA is very high and O_3 UV photolysis is low, and insufficient HO_2 is produced to reduce BrO mixing ratios significantly to give a noon minimum. The BrO mixing ratios in Fig. 6b, however, show a clear morning peak followed by a minimum around noon and rising again to a second less-well-defined maximum just prior to sunset. Here days are long enough to allow sufficiently low noon-time SZAs, implying that sufficient HO_2 is produced to reduce BrO mixing ratios leading to a minimum around noon.

Figure 7 shows the hourly mean diurnal variability for the entire measurement period for Br_2 (Fig. 7a) and BrCl (Fig. 7b), the three lines on each plot representing (i) all data, (ii) air with a sea ice zone origin, and (iii) air with a continental origin (as determined from local wind direction). Daytime components of Br_2 and BrCl are indicated by black lines. The data immediately demonstrate the importance of filtering according to air mass origin when calculating averaged diurnal cycles for these halogen species from coastal observations.

Focussing on the hours from midnight to dawn, we note (Fig. 7a) that the hourly-averaged Br_2 mixing ratios increase over this time period in air with a sea ice zone origin. The potential for outgassing of Br_2 from sea salt aerosol at night has been demonstrated in modelling calculations by von Glasow et al. (2002), driven by gas-aqueous partitioning from gas-phase BrCl. Such increases in Br_2 are not evident in air with a continental origin (Fig. 7a), where the Br_2 mixing ratios decrease between midnight and dawn.

The reduction in hourly-averaged BrCl between midnight and dawn in sea ice zone air (Fig. 7b) is consistent with uptake and re-partitioning to Br_2 (although not sufficient to account for all the observed Br_2 increase). It is somewhat surprising, however, that BrCl mixing ratios decrease also in air with a continental origin, particularly given that Br_2 mixing ratios in the same air masses also decrease. The observations suggest uptake of both Br_2 and BrCl onto surfaces at night.

3.2.3 Period of sustained surface O_3 depletion

From 14 to 16 August the most sustained (> 24 h) ODE of the whole measurement period was observed. O_3 mixing ratios dropped from a background of 33 ppbv to 18 ppbv (a change in 15 ppbv) over a 20 min period (15:20–15:40) on 14 August and continued to fall to a minimum of 6 ppbv. This rapid change in $[O_3]$ suggests transport of an ozone depleted air mass to Halley. ECMWF ERA Interim re-analysis plots of mean surface pressure and 10 m wind speed vectors indicate that a low pressure system was present over the Weddell Sea sea ice for several days before coming into contact with Halley (not shown). At noon on 13 August, 10 m wind speeds were $> 12\,m\,s^{-1}$ over the central Weddell Sea and $> 16\,m\,s^{-1}$ at the northern Weddell Sea near the sea ice edge. Wind speeds $> 12\,m\,s^{-1}$ can create "blowing snow" conditions (Jones et al., 2009), and Yang et al. (2008) suggest lofted snow on sea ice can give rise to enhanced tropospheric bromine which can then react to destroy ozone. As the low pressure system moved over Halley wind speeds dropped to $< 4\,m\,s^{-1}$. This suggests that the high wind speeds ($> 16\,m\,s^{-1}$) observed at the northern Weddell Sea sea ice zone on 13 August could be the driver of the ODE measured at Halley on 14–16 August. The air mass is first depleted in ozone, then transported to Halley where the wind speeds drop and the ozone depleted air mass resides over Halley for > 24 h. There is then a rise in O_3 from 10–25 ppbv from 04:00–06:00 on 16 August, signalling the end of the ODE. This replenishment of O_3 may be caused by a shift in the balance of air flow from sea ice zone (low pressure system) and from the continent (orographic flow).

3.3 Br_2 : BrCl ratios

As discussed in Sect. 1, air masses arriving at Halley during spring generally have either a continental or a sea ice zone influence. We have discussed the potential importance of the sea ice zone for halogen release and ozone depletion, but here we will look at a more detailed picture of the influence these different source regions have on Br_2 : BrCl ratios.

Figure 8 shows the ratio of Br_2 : BrCl derived from the Halley nighttime observations, and colour coded for local wind direction. There is considerable variability in the ratio much of which is clearly associated with wind direction

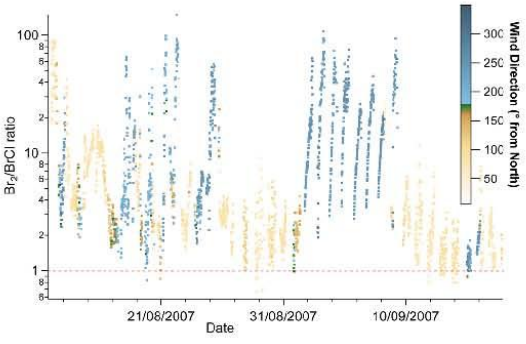

Fig. 8. Nighttime ratio of Br_2 : BrCl throughout the measurement period on a log scale. The colour coding indicates local wind direction (blues indicate sea ice zone origin; oranges indicate continental origin), emphasising the influence of air mass origin on the calculated ratio. A red dashed line is drawn at a ratio of one to highlight the small number of values found below it.

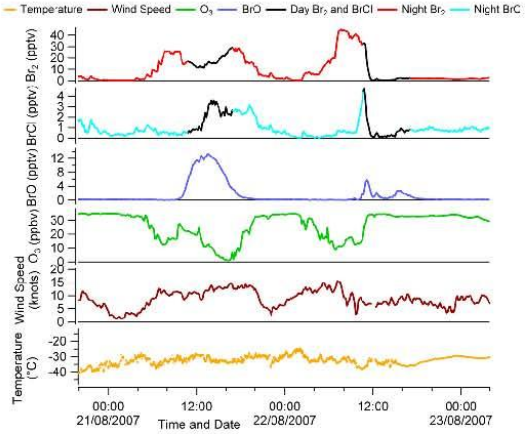

Fig. 9. Wind speed, temperature, surface O_3 and CIMS Br_2, BrCl and BrO measurements from Halley on 21 and 22 August 2007.

and thereby halogen source region. For example, from 10 September onwards, the ratio is very low, as are the mixing ratios of both Br_2 and BrCl (see Fig. 4), resulting from air masses with little/no sea ice contact. These air masses have little/no ozone depletion. In contrast, air masses with an origin from the sea ice zone (e.g. 3 to 8 September) which are depleted in ozone and enhanced in halogens, have a Br_2 : BrCl ratio clearly in favour of Br_2 ($\sim$ 2–100). On a very few occasions the Br_2 : BrCl ratio drops below 1 (red dashed line in Fig. 8). Such low ratios can be attributed to the very low (near detection limit) mixing ratios of both Br_2 and BrCl; use of a 3σ LOD filter rather than a 2σ filter (Table 1) would remove these points.

From 10 to 14 September, our data show a decrease in the Br_2 : BrCl ratio with time since the last exposure to sea ice (Fig. 8). As discussed in Sect. 3.2.1, recycling of bromine deposited on the snowpack can be a source of gas phase bromine. One explanation for this decrease in the Br_2 : BrCl ratio could be that the availability of bromine previously deposited to the snowpack reduces over time, leading to less recycling into gas phase bromine.

3.4 Comparison with Arctic Br_2, BrCl and BrO observations

High resolution ground-based measurements of Br_2 and BrCl were previously made in the Arctic as part of the Alert Polar Sunrise Experiment (PSE) (Foster et al., 2001; Spicer et al., 2002). These measurements were conducted prior to first direct sunlight, and continued for a further two weeks after polar sunrise. In the period following first direct sunlight, Spicer et al. (2002) reported Br_2 mixing ratios at Alert that ranged from instrumental detection limits to 27 pptv (which we note was measured when solar irradiance was 0 W m^{-2}, i.e. nighttime observations). For the same period at Alert, Foster et al. (2001) reported BrCl mixing ratios ranging from detection limits to $\sim$ 35 pptv, although without showing whether this was daytime or nighttime data. However, Spicer et al. (2002) measured daytime (i.e. solar irradiance $>$ 0 W m^{-2}) BrCl up to $\sim$ 25 pptv, and nighttime (i.e. solar irradiance = 0 W m^{-2}) BrCl up to $\sim$ 18 pptv. Their nighttime BrCl is considerably larger than was observed at Halley, where nighttime BrCl mixing ratios were never greater than 6 pptv. The data from Spicer et al. (2002) therefore suggest that BrCl in the Arctic can reach considerably greater mixing ratios than were measured at Halley. Furthermore, when 18 pptv of BrCl were measured at Alert, the coincident Br_2 measured was only $\sim$ 4 pptv, i.e. a Br_2 : BrCl ratio of $\sim$ 0.2 – considerably less than observed at Halley. In general Foster et al. (2001) describe the measured ratio of Br_2 to BrCl in the air to be $\sim$ 1, whereas at Halley, the ratio was almost always significantly greater than 1 (see Sect. 3.3). The measurements at Alert were made using a similar CIMS technique to that at Halley, but with a $\sim$ 9 m long teflon inlet (J. Bottenheim, personal communication, 2012), which raises the question of whether they were also subject to an inlet artefact in daytime Br_2 and BrCl observations discussed in Sect. 3.1. If so, this would likely affect both the recorded mixing ratios and ratios.

A more recent study by Liao et al. (2012b), reports measurements of BrO, Br_2 and HOBr made using a modified CIMS technique at Barrow, Alaska, in spring 2009. Their observations show a BrO maximum of $>$ 30 pptv, more than double the observed maximum at Halley of 13 pptv. Maxima in Br_2 at the two stations are very similar, with 46 pptv at Barrow and 45 pptv observed at Halley.

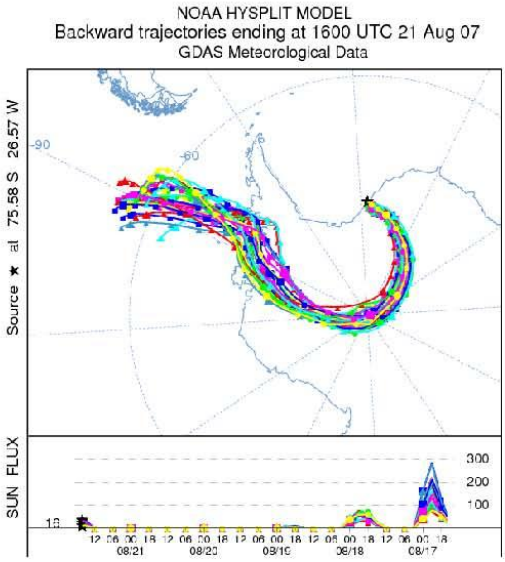

Fig. 10. 5-day HYSPLIT Ensemble back trajectory from Halley. Included is a measure of "Downward Solar Radiation Flux ($W m^{-2}$)" to indicate when the air parcel last experienced light.

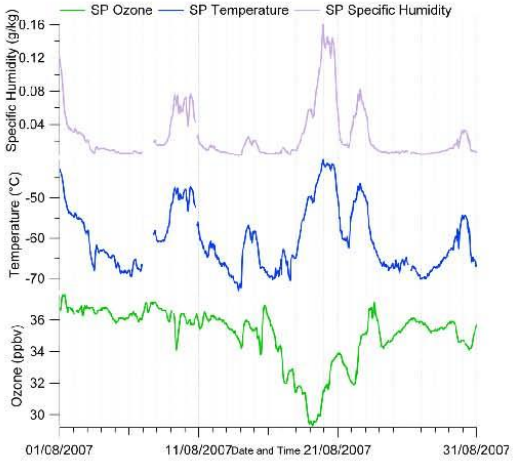

Fig. 11. South Pole surface ozone, temperature and specific humidity, from 1–31 August 2007.

3.5 Long range transport (in darkness) of a halogen enriched, ozone-depleted, air mass

Over a two day period from 21–22 August an intriguing event was observed at Halley, with the lowest measured [O_3] throughout the entire period of observations and the highest mixing ratios of [Br_2] and [BrO] (Fig. 9). The highest measured [Br_2] of the whole spring period occurred after midnight on 22 August, so is not likely to be influenced by the HOBr interferent (discussed in Sect. 3.1). HYSPLIT back trajectories suggest that this ozone depleted air mass had arrived at Halley having travelled across the continent of Antarctica from the Bellingshausen Sea, to the west of the Antarctic Peninsula (Fig. 10). As shown by the lower panel of Fig. 10, the air mass had travelled in darkness for the previous 3 1/2 days with no possibility of photochemical reactions taking place. AMSR-E maps (not shown) show open water leads, with associated sea-ice formation processes, at the coastal edge of the Bellingshausen in the region of the air mass trajectories. This area could be seen as the main source of halogen for the air mass, but it could also be argued that the furthest edge of the sea is the greatest halogen source. A third possibility is that these source regions may have some influence, but what we see is also the result of chemistry in the near-coastal environment at Halley.

Figure 11 shows surface ozone measurements from South Pole from 1–31 August 2007. The outstanding feature is the drop in ozone that occurs on 19–20 August. The back trajectories shown on Fig. 10 indicate that the low-ozone air arriving at Halley on 21 August had passed over South Pole on 19–20 August. While the drop in ozone at South Pole is modest compared with the Halley observations, the HYSPLIT trajectories suggest that the Halley air mass did not skirt the surface, but travelled at some height (> 1000 m) over South Pole. The drop in surface ozone of 7–8 ppb on 19 August is consistent with an ozone depleted air mass following this trajectory over South Pole with only a small influence being evident at the surface. Unfortunately no ozone sonde was launched from South Pole on this day, from which the profile of ozone could be seen. However, data from South Pole of temperature and specific humidity both show significant increases, consistent with passage of marine air. Further, Bromwich et al. (1996) suggest that passage of air across the continent along this route is not uncommon.

In an attempt to understand the halogen chemistry occurring during this period of darkness as the air mass traversed the continent, a run in MISTRA-0D was set up to recreate the conditions the air mass would see (Fig. 12). An initial mixing ratio for Br_2 was set at 40 pptv, with the majority of the remaining parameters set for a typical Halley model run. HYSPLIT trajectories were used to determine the length of run required, and the influence of light on the air mass. The result is shown in Fig. 12. It is clear that the initial influence of sunlight is of vital importance in the partitioning of halogen species between Br_2 and BrCl, but it appears that the lack of photolysis thereafter effectively "stalls" the ozone depleting reactions. This implies that the majority of ozone depletion would have to occur prior to the period of darkness, although there is some photolytic influence near the end

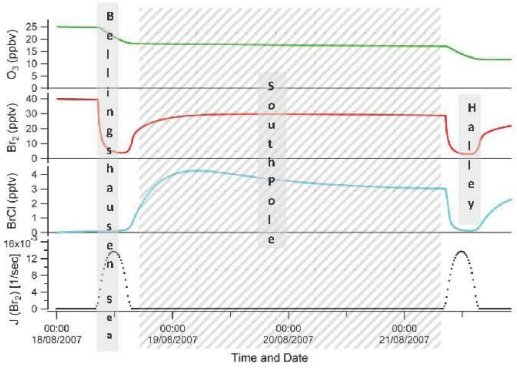

Fig. 12. MISTRA 0-D run 4 days in length showing [Br_2], [BrCl], [O_3] and $J(Br_2)$ model output. Only the first and last of those days under the influence of sunlight (darkness is highlighted with the hashed grey box). Mixing ratio on the left axis, and time in hours since the start of the run along the bottom. The location of the air mass is highlighted at key stages of its transcontinental path.

of the run. Although the model run does not show complete ozone depletion as observed at Halley, the run does highlight the transport of the depleted air mass in the dark. We also note that the final [Br_2] and [BrCl] output from the model run is comparable to the halogen observations from Halley on 21 August 2007 (see Fig. 9).

4 Conclusions

We report the first high temporal resolution measurements of BrO, Br_2 and BrCl in coastal Antarctica, made during spring 2007 using a CIMS instrument. The previously-reported artefact, arising from an inlet conversion of HOBr and affecting Br_2 observations, may also be apparent in our data; we also suggest there may be a minor artefact on BrCl. This is not, however, a fundamental instrument restriction and refers more to our specific sampling methodology. Results from the MISTRA 0-D and 1-D model runs indicate that the artefact represents a conversion of HOBr to Br_2 of the order of several tens of percent, while that for HOBr to BrCl is less but non-negligible. Conclusions can be drawn about the Br_2 and BrCl observations by restricting focus to their nighttime results only. Mixing ratios of BrO, Br_2 and BrCl ranged from instrumental detection limits to 13 pptv (daytime), 45 pptv (nighttime), and 6 pptv (nighttime), respectively. It is interesting to note that as the spring season progressed, the diurnal shape of BrO changed from a sharp single peak, to a broad/ flat-topped peak and finally to a double peak with BrO maxima in the morning and evening along with noon time minima. This suite of Antarctic data provides the first analogue to similar measurements made in the Arctic. Previously-reported nighttime maxima for Br_2 (46 pptv at Barrow, Liao et al., 2012b and 27 pptv at Alert, Spicer et al., 2002) are in line with the Halley observations. Arctic nighttime BrCl mixing ratios up to 18 pptv (Spicer et al., 2002), however, are considerably larger than observed at Halley. Further, ratios of Br_2 : BrCl at Alert appear to be lower than measured at Halley, where air masses with an origin from the sea ice zone have a ratio in favour of Br_2 and are never less than 1 if filtered using a 3σ LOD. An unusual event of trans-continental air mass transport in darkness was associated with severe surface ozone depletion observed at Halley. Model calculations were consistent with the halogen source region being to the west of the Antarctic Peninsula, with the air mass having spent 3 1/2 days in complete darkness crossing the continent prior to arrival at Halley. Not only was this air mass strongly depleted in O_3, it was also the source of both the highest measured [Br_2] and [BrO] for the whole measurement period. Although there are several possible explanations for these measurements (discussed in Sect. 3.5), the evidence suggests that this ozone depleted, halogen-enriched air mass was transported over thousands of kilometres in complete darkness with its halogen source being the sea ice zone on the West side of the Antarctic Peninsula.

Acknowledgements. The authors gratefully acknowledge the NOAA Air Resources Laboratory (ARL) for the provision of the HYSPLIT transport and dispersion model and/or READY website (http://www.arl.noaa.gov/ready.php) used in this publication.

Surface ozone and meteorological data was provided by NOAA's Climate Monitoring and Diagnostics Laboratory (CMDL) via their data archive http://www.cmdl.noaa.gov/info/ftpdata.html.

We thank Tony Phillips of the British Antarctic Survey for giving us access to an experimental service providing web access to IDL-based PP plotting routines of ECMWF operational analysis data.

This study is part of the British Antarctic Survey Polar Science for Planet Earth programme. Zak Buys' studentship was funded by the Natural Environment Research Council through a BAS Algorithm grant.

Edited by: J. W. Bottenheim

References

Abbatt, J. P. D.: Heterogeneous reaction of HOBr with HBr and HCl on ice surfaces at 228 K, Geophys. Res. Lett., 21, 665–668, doi:10.1029/94GL00775, 1994.

Abbatt, J. P. D., Thomas, J. L., Abrahamsson, K., Boxe, C., Granfors, A., Jones, A. E., King, M. D., Saiz-Lopez, A., Shepson, P. B., Sodeau, J., Toohey, D. W., Toubin, C., von Glasow, R., Wren, S. N., and Yang, X.: Halogen activation via interactions with environmental ice and snow in the polar lower troposphere and other regions, Atmos. Chem. Phys., 12, 6237–6271, doi:10.5194/acp-12-6237-2012, 2012.

Adams, J. W., Holmes, N. S., and Crowley, J. N.: Uptake and reaction of HOBr on frozen and dry NaCl/NaBr surfaces between 253 and 233 K, Atmos. Chem. Phys., 2, 79–91, doi:10.5194/acp-2-79-2002, 2002.

Anderson, P. S. and Neff, W. D.: Boundary layer physics over snow and ice, Atmos. Chem. Phys., 8, 3563–3582, doi:10.5194/acp-8-3563-2008, 2008.

Arnold, S. T. and Viggiano, A. A.: Turbulent ion flow tube study of the cluster-mediated reactions of SF_6^- with H_2O, CH_3OH, and C_2H_5OH from 50 to 500 torr, J. Phys. Chem. A, 105, 3527–3531, 2001.

Barrie, L. A., Bottenheim, J. W., Schnell, R. C., Crutzen, P. J., and Rasmussen, R. A.: Ozone Destruction and Photochemical-Reactions at Polar Sunrise in the Lower Arctic Atmosphere, Nature, 334, 138–141, 1988.

Berresheim, H., Elste, T., Plass-Dulmer, C., Eisele, F. L., and Tanner, D. J.: Chemical ionization mass spectrometer for long-term measurements of atmospheric OH and H_2SO_4, Int. J. Mass Spectrom., 202, 91–109, 2000.

Bottenheim, J. W., Gallant, A. G., and Brice, K. A.: Measurements of NO_y Species and O_3 at 82° N Latitude, Geophys. Res. Lett., 13, 113–116, 1986.

Bromwich, D. H., Carrasco J. F., and Turner J.: A Downward Developing Mesoscale Cyclone Over the Ross Ice Shelf During Winter, Global Atmos. Ocean Syst., 4, 125–147, 1996.

Damian, V., Sandu, A., Damien, M., Potra, F., and Carmichael, G. R.: The kinetic preprocessor kpp – a software environment for solving chemical kinetics, Comp. Chem. Eng., 26, 1567–1579, 2002.

Draxler, R. R. and Rolph, G. D.: HYSPLIT (HYbrid Single-Particle Lagrangian Integrated Trajectory) Model access via NOAA ARL READY Website (http://ready.arl.noaa.gov/HYSPLIT.php), NOAA Air Resources Laboratory, Silver Spring, MD, 2012.

Fickert, S., Adams, J. W., and Crowley, J. N.: Activation of Br_2 and BrCl via uptake of HOBr onto aqueous salt solutions, J. Geophys. Res., 104, 23719–23727, doi:10.1029/1999JD900359, 1999.

Foster, K. L., Plastridge, R. A., Bottenheim, J. W., Shepson, P. B., Finlayson-Pitts, B. J., and Spicer, C. W.: The role of Br_2 and BrCl in surface ozone destruction at polar sunrise, Science, 291, 471–474, 2001.

Gilman, J. B., Burkhart, J. F., Lerner, B. M., Williams, E. J., Kuster, W. C., Goldan, P. D., Murphy, P. C., Warneke, C., Fowler, C., Montzka, S. A., Miller, B. R., Miller, L., Oltmans, S. J., Ryerson, T. B., Cooper, O. R., Stohl, A., and de Gouw, J. A.: Ozone variability and halogen oxidation within the Arctic and sub-Arctic springtime boundary layer, Atmos. Chem. Phys., 10, 10223–10236, doi:10.5194/acp-10-10223-2010, 2010.

Huey, L. G., Hanson, D. R., and Howard, C. J.: Reactions of SF_6^- and I^- with Atmospheric Trace Gases, J. Phys. Chem., 99, 5001–5008, doi:10.1021/j100014a021, 1995.

Huey, L. G., Dunlea, E. J., Lovejoy, E. R., Hanson, D. R., Norton, R. B., Fehsenfeld, F. C., and Howard, C. J.: Fast time response measurements of HNO_3 in air with a chemical ionization mass spectrometer, J. Geophys. Res.-Atmos., 103, 3355–3360, 1998.

Huey, L. G., Tanner, D. J., Slusher, D. L., Dibb, J. E., Arimoto, R., Chen, G., Davis, D., Buhr, M. P., Nowak, J. B., Mauldin, R. L., Eisele, F. L., and Kosciuch, E.: CIMS measurements of HNO_3 and SO_2 at the South Pole during ISCAT 2000, Atmos. Environ., 38, 5411–5421, doi:10.1016/j.atmosenv.2004.04.037, 2004.

Jacobi, H.-W., Morin, S., and Bottenheim, J. W.: Observation of widespread depletion of ozone in the springtime boundary layer of the central Arctic linked to mesoscale synoptic conditions, J. Geophys. Res., 115, D17302, doi:10.1029/2010JD013940, 2010.

Jones, A. E., Anderson, P. S., Wolff, E. W., Turner, J., Rankin, A. M., and Colwell, S. R.: A role for newly forming sea ice in springtime polar tropospheric ozone loss? Observational evidence from Halley station, Antarctica, J. Geophys. Res., 111, D08306, doi:10.1029/2005JD006566, 2006.

Jones, A. E., Wolff, E. W., Salmon, R. A., Bauguitte, S. J.-B., Roscoe, H. K., Anderson, P. S., Ames, D., Clemitshaw, K. C., Fleming, Z. L., Bloss, W. J., Heard, D. E., Lee, J. D., Read, K. A., Hamer, P., Shallcross, D. E., Jackson, A. V., Walker, S. L., Lewis, A. C., Mills, G. P., Plane, J. M. C., Saiz-Lopez, A., Sturges, W. T., and Worton, D. R.: Chemistry of the Antarctic Boundary Layer and the Interface with Snow: an overview of the CHABLIS campaign, Atmos. Chem. Phys., 8, 3789–3803, doi:10.5194/acp-8-3789-2008, 2008.

Jones, A. E., Anderson, P. S., Begoin, M., Brough, N., Hutterli, M. A., Marshall, G. J., Richter, A., Roscoe, H. K., and Wolff, E. W.: BrO, blizzards, and drivers of polar tropospheric ozone depletion events, Atmos. Chem. Phys., 9, 4639–4652, doi:10.5194/acp-9-4639-2009, 2009.

Kirchner, U., Benter, T. H., and Schindler, R. N.: Experimental verification of gas phase bromine enrichment in reactions of HOBr with sea salt doped ice surfaces, Ber. Bunsen Ges. Phys. Chem., 101, 975–977, 1997.

König-Langlo, G., King, J. C., and Pettre, P.: Climatology of the three coastal Antarctic stations Dumont d'Urville, Neumayer, and Halley, J. Geophys. Res.-Atmos., 103, 10935–10946, doi:10.1029/97jd00527, 1998.

Kreher, K., Keys, J. G., Johnston, P. V., Platt, U., and Liu, X.: Ground-based measurements of OClO and HCl in austral spring 1993 at Arrival Heights, Antarctica, Geophys. Res. Lett., 23, 1545–1548, doi:10.1029/96gl01318, 1996.

Kreher, K., Johnston, P. V., Wood, S. W., Nardi, B., and Platt, U.: Ground-based measurements of tropospheric and stratospheric BrO at Arrival Heights, Antarctica, Geophys. Res. Lett., 24, 3021–3024, doi:10.1029/97gl02997, 1997.

Landgraf, J. and Crutzen, P. J.: An Efficient Method for Online Calculations of Photolysis and Heating Rates, J. Atmos. Sci., 55, 863–878, doi:10.1175/1520-0469(1998)055<0863:AEMFOC>2.0.CO;2, 1998.

Leibrock, E. and Huey, L. G.: Ion chemistry for the detection of isoprene and other volatile organic compounds in ambient air, Geophys. Res. Lett., 27, 1719–1722, 2000.

Liao, J., Huey, L. G., Tanner, D. J., Brough, N., Brooks, S., Dibb, J. E., Stutz, J., Thomas, J. L., Lefer, B., Haman, C., and Gorham, K.: Observations of hydroxyl and peroxy radicals and the impact of BrO at Summit, Greenland in 2007 and 2008, Atmos. Chem. Phys., 11, 8577–8591, doi:10.5194/acp-11-8577-2011, 2011a.

Liao, J., Sihler, H., Huey, L. G., Neuman, J. A., Tanner, D. J., Friess, U., Platt, U., Flocke, F. M., Orlando, J. J., Shepson, P. B., Beine, H. J., Weinheimer, A. J., Sjostedt, S. J., Nowak, J. B., Knapp, D. J., Staebler, R. M., Zheng, W., Sander, R., Hall, S. R., and Ullmann, K.: A comparison of Arctic BrO measurements by chemical ionization mass spectrometry and long path-differential optical absorption spectroscopy, J. Geophys. Res.-Atmos., 116,

D00r02, doi:10.1029/2010jd014788, 2011b.

Liao, J., Huey, L. G., Scheuer, E., Dibb, J. E., Stickel, R. E., Tanner, D. J., Neuman, J. A., Nowak, J. B., Choi, S., Wang, Y., Salawitch, R. J., Canty, T., Chance, K., Kurosu, T., Suleiman, R., Weinheimer, A. J., Shetter, R. E., Fried, A., Brune, W., Anderson, B., Zhang, X., Chen, G., Crawford, J., Hecobian, A., and Ingall, E. D.: Characterization of soluble bromide measurements and a case study of BrO observations during ARCTAS, Atmos. Chem. Phys., 12, 1327–1338, doi:10.5194/acp-12-1327-2012, 2012a.

Liao, J., Huey, L. G., Tanner, D. J., Flocke, F. M., Orlando, J. J., Neuman, J. A., Nowak, J. B., Weinheimer, A. J., Hall, S. R., Smith, J. N., Fried, A., Staebler, R. M., Wang, Y., Koo, J.-H., Cantrell, C. A., Weibring, P., Walega, J., Knapp, D. J., Shepson, P. B., and Stephens, C. R.: Observations of inorganic bromine (HOBr, BrO, and Br_2) speciation at Barrow, Alaska, in spring 2009, J. Geophys. Res., 117, D00R16, doi:10.1029/2011JD016641, 2012b.

Neuman, J. A., Nowak, J. B., Huey, L. G., Burkholder, J. B., Dibb, J. E., Holloway, J. S., Liao, J., Peischl, J., Roberts, J. M., Ryerson, T. B., Scheuer, E., Stark, H., Stickel, R. E., Tanner, D. J., and Weinheimer, A.: Bromine measurements in ozone depleted air over the Arctic Ocean, Atmos. Chem. Phys., 10, 6503–6514, doi:10.5194/acp-10-6503-2010, 2010.

Oltmans, S. J.: Surface Ozone Measurements in Clean Air, J. Geophys. Res., 86, 1174–1180, 1981.

Piot, M. and von Glasow, R.: The potential importance of frost flowers, recycling on snow, and open leads for ozone depletion events, Atmos. Chem. Phys., 8, 2437–2467, doi:10.5194/acp-8-2437-2008, 2008.

Pöhler, D., Vogel, L., Friess, U., and Platt, U.: Observation of halogen species in the Amundsen Gulf, Arctic, by active long-path differential optical absorption spectroscopy, P. Natl. Acad. Sci. USA, 107, 6582–6587, doi:10.1073/pnas.0912231107, 2010.

Rankin, A. M. and Wolff, E. W.: A year-long record of size-segregated aerosol composition at Halley, Antarctica, J. Geophys. Res.-Atmos., 108, 4775, doi:10.1029/2003jd003993, 2003.

Rankin, A. M., Wolff, E. W., and Martin, S.: Frost flowers: Implications for tropospheric chemistry and ice core interpretation, J. Geophys. Res.-Atmos., 107, 4683, doi:10.1029/2002jd002492, 2002.

Ridley, B. A., Walega, J. G., Dye, J. E., and Grahek, F. E.: Distributions of NO, NO_x, NO_y, and O_3 to 12 km altitude during the summer monsoon season over New Mexico, J. Geophys. Res., 99, 25529–25534, doi:10.1029/94JD02210, 1994.

Rolph, G. D.: Real-time Environmental Applications and Display sYstem (READY) Website (http://ready.arl.noaa.gov), NOAA Air Resources Laboratory, Silver Spring, MD, 2012.

Roscoe, H. K. and Roscoe, J.: Polar tropospheric ozone depletion events observed in the International Geophysical Year of 1958, Atmos. Chem. Phys., 6, 3303–3314, doi:10.5194/acp-6-3303-2006, 2006.

Saiz-Lopez, A., Mahajan, A. S., Salmon, R. A., Bauguitte, S. J. B., Jones, A. E., Roscoe, H. K., and Plane, J. M. C.: Boundary layer halogens in coastal Antarctica, Science, 317, 348–351, doi:10.1126/science.1141408, 2007.

Simpson, W. R., von Glasow, R., Riedel, K., Anderson, P., Ariya, P., Bottenheim, J., Burrows, J., Carpenter, L. J., Frieß, U., Goodsite, M. E., Heard, D., Hutterli, M., Jacobi, H.-W., Kaleschke, L., Neff, B., Plane, J., Platt, U., Richter, A., Roscoe, H., Sander, R., Shepson, P., Sodeau, J., Steffen, A., Wagner, T., and Wolff, E.: Halogens and their role in polar boundary-layer ozone depletion, Atmos. Chem. Phys., 7, 4375–4418, doi:10.5194/acp-7-4375-2007, 2007.

Sjostedt, S. J. and Abbatt, J. P. D.: Release of gas-phase halogens from sodium halide substrates: heterogeneous oxidation of frozen solutions and dessicated salts by hydroxyl radicals, Environ. Res. Lett., 3, 045007, doi:10.1088/1748-9326/3/4/045007, 2008.

Slusher, D. L., Pitteri, S. J., Haman, B. J., Tanner, D. J., and Huey, L. G.: A chemical ionization technique for measurement of pernitric acid in the upper troposphere and the polar boundary layer, Geophys. Res. Lett., 28, 3875–3878, 2001.

Slusher, D. L., Huey, L. G., Tanner, D. J., Flocke, F. M., and Roberts, J. M.: A thermal dissociation-chemical ionization mass spectrometry (td-cims) technique for the simultaneous measurement of peroxyacyl nitrates and dinitrogen pentoxide, J. Geophys. Res., 109, D19315, doi:10.1029/2004JD004670, 2004.

Spicer, C. W., Plastridge, R. A., Foster, K. L., Finlayson-Pitts, B. J., Bottenheim, J. W., Grannas, A. M., and Shepson, P. B.: Molecular halogens before and during ozone depletion events in the Arctic at polar sunrise: concentrations and sources, Atmos. Environ., 36, 2721–2731, 2002.

Spreen, G., Kaleschke, L., and Heygster, G.: Sea ice remote sensing using AMSR-E 89-GHz channels, J. Geophys. Res.-Oceans, 113, C02s03, doi:10.1029/2005jc003384, 2008.

Toyota, K., McConnell, J. C., Lupu, A., Neary, L., McLinden, C. A., Richter, A., Kwok, R., Semeniuk, K., Kaminski, J. W., Gong, S.-L., Jarosz, J., Chipperfield, M. P., and Sioris, C. E.: Analysis of reactive bromine production and ozone depletion in the Arctic boundary layer using 3-D simulations with GEM-AQ: inference from synoptic-scale patterns, Atmos. Chem. Phys., 11, 3949–3979, doi:10.5194/acp-11-3949-2011, 2011.

von Glasow, R., Sander, R., Bott, A., and Crutzen, P. J.: Modeling halogen chemistry in the marine boundary layer – 1. Cloud-free MBL, J. Geophys. Res.-Atmos., 107, 4341, doi:10.1029/2001JD000942, 2002.

Wesely, M. L.: Parameterization of surface resistances to gaseous dry deposition in regional-scale numerical models, Atmos. Environ., 23, 1293–1304, 1989.

Wessel, S., Aoki, S., Winkler, P., Weller, R., Herber, A., Gernandt, H., and Schrems, O.: Tropospheric ozone depletion in polar regions - A comparison of observations in the Arctic and Antarctic, Tellus B, 50, 34–50, 1998.

Wilson, K. L. and Birks, J. W.: Mechanism and Elimination of a Water Vapour Interference in the Measurement of Ozone by UV Absorbance, Environ. Sci. Technol., 40, 6361–6367, doi:10.1021/es052590c, 2006.

Yang, X., Pyle, J. A., and Cox, R. A.: Sea salt aerosol production and bromine release: Role of snow on sea ice, Geophys. Res. Lett., 35, L16815, doi:10.1029/2008GL034536, 2008.

Bibliography

Abbatt, J. P. D.: Heterogeneous reaction of HOBr with HBr and HCl on ice surfaces at 228 K, Geophys. Res. Lett., 21, 665–668, doi:10.1029/94GL00775, 1994.

Abbatt, J. P. D.: Interactions of Atmospheric Trace Gases with Ice Surfaces: Adsorption and Reaction, Chem. Rev., 103, 4783–4800, doi:10.1021/cr0206418, 2003.

Abbatt, J. P. D., Thomas, J. L. , Abrahamsson, K., Boxe, C., Granfors, A., Jones, A. E., King, M. D., Saiz-Lopez, A., Shepson, P. B., Sodeau, J., Toohey, D. W., Toubin, C., von Glasow, R., Wren, S. N. and X. Yang: Halogen activation via interactions with environmental ice and snow in the polar lower troposphere and other regions, Atmos. Chem. Phys., 12, 6237-6271, 2012.

Adams, J. W., Holmes, N. S., and Crowley, J. N.: Uptake and reaction of HOBr on frozen and dry NaCl/NaBr surfaces between253 and 233 K, Atmos. Chem. Phys., 2, 79–91, doi:10.5194/acp- 2-79-2002, 2002.

Albert, M. R., Grannas, A. M., Bottenheim, J., Shepson, P. B., and Peron Jr., F. E.: Processes and properties of snow-air transfer in the High Arctic with application to interstitial ozone at Alert, Canada, Atmos. Environ., 36, 2779–2787, 2002.

Albert, M. R. and Shultz, E. F.: Snow and firn properties and air-snow transport processes at Summit, Greenland, Atmos. Environ., 36, 2789–2797, 2002.

Anderson, P. S., and Neff, W. D.: Boundary layer physics over snow and ice, Atmospheric Chemistry and Physics, 8, 3563-3582, 2008.

Arnold, S. T., and Viggiano, A. A.: Turbulent ion flow tube study of the cluster-mediated reactions of SF_6^- with H_2O, CH_3OH, and C_2H_5OH from 50 to 500 torr, J. Phys. Chem. A, 105, 3527-3531, 2001.

Barrie, L. A., Bottenheim, J. W., Schnell, R. C., Crutzen, P. J., and Rasmussen, R. A.: Ozone Destruction and Photochemical-Reactions at Polar Sunrise in the Lower Arctic Atmosphere, Nature, 334, 138-141, 1988.

Barrie, L. A., Denhartog, G., Bottenheim, J. W., and Landsberger, S.: ANTHROPOGENIC AEROSOLS AND GASES IN THE LOWER TROPOSPHERE AT ALERT CANADA IN APRIL 1986, Journal of Atmospheric Chemistry, 9, 101-127, 10.1007/bf00052827, 1989.

Bartlett, W. P. and Margerum, D. W.: Temperature dependencies of the Henry's law constant and the aqueous phase dissociation constant of bromine chloride, Environ. Sci. Technol., 33, 3410–3414, 1999.

Begoin, M., Richter, A., Weber, M., Kaleschke, L., Tian-Kunze, X., Stohl, A., Theys, N., and Burrows, J. P.: Satellite observations of long range transport of a large BrO plume in the Arctic, Atmos. Chem. Phys., 10, 6515–6526, doi:10.5194/acp-10-6515- 2010, 2010.

Beine, H., Colussi, A. J., Amoroso, A., Esposito, G., Montagnoli, M., and Hoffmann, M. R.: HONO emissions from snow surfaces, Environ. Res. Lett., 3, 045005, doi:10.1088/1748-9326/3/4/045005, 2008.

Berresheim, H., Elste, T., Plass-Dulmer, C., Eisele, F. L., and Tanner, D. J.: Chemical ionization mass spectrometer for long-term measurements of atmospheric OH and H_2SO_4, International Journal of Mass Spectrometry, 202, 91-109, 2000.

Bloss, W. J., Lee, J. D., Heard, D. E., Salmon, R. A., Bauguitte, S. J.-B., Roscoe, H. K., and Jones, A. E.: Observations of OH and HO2 radicals in coastal Antarctica, Atmos. Chem. Phys., 7, 4171-4185, 2007

Bott, A. A numerical model of the cloud-topped planetary boundary-layer: Impact of aerosol particles on the radiative forcing of stratiform clouds. Q. J. R. Meteorol. Soc., 123 , 631-656, 1997.

Bottenheim, J. W., Gallant, A. G., and Brice, K. A.: Measurements of NO_Y Species and O_3 at 82°N Latitude, Geophysical Research Letters, 13, 113-116, 1986.

Bromwich, D. H., Carrasco J. F., and Turner J.: A Downward Developing Mesoscale Cyclone Over the Ross Ice Shelf During Winter. The Global Atmosphere and Ocean System, 4, 125-147, 1996.

Buys, Z., Brough, N., Huey, L. G., Tanner, D. J., von Glasow, R., and Jones, A. E.: High temporal resolution Br_2, BrCl and BrO observations in coastal Antarctica, Atmos. Chem. Phys., 13, 1329-1343, doi:10.5194/acp-13-1329-2013, 2013.

Cho, H., Shepson, P. B., Barrie, L. A., Cowin, J. P., and Zaveri, R.: NMR Investigation of the Quasi-Brine Layer in Ice/Brine Mixtures, J. Phys. Chem. B, 106, 11226–11232, doi:10.1021/jp020449+, 2002.

Clemitshaw, K. C.: Coupling between the tropospheric photochemistry of nitrous acid (HONO) and nitric acid (HNO3), Environmental Chemistry, 3, 31-34, 2006.

Cunningham, J. and Waddington, E. D.: Snow physics as Air flow and dry deposition of non-sea salt sulphate in polar firn: paleoclimatic implications, Atmos. Environ., 27A, 2943–2956, 1993.

Damian, V., Sandu, A., Damien, M., Potra, F., and Carmichael, G. R.: The kinetic preprocessor kpp - a software environment for solving chemical kinetics. Comp. Chem. Eng., 26:1567 – 1579, 2002.

Davies, R. Response of Cloud Supersaturation to Radiative Forcing. J. Atmos. Sci., 42 , 2820{2825, 1985.

de Serves, C.: Gas phase formaldehyde and peroxide measurements in the Arctic atmosphere, J. Geophys. Res., 99 (D12), 25 391–25 398, 1994.

DeMore, W. B., Sander, S. P., Golden, D. M., Hampson, R. F., Kurylo, M. J., Howard, C. J., Ravishankara, A. R., Kolb, C. E., and Molina, M. J.: Chemical Kinetics and Photochemical Data for Use in Stratospheric Modeling, Tech. Rep. JPL Publication 97-4, Jet Propulsion Laboratory, Pasadena, CA, 1997.

Dieckmann, G. S., Nehrke, G., Papadimitriou, S., G¨ottlicher, J., Steininger, R., Kennedy, H., Wolf-Gladrow, D., and Thomas, D. N.: Calcium carbonate as ikaite crystals in Antarctic sea ice, Geophys. Res. Lett., 35, L08501, doi:10.1029/2008GL033540, 2008.

Dieckmann, G. S., Nehrke, G., Uhlig, C., G¨ottlicher, J., Gerland, S., Granskog, M. A., and Thomas, D. N.: Brief Communication: Ikaite ($CaCO_3 \cdot 6H_2O$) discovered in Arctic sea ice, The Cryosphere, 4, 227–230, doi:10.5194/tc-4-227-2010, 2010.

Döppenschmidt, A. and Butt, H.-J.: Measuring the thickness of the liquid-like layer on ice surfaces with atomic force microscopy, Langmuir, 16, 6709–6714, doi:10.1021/la990799w, 2000.

Draxler, R.R. and Rolph, G.D., HYSPLIT (HYbrid Single-Particle Lagrangian Integrated Trajectory) Model access via NOAA ARL READY Website (http://ready.arl.noaa.gov/HYSPLIT.php). NOAA Air Resources Laboratory, Silver Spring, MD. 2012

Ehn, J. K., Hwang, B. J., Galley, R., and Barber, D. G.: Investigations of newly formed sea ice in the Cape Bathurst polynya: 1. Structural, physical, and optical properties, J. Geophys. Res., 112, C05002, doi:10.1029/2006JC003702, 2007.

Eicken, H.: The role of sea ice in structuring Antarctic ecosystems, *Polar. Biol*., *12*(1), 3–13, 1992.

Fickert, S., Adams, J. W., and Crowley, J. N.: Activation of Br_2 and BrCl via uptake of HOBr onto aqueous salt solutions, J. Geophys. Res., 104, 1999.

Foster, K. L., Plastridge, R. A., Bottenheim, J. W., Shepson, P. B., Finlayson-Pitts, B. J., and Spicer, C. W.: The role of Br_2 and BrCl in surface ozone destruction at polar sunrise, Science, 291, 471-474, 2001.

Frieß, U., Hollwedel, J., K¨onig-Langlo, G., Wagner, T., and Platt, U.: Dynamics and chemistry of tropospheric bromine explosion events in the Antarctic coastal region, J. Geophys. Res., 109, D06305, doi:10.1029/2003JD004133, 2004.

Frieß, U., Sihler, H., Sander, R., P¨ohler, D., Yilmaz, S., and Platt, U.: The vertical distribution of BrO and aerosols in the Arctic: Measurements by active and passive differential optical absorption spectroscopy, J. Geophys. Res., 116, D00R04, doi:10.1029/2011JD015938, 2011.

Frinak, E. K. and Abbatt, J. P. D.: Br2 production from the heterogeneous reaction of gas-phase OH with aqueous salt solutions: Impacts of acidity, halide concentration, and organic surfactants, J. Phys. Chem. A, 110, 10456–10464, doi:10.1021/jp063165o, 2006.

Gilman, J. B., Burkhart, J. F., Lerner, B. M.,Williams, E. J., Kuster, W. C., Goldan, P. D., Murphy, P. C., Warneke, C., Fowler, C., Montzka, S. A., Miller, B. R., Miller, L., Oltmans, S. J., Ryerson, T. B., Cooper, O. R., Stohl, A., and de Gouw, J. A.: Ozone variability and halogen oxidation within the Arctic and sub-Arctic springtime boundary layer, Atmos. Chem. Phys., 10, 10223–10236, doi:10.5194/acp-10-10223-2010, 2010.

Gladich, I., Shepson, P. B., Carignano, M. A., and Szleifer, I.: Halide affinity for the water air interface in aqueous solutions of mixtures of sodium salts, J. Phys. Chem. A, 115, 5895–5899, doi:10.1021/jp110208a, 2011.

Grannas, A. M., Jones, A. E., Dibb, J., Ammann, M., Anastasio, C., Beine, H. J., Bergin, M., Bottenheim, J., Boxe, C. S., Carver, G., Chen, G., Crawford, J. H., Domine, F., Frey, M. M., Guzman, M. I., Heard, D. E., Helmig, D., Hoffmann, M. R., Honrath, R. E., Huey, L. G., Hutterli, M., Jacobi, H. W., Klan, P., Lefer, B., McConnell, J., Plane, J., Sander, R., Savarino, J., Shepson, P. B., Simpson, W. R., Sodeau, J. R., von Glasow, R., Weller, R., Wolff, E. W., and Zhu, T.: An overview of snow photochemistry: evidence, mechanisms and impacts, Atmospheric Chemistry and Physics, 7, 4329-4373, 2007.

Hamilton, J. F., Allen, G., Watson, N. M., Lee, J. D., Saxton, J. E., Lewis, A. C., Vaughan, G., Bower, K. N., Flynn, M. J., Crosier, J., Carver, G. D., Harris, N. R. P., Parker, R. J., Remedios, J. J., and Richards, N. A. D.: Observations of an atmospheric chemical equator and its implications for the tropical warm pool region, Journal of Geophysical Research-Atmospheres, 113, D20313 10.1029/2008jd009940, 2008.

Hanson, D. R. and Ravishankara, A. R.: Heterogeneous chemistry of HBr and HF, J. Phys. Chem., 96, 9441–9446, doi:10.1021/j100202a069, 1992.

Helmig, D., Bocquet, F., Cohen, L., and Oltmans, S.: Ozone Uptake to the Summit, Greenland Snowpack, Atmos. Environ., in press, 2006.

Helmig, D., Ganzeveld, L., Butler, T., and Oltmans, S. J.: The role of ozone atmosphere-snow gas exchange on polar, boundary-layer tropospheric ozone – a review and sensitivity analysis, Atmos. Chem. Phys., 7, 15–30, doi:10.5194/acp-7-15-2007, 2007.

Honrath, R., Lu, Y., Peterson, M., Dibb, J., Arsenault, M., Cullen, N., and Steffen, K.: Vertical fluxes of NOx, HONO, and HNO3 above the snowpack at Summit, Greenland, Atmos. Environ., 36, 2629–2640, doi:10.1016/S1352-2310(02)00132-2, 2002.

Huey, L. G., Hanson, D. R., and Howard, C. J.: Reactions of SF_6^- and I^- with Atmospheric Trace Gases, Journal of Physical Chemistry, 99, 5001-5008, 10.1021/j100014a021, 1995.

Huey, L. G., Dunlea, E. J., Lovejoy, E. R., Hanson, D. R., Norton, R. B., Fehsenfeld, F. C., and Howard, C. J.: Fast time response measurements of HNO_3 in air with a chemical ionization mass spectrometer, Journal of Geophysical Research-Atmospheres, 103, 3355-3360, 1998.

Huey, L. G., Tanner, D. J., Slusher, D. L., Dibb, J. E., Arimoto, R., Chen, G., Davis, D., Buhr, M. P., Nowak, J. B., Mauldin, R. L., Eisele, F. L., and Kosciuch, E.: CIMS measurements of HNO_3 and SO_2 at the South Pole during ISCAT 2000, Atmospheric Environment, 38, 5411-5421, 10.1016/j.atmosenv.2004.04.037, 2004.

Huff, A. K. and Abbatt, J. P. D.: Gas-Phase Br_2 Production in Heterogeneous Reactions of Cl_2, HOCl, and BrCl with Halide-Ice Surfaces, J. Phys. Chem. A, 104, 7284–7293, 2000.

Huff, A. K. and Abbatt, J. P. D.: Kinetics and product yields in the heterogeneous reactions of HOBr with ice surfaces containing NaBr and NaCl, J. Phys. Chem. A, 106, 5279–5287, doi:10.1021/jp014296m, 2002.

Huthwelker, T., Ammann, M., and Peter, T.: The uptake of acidic gases on ice, Chem. Rev., 106, 1375–1444, doi:10.1021/cr020506v, 2006.

Jacobi, H.-W., Morin, S., and Bottenheim, J. W.: Observation of widespread depletion of ozone in the springtime boundary layer of the central Arctic linked to mesoscale synoptic conditions, J. Geophys. Res., 115, D17302, doi:10.1029/2010JD013940, 2010.

Jacobson, M. Z.: Fundamentals of Atmospheric Modeling, Cambridge University Press, 1999.

Jaenicke, R.: Aerosol Physics and Chemistry, in Landolt-Börnstein ”Zahlenwerte und Funktione aus Naturwissenschaften und Technik”, vol. V 4b, pp. 391–457, Springer, 1988.

Jones, A. E., Anderson, P. S., Wolff, E. W., Turner, J., Rankin, A. M., and Colwell, S. R.: A role for newly forming sea ice in springtime polar tropospheric ozone loss? Observational evidence from Halley station, Antarctica, J. Geophys. Res., 111, 2006.

Jones, A. E., Wolff, E. W., Ames, D., Bauguitte, S. J.-B., Clemitshaw, K. C., Fleming, Z., Mills, G. P., Saiz-Lopez, A., Salmon, R. A., Sturges, W. T., and Worton, D. R.: The multi-seasonal NOy budget in coastal Antarctica and its link with surface snow and ice core nitrate: Results from the CHABLIS campaign, Atmos. Chem. Phys. Discuss., 7, 4127–4163, 2007.

Jones, A. E., Wolff, E. W., Salmon, R. A., Bauguitte, S. J. B., Roscoe, H. K., Anderson, P. S., Ames, D., Clemitshaw, K. C., Fleming, Z. L., Bloss, W. J., Heard, D. E., Lee, J. D., Read, K. A., Hamer, P., Shallcross, D. E., Jackson, A. V., Walker, S. L., Lewis, A. C., Mills, G. P., Plane, J. M. C., Saiz-Lopez, A., Sturges, W. T., and Worton, D. R.: Chemistry of the Antarctic Boundary Layer and the Interface with Snow: an overview of the CHABLIS campaign, Atmospheric Chemistry and Physics, 8, 3789-3803, 2008.

Jones, A. E., Anderson, P. S., Begoin, M., Brough, N., Hutterli, M. A., Marshall, G. J., Richter, A., Roscoe, H. K., and Wolff, E. W.: BrO, blizzards, and drivers of polar tropospheric ozone depletion events, Atmospheric Chemistry and Physics, 9, 4639-4652, 2009.

Jones, A. E., Anderson, P. S., Wolff, E. W., Roscoe, H. K., Marshall, G. J., Richter, A., Brough, N., and Colwell, S. R.: Vertical structure of Antarctic tropospheric ozone depletion events: characteristics and broader implications, Atmospheric Chemistry and Physics, 10, 7775-7794, 10.5194/acp-10-7775-2010, 2010.

Jourdain, B., and Legrand, M.: Year-round records of bulk and size-segregated aerosol composition and HCl and HNO3 levels in the Dumont d'Urville (coastal Antarctica) atmosphere: Implications for sea-salt aerosol fractionation in the winter and summer, Journal of Geophysical Research: Atmospheres, 107, 4645, 2002.

Jungwirth, P. and Tobias, D. J.: Molecular structure of salt solutions: A new view of the interface with implications for heterogeneous atmospheric chemistry, J. Phys. Chem. B, 105, 10468–10472, doi:10.1021/jp012750g, 2001.

Jungwirth, P. and Tobias, D. J.: Ions at the Air/Water Interface, J. Phys. Chem. B, 106, 6361–6373, 2002.

Jungwirth, P. and Tobias, D. J.: Specific ion effects at the air/water interface, Chem. Rev., 106, 1259–1281, doi:10.1021/cr0403741, 2006.

Kaleschke, L., Richter, A., Burrows, J., Afe, O., Heygster, G., Notholt, J., Rankin, A. M., Roscoe, H. K., Hollwedel, J., Wagner, T., and Jacobi, H. W.: Frost flowers on sea ice as a source of sea salt and their influence on tropospheric halogen chemistry, Geophysical Research Letters, 31, 10.1029/2004gl020655, 2004.

Kalnajs, L. E. and Avallone, L. M.: Frost flower influence on springtime boundary-layer ozone depletion events and atmospheric bromine levels, Geophys. Res. Lett., 33, L10810, doi:10.1029/2006GL025809, 2006.

King, D. and W.R. Simpson.: Extinction of UV radiation in Arctic snow at Alert, Canada (82 8 N). J. Geophys. Res., 106 (D12), 12,499–12,507. 2001.

Kirchner, U., Benter, T. H., and Schindler, R. N.: Experimental verification of gas phase bromine enrichment in reactions of HOBr with sea salt doped ice surfaces, Ber. Bunsen Ges. Phys. Chem., 101, 975–977, 1997.

Koop, T., Kapilashrami, A., Molina, L. T., and Molina, M. J.: Phase transitions of sea-salt/water mixtures at low temperatures: Implications for ozone chemistry in the polar marine boundary layer, Journal of Geophysical Research-Atmospheres, 105, 26393-26402, 2000.

König-Langlo, G., King, J. C., and Pettre, P.: Climatology of the three coastal Antarctic stations Dumont d'Urville, Neumayer, and Halley, Journal of Geophysical Research-Atmospheres, 103, 10935-10946, 10.1029/97jd00527, 1998.

Kreher, K., Keys, J. G., Johnston, P. V., Platt, U., and Liu, X.: Ground-based measurements of OClO and HCl in austral spring 1993 at Arrival Heights, Antarctica, Geophysical Research Letters, 23, 1545-1548, 10.1029/96gl01318, 1996.

Kreher, K., Johnston, P. V., Wood, S. W., Nardi, B., and Platt, U.: Ground-based measurements of tropospheric and stratospheric BrO at Arrival Heights, Antarctica, Geophysical Research Letters, 24, 3021-3024, 10.1029/97gl02997, 1997.

Kuo, M. H., Moussa, S. G., and McNeill, V. F.: Modeling interfacial liquid layers on environmental ices, Atmos. Chem. Phys., 11, 9971–9982, 10.5194/acp-11-9971-2011, 2011.

Landgraf, J., and Crutzen, P. J.: An Efficient Method for Online Calculations of Photolysis and Heating Rates, Journal of the Atmospheric Sciences, 55, 863-878, doi:10.1175/1520-0469(1998)055<0863:AEMFOC>2.0.CO;2, 1998.

Leibrock, E., and Huey, L. G.: Ion chemistry for the detection of isoprene and other volatile organic compounds in ambient air, Geophysical Research Letters, 27, 1719-1722, 2000.

Liao, J., Huey, L. G., Tanner, D. J., Brough, N., Brooks, S., Dibb, J. E., Stutz, J., Thomas, J. L., Lefer, B., Haman, C., and Gorham, K.: Observations of hydroxyl and peroxy radicals and the impact of BrO at Summit, Greenland in 2007 and 2008, Atmospheric Chemistry and Physics, 11, 8577-8591, 10.5194/acp-11-8577-2011, 2011a.

Liao, J., Sihler, H., Huey, L. G., Neuman, J. A., Tanner, D. J., Friess, U., Platt, U., Flocke, F. M., Orlando, J. J., Shepson, P. B., Beine, H. J., Weinheimer, A. J., Sjostedt, S. J., Nowak, J. B., Knapp, D. J., Staebler, R. M., Zheng, W., Sander, R., Hall, S. R., and Ullmann, K.: A comparison of Arctic BrO measurements by chemical ionization mass spectrometry and long path-differential optical absorption spectroscopy, Journal of Geophysical Research-Atmospheres, 116, 14, D00r02 10.1029/2010jd014788, 2011b.

Liao, J., Huey, L. G., Scheuer, E., Dibb, J. E., Stickel, R. E., Tanner, D. J., Neuman, J. A., Nowak, J. B., Choi, S., Wang, Y., Salawitch, R. J., Canty, T., Chance, K., Kurosu, T., Suleiman, R., Weinheimer, A. J., Shetter, R. E., Fried, A., Brune, W., Anderson, B., Zhang, X., Chen, G., Crawford, J., Hecobian, A., and Ingall, E. D.: Characterization of soluble bromide measurements and a case study of BrO observations during ARCTAS, Atmos. Chem. Phys., 12, 1327-1338, doi:10.5194/acp-12-1327-2012, 2012a.

Liao, J., Huey, L. G., Tanner, D. J., Flocke, F. M., Orlando, J. J., Neuman, J. A., Nowak, J. B., Weinheimer, A. J., Hall, S. R., Smith, J. N., Fried, A., Staebler, R. M., Wang, Y., Koo, J.-H., Cantrell, C. A., Weibring, P., Walega, J., Knapp, D. J., Shepson, P. B., and Stephens, C. R.: Observations of inorganic bromine (HOBr, BrO, and Br_2) speciation at Barrow, Alaska, in spring 2009, J. Geophys. Res., 117, D00R16, doi:10.1029/2011JD016641, 2012b.

Mahajan, A. S., Oetjen, H., Lee, J. D., Saiz-Lopez, A., McFiggans, G. B., and Plane, J. M. C.: High bromine oxide concentrations in the semi-polluted boundary layer, Atmospheric Environment, 43, 3811-3818, 2009.

Maric, D., J. P. Burrows, and G. K. Moortgat, A Study of the UV-Visible Absorption Spectra of Br_2 and BrCl, *J. Photochem. Photobiol. A: Chem.* **83**, 179-192, 1994.

Massom, R. A., Eicken, H., Haas, C., Jeffries, M. O., Drinkwater, M. R., Sturm, M., Worby, A. P., Wu, X. R., Lytle, V. I., Ushio, S., Morris, K., Reid, P. A., Warren, S. G., and Allison, I.: Snow on Antarctic Sea ice, Reviews of Geophysics, 39, 413-445, 10.1029/2000rg000085, 2001.

McConnell, J. C., Henderson, G. S., Barrie, L., Bottenheim, J., Niki, H., Langford, C. H., and Templeton, E. M. J.: Photochemical bromine production implicated in Arctic boundary-layer ozone depletion, Nature, 355, 150-152, 1992.

McNeill, V. F., Loerting, T., Geiger, F. M., Trout, B. L., and Molina, M. J.: Hydrogen chloride-induced surface disordering on ice, P. Natl. Acad. Sci., 103, 9422–9427, doi:10.1073/pnas.0603494103, 2006.

Mellor, G. and Yamada, T.: Development of a Turbulence Closure Model for Geophysical Fluid Problems, Rev. Geophys. Space Ph., 20, 851–875, 1982.

Michalowski, B. A., Francisco, J. S., Li, S.-M., Barrie, L. A., Bottenheim, J. W., and Shepson, P. B.: A computer model study of multiphase chemistry in the Arctic boundary layer during polar sunrise, J. Geophys. Res., 105, 15131–15145, doi:10.1029/2000JD900004, 2000.

Mills, G. P., Sturges, W. T., Salmon, R. A., Bauguitte, S.-B., Read, K. A., and Bandy, B. J.: Seasonal variation of peroxyacetylnitrate (PAN) in coastal Antarctica measured with a new instrument for the detection of sub-part per trillion mixing ratios of PAN, Atmospheric Chemistry and Physics, 7, 4589-4599, 2007.

Morin, S., Marion, G. M., von Glasow, R., Voisin, D., Bouchez, J., and Savarino, J.: Precipitation of salts in freezing seawater and ozone depletion events: a status report, Atmospheric Chemistry and Physics, 8, 7317-7324, 2008.

Neuman, J. A., Nowak, J. B., Huey, L. G., Burkholder, J. B., Dibb, J. E., Holloway, J. S., Liao, J., Peischl, J., Roberts, J. M., Ryerson, T. B., Scheuer, E., Stark, H., Stickel, R. E., Tanner, D. J., and Weinheimer, A.: Bromine measurements in ozone depleted air over the Arctic Ocean, Atmospheric Chemistry and Physics, 10, 6503-6514, 10.5194/acp-10-6503-2010, 2010.

Obbard, R. W., Roscoe, H. K., Wolff, E. W., and Atkinson, H. M.: Frost flower surface area and chemistry as a function of salinity and temperature, Journal of Geophysical Research-Atmospheres, 114, 10.1029/2009jd012481, 2009.

Oltmans, S. J.: Surface Ozone Measurements in Clean Air, J. Geophys. Res., 86, 1174-1180, 1981.

Pechtl, S., Schmitz, G., and von Glasow, R.: Modelling iodide-iodate speciation in atmospheric aerosol: Contributions of inorganic and organic iodine chemistry, Atmospheric Chemistry and Physics, 7, 1381-1393, 2007.

Peterson, M. C. and Honrath, R. E.: Observations of rapid photochemical destruction of ozone in snowpack interstitial air, Geophys. Res. Lett., 28, 511–514, doi:10.1029/2000GL012129, 2001.

Piot, M.: Modeling Halogen Chemistry during Ozone Depletion Events in Polar Spring: A Model Study, Thesis, 2007.

Piot, M., and von Glasow, R.: The potential importance of frost flowers, recycling on snow, and open leads for ozone depletion events, Atmospheric Chemistry and Physics, 8, 2437-2467, 2008.

Platt, U. and Janssen, C.: Observation and Role of the Free Radicals NO3, ClO, BrO and IO in the Troposphere, Faraday Discuss., 100, 175–198, 1995

Pöhler, D., Vogel, L., Friess, U., and Platt, U.: Observation of halogen species in the Amundsen Gulf, Arctic, by active long-path differential optical absorption spectroscopy, Proceedings of the National Academy of Sciences of the United States of America, 107, 6582-6587, 10.1073/pnas.0912231107, 2010.

Pratt, K. A., Custard, K. D., Shepson, P. B., Douglas, T. A., Pohler, D., General, S., Zielcke, J., Simpson, W. R., Platt, U., Tanner, D. J., Gregory Huey, L., Carlsen, M., and Stirm, B. H.: Photochemical production of molecular bromine in Arctic surface snowpacks, Nature Geosci, 6, 351-356, 2013.

Pruppacher, H. R. and J. D. Klett.: Microphysics of Clouds and Precipitation. Kluwer Academic Pub., Dordrecht/Boston/London, 1997.

Rankin, A. M., Wolff, E. W., and Martin, S.: Frost flowers: Implications for tropospheric chemistry and ice core interpretation, Journal of Geophysical Research-Atmospheres, 107, 10.1029/2002jd002492, 2002.

Rankin, A. M., and Wolff, E. W.: A year-long record of size-segregated aerosol composition at Halley, Antarctica, Journal of Geophysical Research-Atmospheres, 108, 10.1029/2003jd003993, 2003.

Read, K. A., Lewis, A. C., Bauguitte, S., Rankin, A. M., Salmon, R. A., Wolff, E. W., Saiz-Lopez, A., Bloss, W. J., Heard, D. E., Lee, J. D., and Plane, J. M. C.: DMS and MSA measurements in the Antarctic Boundary Layer: Impact of BrO on MSA production, Atmospheric Chemistry and Physics, 8, 2985-2997, 2008.

Ridley, B. A., Walega, J. G., Dye, J. E., and Grahek, F. E.: Distributions of NO, NOx, NOy , and O3 to 12 km altitude during the summer monsoon season over New Mexico, Journal of Geophysical Research, 99, 25529–25534, 10.1029/94JD02210, 1994

Riedel, K., Weller, R., and Schrems, O.: Variability of formaldehyde in the Antarctic troposphere, Physical Chemistry Chemical Physics, 1, 5523-5527, 1999.

Rolph, G.D., Real-time Environmental Applications and Display sYstem (READY) Website (http://ready.arl.noaa.gov). NOAA Air Resources Laboratory, Silver Spring, MD. 2012.

Roscoe, H. K., and Roscoe, J.: Polar tropospheric ozone depletion events observed in the International Geophysical Year of 1958, Atmospheric Chemistry and Physics, 6, 3303-3314, 2006.

Rosenberg, R.: Why Is Ice Slippery?, Phys. Today, 58, 50–55, doi:10.1063/1.2169444, 2005.

Rudolph, J., Khedim, A., Clarkson, T., and Wagenbach, D.: Long-term measurements of light alkanes and acetylene in the Antarctic troposphere, Tellus, 44, 252–261, 1992.

Saiz-Lopez, A., Mahajan, A. S., Salmon, R. A., Bauguitte, S. J. B., Jones, A. E., Roscoe, H. K., and Plane, J. M. C.: Boundary layer halogens in coastal Antarctica, Science, 317, 348-351, 10.1126/science.1141408, 2007.

Saiz-Lopez, A., Plane, J. M. C., Mahajan, A. S., Anderson, P. S., Bauguitte, S. J.-B., Jones, A. E., Roscoe, H. K., Salmon, R. A., Bloss, W. J., Lee, J. D., and Heard, D. E.: On the vertical distribution of boundary layer halogens over coastal Antarctica: implications for O3, HOx, NOx and the Hg lifetime, Atmos. Chem. Phys., 8, 887–900, doi:10.5194/acp-8-887-2008, 2008.

Salmon, R. A., Bauguitte, S.-B., Bloss, W., Hutterli, M. A., Jones, A. E., Read, K., and Wolff, E. W.: Measurement and interpretation of gas phase formaldehyde concentrations obtained during the CHABLIS campaign in coastal Antarctica, Atmospheric Chemistry and Physics, 8, 4085-4093, 2008.

Sander, R. and P. J. Crutzen.: Model study indicating halogen activation and ozone destruction in polluted air masses transported to the sea. J. Geophys. Res., 101 , 9121-9138, 1996.

Sander, R., Burrows, J., and Kaleschke, L.: Carbonate precipitation in brine - a potential trigger for tropospheric ozone depletion events, Atmos. Chem. Phys., 6, 4653-4658, 2006.

Sandu, A., Verwer, J. G., Blom, J. G., Spee, E. J., Carmichael, G. R., and Potra, F. A.: Benchmarking stiff ODE solvers for atmospheric chemistry problems - II. Rosenbrock Solvers, Atmos. Environ., 31, 3459–3472, 1997.

Simpson, W. R., von Glasow, R., Riedel, K., Anderson, P., Ariya, P., Bottenheim, J., Burrows, J., Carpenter, L. J., Friess, U., Goodsite, M. E., Heard, D., Hutterli, M., Jacobi, H. W., Kaleschke, L., Neff, B., Plane, J., Platt, U., Richter, A., Roscoe, H., Sander, R., Shepson, P., Sodeau, J., Steffen, A., Wagner, T., and Wolff, E.: Halogens and their role in polar boundary-layer ozone depletion, Atmospheric Chemistry and Physics, 7, 4375-4418, 2007.

Sjostedt, S. J., and Abbatt, J. P. D.: Release of gas-phase halogens from sodium halide substrates: heterogeneous oxidation of frozen solutions and desiccated salts by hydroxyl radicals, Environ. Res. Lett., 3, 7, 045007 10.1088/1748-9326/3/4/045007, 2008.

Slusher, D. L., Pitteri, S. J., Haman, B. J., Tanner, D. J., and Huey, L. G.: A chemical ionization technique for measurement of pernitric acid in the upper troposphere and the polar boundary layer, Geophysical Research Letters, 28, 3875-3878, 2001.

Slusher, D. L., Huey, L. G., Tanner, D. J., Flocke, F. M., and Roberts, J. M.: A thermal dissociation-chemical ionization mass spectrometry (td-cims) technique for the simultaneous measurement of peroxyacyl nitrates and dinitrogen pentoxide, J. Geophys. Res., 109(13), 5 D19315, doi:10.1029/2004JD004670, 2004.

Smoydzin, L., and von Glasow, R.: Modelling chemistry over the Dead Sea: bromine and ozone chemistry, Atmospheric Chemistry and Physics, 9, 5057-5072, 2009.

Snow, J. A., Heikes, B. G., Merrill, J. T., Wimmers, A. J., Moody, J. L., and Cantrell, C. A.: Winter-spring evolution and variability of HOx reservoir species, hydrogen peroxide and methyl hydroperoxide, in the northern mid to high-latitudes, J. Geophys. Res., 108 (D4), doi:10.1029/2002JD002 172, 2002.

Spicer, C. W., Plastridge, R. A., Foster, K. L., Finlayson-Pitts, B. J., Bottenheim, J. W., Grannas, A. M., and Shepson, P. B.: Molecular halogens before and during ozone depletion events in the Arctic at polar sunrise: concentrations and sources, Atmospheric Environment, 36, 2721-2731, 2002.

Spolaor, A., Vallelonga, P., Plane, J. M. C., Kehrwald, N., Gabrieli, J., Varin, C., Turetta, C., Cozzi, G., Kumar, R., Boutron, C., and Barbante, C.: Halogen species record Antarctic sea ice extent over glacial-interglacial periods, Atmos. Chem. Phys., 13, 6623-6635, 2013.

Spreen, G., Kaleschke, L., and Heygster, G.: Sea ice remote sensing using AMSR-E 89-GHz channels, J. Geophys. Res.-Oceans, 113, C02s03 10.1029/2005jc003384, 2008.

Sturges, W. T.: EXCESS PARTICULATE AND GASEOUS BROMINE AT A REMOTE COASTAL LOCATION, Atmospheric Environment Part a-General Topics, 24, 167-171, 1990.

Tarasick, D. W. and Bottenheim, J. W.: Surface ozone depletion episodes in the Arctic and Antarctic from historical ozonesonde records, Atmos. Chem. Phys., 2, 197–205, doi:10.5194/acp-2- 197-2002, 2002.

Timco, G. W. and Weeks, W. F.: A review of the engineering properties of sea ice, Cold Reg. Sci. Technol., 60, 107–129, doi:10.1016/j.coldregions.2009.10.003, 2010.

Thomas, J. L., Stutz, J., Lefer, B., Huey, L. G., Toyota, K., Dibb, J. E., and von Glasow, R.: Modeling chemistry in and above snow at Summit, Greenland - Part 1: Model description and results, Atmospheric Chemistry and Physics, 11, 4899-4914, 10.5194/acp-11-4899-2011, 2011.

Thomas, J. L., Dibb, J. E., Huey, L. G., Liao, J., Tanner, D., Lefer, B., von Glasow, R., and Stutz, J.: Modeling chemistry in and above snow at Summit, Greenland - Part 2: Impact of snowpack chemistry on the oxidation capacity of the boundary layer, Atmos. Chem. Phys., 12, 6537-6554, 2012.

Toyota, K., McConnell, J. C., Lupu, A., Neary, L., McLinden, C. A., Richter, A., Kwok, R., Semeniuk, K., Kaminski, J. W., Gong, S. L., Jarosz, J., Chipperfield, M. P., and Sioris, C. E.: Analysis of reactive bromine production and ozone depletion in the Arctic boundary layer using 3-D simulations with GEM-AQ: inference from synoptic-scale patterns, Atmos. Chem. Phys., 11, 3949-3979, 2011.

Vogt, R., Crutzen, P. J., and Sander, R.: A mechanism for halogen release from sea-salt aerosol in the remote marine boundary layer, Nature, 383, 327–330, doi:10.1038/383327a0, 1996.

von Glasow, R.: Modeling the gas and aqueous phase chemistry of the marine boundary layer, Thesis, 2000

von Glasow, R., Sander, R., Bott, A., and Crutzen, P. J.: Modeling halogen chemistry in the marine boundary layer - 1. Cloud-free MBL, Journal of Geophysical Research-Atmospheres, 107, 10.1029/2001jd000942, 2002a.

von Glasow, R., Sander, R., Bott, A., and Crutzen, P. J.: Modeling halogen chemistry in the marine boundary layer 2. Interactions with sulfur and the cloud-covered MBL, J. Geophys. Res., 107, 2002b.

von Glasow, R., and Crutzen, P. J.: Model study of multiphase DMS oxidation with a focus on halogens, Atmospheric Chemistry and Physics, 4, 589-608, 2004.

Voulgarakis, A., Yang, X., and Pyle, J. A.: How different would tropospheric oxidation be over an ice-free Arctic?, Geophysical Research Letters, 36, L23807, 2009.

Vrbka, L. and Jungwirth, P.: Brine rejection from freezing salt solutions: A molecular dynamics study, Phys. Rev. Lett., 95, 148501, doi:10.1103/PhysRevLett.95.148501, 2005.

Wagner, T., Leue, C., Wenig, M., Pfeilsticker, K., and Platt, U.: Spatial and temporal distribution of enhanced boundary layer BrO concentrations measured by the GOME instrument aboard ERS-2, J. Geophys. Res., 106, 24225–24235, doi:10.1029/2000JD000201, 2001.

Wesely, M. L.: Parameterization of surface resistances to gaseous dry deposition in regional-scale numerical models, Atmospheric Environment (1967), 23, 1293-1304, 1989.

Wessel, S., Aoki, S., Winkler, P., Weller, R., Herber, A., Gernandt, H., and Schrems, O.: Tropospheric ozone depletion in polar regions - A comparison of observations in the Arctic and Antarctic, Tellus Series B-Chemical and Physical Meteorology, 50, 34-50, 1998.

Williams, J. E., Landgraf, J., Bregman, A., and Walter, H. H.: A modified band approach for the accurate calculation of online photolysis rates in stratospheric-tropospheric Chemical Transport Models, Atmos. Chem. Phys., 6, 4137-4161, 2006.

Wilson, K. L., and Birks, J. W.: Mechanism and Elimination of a Water Vapour Interference in the Measurement of Ozone by UV Absorbance, Environmental Science and Technology, 40 (20), 6361–6367**,** 10.1021/es052590c, 2006.

Yang, X., Pyle, J. A., and Cox, R. A.: Sea salt aerosol production and bromine release: Role of snow on sea ice, Geophysical Research Letters, 35, 10.1029/2008gl034536, 2008.

Yang, X., Pyle, J. A., Cox, R. A., Theys, N., and Van Roozendael, M.: Snow-sourced bromine and its implications for polar tropospheric ozone, Atmos. Chem. Phys., 10, 7763–7773, doi:10.5194/acp-10-7763-2010, 2010.